The conservation of polymeric materials in museum collections using advanced surface science and surface analysis techniques

Anna L Fricker

2016

Supervised by Professor D. S. McPhail, Dr. B. Keneghan and Dr. T. Georgiou

Department of Materials

Imperial College London

Submitted in partial fulfilment of the requirements for the degree of Doctor of Philosophy

Declaration of originality

I hereby declare that the work contained within this thesis is my own and that all else has been properly acknowledged.

Anna L Fricker

Acknowledgements

First and foremost I would like to thank my supervisors, Professor David S McPhail, Dr Brenda Keneghan and Dr Theoni Georgiou as well as Boris Pretzel at the Victoria and Albert Museum for their guidance, encouragement and scientific advice. I am very grateful for the generosity with which they have given their time and support throughout the last three years.

This work was funded by the Arts and Humanities Research Council as part of the Collaborative Doctoral Award scheme and would not have been possible without the advice and expertise of numerous people within the Department of Materials at Imperial College London. I am especially grateful to Dr Sarah Fearn for her invaluable assistance with the ToF-SIMS analysis and Dr Richard Chater for his help with both SIMS and interferometry. I would also like to express my thanks for the training and assistance provided by Dr Victoria Bemmer for AFM analysis and Richard Sweeney for thermal analysis as well as Ecaterina Ware and Mahmoud Ardakani for SEM. My thanks also go to Russell Stracey, Ben Chan and Ignacio Villar Garcia for their technical expertise. I am grateful to Professor Jason Riley and Professor Natalie Stingelin for allowing me to work in their laboratories throughout my PhD. I would also like to take this opportunity to thank Dr Alex Henderson for his very useful advice on PCA analysis and Anna Constantinou for her help with the GPC analysis. My thanks go to Dr Ambrose Taylor for generously allowing me to use the accelerated ageing chamber in the Department of Mechanical Engineering and to Dr Judith Thei for her assistance with the equipment. I am also grateful to Professor John Watts and Dr Steve Hinder at the University of Surrey for allowing me time on their ToF-SIMS.

Finally, I would like to thank my friends and colleagues in the Department of Materials and the Victoria and Albert Museum for making my time over the last three years hugely enjoyable. Last but not least, I cannot express how much I owe to my family, especially my parents, Celia and Jeffrey, and my sister Laura for their constant love, support and encouragement. Thank you.

Abstract

This thesis describes the research work performed to determine the effect of conservation cleaning treatments on plastics that might be encountered in the museum environment. As part of this work, surface analysis techniques were used to examine the changes occurring to the surfaces of two plastics, polystyrene and poly(methyl methacrylate), following the application of seven different cleaning treatments. Substrates were analysed using optical microscopy, white light interferometry, scanning electron microscopy, atomic force microscopy and time-of-flight secondary ion mass spectrometry in conjunction with principal component analysis of the data. The use of sophisticated analysis techniques enabled the characterisation of surface changes at the sub-micron scale.

Experimental data obtained for virgin sheet polystyrene substrates revealed surface damage due to cleaning in the form of scratching, attributed in part to the mechanical action of the cloth over the substrate. Residues from surfactants were also detected and were still present after repeated rinsing. The addition of an artificial carbonaceous soil to the surface was found to result in the appearance of scratches on PMMA and a change in the topography of scratches formed on polystyrene due to abrasion from the soil. Accelerated ageing of the substrates revealed changes to the plastics' bulk properties and surface chemistry, as well as the appearance of formations on the polystyrene surface. Further indications of damage caused by cleaning also became apparent with ageing. The cleaning behaviour of aged polystyrene substrates was found to be notably different to that of the unaged substrates. Finally, the initial physical and chemical condition of a real-world object was characterised and its cleaning behaviour evaluated, enabling comparison with the virgin polystyrene substrate. The findings from this work provide valuable information regarding the microscopic changes that can occur to plastic substrates as a result of cleaning and the implications for their future stability.

Table of contents

List of figures

List of tables

List of abbreviations

ABS	Acrylonitrile butadiene styrene
AFM	Atomic force microscopy
AHRC	Arts and Humanities Research Council (UK)
ASTM	American Society for Testing and Materials
ATR-FTIR	Attenuated total reflectance Fourier transform infra-red spectroscopy
CA	Cellulose acetate
CIE	International Commission on Illumination
CN	Cellulose nitrate
DSC	Differential scanning calorimetry
EFI	Extended focal imaging mode
EM	Electromagnetic
EPS	Expanded polystyrene
ESC	Environmental stress cracking
GCI	The Getty Conservation Institute
GC/MS	Gas chromatography mass spectrometry
GPC	Gel permeation chromatography
HALS	Hindered amine light stabilisers
HCBM	High current bunched mode
HDPE	High density polyethylene
HIPS	High impact polystyrene
HV	High vacuum
ICOM-CC	The International Council of Museums - Committee for Conservation
ICON	The Institute of Conservation (UK)
ISO	International Organization for Standardization
LDPE	Low density polyethylene
LED	Light emitting diode
MVA	Multivariate analysis
NPL	The National Physical Laboratory (UK)

PC	Polycarbonate
PCA	Principal component analysis
PC1	Principal component 1
PDMS	Polydimethylsiloxane
PE	Polyethylene
PET	Poly(ethylene teraphthalate)
PHS	Plastics Historical Society
PM	Particulate matter
PMMA	Poly(methyl methacrylate)
POPART	Preservation of plastic artefacts in museum collections study
PP	Polypropylene
PS	Polystyrene
PTFE	Polytetrafluoroethylene
PUR	Polyurethane
PV	Peak-to-valley height
PVC	Poly(vinyl chloride)
RH	Relative humidity
SEM	Scanning electron microscopy
SEM-EDX	Scanning electron microscopy - energy dispersive spectroscopy
SLS	Sodium lauryl sulphate
TGA	Thermogravimetric analysis
THF	Tetrahydrofuran
ToF-SIMS	Time-of-flight secondary ion mass spectrometry
UHV	Ultra high vacuum
UV	Ultraviolet
V&A	Victoria and Albert Museum
VOC	Volatile organic compound
XPS	X-ray photoelectron spectroscopy
XRF	X-ray fluorescence spectrometry
YI	Yellowness index

Chapter 1

Plastics in the museum environment

Plastics. The wonder material of the 20th century. It is difficult to imagine a world without them. They have revolutionised manufacturing, transformed healthcare and facilitated numerous technological and societal advancements. Barely a corner of our modern life remains untouched by their presence. Yet plastics have an increasingly bad reputation in today's world. Originally cherished for their scarcity and novelty, they are now seen as cheap, tacky, and responsible for some of our most challenging environmental problems.

The development of plastics and their rise to prominence has been swift. They are now a ubiquitous, and indispensable, part of modern life. Nowhere is this more clearly encapsulated than in the artefacts of our cultural heritage and the institutions that preserve them for the generations to come.

1.1 History of plastics

In many heritage institutions, plastics come under the umbrella term of 'modern materials'. Yet the first plastic was created over 150 years ago. The International Organization for Standarization (ISO) defines a plastic as a 'material which contains as an essential ingredient a high polymer and which, at some stage in its processing into finished products, can be shaped by flow' (ISO 472:2013) [1]. While all plastics are polymers, not all polymers are plastics. In this work the term 'plastic' will be used to describe a material consisting of one or more polymers to which one or more additives may be added.

Polymers occur naturally, and include many traditional materials such as wool and cellulose. Early plastics were made partly of these natural polymers and are termed semi-synthetic plastics. The first man-made plastic, named Parkesine, was unveiled at the Great London Exposition in 1862 and is now known to be cellulose nitrate (CN). Cellulose nitrate and other semi-synthetic plastics, including cellulose acetate (CA) and casein formaldehyde are commonly found in museum collections today.

The first completely synthetic plastic was invented by Leo Baekeland in 1907 and was named Bakelite. This was a thermosetting plastic which was strengthened with wood fillers and was consequently only available in shades of brown or black. The first thermoplastics were developed during the inter-war years and included poly(vinyl) chloride (PVC), polystyrene (PS) and polyethylene (PE). Mass manufacture of these plastics began during the 1940s and 1950s, a period which also saw the development of new plastics. The discovery of these plastics in the first half of the 20th century resulted in many of the common plastics in use today. The latter half of the 20th century saw developments in polymer synthesis which resulted in the manufacture of polymers with specific properties. More recently bio-degradable plastics have become a focus of much interest. A timeline showing the development of some common plastics is shown in figure 1.1.

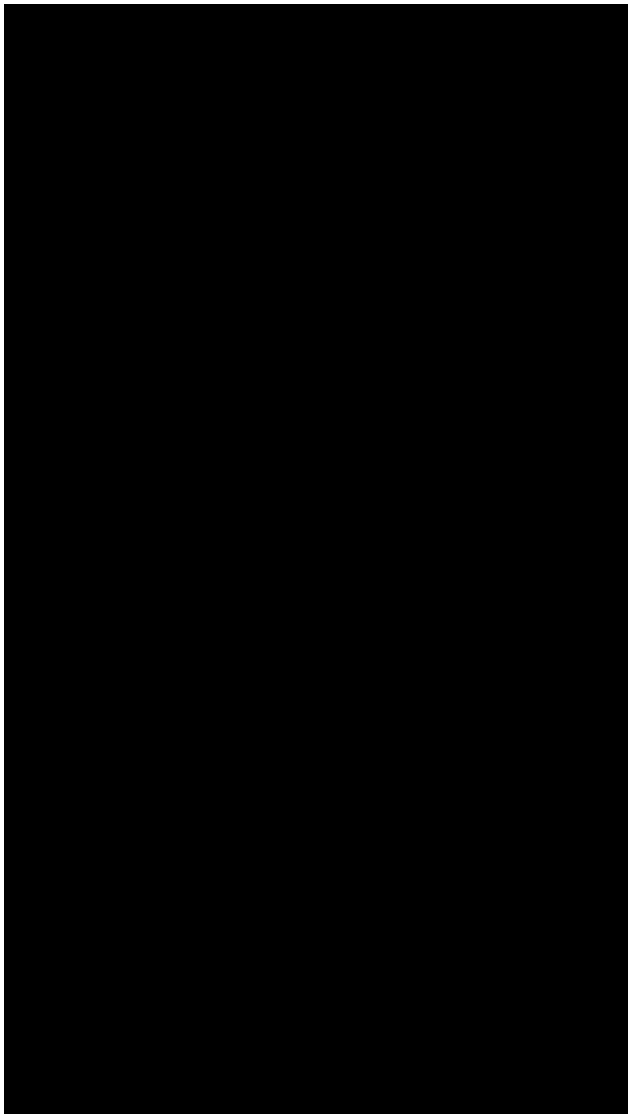

Figure 1.1 Timeline of plastics manufacture.

Today the range of synthetic plastics is vast, but in Europe there are seven main plastics in common use [2]: high density polyethylene (HDPE), low density polyethylene (LDPE), polypropylene (PP), poly(vinyl chloride) (PVC), polyurethane (PUR), polystyrene (PS), including expanded polystyrene (EPS) and poly(ethylene terephthalate) (PET). Others include poly(methyl methacrylate) (PMMA), commonly known as acrylic or Plexiglas®, polytetrafluoroethylene (PTFE), otherwise known as Teflon™, and polycarbonate (PC). The European demand for plastics according to polymer type in 2015 is shown in figure 1.2 [2]. Combined, LDPE and HDPE constitute almost 30% of all plastic demand in Europe and are commonly used for packaging applications.

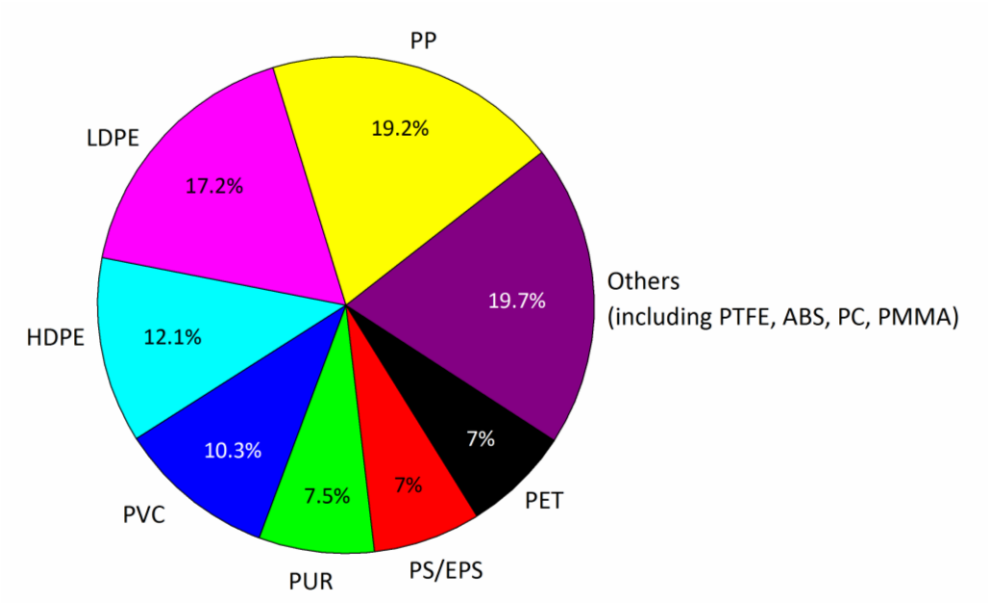

Figure 1.2 Pie chart showing the plastic demand in Europe in 2015 according to polymer type [2].

Plastics are used in a wide variety of industrial and commercial applications. In Europe, the largest demand for plastics is for packaging (39.5% of all markets), followed by building applications (20.1%), the automotive sector (8.6%) and electrical and electronic applications (5.7%) [2]. Items such as household appliances, furniture and personal effects, which might be expected to form a significant part of museum collections, individually comprise less than 3.4% of the total. New demands for plastics are continually created; at the time of writing the UK government has issued its first polymer £5 banknote manufactured from polypropylene [3]. This step was taken for security considerations and to increase the durability and cleanliness of banknotes.

1.2 Plastics in museum collections

The first attempts to understand the extent to which plastics were present in the UK's museums were performed in the 1990s. Surveys at the Victoria and Albert Museum (V&A) [4], the British Museum [5] and the Science Museum [6] were undertaken to quantify the plastics in their collections and to determine their condition. A questionnaire by the Plastics Historical Society (PHS) and the Conservation Unit of the Museums & Galleries Commission was also circulated to museums and private collections in 1994 to gain information concerning the number, type and condition of plastic objects in these institutions [7]. At this time, the presence of plastic materials in collections was not widely appreciated and many museum curators were unaware that plastics might comprise a part or the whole of objects in their care [8]. Since then, awareness of plastic artefacts has grown, along with an acceptance that the behaviour of these materials requires investigation. An EU-FP7 funded project 'Preservation of Plastic Artefacts in Museum Collections' (POPART), ran from 2008 to 2012. This project focused on the identification of plastics in museum collections, including collection surveys,

as well as degradation mechanisms and conservation treatments for plastics. This brought together partners from 13 heritage institutions in Europe and the USA, including the V&A.

The distribution of plastics in museum collections is rather different to that seen in figure 1.2. Instead, collections contain plastics whose distribution reflects their cultural significance. Figure 1.3 shows the average distribution, by type, of plastics contained in the collections of three French museums surveyed as part of POPART [9]. These include early plastics such as cellulose nitrate and cellulose acetate which, along with polyurethane and PVC, comprise what are thought to be the four most vulnerable plastics in museum collections.

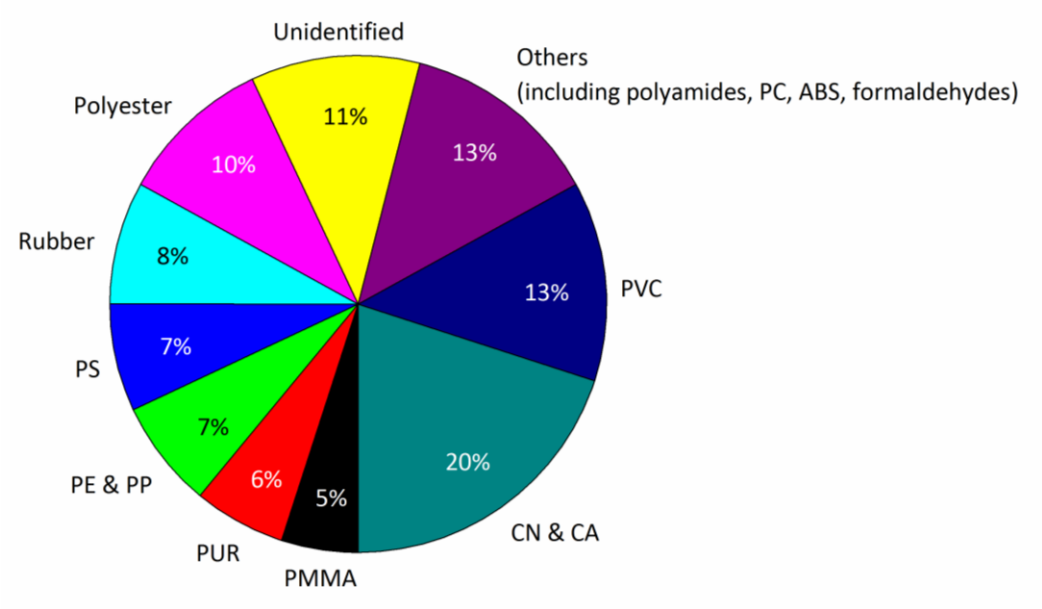

Figure 1.3 Pie chart showing the average distribution of plastics in three French museum collections surveyed as part of POPART [9].

According to a survey of natural, semi-synthetic and synthetic plastics performed in the 1990s, many of the plastic objects in collections date from the mid-20th century [7]. Approximately 60% of the V&A's collections was surveyed in 1996; at that time it was estimated there were over 8000 plastic artefacts in the collections [8]. The surveys revealed that the date of manufacture of the majority (68%) of plastics was unknown and that the composition of 94% of the plastics surveyed was unidentified [10]. Many of the plastics are found in the V&A's Museum of Childhood collection, where many of the objects are thought to be made of polystyrene [4]. However, plastics are distributed throughout the collections and may be found in collections as diverse as furniture, jewellery, sculpture, or domestic items, to name a few. It is inevitable that the number of plastics from the late 20th century and early 21st century will increase over time, and that new plastics will join them as a result of advances in technology. The advent of 3D printing, plastic electronics and bioplastics have the potential to introduce novel plastics to the museum environment.

As awareness of plastics in heritage has grown, so too has the literature surrounding their composition and care. A number of conferences have been devoted to plastics in the heritage environment and the membership of the 'Modern Materials and Contemporary Art' working group of The International Council of Museums - Committee for Conservation (ICOM-CC) has grown steadily since its inception at the turn of the century [11]. Museums specifically devoted to plastic materials include the Museum of Design in Plastics in Bournemouth, which changed its name and focus to plastics in 2007, and the Plastics Museum near Turin in Italy (first established in 1985). More recently plastics have been the focus of an issue of the Getty Conservation Institute's Newsletter titled 'Conservation of Plastics' [12]. This increasing interest in plastic artefacts is reflected by more mainstream articles concerning their fragility and demonstrates the awareness of the issues facing conservators outside of the academic or heritage environment [13, 14].

1.3 Issues in plastics conservation

One of the first indications that plastics might be problematic materials to preserve came in the early 1960s, when curators at the Philadelphia Museum of Art reported that a sculpture by Gabo entitled 'Construction in Space: Two Cones', was showing signs of deterioration [15]. By 1968, only 41 years after it was made, the sculpture was taken off display. The rapid deterioration of the cellulose acetate sculpture was initially blamed on poor exhibition conditions. However, a replica of the same piece at the Tate showed the same behaviour, and when other museums reported similar experiences with cellulose acetate, it soon became apparent that the plastic was degrading.

Degradation is the change in a material's physical and/or chemical properties. These changes are usually detrimental, resulting in alterations in the object's visual appearance and structural integrity. In museum objects the limit of acceptable degradation can be subjective. One definition is that an artefact may be considered as to have lost all meaning when its form can no longer be discerned [16]. There are also differences between acceptable changes for plastics and more traditional materials. While patina on antique bronze is acceptable and can add both monetary and cultural value, the yellowing of a plastic artefact is generally undesired.

One of the characteristics that distinguishes plastic materials from more traditional materials is the very short time span in which degradation can occur. The primary concern for museum curators and conservators is therefore not only that plastic artefacts will degrade but that this degradation may occur over a shorter time period than is acceptable. A museum may not wish to acquire an artefact only for it to crumble to dust in the next 10 or 20 years.

1.3.1 Artefact condition and degradation

Two individual surveys into the condition of plastic artefacts housed in the British Museum and the V&A were carried out in the 1990s and 2000s [5, 10]. The findings from these surveys were classified into categories according to the condition of the artefacts and are shown in figure 1.4.

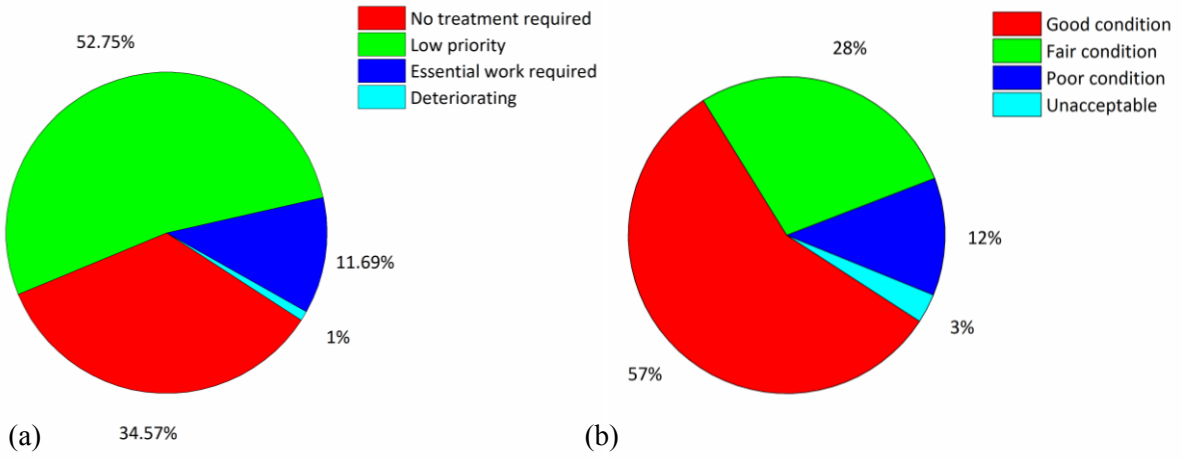

Figure 1.4 Pie charts showing the condition of plastics in the collections of a) the British Museum and b) the Victoria & Albert Museum.

The findings revealed that, on average, 86% of the artefacts surveyed were in a good or fair condition and required little conservation treatment. This category included objects in need of cleaning but which were otherwise stable. However, approximately 12% were found to be in need of essential conservation, such as repair or strengthening, while an average of 2% were of high conservation priority. This 2% encompassed objects which were actively degrading and therefore in need of stabilisation. Four plastics were highlighted as showing severe degradation: cellulose acetate, cellulose nitrate, PVC and polyurethane.

In 2010 a survey undertaken at the Stedelijk Museum in Amsterdam as part of POPART [9] revealed that 80% of plastic artefacts needed minor or no intervention while 12.5% were in need of restoration and 7.5% had severely degraded. In this survey, PMMA artworks had undergone severe degradation due to mechanical damage or a poor choice of adhesive [9]. The three French museums surveyed during POPART (figure 1.3) revealed a greater proportion of plastic artefacts (32%) that were considered to be in poor or severe condition. All of the surveys noted that artefacts may consist of more than one polymer and that the degradation observed was related to the function of the object as well as its composition. It should be noted that only a sample of these collections was surveyed and that storage conditions for plastic artefacts vary widely depending on the institution.

With this focus on the condition of plastic artefacts it is unsurprising that much of the literature about the conservation of plastic objects is concerned with their degradation. Many of the papers on this

topic focus on cellulose acetate, cellulose nitrate, PVC and polyurethane, as plastics that are giving most cause for concern. The general aim of these studies is to understand the degradation mechanisms taking place and to identify ways to prevent or retard deterioration. In addition a sizeable number of case studies have been performed on the conservation of particular artworks or artefacts. The degradation mechanisms of polymers are discussed further in Chapter 2.

1.3.2 Indicators of degradation

The first indications of degradation are usually identified by the appearance, odour or feel of the object. In many cases degradation causes a change in appearance in the form of discolouration, loss of gloss or yellowing. Warping or other deformation may be seen. Physical damage can range from small cracks or crazing on the surface to total disintegration of the object. A whitish film on the surface is defined as 'bloom' and indicates the migration of additives to the surface. Tackiness is commonly observed for PVC artefacts as a result of plasticiser migration. Weeping or sweating may be due to the migration of additives or the formation of degradation products on the surface of the plastic. The mechanical properties of a plastic may also change with degradation; embrittlement is most commonly observed as a result of plasticiser loss or cross-linking [10, 17]. Some examples of degradation are shown in figure 1.5.

Figure 1.5 Examples of degradation a) discoloration in areas not previously covered by clothing, b) severe cracking of a cellulose acetate handbag, c) warping of cellulose acetate Lego® bricks. (Images 1.5b and c courtesy of the Victoria and Albert Museum, photographer Mark Kearney).

Cellulose acetate and cellulose nitrate are notable for producing acetic acid and nitric acid as degradation products. This results in the distinctive vinegar odour for objects made from cellulose acetate. The deterioration of PVC may also be accompanied by a sweet smell [18]. This production of degradation products that may be detected by smell has resulted in studies into the detection of volatile organic compounds (VOCs) to determine both the onset and extent of plastics degradation [19, 20]. The interaction of acidic products with other plastics can cause damage while contact with metals results in corrosion. PVC also exudes plasticiser which can be absorbed by other plastics.

1.4 Conservation treatments for plastics

Conservation is broadly defined as the 'preservation, protection, care and restoration of our cultural heritage' [21]. Conservation treatments can be divided into two types: preventive and interventive. Both are designed to extend the lifetime of the object by preventing or inhibiting degradation and are performed for reasons of stability and appearance. In 2014 the Institute of Conservation (ICON) updated its code of conduct for its membership [22], which requires that any conservation treatment undertaken is documented. Added to this is the requirement that any treatment performed is both minimal and reversible.

1.4.1 Preventive conservation

Preventive conservation involves monitoring and controlling environmental conditions to maintain the stability of an artefact. This includes controlling illumination levels, temperature, relative humidity and pollutants. It may also include the placement of a fragile or vulnerable artefact in an enclosure. In rare cases, the local environmental conditions of an object may be controlled via, for example, flooding an enclosure with nitrogen gas to eliminate the presence of oxygen, thereby reducing the likelihood of oxidation. Sensitive materials may be rotated in and out of storage to limit their exposure to display conditions.

The storage conditions for plastic artefacts vary according to institution and often have to take practical considerations into account. In general, storage conditions for plastics and other organic materials include illumination levels below 50 lux, temperatures below 20°C and a relative humidity of 50% or lower [23]. The latter depends on the object: plastics which are prone to hydrolysis should be stored at low relative humidity while those objects which are plasticised via water should be stored at higher relative humidities to prevent cracking. It is generally accepted that lower temperatures result in reduced degradation, however the transfer of objects from cold storage to an ambient temperature should be performed in stages to minimise damage from thermal expansion [23]. The use of oxygen scavengers is also advised and it is recommended that plastics such as cellulose acetate and PVC are stored separately from other materials to prevent damage occurring from exposure to acidic products or contact with exuded plasticiser [18, 24]. Cellulose nitrate is highly flammable and can spontaneously combust, emitting noxious fumes [25]; objects such as motion-picture film are required by law to be stored separately in ventilated containers in a cool environment to limit the likelihood of combustion.

1.4.2 Interventive conservation

Interventive conservation encompasses all conservation treatments that involve contact with the object in question. This includes consolidation (using one material to strengthen another), repairs and cleaning. Ethical considerations are instrumental in decisions concerning interventive treatment. Any treatment undertaken should not affect the artistic integrity of the object, for example the application

of a protective coating to an object may be prohibited. Coatings can also trap harmful products and may be difficult to remove at a later date [26].

Any interventive treatment performed must satisfy the museum's own requirements and protocols. The V&A's Collections Care and Conservation Policy states that 'Interventive or remedial treatment is undertaken to stabilise the collections, to enhance intellectual access and accuracy and to improve their visual appearance. Treatments are intended to prolong and extend the useable lifetimes of the collections in accordance with the international ethical guidelines. Treatments will be agreed with the relevant curator taking into account the purpose for which the object is to be used.' [27].

1.5 Cleaning in the conservation sector

The work described in this thesis focuses on one interventive treatment: cleaning. Cleaning is performed for many materials that are found in the museum environment and may be defined as the removal of foreign or undesirable matter from the surface of an object. This can include contamination from external sources but also can result from the object itself. The reasons for cleaning are three-fold: to improve the appearance of the object, to maintain its artistic integrity and to increase its stability. However, it is also recognised that the act of cleaning may itself cause damage or irreversible changes to the object in question. It is estimated that approximately 75% of plastics in museum collections are in need of cleaning [17].

1.5.1 Current protocols for cleaning

There are currently no universal cleaning protocols or standards for plastic artefacts. Dry cleaning with cotton swabs or microfibre cloths is commonly advised, while the dampening of a cloth with deionised water may be acceptable for plastics that are not vulnerable to hydrolysis. The use of solvents is not recommended [18, 24]. However, there is very little advice for soiling that is not easily removed via dry cleaning methods. This is most likely due to the sheer range of plastics available as well as a lack of knowledge around cleaning treatments for these materials.

The use of gloves is requisite when handling museum objects to avoid the deposition of skin oils or other contaminants. Nitrile gloves are commonly recommended for cleaning procedures as latex gloves can cause allergies and potentially leave residues [28]. However, analysis of nitrile gloves has revealed that these can also be a source of contamination [29, 30].

1.5.2 Prior work on cleaning plastics

To date the most extensive study on the cleaning of plastics was performed as part of the POPART project [31]. A wide range of plastics, cleaning agents and application methods were investigated in this study, with initial tests reducing the number of variables to those summarised in table 1.1. The study examined both virgin substrates as well as substrates that had been soiled with two artificial soils designed to replicate carbonaceous soil and fingerprints.

Table 1.1 Cleaning combinations studied during POPART [31].

Plastics	**Cleaning agents**	**Application tools**
Cellulose acetate	Distilled water	PVA sponge
HDPE	Dehypon LS45	Cotton bud
HIPS	*(non-ionic surfactant)*	Cotton cloth
PMMA	Judith Hofenk de Graff detergent	Leather chamois
PVC	*(non-ionic surfactant)*	Spectacles cloth
	Orvus WA Paste	Microfibre cloth
	(anionic surfactant)	
	Synthetic saliva	
	Tri-ammonium citrate	
	Ethanol	
	Isopropyl alcohol	
	White spirit	
	Xylene	

The findings from the POPART project were varied and the effect of cleaning agents was highly dependent on the plastic under investigation. However, mechanical cleaning introduced scratches to all plastics. In general, the use of cloths or brushes resulted in shallower scratches. In the case of PVC, scratches were observed to become less visible with time. This was attributed to plasticiser migration resulting in the scratches being filled. The use of some cleaning tools, particularly sponges, resulted in residues after cleaning, while cloths, leather chamois and feather dusters were least damaging to the surface.

The use of cleaning agents changed the observed behaviour. It was suggested that aqueous agents acted as lubricants during the cleaning process to reduce damage in the form of scratching. However, this effect was not observed for solvents, with the exception of isopropyl alcohol and white spirit. The least damaging cleaning agents were distilled water, Judith Hofenk de Graff detergent and Dehypon LS45. Acetone was observed to be highly damaging to plastic surfaces.

The presence of soiling on the surface of the plastic substrate was reported, in some cases, to result in the absorbance of oil by the plastic. Unsurprisingly, distilled water was ineffective in removing soiling; some success was reported for the other aqueous agents. Solvents were generally found to be more effective for soil removal, particularly for the fingerprint soil. The use of the leather chamois and sponges with solvents resulted in the appearance of residues. A more extensive treatment of the

findings can be found in the POPART book [31]. The plastic-cleaning agent combinations studied in this thesis are reviewed in more detail in Chapter 4.

Other investigators have also studied the cleaning of plastics. Findings from a study by Morales Muñoz on the dry cleaning of PVC with cotton swabs and three different microfibre cloths [32] revealed that cotton swabs damaged the surface. Short cleaning periods for two out of the three microfibre cloths did not cause damage that was detectable via profilometry. These findings are consistent with those from POPART [31, 33] in that cotton swabs were observed to result in more noticeable scratch damage to the surface of plastics. ATR-FTIR data from the same study by Morales Muñoz suggested that plasticiser was removed from the surface during cleaning treatments and that fibres from one microfibre cloth adhered to plasticiser on the surface after cleaning.

Morales Muñoz also investigated the use of wet cleaning treatments for plasticised PVC [34]. The use of attenuated total reflectance Fourier transform infrared spectroscopy (ATR-FTIR) to examine the PVC surface after cleaning detected residues from a non-ionic surfactant (Dehypon LS45, 5 vol.% concentration) but not from an anionic surfactant (Hostapon T, 5 vol.% concentration). This was attributed to the solubility of the non-ionic surfactant in water. In both cases the surfactants were applied with cotton swabs and the surface was rinsed with deionised water after cleaning. Cleaning with deionised water did not cause any changes to the FTIR spectrum. The use of the organic solvents ethanol, propanol and heptane were observed to result in a decrease in the intensity of the bands attributed to plasticiser, which was attributed to extraction of the additive.

Waentig investigated conservation treatments for a transparent violin dating from the 1930s which was made from PMMA [35]. In this case a layer of dust covering the inside surfaces of the violin was removed using a microfibre cloth dampened with a solution containing a non-ionic surfactant and deionised water. The surfaces were then rinsed using a cloth dampened with deionised water. The use of a dry cloth was avoided due to the potential for electrostatic charging during cleaning.

In the last few years, the use of gels as cleaning agents has become a focus of study. Much of the literature surrounding the use of gels has focused on their ability to clean paintings. Many are designed to remove degraded polymer coatings from the painted surface [36] and would therefore not be suitable for the cleaning of plastic substrates. One of the potential problems surrounding the use of gels is that they can leave residues on the surface which may then need to be removed.

1.5.3 Cleaning considerations

Prior to cleaning there are a number of considerations that must be addressed. Firstly, and most importantly, is the type of plastic. POPART highlighted the fact that an appropriate cleaning treatment for one plastic may not be suitable for another. Unfortunately, the composition of many plastic objects in museum collections is unknown, and it can be a time consuming task to identify them. In some

cases identification may not be possible. Secondly, it is desirable to determine the type of contamination present on the surface. The presence of oily fingerprints for example may be more suited to a surfactant while an adhesive residue might be expected to require treatment with an organic solvent. The third consideration encompasses both the composition of the cleaning agent and the method of application. It is well known that organic solvents can cause polymer dissolution, while POPART found that latex, rubber and synthetic sponges left a residue on the substrate after cleaning [31]. Finally it must be considered whether the cleaning treatment is likely to change the substrate in ways that are not immediately apparent, and that only become clear weeks, months or years in the future.

Not all changes are visible to the naked eye. Microscopic changes may take place that can only be detected via the use of sophisticated instrumentation. Techniques that enable imaging at very high magnifications along with highly sensitive surface analysis techniques have the potential to identify very small changes that may affect the stability of the plastic in the future. The use of sophisticated techniques to identify changes due to cleaning is the focus of the work contained within this thesis.

1.5.3.1 Sources of contamination and distribution

The contamination and soiling present on the surfaces of museum objects varies in its composition and distribution. Soil includes any foreign matter that is present on the surface, including dust, oils and adhesives. Surveys of the environment in the V&A reveal that dust is comprised of human hair, skin flakes, clothing fibres, carbon particulates, mineral fragments, insect parts, pollen and pollutants [37]. Many of these come from the millions of visitors that the V&A welcomes each year; over 3.7m visitors passed through its doors in 2015 alone [38]. Particulate matter from combustion engines is another major source of contamination [39]. Oily carbonaceous particles may also be produced during cooking and many museums have cafes or restaurants. In very rare cases, soiling may result from natural disasters or accidental events such as fire [40].

The term 'particulate matter' (PM) includes all particles found in the atmosphere and which characteristically display a size distribution which can be divided into three broad categories, according to particle diameter: ultrafine mode (<0.1 μm), accumulation mode (0.1 μm - 1 μm) and coarse mode (>1 μm) [39]. However, quantification of particulate matter is commonly achieved by separating all particles with diameters less than 1 μm, 2.5 μm, 5 μm and 10 μm. These classifications are known as PM1, PM2.5, PM5 and PM10 respectively.

Many museums are located in major cities and are consequently surrounded by high levels of environmental pollution. The V&A is situated on a busy main road with high traffic flow in the South Kensington area of London. Environmental data for this region is available via the London Air

Quality Network (King's College London) [41]. Figure 1.6 shows the mean PM10 levels for the year 2010. Figure 1.7 shows the mean levels of NO_2 for the same year.

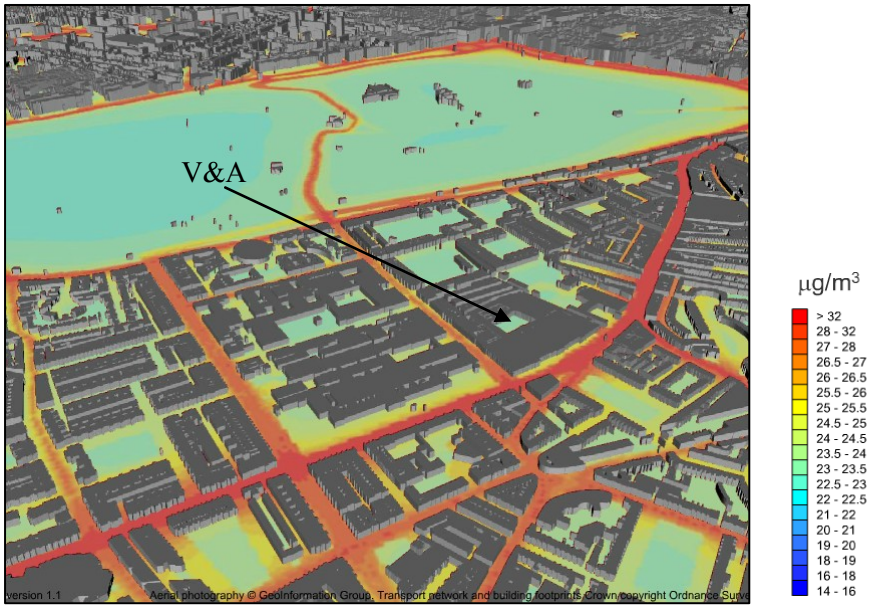

Figure 1.6 Annual mean PM10 levels in South Kensington in 2010 [41].

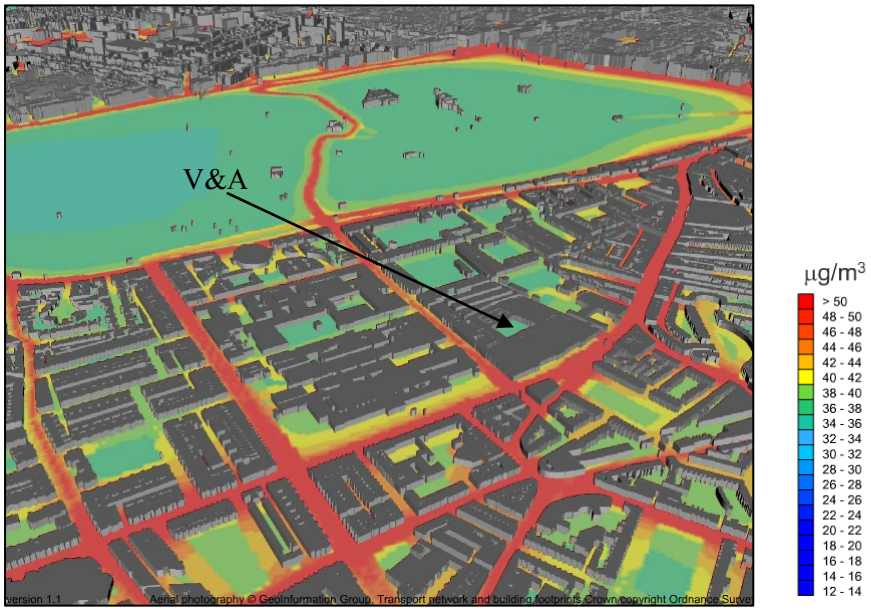

Figure 1.7 Annual mean NO_2 levels in South Kensington in 2010 [41].

Particles enter buildings via large opening such as doors and windows or through smaller cracks or gaps which connect the indoor environment to the outside. A review of studies into particulate matter in the heritage environment by Grau-Bové and Strlič [39] stated that, in general, the concentration and distribution of particles greater than 1 µm in the indoor environment was found to correspond to museum opening hours. This is due to the potential for air flow to re-suspend particles with a diameter

greater than 1 μm. However, the distribution of fine particulate matter (<1 μm) is generally unaffected.

At the time of writing the V&A is undergoing extensive building work to construct a new entrance and gallery. While hoardings are in place to reduce dust ingress into the exhibition areas, examination of dust levels has revealed a notable increase in particulate counts in areas that are closest to the construction area. It has also been observed that dust levels are elevated in the morning when building work starts for the day [42].

Many museums implement environmental measures in an effort to prevent pollutants and particulate matter from reaching the inside of their buildings and therefore the collections. In the case of the V&A this is achieved via the use of revolving doors and a large entrance area which divides the collections from the outside environment. The Porter Gallery, which is located near the museum's main entrance, consists of a second room which has been built inside the main building and which offers a level of protection to the objects displayed inside. Air filtration systems for the V&A's new exhibition space are required to remove 85% of particles with a diameter greater than 5 μm from permanent collections [43]. This is increased to 95% of particles with a diameter greater than 2 μm for sensitive or fragile displays.

While visitors are a source of contamination, they also affect the distribution of dust in the museum environment. Dust particles present on surfaces may be re-suspended due to changes in air flow caused by visitor movement, however this is mainly observed for particles with a diameter greater than 1 μm [39]. Efforts to reduce dust deposition in exhibition areas include planning the layout so that any dust brought in on visitors' clothing has a reduced chance of depositing on the exhibition items [37]. This may incorporate a lengthy walkway at the entrance of the exhibition to allow for the removal of outer clothing. Increasing the distance between the exhibition entrance and the objects on display also reduces the deposition of dust originating from outside the exhibition area. Physical barriers between visitors and objects reduce the likelihood of dust deposition as well as limiting direct contact through touching. Plinths are used to raise exhibition objects off the floor and protective casings may be used in areas where heavy soiling is expected to occur or to protect particularly fragile items. Dust deposition may also be reduced via the use of false ceilings. At floor level, dust mats may be placed at room entrances and exits while regularly vacuumed carpets can also reduce dust levels. The placing of artefacts in protective enclosures would further reduce soiling but this is limited by cost and also by the museum's mandate to facilitate public access [37].

Many objects acquired by museums have a prior history. Unless objects are acquired directly from the manufacturer in the form of prototypes, it is likely that they will have been handled or come into contact with human skin. In other cases, the handling of certain objects designated as a teaching collection is encouraged as part of public engagement. This results in the deposition of oils, acids and

potentially other foreign products onto the surface of the plastic. Some plastics objects, particularly those such as toys or jewellery, may have been handled extensively before acquisition. This not only results in contamination but also potentially in physical degradation due to wear and tear, which may be manifested as changes in surface characteristics such as gloss, colour or roughness. Damage may also be the result of previous museum or conservation practices. The application of inappropriate adhesives has been reported to result in damage to PMMA artwork [31], while labelling of objects with a pen or adhesive label can cause localised damage [44].

The degradation of plastics such as cellulose acetate or cellulose nitrate results in the production of acidic species. These can redeposit on the plastic itself or on surrounding objects, causing degradation. Contamination is also possible from other materials contained in plastic objects such as metals. In some cases complex systems can be set up as degradation of the plastic causes changes in other parts of the object which then proceed to contaminate the plastic.

1.5.3.2 Soiling and surface energy

With the exception of soil that is transferred via direct contact, soiling generally takes place as particles in the air deposit on a surface under the influence of gravity or via Brownian motion. Coarse particles deposit in a shorter period of time than fine particles and the size distribution of particulate matter has been found to vary with height above floor level [39]. Temperature gradients will affect the movement of particles and can be set up due to the presence of lighting, windows, thermal sources or visitor presence [39].

The surface energy of a material also affects its soiling behaviour as it governs the degree of attraction or repulsion between a surface and another material. The surface energy of a substrate is a result of atoms or molecules on the surface having fewer nearest neighbours than those in the bulk of the material. A molecule on the surface of a material therefore experiences a net inward force due to attractive intermolecular forces. As energy is needed to overcome these attractive forces to create a new surface, molecules on the surface have greater energy than those in the bulk. In liquids it is more common to refer to the surface tension, which has the same dimensions as surface energy. The surface energy (γ) is the work done (W) per unit area (A) and the surface tension (γ) is the force (F) required per unit length (l) as in equations 1.1 and 1.2.

$$\gamma = \frac{W}{A} \tag{1.1}$$

$$\gamma = \frac{F}{l} \tag{1.2}$$

The surface energy of a material may be considered as being comprised of two components, the dispersive component (γ_d) which is present in all intermolecular interactions and the polar component

(γ_p) which, for polymers, is only present in those polymers containing polar groups (equation 1.3). Interactions due to hydrogen bonding are contained within the polar component.

$$\gamma = \gamma_d + \gamma_p \quad (1.3)$$

Polymers typically have low surface energies due to the low polarity of the functional groups present on the surface [45]. It follows that the surface energy varies according to the polymer: more polar polymers have relatively high surface energies, while a non-polar polymer such as polyethylene has a lower surface energy.

The surface energy also has implications for cleaning as the wetting of a plastic substrate is dependent on the surface energies of both the wetting agent and the plastic. In order for wetting to occur, the agent should have a lower surface tension than the plastic. Due to their low surface energy, plastics are difficult to wet, which can cause problems with finding suitable adhesives for conservation purposes. However, all organic solvents used in this work have lower surface tensions than the plastics investigated. Water has a high surface tension due to hydrogen bonding and tends to form droplets on a plastic surface. Surfactants reduce the surface tension of water to enable wetting. The typical surface tension values for a range of plastics and cleaning agents, including those studied in this work, are given in table 1.2.

Table 1.2 Typical surface energies and surface tensions of selected plastics [46] and cleaning agents [47].

	Surface tension (mNm^{-1}) at 20°C
Polystyrene	40.7
PMMA	41.1
Polyethylene (HDPE)	35.7
PVC	36.5
PTFE	23.9
Acetone	23.46
Ethanol	22.39
Isopropyl alcohol	23.71
Water	72.75

An increase in the surface energy will increase the attraction exerted on another material. Oxidation of the surface is one of the routes by which the surface energy may be intentionally or non-intentionally

increased due to the formation of polar groups on the surface of the plastic. Therefore, oxidative degradation of a plastic material may result in increased wetting behaviour as well as an increased attraction between the surface and foreign material.

Other factors also influence soil deposition and adhesion. Dust may be attracted to the surface as a result of electrostatic forces, which can occur during or after cleaning due to the movement of a cloth or other cleaning tool over the surface. Static electricity has been found to result from dry cleaning of plastics, particularly HIPS [31, 33]. The surface roughness will also affect adhesion due to the greater surface area available on a surface with a higher roughness value.

1.5.3.3 Solubility, dissolution and scratching

The susceptibility of plastics to some organic solvents is well known. For this reason conservation recommendations preclude the use of organic solvents to clean plastics. However, it may be necessary to consider their use for the removal of residues which themselves may be damaging to the object and which cannot be removed by any other means. The findings from POPART indicated that, in many cases, the use of organic solvents caused damage to plastics in the form of scratching. However, in some cases the condition of the surface after cleaning was better than, or comparable to, that achieved using aqueous agents [31]. The interaction of plastics with organic solvents is further discussed in Chapter 2. It has already been reported that the application of dry cleaning methods or aqueous cleaning agents to plastics can also result in the formation of scratches. Aside from the obvious detrimental changes to the object's appearance, scratches can also create areas of weakness on the plastic surface, potentially resulting in localised degradation.

1.5.3.4 Residues

Any application of cleaning treatments must consider the possibility that residues from the cleaning agent or the application method may remain on the surface after cleaning. The application of clearing steps, namely rinsing with deionised or distilled water, is undertaken to reduce or remove any residues from the substrate. Previous work using ATR-FTIR has indicated that surfactant residues are present on the surface of plasticised PVC after cleaning [34]. The use of gels in conservation also has the potential to leave residues, which may then need to be removed with another agent.

The presence of residues is detrimental for reasons of appearance and stability. Firstly they may adversely affect the appearance of the object by forming a thin film on the surface. They may also potentially act as sites for future degradation by providing small microclimates which are different to the object as a whole. Residues present on the surface can cause local variations in surface energy which increase or decrease adhesion and which may affect the object's propensity towards soiling in the future.

1.6 Aims and objectives

Questions remain concerning the effect of cleaning agents and procedures on plastic artefacts. Much of the work performed in this area to date examines the plastic surface with low magnification techniques such as optical microscopy and profilometry or analytical techniques such as ATR-FTIR which are not sufficiently sensitive to detect changes which occur to the topmost layers of the plastic surface. There is therefore an interest in determining whether changes are occurring to the surface which may be invisible at low magnification but which may nonetheless affect the stability of the plastic at some point in the future. In this work, sophisticated surface analysis techniques will be used to detect changes occurring at the sub-micron scale, thus enabling the identification of changes before they can be observed using conventional light microscopy or the naked eye. This work will therefore add to current knowledge about the cleaning of plastics for conservation purposes and it is anticipated that the findings will help to inform cleaning protocols for future conservation practice.

This work aims to identify and characterise the physical and chemical changes occurring to the surfaces of PMMA and polystyrene substrates as a result of the application of conventional cleaning treatments used in conservation. The effect of cleaning treatments on virgin plastic substrates will be examined in Chapter 5. In order to evaluate the effect of surface soiling, the cleaning of artificially soiled substrates will also be examined and discussed in Chapter 6.

One of the potential issues resulting from cleaning treatments is that they may result in detrimental changes to the surface which only become apparent at a later date. The use of accelerated ageing techniques to simulate the ageing behaviour of cleaned plastic substrates will be discussed in Chapter 7. In addition aged polystyrene substrates will undergo cleaning to evaluate any differences in their behaviour. Finally the findings from the virgin polystyrene substrate will be related to a naturally aged polystyrene object and detailed in Chapter 8.

Chapter 2

Plastics and their properties

The terms 'plastic' and 'polymer' are commonly used interchangeably, however a distinction should be drawn between the two terms. The primary constituent of a plastic is a polymer, and therefore a plastic may be defined as a polymeric material [17]. However, plastics contain other additives to improve their performance and properties.

2.1 Composition and classification

The term polymer comes from the Greek 'poly', meaning many and 'meros', meaning parts. Polymers are comprised of macromolecules: long hydrocarbon chains of many repeating units or monomers. These monomers may be identical, in which case the polymer is known as a homopolymer. Polymers consisting of macromolecules with two or more monomers are called copolymers.

2.1.1 Atomic composition and molecular structure

Many different polymers exist. The most fundamental difference between polymers is their atomic composition. The molecular structure of the most common polymer, polyethylene ($(C_2H_4)_n$), is shown in figure 2.1. A chain of covalently bonded carbon atoms commonly forms the polymer backbone, although some polymers also contain heteroatoms or phenyl groups in the backbone. Side groups or side chains may extend from this main chain. Aside from carbon and hydrogen, polymers commonly contain other elements including oxygen, chlorine and nitrogen which can account for certain properties. The presence of chlorine in PVC imparts flame resistance to the polymer as the chlorine reacts with hydrogen to form hydrogen chloride which in turn acts as a fire suppressant [48].

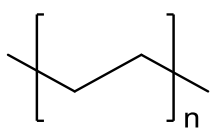

Figure 2.1 Molecular structure of polyethylene.

The molecular weight (M) of a polymer is related to the degree of polymerisation, that is the number of repeat units in the polymer chain, according to equation 2.1 [49].

$$M = xM_0 \tag{2.1}$$

Where x is the degree of polymerisation and M_0 is the molar mass of the repeat unit.

In reality, the length of the chains in a polymer varies, giving rise to a molecular weight distribution. The average molecular weight is commonly expressed in terms of the number average molecular weight ($\overline{M}_n$) or the weight average molecular weight ($\overline{M}_w$), defined as in equations 2.2 and 2.3 [49]. In this work the term 'molecular weight' refers to the number average molecular weight unless otherwise specified.

$$\overline{M}_n = \frac{\sum_{i=1}^{n} N_i M_i}{\sum_{i=1}^{n} N_i} \tag{2.2}$$

$$\overline{M}_w = \frac{\sum_{i=1}^{n} N_i M_i^2}{\sum_{i=1}^{n} N_i M_i} \tag{2.3}$$

Where N_i is the number of molecules of length i and M_i is the molar mass of molecules of length i, where i is discrete and related to the number of monomers in the polymer chain.

Polymers may display a linear, branched or cross-linked structure, as shown in figure 2.2. Cross-linked polymers have a network of interconnected polymer chains. Multiple branched architectures are possible, such as the star structure created when the polymer chains radiate out from a central point.

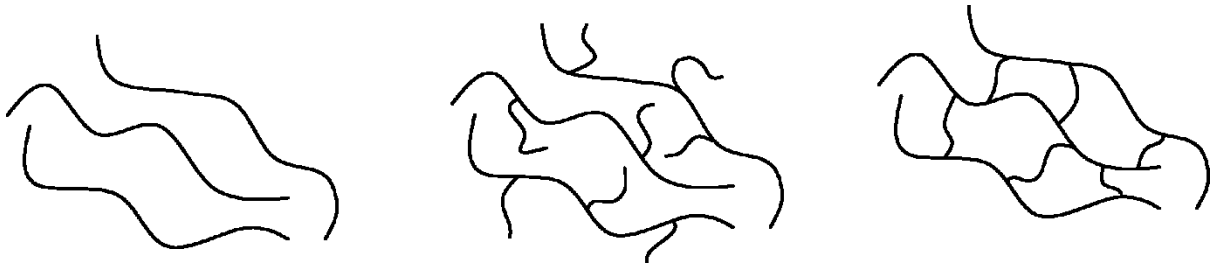

(a) (b) (c)

Figure 2.2 Types of polymer structure a) linear, b) branched and c) cross-linked.

Not all of the volume in a polymer is occupied by the polymer chains. This unoccupied volume is known as the free volume of the polymer and it allows space for the molecules to rotate, bend and move. The free volume is linked to the polymer's molecular weight, physical structure and temperature. Lower molecular weight polymers and branched structures have greater free volume than high molecular weight or linear polymers. This is because the distance between neighbouring molecules is greater at the end of the polymer chains compared to the middle. A decrease in temperature results in a reduction in the free volume available [49].

The polymer chains are held together by secondary intermolecular Van der Waals forces. These are comprised of three separate components: the dispersion, polar and hydrogen bonding forces.

London dispersion forces

Dispersion forces are present in all intermolecular interactions. Fluctuations in the density of the electron cloud result in the formation of temporary dipoles. When two or more molecules are close to one another, the changing polarity of one molecule induces a corresponding change in the polarity of its neighbouring molecules (figure 2.3). This results in the creation of attractive forces between the two molecules. The number of temporary dipoles increases with the size of the molecule; greater attractive forces are experienced between polymer chains with greater surface area. A straight chain polymer will therefore display greater dispersion forces than a branched chain of the same molecular weight.

Figure 2.3 Fluctuating dipoles giving rise to London dispersion forces.

Polar forces

Unlike dispersion forces, polar forces are only present in molecules which have a permanent dipole. The difference in electronegativity between two or more atomic elements in a molecule results in a permanent imbalance in the electron distribution. In symmetrical molecules these dipoles cancel out. Polar forces can be divided into two types: Keesom and Debye forces. Keesom forces are due to the interactions between two permanent dipoles. Debye forces result when a permanent dipole induces a dipole in a neighbouring molecule. Both Keesom and Debye forces are dependent on temperature, but Keesom forces exhibit a greater dependency on temperature due to both dipoles being permanent. As the temperature of the system increases, greater molecular motion results in a reduction in the polar forces.

Hydrogen bonding forces

Hydrogen bonding is a particular case of polar interactions. A strong dipole occurs when a hydrogen atom is bonded to a highly electronegative atom such as oxygen, nitrogen or fluorine. The attraction of electrons to the electronegative atom means that the positive hydrogen nucleus is exposed. This creates an area of positive charge that can attract electrons from neighbouring molecules.

2.1.2 Tacticity

The asymmetry of the arrangement of the pendant groups in some polymers means that they can display different tacticities, where the distribution of side groups varies in relation to the polymer backbone as in figure 2.4. These side groups can be all on one side of the polymer chain as in isotactic polymers or alternate sides as for syndiotactic polymers. A third tacticity, where the placement of the side groups is random, is termed atactic. The tacticity of a polymer affects its degree of crystallinity and glass transition temperature (T_g). As the side groups are all on the same side in isotactic polymers, the polymer chains can pack together in a crystalline arrangement.

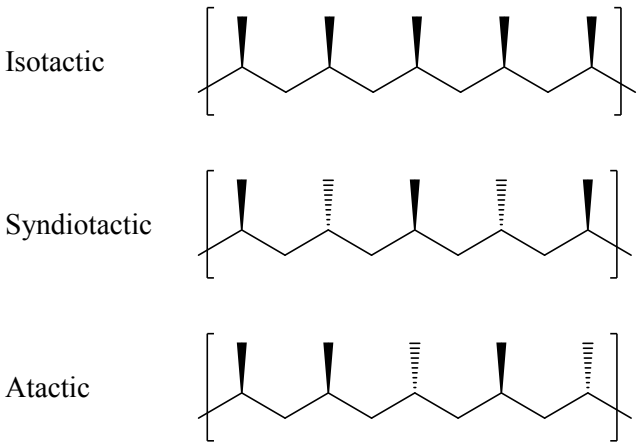

Figure 2.4 Schematic showing the different tacticities of vinyl polymers [48].

2.1.3 Amorphous and crystalline polymers

The arrangement of the individual chains in a polymer determines its degree of crystallinity. Amorphous polymers are characterised by the random arrangement of their chains. Other polymers display areas where the polymer chains are arranged in a regular configuration, rendering the polymer semi-crystalline. Crystallinity is affected by the polymer's molecular structure: polymers with short side chains are able to arrange themselves closely to create crystalline areas. Similarly, isotactic polymer chains pack together more easily than those in atactic polymers. The degree of crystallinity can range from 0% in the case of amorphous polymers to 90% in the case of high density polyethylene (HDPE) [50].

Due to the presence of amorphous and crystalline areas in a semi-crystalline polymer, incoming light in the visible spectrum scatters at the interface between the two areas. Polymers with a high degree of crystallinity, such as HDPE, are therefore opaque in appearance. In contrast, amorphous polymers such as PMMA allow light to pass through. According to product literature PMMA of thickness 6 mm has a light transmission of 92% [51] compared to 91% for glass [52]. PMMA is therefore commonly used in applications which require high optical clarity, such as eyeglass lenses.

The degree of crystallinity also affects the thermal behaviour of a polymer. Semi-crystalline polymers will exhibit a melting point (T_m) corresponding to the transition from a crystalline to an amorphous, liquid phase. This is accompanied by a step change in the specific heat due to the latent heat of vaporisation required for the transition. Amorphous polymers display a glass transition temperature (T_g) which corresponds to the increase in movement of the polymer chains. Energy supplied in the form of heat enables rotational and translational movement of the polymer chains and also results in thermal expansion, which increases the free volume available in the polymer [49]. As this transition does not involve a phase change, it is termed a secondary transition and is not accompanied by a discontinuity in the specific heat, as shown in figure 2.5. Semi-crystalline polymers will display a T_g and T_m due to the presence of amorphous and crystalline areas, where $T_g<T_m$.

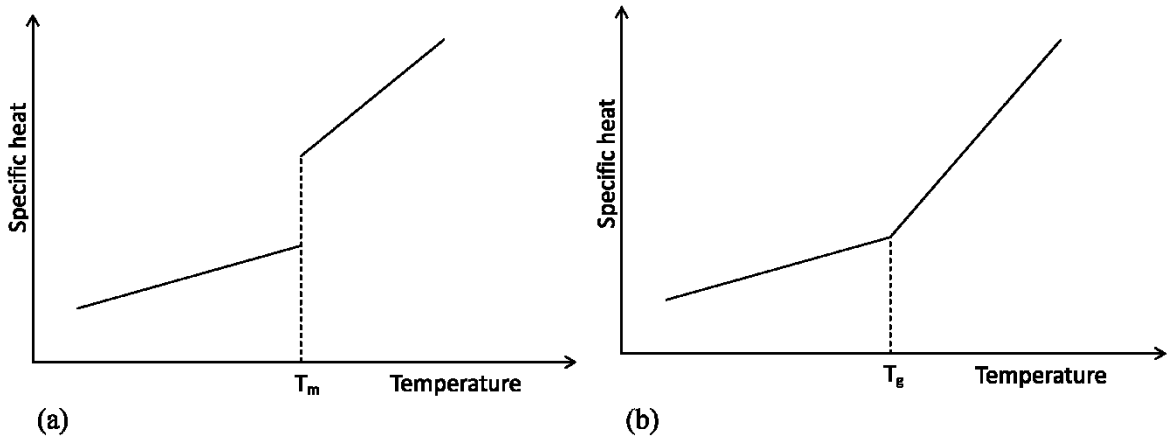

Figure 2.5 First and second order transitions of crystalline and amorphous polymers showing a) the melting point (T_m) and b) the glass transition temperature (T_g).

2.1.4 Factors affecting the glass transition temperature

The glass transition temperature is dependent on the mobility of the polymer chain, which in turn is dependent on several factors. The flexibility of the polymer backbone is perhaps the most significant. While single bonded carbon atoms can rotate freely around their axis, the presence of phenyl groups or double bonds in the polymer backbone increases the chain rigidity and reduces mobility, resulting in an increase in T_g.

The presence of long or bulky pendant groups can have two effects. They can restrict rotation of the backbone or come into contact with other polymer chains and become entangled. Both actions increase the T_g. However, pendant groups can also increase the free volume of the polymer due to the greater spacing between polymer chains. This has the effect of decreasing the T_g as shown for the methacrylate polymers in table 2.1.

Table 2.1 Dependency of T_g on side chain length for polymethacrylates. T_g values from [53].

Poly(methyl methacrylate)	Poly(ethyl methacrylate)	Poly(propyl methacrylate)	Poly(butyl methacrylate)
T_g = 105°C	T_g = 65°C	T_g = 35°C	T_g = 20°C
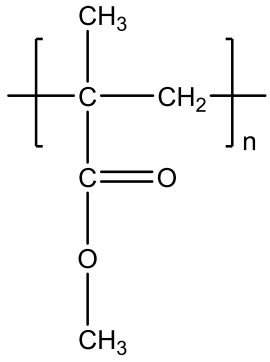	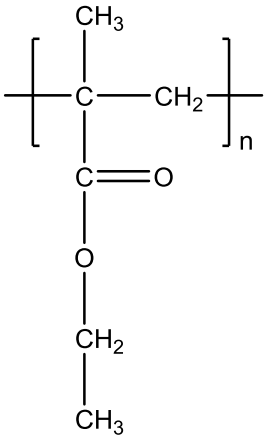	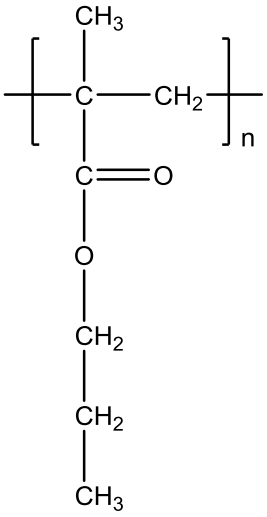	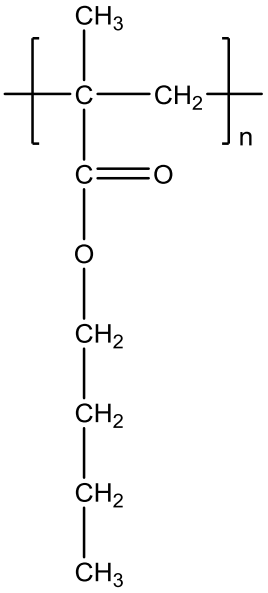

Higher molecular weight polymers have a greater T_g due to the decrease in free volume associated with longer chain lengths. Branching results in a decrease in the T_g when the degree of branching is low but the presence of a greater number of branches causes an increase in T_g due to the restricted mobility of the chains. Cross-linked polymers display a further increase in T_g. However, this is dependent on the degree of cross-linking as the T_g and T_m of cross-linked polymers may be greater than the temperature at which they disintegrate [49].

As previously mentioned the T_g is also affected by tacticity; this is more pronounced for larger side groups. For example T_g values for PMMA vary widely and are around 45°C for isotactic PMMA, 105°C for atactic PMMA and 130°C for syndiotactic PMMA [48]. This is thought to be due to the alternate asymmetrical pendant groups hindering rotation of the chain [54]. Other factors including plasticiser content and water absorption also affect T_g.

2.1.5 Polymer classification

Polymers can be classified based on their behaviour when exposed to external environmental changes. Two such classifications are described below.

2.1.5.1 Thermal behaviour

One of the clearest distinctions between different polymers depends on whether or not they undergo a chemical change when they are heated. Thermosetting plastics become highly cross-linked once cured and cannot be re-melted. In contrast thermoplastics undergo repeated softening and hardening as they are heated and cooled. Thermosets have several advantages over thermoplastics: they are harder and have higher tensile strength as well as being resistant to high temperatures and solvents. However, they are also brittle and cannot be remoulded.

2.1.5.2 Radiation

The exposure of polymers to high energy radiation such as gamma rays and x-rays results in chain scission or cross-linking of the polymer chains [55, 56]. Both may occur, however the dominant pathway depends on the polymer in question. Type I polymers cross-link under irradiation while type II undergo chain scission. This difference between the two types is thought to be due to the presence of the quaternary carbon atom in type II polymers (table 2.2) which weakens the carbon-carbon bond in the backbone due to steric repulsion effects [55].

Table 2.2 Molecular structure of type I and type II polymers [56].

Type I	Type II
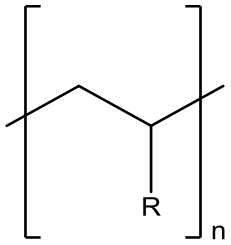	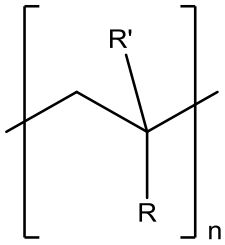
e.g. Polystyrene	e.g. Poly(methyl methacrylate)

In the case of type I polymers such as PVC, where R = halogen, the carbon-halide bond is broken on exposure to radiation [56]. In PVC this will result in dehydrochlorination. Type I polymers containing aromatic rings, such as polystyrene, show an increased resistance to irradiation. This is due to the absorption of energy by the aromatic ring, which protects the rest of the polymer chain [56].

2.2 Plastics manufacture

The manufacture of plastics involves several steps which are detailed in this section.

2.2.1 Polymerisation

Polymerisation can proceed via one of two pathways: step-growth polymerisation and chain-growth polymerisation, first defined by Flory in 1953 [49]. Step-growth polymerisation occurs when reactions between any two molecules results in the growth of the polymer chain. Chain-growth polymerisation occurs when only the end group of the polymer chain reacts with a monomer.

2.2.1.1 Step-growth polymerisation

Step-growth polymerisation proceeds via reactions between functional groups. Monomers with two functional sites can initially react with each other to produce linear dimers which then go on to react with other monomers or dimers (figure 2.6). In this way multiple individual chains can grow throughout the polymer matrix. Monomers with a functionality of three or more give rise to branched polymer chains. Step-growth polymerisation is commonly accompanied by the loss of small molecules such as water [49].

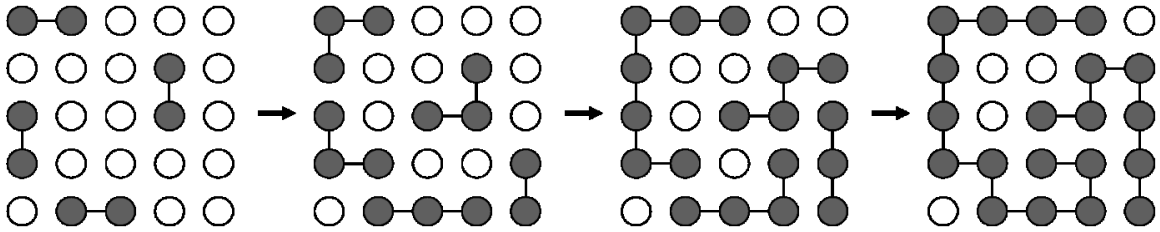

Figure 2.6 Schematic showing step-growth polymerisation. Unfilled circle = monomer, filled circle = oligomer.

2.2.1.2 Chain-growth polymerisation

Chain-growth polymerisation is initiated by a reaction between a monomer and an initiator. The growth of the chain can proceed via various mechanisms with the reaction site, known as the active centre, always transferring to the end of the polymer chain [49] (figure 2.7). Unlike step-growth polymerisation, chain-growth polymerisation ends with the termination of the reaction.

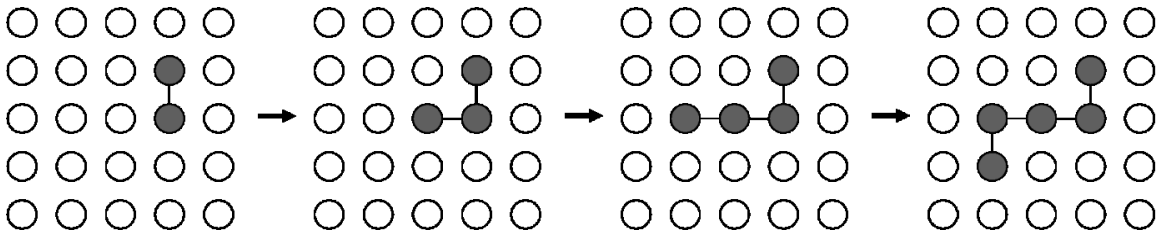

Figure 2.7 Schematic showing chain-growth polymerisation. Unfilled circle = monomer, filled circle = oligomer.

2.2.1.3 Polymerisation methods

Polymerisation may be performed in bulk, solution, suspension, or emulsion. Bulk polymerisation is the most straightforward process but can be susceptible to overheating [48]. However, the potential for contamination is low [49] and polystyrene, PMMA and polyethylene are produced via this method. Solution polymerisation involves the dissolution of the monomer in a solvent which absorbs heat produced during the reaction. The drawback to solution polymerisation is the difficulty in removing all residual solvent after polymerisation has taken place [49]. Suspension polymerisation takes place in water with each monomer forming separate polymer spheres. Agents such as talc or gelatine are added to aid dispersion and prevent agglomeration [17]. This method requires significant agitation of the water during polymerisation to prevent the separate spheres coming into contact [49]. It is commonly used to manufacture PVC. Emulsion polymerisation adds a surfactant to the water which acts to protect the polymer spheres as they form. However surfactant residues may be difficult to remove after polymerisation [57].

2.2.2 Formation

Additives are introduced into the plastic prior to formation and are discussed further in section 2.3. Thermoplastics can be moulded using a variety of methods; four common processes are described below.

2.2.2.1 Casting

Casting is the most straightforward of the manufacturing methods and is used for the production of flat plastic sheets or films. Following bulk polymerisation the resulting plastic melt is poured onto a highly polished flat metal sheet which then passes through a series of heating and cooling rollers to shape the plastic sheet to the desired thickness, a process known as calendering [48]. Following formation, the plastic sheet is usually protected by means of a thin film which is weakly adhered to the surface [57].

2.2.2.2 Extrusion

Extruded plastics use small plastic pellets or flakes which are placed into a hopper connected to a screw and barrel assembly. As the screw rotates the pellets pass down the barrel and through a series of heating units. The pressure of the rotating screw then extrudes the molten plastic through a die. The molten polymer may be extruded onto a flat sheet to undergo calendering, shaped by the die, or it may pass into a mould. Hollow products such as bottles or cartons may be produced by inflating the still softened plastic in a process called blow-moulding [57].

2.2.2.3 Injection moulding

Injection moulding is used to create a wide variety of objects, ranging from toys to wheelie bins [58]. In this process the plastic melt is extruded into a cooled mould where it rapidly solidifies [57]. The mould is commonly of a split design so that the object can be easily removed.

2.2.2.4 Polymer foams

Polymer foams are created by the addition of blowing agents into the plastic during processing [17]. These may be liquids or gases and commonly include carbon dioxide and air. During processing these blowing agents either expand or evaporate with the increase in temperature, resulting in the formation of voids within the polymer matrix. Common polymer foams included expanded polystyrene which is used in packaging applications worldwide.

2.3 Additives

Additives are introduced into plastics to change their behavioural properties. They include fillers to improve the plastic's stability, flexibility, visual appearance and processing performance. The quantity and type of fillers depends on the end use of the plastic and its life expectancy [17]. Consequently, items such as PVC window frames contain a relatively high proportion of stabilisers while plastics used in food packaging are subject to food safety legislation and do not need a high life expectancy.

2.3.1 Antioxidants and ultraviolet stabilisers

One of the most damaging environmental factors for polymers is exposure to ultraviolet (UV) radiation and heat, which results in oxidation and is discussed further in section 2.4. Most plastics therefore contain additives to reduce or prevent oxidation resulting from high temperatures during processing and exposure to UV radiation. These commonly take two forms, antioxidants or UV stabilisers [48].

Antioxidants are used to inhibit oxidation of the polymer that occurs as a result of exposure to heat or UV radiation. Primary antioxidants work by reacting with the radicals that are produced during oxidation to form stable species. They are commonly used with secondary antioxidants which prevent the decomposition of hydroperoxides which would otherwise produce free radicals [57]. UV stabilisers include absorbers which preferentially absorb ultraviolet radiation and re-radiate it as heat. This prevents the formation of free radicals in the polymer. Other types of stabilisers commonly found in plastics are hindered amine light stabilisers (HALS). These form nitroxyl radicals which then react with radical species to stabilise the polymer.

2.3.2 Plasticisers

As many polymers are rigid at room temperature, plasticisers are added to polymers to increase their flexibility. Plasticisers are dispersed within the polymer matrix and are only weakly bonded to the polymer chains via Van der Waals forces. They increase the free volume between the polymer chains

and allow them to move easily past each other. This in turn lowers the plastic's T_g and results in increased flexibility. The addition of plasticisers also enables lower processing temperatures to be used, reducing the potential for thermal degradation. The quantity of plasticiser in a plastic can range from zero in un-plasticised plastics to 50 %wt. in the case of plasticised PVC [59]. The reduction in T_g is dependent on the type and quantity of plasticiser used. The most common plasticisers are phthalates which are used in PVC [60]. The unmodified polymer has a T_g of 80 °C [53], while PVC plasticised with 30-40 %wt. phthalate plasticiser can lower the T_g to -40 °C [17]. Health concerns around these additives have resulted in restrictions relating to children's toys, particularly for those which may come into contact with children's mouths [61].

2.3.3 Colorants

Perhaps one of most obvious properties of a plastic object is its colour. Dyes, organic pigments and inorganic pigments are used to colour plastics; the type of colorant used is dependent on the polymer and the requirements of the finished product. Dyes dissolve within the polymer matrix and are generally used to colour translucent plastics. Pigments are insoluble and inorganic pigments in particular offer greater opacity [48]. Some colorants are incompatible with certain polymers as they can migrate out of the polymer matrix or exhibit low thermal stability.

2.3.4 Other additives

Other additives include fire retardants which are added to plastics used in buildings or furniture. These can act to suppress fire propagation through inhibition of the combustion process and typically consist of halogen-containing compounds [62]. Other flame retardants react to form a protective carbonaceous layer on the plastic surface which also prevents oxygen penetration. Additives added to plastics can also include anti-static agents to dissipate electrical charge, mould release agents to aid processing and blowing agents for the manufacture of polymer foams [48].

2.4 Degradation mechanisms

The inevitable exposure of plastics to light and air means that many plastics will degrade, though degradation can proceed very slowly and be invisible to the naked eye. Much of the interaction of a plastic with its environment occurs at its surface and plastics failure does not necessarily require that degradation extends significantly into the bulk material [63]. Degradation is highly complex due to the number of factors which can potentially be involved. It is highly unlikely that a plastic will degrade via one route alone, rather a combination of factors must be considered.

The degradation of plastic materials is dependent on both their composition and environment, and while degradation cannot be stopped or reversed, it may be slowed [17, 24]. For museums, it is a somewhat impossible task to tailor storage and display conditions to many different plastics. Instead, environmental conditions must be chosen which pose the least risk to the plastics involved.

2.4.1 Irradiation

The degradation of plastics due to irradiation is principally due to exposure to radiation in the short wavelength ultraviolet range of the electromagnetic spectrum, but longer wavelengths can also cause damage if the plastic contains additives or impurities that absorb at these wavelengths [64].

2.4.1.1 Light

While solar radiation contains electromagnetic radiation of all wavelengths, much of the highly energetic and highly damaging radiation is absorbed by the Earth's atmosphere. The spectral distribution of solar radiation reaching the Earth's surface in North America is shown in figure 2.8 as detailed in British Standard EN 60904-3:2008 [65].

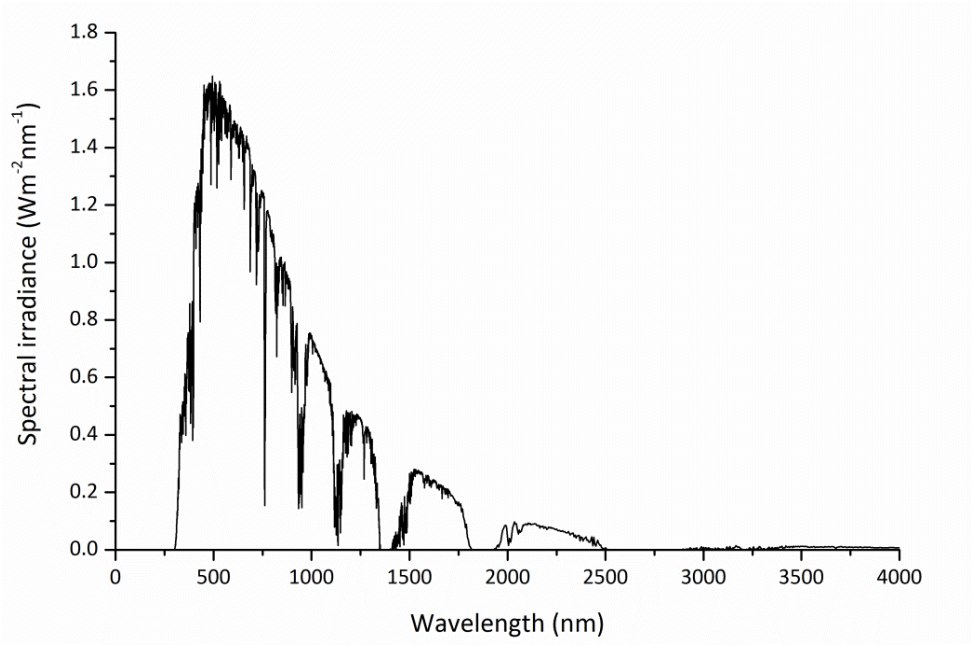

Figure 2.8 Spectral distribution of solar radiation reaching the Earth's surface [65].

The highest energy photons that reach the Earth's surface have a wavelength of 280 nm and fall in the ultraviolet region of the electromagnetic spectrum. Radiation in the ultraviolet region is highly damaging to most plastics, particularly radiation in the UVB region with wavelengths between 280 nm and 320 nm as this is the most energetic.

According to Planck's equation (2.4), the energy of incoming radiation (E) is inversely proportional to its wavelength.

$$E = h\upsilon = \frac{hc}{\lambda} \tag{2.4}$$

Where h is Planck's constant (6.62×10^{-34} m^2kgs^{-1}), ν is the radiation frequency, c is the speed of light in a vacuum and λ is the wavelength of radiation.

Radiation reaching the Earth's surface has wavelengths in the range 280 nm - 400 nm in the UV region, which equals photon energies in the range 299 $kJmol^{-1}$ (3.1 eV) to 427 $kJmol^{-1}$ (4.4 eV). These wavelengths can be absorbed by chromophoric groups in polymers; some common chromophores and their maximum wavelengths of absorption are shown in table 2.3. Radiation may also be absorbed by impurities contained within the plastic which result from processing residues, pollutants or raw material. These commonly include hydroperoxide or carbonyl groups and their presence means that even polymers that do not contain chromophoric groups may be affected by UV radiation [63].

Table 2.3 Common chromophore groups and their associated wavelengths and energies of maximum absorption [49] R = alkyl, R' = alkyl or H.

Chromophore	λ_{max} (nm)	E (eV)
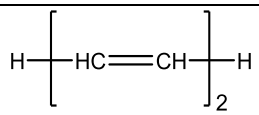	217	5.7
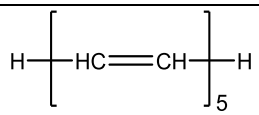	335	3.7
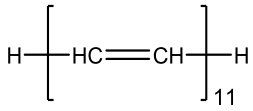	470	2.6
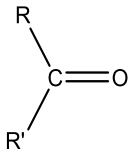	270-300	4.1-4.6
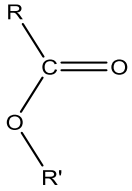	~200	~6.2
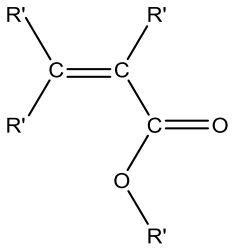	200-220	5.6-6.2
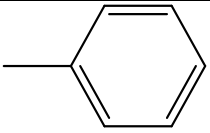	200-240 250-280	5.2-6.2 4.4-5.0

It can be seen from table 2.3 that increasingly conjugated chains result in the absorption of radiation at longer wavelengths. Long conjugated polymer chains can result in the absorption of wavelengths in the visible spectrum. This is most apparent in the degradation of PVC, which degrades via de-hydrochlorination or unzipping of the polymer chain. This results in an increasingly conjugated polymer chain which absorbs light at longer wavelengths as degradation proceeds, resulting in a colour change from white to yellow to red and finally to black [59].

Absorption of radiation results in the excitation of the chromophore to an excited state. Relaxation of the chromophore to the ground state is accompanied by the emission of energy which may be radiated as heat or can cause chain scission. The energy required to break chemical bonds is given by the bond dissociation energy. The typical dissociation energies for chemical bonds in polymers lie between 290 - 420 $kJmol^{-1}$ [63]. Therefore, the energy of UV radiation is sufficient to break interatomic bonds, which can occur in the polymer backbone or in side chains. Scission of the polymer backbone reduces its molecular weight which in turn results in a reduction in its mechanical properties. Tertiary hydrogen atoms are particularly vulnerable to abstraction as the bond dissociation energies for these are lower than for other carbon-carbon or carbon-hydrogen bonds [64]. The breakage of bonds at any site in the polymer chain can create potential sites for oxidation, which is discussed further in section 2.4.3.

The surface of the plastic is most vulnerable to degradation as light is attenuated as it passes into the bulk. The absorbance (A) of UV-visible radiation by a substrate is described by the Lambert-Beer law (equation 2.5) [64].

$$A = \varepsilon c d \qquad (2.5)$$

Where ε is the molar absorption co-efficient, c is the concentration of the absorbing species and d is the path length of the radiation. For polymers the absorbing species are chromophoric groups such as C=O, ROOH and aromatic rings. However, the equation is only valid for low concentrations of absorbing species and for low intensity radiation [64]. Oxidation of the polymer may result in the formation of additional chromophores which absorb radiation in the UV and visible wavelengths [63]. Cross-linking can also occur due to exposure to UV-visible radiation and is more likely in linear polymers such as polystyrene and PVC [17].

2.4.1.2 Other sources of irradiation

Other potential sources of irradiation in the museum environment originate from artificial lighting. Historically museum lighting has used tungsten-halogen lamps although there is currently a move towards the use of LED lighting. The spectrum of tungsten-halogen lighting typically contains a significant component at longer wavelengths in the visible spectrum and in the infra-red. While LED lighting does not generally contain a UV component, some LED light sources do exhibit a peak in the

blue region of the spectrum which can potentially be problematic for light-sensitive objects. The spectral power distributions of a typical tungsten-halogen lamp and an LED light source are shown in figure 2.9 [66].

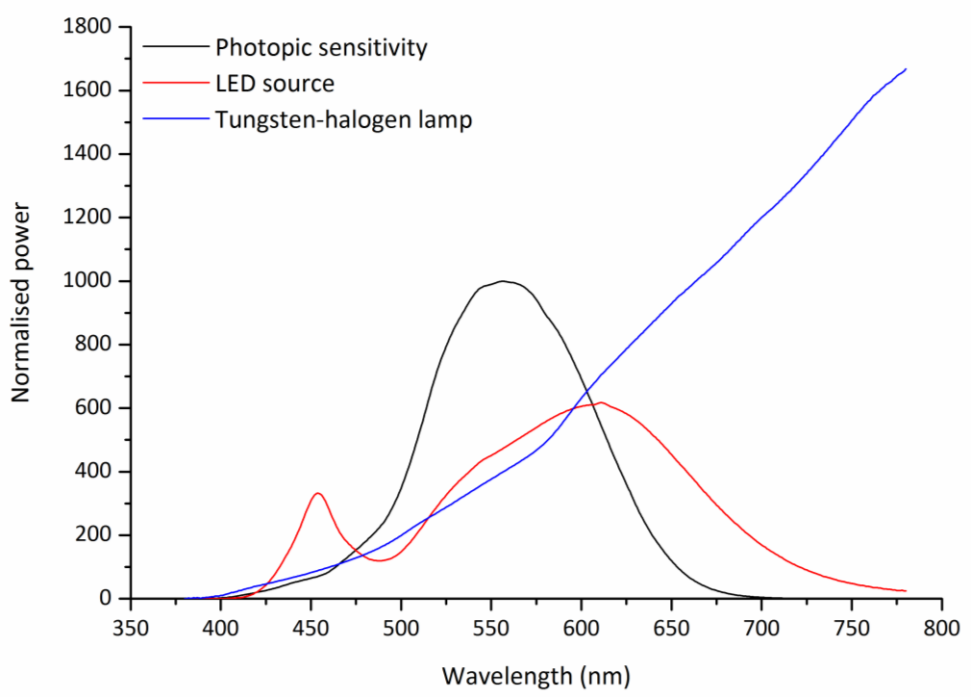

Figure 2.9 Normalised spectral power distribution for a standard tungsten-halogen lamp and an LED light source in the wavelength range 380-780 nm compared to the photopic sensitivity curve. Data courtesy of the National Gallery [66].

Environmental damage due to radiation is principally a result of exposure to UV radiation. Higher energy radiation of the order 10 MeV, such as gamma rays and x-rays, is unlikely to be found in a normal environment. However, due to their historic and cultural value, plastic objects that have been exposed to extra-terrestrial environmental conditions, such as spacesuits, may be found in museum collections [67]. The use of high energy radiation for analytical purposes can result in the degradation of polymers through chain scission or cross-linking as discussed in section 2.1.5.2. Unlike UV radiation, high energy radiation is not selectively absorbed by polymers [56].

2.4.2 Thermolysis

The exposure of polymers to high temperatures can also result in scission of the polymer chain. Bond breakages may occur anywhere in the polymer chain although the incorporation of impurities during polymer processing can result in sites that are more vulnerable to scission. Side chains often experience scission at lower temperatures compared to the polymer backbone [17]. Side chain scission in PMMA has been observed to occur at lower temperatures than main chain scission, which

starts to occur at around 270 °C [68]. Bonds with lower bond energies such as N-O (E=201 $kJmol^{-1}$) which are found in the side groups of cellulose nitrate are also more vulnerable to temperature [17]. It should be noted that the temperatures required for chain scission are unlikely to occur in the museum environment. The polymer is most vulnerable to degradation via thermolysis during processing; scission of bonds at this point in the polymer's lifetime can create potential sites for oxidation in the future. At very cold temperatures plastics containing plasticisers may distort or become brittle due to the temperature being below the T_g of the plasticiser. Commonly used phthalate plasticisers have a T_g around -50 °C [60].

2.4.3 Oxidation

Oxidation is involved in the degradation of most polymers. Exposure to atmospheric oxygen occurs at all points in the life of the polymer. The interaction of oxygen with the polymer during manufacture results in the incorporation of oxygen impurities in the bulk [17] while after manufacture the surface of the polymer is exposed to oxygen in the atmosphere. Oxidation occurring as a result of direct exposure to molecular oxygen is known as auto-oxidation.

Some polymers are more vulnerable to oxidation than others, due to their molecular composition and structure. In general the greater free volume and chain flexibility of amorphous polymers renders them more vulnerable than crystalline polymers [69]. Kazmarek et al. found that the rate of oxidation increases with the length of the pendant group in poly(alkyl methacrylate)s [70]. This was attributed to the increase in chain flexibility lowering the T_g, which in turn increases the rate of oxygen diffusion into the polymer. For a polymer with a given T_g, the permeability of oxygen also increases with temperature as the polymer becomes more flexible. The reaction of polymers with oxygen is highly dependent on the type of bonds present in the polymer chain. Unsaturated bonds are more reactive than saturated bonds. Polymer chains containing tertiary carbon atoms are also more reactive due to the localised area of negative charge around the tertiary carbon [17].

Oxidation can be considered as occurring in three stages: initiation, propagation and termination, as shown in figure 2.10 [17]. Initiation of the process occurs with the application of light or heat which results in the formation of free radicals (R•). These react with molecular oxygen to form hydroperoxy radicals (ROO•) which in turn react with the polymer to form hydroperoxides (ROOH). The production of free radicals during this stage enables continued degradation and is known as the propagation stage. Termination is achieved only by the reaction of radicals with each other. Following initiation, autocatalytic oxidation proceeds via a chain reaction which cannot be stopped.

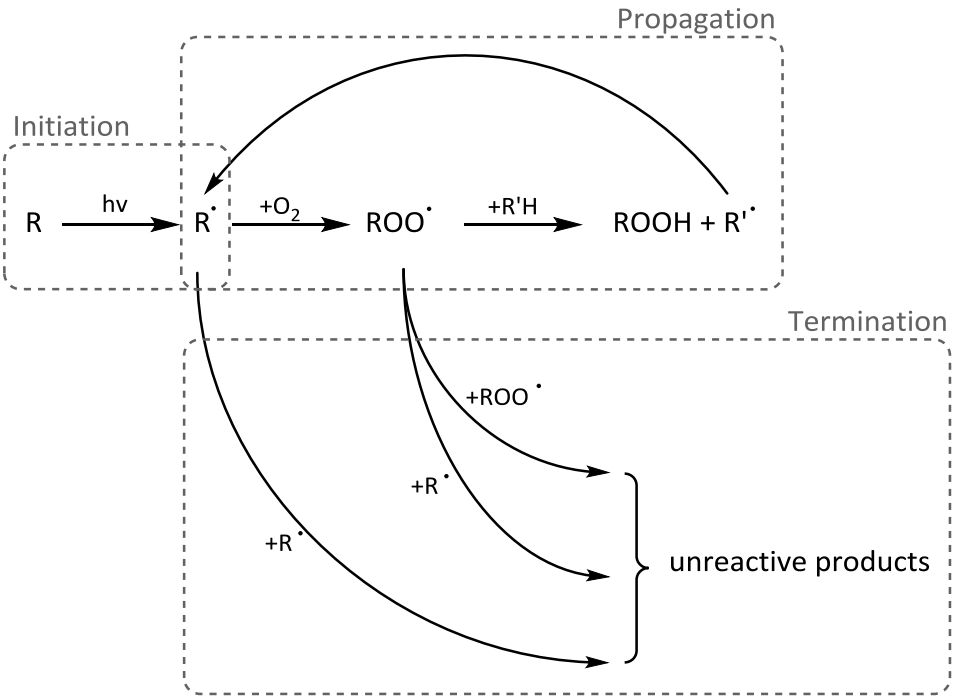

Figure 2.10 General photo-oxidation mechanism.

Oxidative degradation may be divided into four stages: inception, induction, maximum rate and decreasing rate (figure 2.11) [71, 72]. Inception is a potentially lengthy period of time when there is no visible change to the plastic. Induction is the period in which degradation starts to accelerate rapidly until it reaches the maximum rate where there is a steady rate of deterioration. Close to the end of the object's lifetime, the rate of oxidation decreases. This is thought to be due to the reduction in the conditions favourable for oxidation. Oxidation results in discoloration, the loss of mechanical strength and embrittlement.

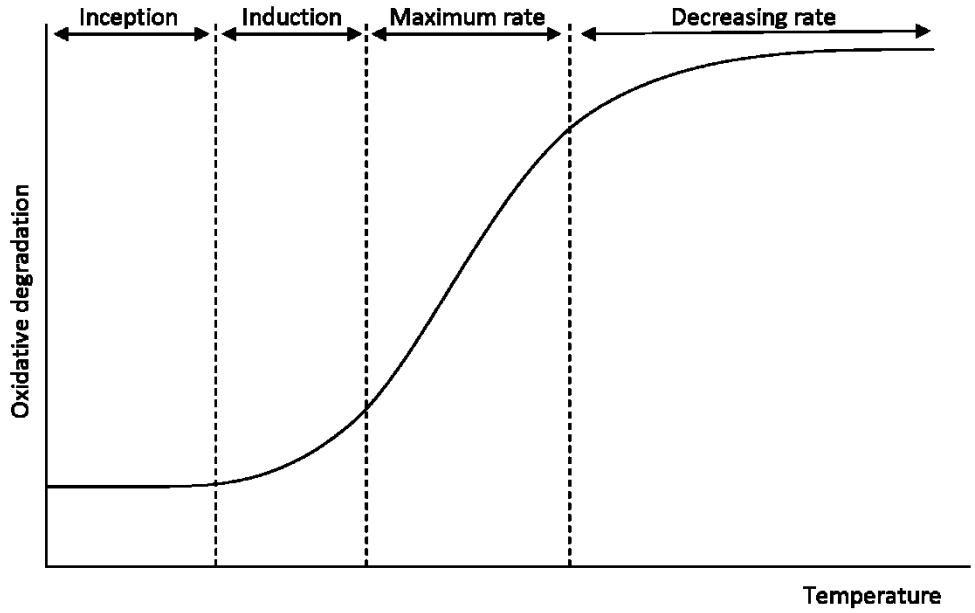

Figure 2.11 Schematic illustrating the four stages of oxidative degradation [71].

2.4.3.1 Photo-oxidation

Photo-oxidation is the term given to oxidation that occurs as a result of exposure to light. As previously discussed, incoming radiation in the 280 nm - 400 nm range can result in the scission of chemical bonds and the production of free radicals. The reaction of the free radicals with molecular oxygen initiates oxidation. Due to the limited penetration of light into the material, photo-oxidation is limited to the surface and subsurface layers.

2.4.3.2 Thermal oxidation

Thermal oxidation refers to oxidation that occurs as a result of an increase in temperature. In this case the initial scission of bonds is due to energy in the form of heat. Unlike photo-oxidation, the application of heat can result in the breakage of bonds throughout the material. Thermal oxidation is therefore not limited solely to the plastic surface. The presence of oxygen has been reported to increase the rate of chain scission in PMMA when compared to anoxic conditions [68].

2.4.4 Hydrolysis

Hydrolysis is the occurrence of degradation due to exposure to water or water vapour. Interaction of the polymer with water results in cleavage of molecular bonds. Some polymers are more susceptible to hydrolysis than others due to the presence of heteroatoms in their backbone which react with water and result in main chain scission [48]. These include polycarbonates, polyesters and polyurethanes. Scission may also occur on the side chains but is not as detrimental as main chain scission. Polymers which are formed by processes involving the elimination of a water molecule are particularly vulnerable to hydrolysis [63]. Guidelines for polycarbonate recommend a maximum water content so that degradation does not occur in subsequent high temperature processing [73]. The hydrolysis of cellulose acetate is accompanied by the production of acetic acid. This gives rise to the distinctive 'vinegar syndrome' which heralds the degradation of cellulose acetate [17].

The sensitivity of a polymer to hydrolysis is also dependent on its water permeability. Diffusion of water into the polymer matrix is greater for amorphous areas compared to crystalline regions. The rate of diffusion also increases with temperature and relative humidity [63]. In the case of polyamides, water acts as a plasticiser by disrupting the hydrogen bonding between the polymer chains and decreasing the T_g [63]. Polymers can also become more sensitive to water as they age due to their polarity increasing as a result of oxidation [17].

2.4.5 Environmental pollutants

The most detrimental pollutants for plastics are nitrogen dioxide (NO_2), sulphur dioxide (SO_2) and ozone (O_3) [69]. In urban areas the source of the former two pollutants is the combustion of fossil fuels while ozone occurs naturally and as a result of human emissions [74]. The degradation of polymers via NO_2 is complex and is exacerbated by exposure to UV radiation, heat and oxygen [69].

Unsaturated polymers are more susceptible to attack. Nitrogen dioxide removes a tertiary hydrogen atom from the polymer as in figure 2.12 which eventually results in chain scission. Moisture in the air can also react with NO_2 to form nitric acid [17].

$$NO_2 + RH \rightarrow HNO_2 + R\bullet$$

$$R\bullet + NO_2 \rightarrow RONO$$

$$R\bullet + O_2 \rightarrow RO_2$$

Figure 2.12 Interaction of NO_2 with an unsaturated polymer [69].

Ultraviolet light can cause excitation of SO_2 which can react with saturated polymers as in figure 2.13 to form sulfinic acids [75].

$$SO_2^* + RH \rightarrow RSO_2H$$

Figure 2.13 Interaction of SO_2 with a saturated polymer [75].

Ozone can also cause the degradation of polymers. Rubber is particularly vulnerable to this pollutant which causes the formation of large cracks in the rubber and is known as ozone cracking. Ozone reacts with double bonds in the polymer backbone, causing main chain scission and resulting in the loss of mechanical properties. Fossil fuel combustion can also result in the formation of airborne particles, such as carbon particulates from diesel engines. These particles may contain acidic species such as sulfinic acids [76] which can deposit on the polymer and adversely affect the surface.

2.4.6 Biological attack

Compared to more traditional materials such as wood and natural textiles, plastics are relatively resistant to biological attack. However, they are not immune [77]. Lower molecular weight polymers are more vulnerable to biodegradation [63], therefore it follows that degradation of the polymer via chain scission will result in greater susceptibility to microbial attack. Micro-organisms may preferentially attack additives rather than the polymer itself. This has been seen in the case of plasticisers in PVC [78] where the presence of water has contributed to microbial attack. A number of studies have reported that polyurethane is particularly prone to degradation [79]. Fungal growth on PMMA artwork containing water has also been observed (personal communication from A Riquier, November 2014) while spacesuits, audiotape and habitable structures have been similarly affected [77]. In more recent years increasing environmental concerns about plastics and pollution of the environment have resulted in the advent of biodegradeable plastics which are designed to degrade over time and which may pose a challenge for museum collections in the future.

2.4.7 Influence of additives

Additives introduced during the manufacturing process are designed to last for the expected lifetime of the plastic. The depletion of antioxidants and UV stabilisers therefore eventually results in unchecked oxidation of the polymer and an increased rate of degradation. Plasticisers can also migrate out of the polymer material. This is seen in the case of PVC, where migration of plasticiser to the surface results in tackiness and loss of the plasticiser via evaporation [59].

Additives can also act as potential sources of degradation. Brominated flame retardants used in polystyrene have been observed to preferentially absorb radiation in the 280 nm - 350 nm region, with degradation of the flame retardants resulting in degradation of the polystyrene [80]. Flame retardants have been observed to interfere with the effectiveness of hindered amine light stabilisers (HALS) in polypropylene [81]. The incorporation of colorants in the plastic can also result in degradation [64].

2.4.8 Physical degradation

Physical degradation is primarily a result of stresses incorporated within the plastic due to the manufacturing process. Areas of high stress within an object can be susceptible to degradation via one or more of the processes heretofore described. The hydrolysis of polycarbonate may be increased by significantly by tensile stresses [80]. Environmental stress cracking, discussed further in section 2.5.4.2, is a known failure mode for plastics [82] and occurs as a result of localised stresses increasing the plastic's susceptibility to solvents or other liquids.

Cracks or scratches on the plastic surface can occur as a result of general wear and tear, though they may also form as a result of other degradation processes. Regardless of their source, these can form areas of weakness and potential sites for future degradation [17]. Temperature changes can result in weakened areas due to repeated expansion and contraction of the plastic. The effect of fluctuating temperature has been seen in protective transparent PMMA coverings for slides housed in cardboard frames. In this case temperature changes resulted in the diffusion of water into and out of the cardboard, resulting in stress crazing [83].

2.5 Solubility

One of the key considerations in the conservation of plastics is their compatibility or potential vulnerability to materials used for treatment and repair. When choosing appropriate cleaning agents it is necessary to consider the solubility behaviour of polymers and the types of cleaning agents to be used. This is especially true for the use of organic solvents.

2.5.1 Intermolecular forces

Intermolecular forces are considered when determining the solubility of polymer-solvent systems. The general rule 'like dissolves like' can give an indication of the compatibility between a polymer and a solvent, i.e. polar solvents are more likely to dissolve polar macromolecules. However, solubility

parameters have been defined in order to predict the likely solubility behaviour of a polymer-solvent system.

2.5.2 Hildebrand and Hansen solubility parameters

In 1936 Joel Hildebrand proposed the introduction of a parameter to indicate the solvency behaviour of a specific solvent. The Hildebrand solubility parameter (δ), as it came to be known, is defined as the square root of the cohesive energy density, as shown in equation 2.6 [49].

$$\delta = \sqrt{\frac{E}{V_m}} \tag{2.6}$$

Where E is the cohesive energy and V_m is the molar volume.

The cohesive energy (E) is defined as the energy required to vaporise a liquid to a gas and is given by equation 2.7. It is indicative of the total attractive forces present between the molecules in a solvent.

$$E = H_v - RT \tag{2.7}$$

Where H_v is the latent heat of vaporisation, R is the universal gas constant (8.31 J mol^{-1} K^{-1}) and T is the absolute temperature.

Inconsistencies in the solubility behaviour of solvents with similar Hildebrand parameters led to the development of Hansen parameters. The inconsistencies were thought to be due to the different contributions from the dispersion, polar and hydrogen bonding forces. In 1966 Charles Hansen proposed that the Hildebrand solubility parameter could be defined in terms of three separate components resulting from the dispersion force (δ_d), polar force (δ_p) and hydrogen bonding (δ_h), as in equation 2.8 [84].

$$\delta^2 = \delta_d{}^2 + \delta_p{}^2 + \delta_h{}^2 \tag{2.8}$$

If two molecules such as a polymer and a solvent are considered in three dimensional Hansen space, the distance between them (Ra) is then given by equation 2.9 [84].

$$Ra^2 = 4\left(\delta_{d_1} - \partial_{d_2}\right) + \left(\delta_{p_1} - \delta_{p_2}\right) + \left(\delta_{h_1} - \delta_{h_2}\right) \tag{2.9}$$

The relative energy difference, RED, is defined in equation 2.10 and predicts the compatibility between a solvent and a polymer. The value of the Hansen interaction radius, Ro, is dependent on the polymer.

$$RED = \frac{Ra}{Ro} \tag{2.10}$$

RED values greater than 1 indicate that the polymer and solvent are not compatible, while dissolution is likely for values less than 1. This compatibility can be visualised by considering a sphere of radius Ro, as shown in figure 2.14. Any solvents with a Ra that falls inside this sphere can be said to be compatible.

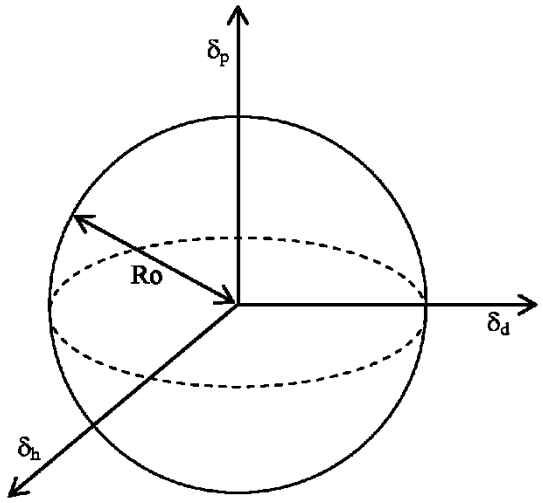

Figure 2.14 Schematic showing the Hansen interaction radius.

2.5.3 Teas chart

An alternate visual representation of solubility parameters, the Teas chart, was first developed in 1968 and is commonly used in conservation [17, 85]. The chart uses the values for the three Hansen parameters expressed as a percentage of the total solubility parameter to obtain fractional parameters for the dispersion (f_d), polar (f_p) and hydrogen bonding (f_h) forces. These fractional parameters are then plotted on a three axis graph, the Teas chart. Figure 2.15 shows a Teas chart with the solubility parameters of some common polymers and solvents indicated. Solvent families lie in the same region of the chart, for example the alcohols are found in the centre while hydrocarbons are located towards the right corner. The greater the distance between two neighbouring points, the less likely they are to be miscible, or in the case of a polymer and solvent, the less likely that the solvent will dissolve the polymer. The Teas chart has its limitations due to the contribution of the individual forces being expressed as a percentage of the total solubility parameter. It therefore does not take into account the different Hildebrand solubility parameters for different materials. However, it does provide a useful indication of solubility behaviour.

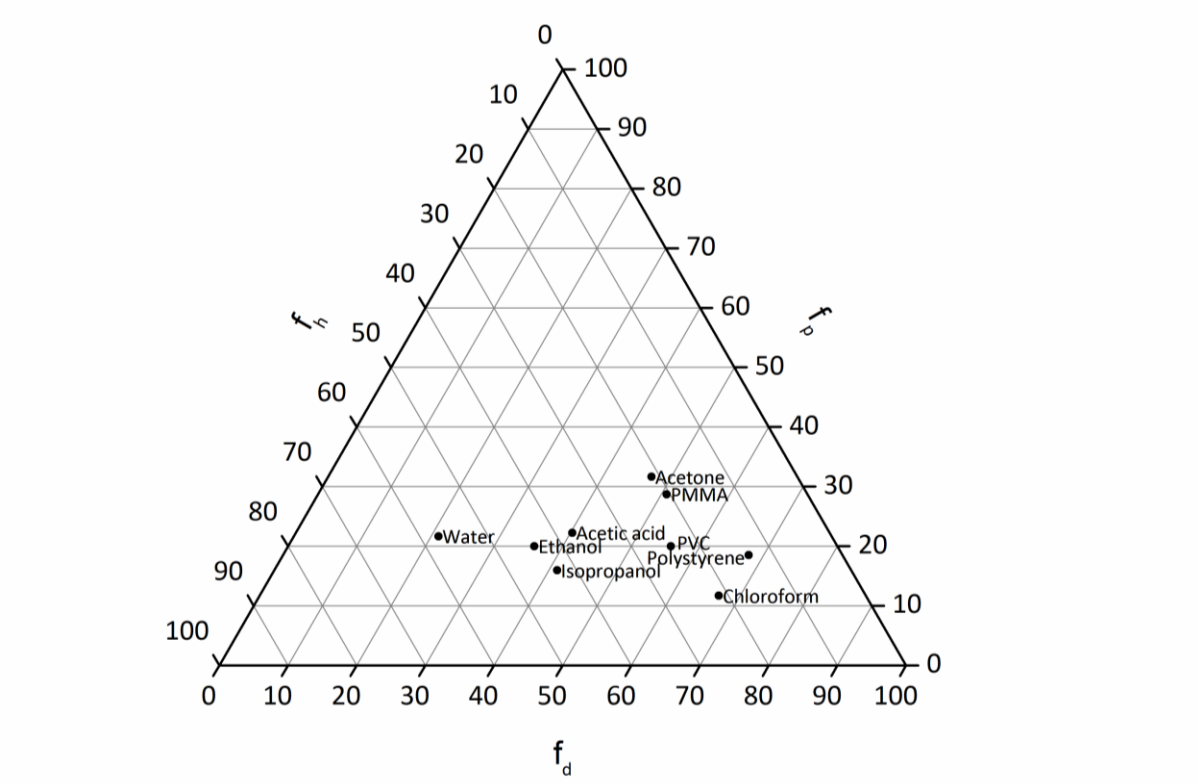

Figure 2.15 Teas chart showing common solvents and polymers.

The determination of solubility parameters is achieved via repeat testing of the polymer to find the solvent or combination of solvents for which dissolution occurs. In the case of cross-linked polymers this is the solvent for which maximum swelling of the polymer occurs [85]. Solubility parameters depend on the type and quantity of fillers and the polymer's molecular weight. The temperature and the molecular size of the solvent also affect solubility behaviour, with smaller molecules exhibiting faster diffusion rates [85]. Solubility parameters can and do change as the polymer ages and degrades [17]. Therefore, they should only be taken as a guide when considering conservation treatments.

2.5.4 Mechanisms and manifestations of solubility

Solubility parameters are commonly used to find solvents and solutes that are compatible, i.e. the solute is completely dissolved by the solvent. However, this compatibility can be undesirable, particularly in cleaning applications and the interaction of solvents with a polymer can result in detrimental changes to the polymer.

2.5.4.1 Dissolution and scratching

The localised dissolution of a plastic that has been exposed to a compatible solvent results in changes to the appearance of the plastic surface. Dissolution of the plastic combined with mechanical action can result in the appearance of scratches or other defects on the plastic surface. Additives can also be extracted from the plastic [63].

2.5.4.2 Environmental stress cracking

Environmental stress cracking is a common cause of failure for plastic materials [82]. In order for stress cracking to occur, the plastic must be under stress and in the presence of a corrosive liquid. This may be a solvent but may also be an acid or alkali.

While the mechanism of stress cracking is not fully understood it is thought that the solvent diffuses into the plastic and causes localised swelling as the polymer chains move apart [82] (figure 2.16). The increased chain mobility causes a decrease in the stress required to form cracks or crazes. Wetting of the plastic surface is also thought to aid the creation of voids and help to propagate crack formation. Photo-degradation of polystyrene has been observed to lower the stress required for cracking to occur [86]. This is thought to be a result of oxidation increasing the polarity of the polystyrene as well as the reduction in the molecular weight of the polymer.

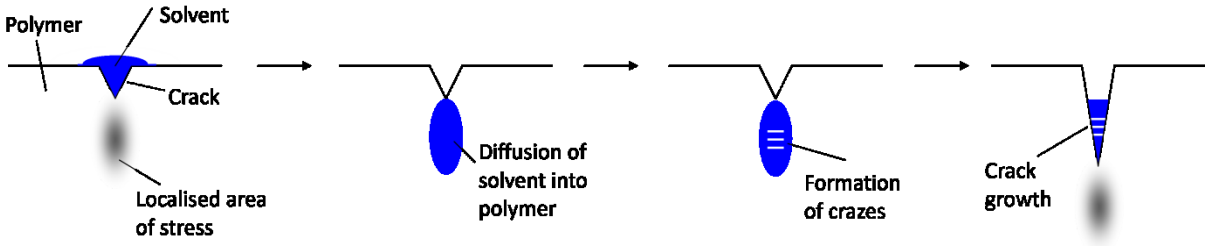

Figure 2.16 Schematic showing the mechanism of environmental stress cracking.

Chapter 3

Analytical techniques

3.1 Introduction

The nature of cultural heritage artefacts does not lend them to straightforward analysis. Often large, bulky, fragile or extremely valuable, it can be difficult to examine artefacts using sophisticated analysis techniques that may potentially cause damage, require vacuum conditions or have maximum size limitations. For this reason, much of the instrumentation used in conservation employs non-destructive analytical techniques that can be used at atmospheric pressure without significant sample preparation. The development of portable instrumentation is an area of great interest due to its potential to be taken to the artefact in question, rather than having to transport an artefact for analysis. In other cases, small samples may be removed for analysis, however this is subject to lengthy conservation protocols. As detailed in Chapter 1, conservation guidelines dictate that any treatment or analysis should be non-destructive and reversible [87].

If sampling does take place, it should also be considered whether the sample is representative of the object in question: a sample removed from the edge of a painting that has been protected by a frame will not necessarily have the same characteristics as an area of the same painting that has been exposed to atmospheric conditions for many years. The question of what exactly constitutes a non-destructive technique is also open for debate. While advanced analytical techniques can remove molecular material from the surface, the amount of material removed can be so small as to be invisible to the naked eye.

This work uses sheet plastics which are commercially available as well as a sacrificial plastic object. For the analyst there are a range of techniques that can be used to characterise the composition and behaviour of polymer materials. In this work, the principal focus lies on the interaction of cleaning agents with the plastic surface. Therefore most of the techniques covered in this section are surface-

sensitive. This section will detail the analytical techniques used in this work to examine the bulk and surface properties of polymeric materials, with reference to their applicability.

3.2 The use of analytical techniques in conservation

The requirements for minimal intervention necessarily means that much of the analytical work performed on artefacts is carried out in-situ, non-destructively and performed at atmospheric pressure. Much of the analysis of plastics and their topography has relied on microscopy techniques. Optical microscopy is widely used to examine objects including plastics and was used to look at the effects of cleaning as part of the POPART project [31]. The effect of cleaning on the surface of PVC has been examined using profilometry [88]. In addition the visual appearance of plastics has been quantified using gloss measurements [31, 33] and colorimetry [88, 89]. Scanning electron microscopy (SEM) is one of the more advanced microscopic techniques used, although due to practical limitations it is used principally to analyse small samples that have been removed from the artefact of interest [90, 91].

The use of attenuated total reflectance Fourier transform infra-red (ATR-FTIR) spectroscopy is also prevalent in conservation science. It has been widely used to examine the composition of plastics, including changes occurring as a result of degradation [83, 92-95]. The composition and identification of historical plastics has also been studied [96]. While less common than ATR-FTIR, Raman spectroscopy has been used to characterise plastics in the conservation environment [97].

Thermal analysis techniques including thermogravimetric analysis (TGA) and differential scanning calorimetry (DSC) have been found to provide information regarding the loss of volatile additives and the presence of degradation products in cellulose acetate [94]. Schilling et al. also used gas chromatography mass spectrometry (GC/MS) to obtain compositional information about cellulose ester plastics and their additives. More recently, the use of GC/MS to analyse and identify volatile organic compounds (VOCs) from degrading plastics has received some attention [19, 20, 98].

More sophisticated surface analysis techniques such as secondary ion mass spectrometry (SIMS), x-ray photoelectron spectroscopy (XPS) and atomic force microscopy (AFM) are rarely used in the practical conservation environment. However, a number of research projects have carried out investigations into heritage materials. These include the use of SIMS to examine corrosion in museum glass [99] and the tarnishing of silver artefacts [100]. The identification and characterisation of degraded polystyrene jewellery [101], the distribution of pigments in a 15th century painting [102] and the identification of historic papers [103] have also been studied using SIMS and XPS. XPS has also been used to study the cleaning of acrylic paints [104], which has enabled the identification of surface residues and modifications. AFM has been used to examine the effect of cleaning on sheet PMMA and to quantify the increase in surface roughness due to polishing [105]. Energy dispersive x-

ray fluorescence spectrometry (XRF) has been used for the non-destructive identification of historic plastics [106].

3.3 Bulk properties

The following sections provide information about the characterisation techniques used to determine the bulk polymer properties. These are of interest due to their ability to characterise the polymer before and after treatment and to determine its composition.

3.3.1 Differential scanning calorimetry

Thermal analysis techniques are used to determine the behaviour of materials with respect to temperature. Of particular interest for thermoplastic polymers are the glass transition temperature (T_g) and the polymer melting point (T_m) as discussed in Chapter 2. Differential scanning calorimetry (DSC) is used to obtain information about the phase transitions of a material. Energy is absorbed by a material when it undergoes a phase change, and is termed the latent heat of fusion for a phase transition from a solid to a liquid. This therefore results in a discontinuity in the specific heat for a first order transition which is not observed for a second order transition, such as the glass transition temperature. The specific heat capacity of the polymer increases at the T_g.

DSC measures the energy required to heat a sample of known mass compared to an empty reference pan and plots the resulting energy as a function of temperature. Figure 3.1 shows three points of interest for polymers on a typical DSC graph: the glass transition, crystallisation and melting temperatures. It should be noted that the y-axis in figure 3.1 is expressed in terms of heat flow which indicates the difference in the heat energy supplied to the reference pan and the sample. In this case, first order endothermic transitions such as melting are identified by a peak in the negative direction. Similarly, first order exothermic transitions such as crystallisation are shown by a peak in the positive direction. As the glass transition is a second order transition it is manifested as a shift in the baseline. The glass transition temperature is commonly calculated as the midway point between the onset and the end of the transition. The DSC instrument used in this work was a Netzsch STA 449 F5 Jupiter (Erich Netzsch GmbH & Co. KG, Germany).

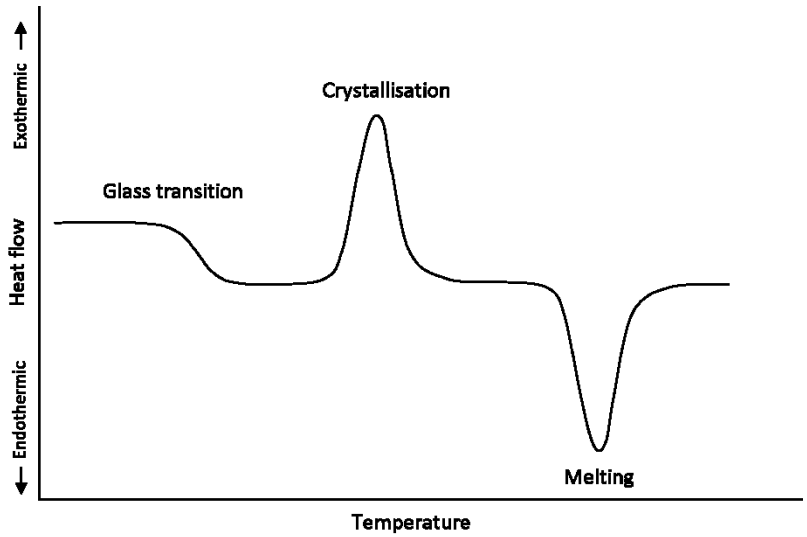

Figure 3.1 Phase transitions observed in a typical DSC plot.

3.3.2 Gel permeation chromatography

Gel permeation chromatography (GPC), also known as size exclusion chromatography (SEC), is used to determine the molecular weight distribution of a polymer. A 1260 Infinity high performance liquid chromatography instrument (Agilent Technologies, USA) was used in this work and a schematic of the GPC process is shown in figure 3.2.

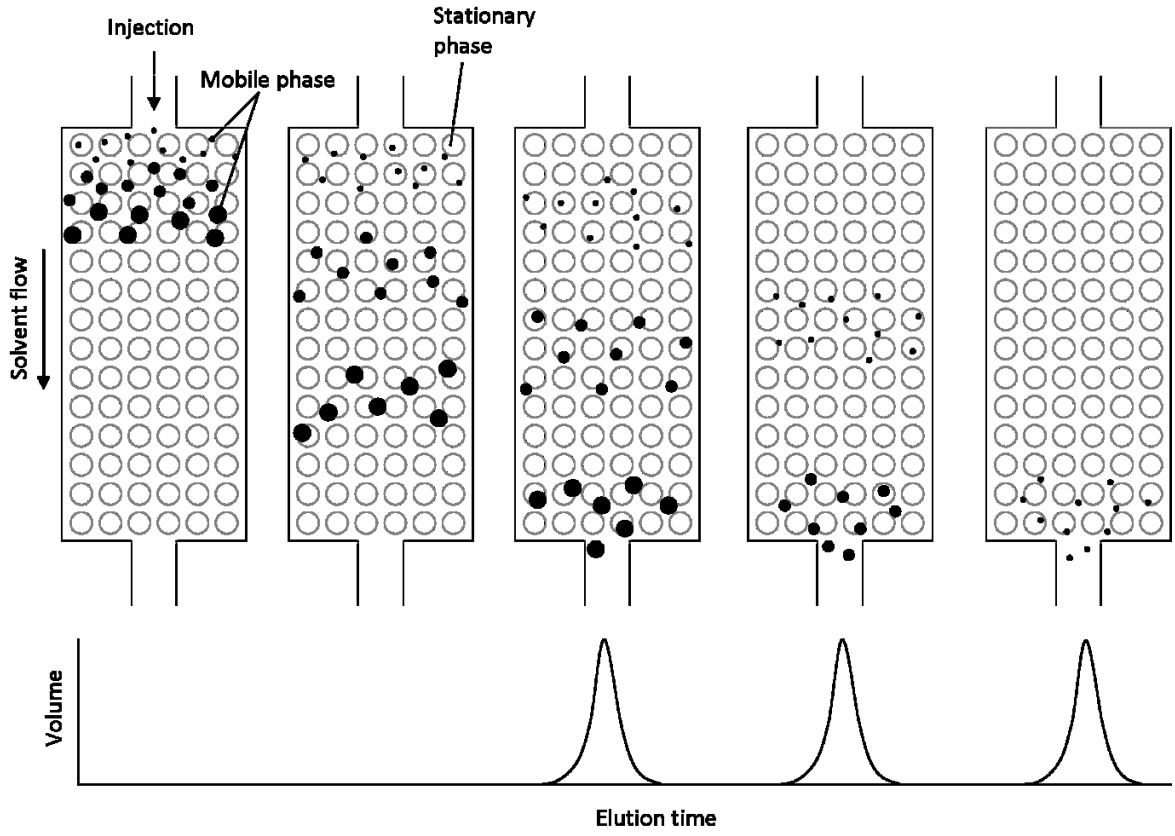

Figure 3.2 Schematic of the GPC process [107]. The filled circles represent the polymer; increasing diameter indicates increasing molecular weight.

Prior to analysis, the polymer under investigation is dissolved in an appropriate solvent such as tetrahydrofuran (THF) and filtered to remove any insoluble material. On dissolution the polymer chains form into balls of diameter corresponding to their molecular weight: a larger diameter corresponds to higher molecular weight. The dissolved polymer is then injected into a stream of flowing solvent, which constitutes the mobile phase, and flows through a column packed with small porous spherical beads which form the stationary phase. These pores are of varying diameters. As the mobile phase flows past these beads, the polymer chains can interact with the beads in several ways depending on their diameter, as shown in figure 3.2. Large polymer chains are unable to enter even the largest pores and are carried to the end of the column by the flowing solvent where they are eluted. Smaller polymer chains may enter some of the pores and therefore take longer to reach the end of the column. The smallest polymer chains can enter all the pores present in the stationary phase and therefore take the longest time to exit the column. A graph of the polymer's molecular weight distribution can therefore be plotted as a function of time, assuming a constant flow rate. The relationship between the elution time and molecular weight is determined by calibrating the instrument using a polymer of a known molecular weight distribution.

3.3.3 Colorimetry

Colorimetry is the measurement of light in the visible part of the electromagnetic (EM) spectrum to determine the perception of colour by the human eye. The percentage of incident light transmitted or reflected by a solid sample is obtained using a dual beam spectrophotometer. A U-4000 dual beam spectrophotometer (Hitachi Ltd., Japan) was used in this work and is shown in figure 3.3.

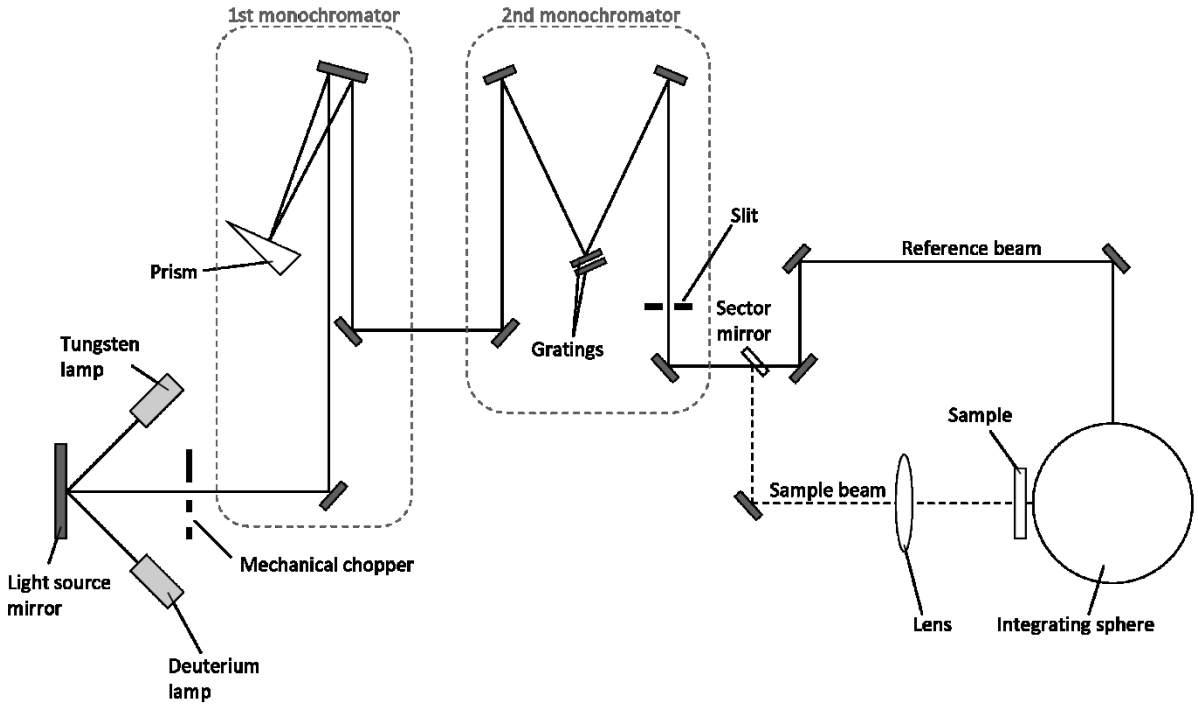

Figure 3.3 Schematic of the optics of the Hitachi dual beam spectrophotometer [108].

Measurement of the visible part of the spectrum incorporates wavelengths in the region 350 nm to 830 nm. It is also possible to obtain data for both the near infra-red and ultraviolet regions of the EM spectrum. Thus the total region measured encompasses wavelengths from 250 nm to 2500 nm, with measurements being taken at intervals of 1 nm. The tungsten lamp is used for wavelengths in the 350-2500 nm region, while the deuterium lamp is used for 250-350 nm wavelengths. Wavelengths are selected in turn via the Littrow prism, which has a reflective coating on the face opposite the 60° angle. A slit defines the width of the incident beam; a narrower width results in increased resolution. The transmitted light is then detected in the integrating sphere. The measurement of transmitted or reflected light is obtained as a percentage of the incident light for each wavelength measured, generating a spectrum over the entire region of interest.

The International Commission on Illumination (CIE) defines standards to accurately measure colour and colour perception. In order to correctly represent the colour observed by the human eye, the raw spectral data undergoes two adjustments. The first adjustment accounts for illumination as the colour perceived by an observer will depend on the light source with which it is illuminated. The CIE standard illuminant D65 [109] is commonly used as it represents the spectrum of average daylight in Europe. The D65 spectrum is shown in figure 3.4.

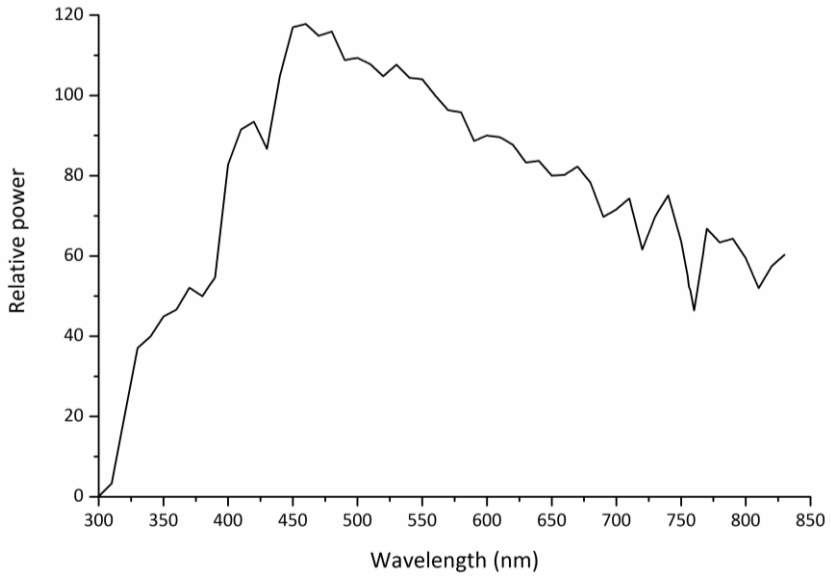

Figure 3.4 D65 illumination spectrum [109].

The second adjustment is performed to account for the human eye. Colour vision in medium or bright light is facilitated by three types of cone cells. The sensitivity of these cells to spectral wavelengths peak in the short (420 nm), medium (530 nm) and long (560 nm) wavelengths of the visible spectrum. Colorimetry defines three colour matching functions: $\bar{x}(\lambda)$, $\bar{y}(\lambda)$ and $\bar{z}(\lambda)$ which describe the sensitivity of the human eye to different wavelengths and which form the CIE standard observer. Two sets of colour matching functions exist. The 2° observer assumes that all cone cells are found within

2° of the fovea (the point of sharpest vision) in the retina and is commonly used for objects that will be viewed from a distance. The 10° observer corresponds to the cone cells being found within 10° of the fovea. In this work the colour matching functions corresponding to the 2° observer are used and are shown in figure 3.5 [110].

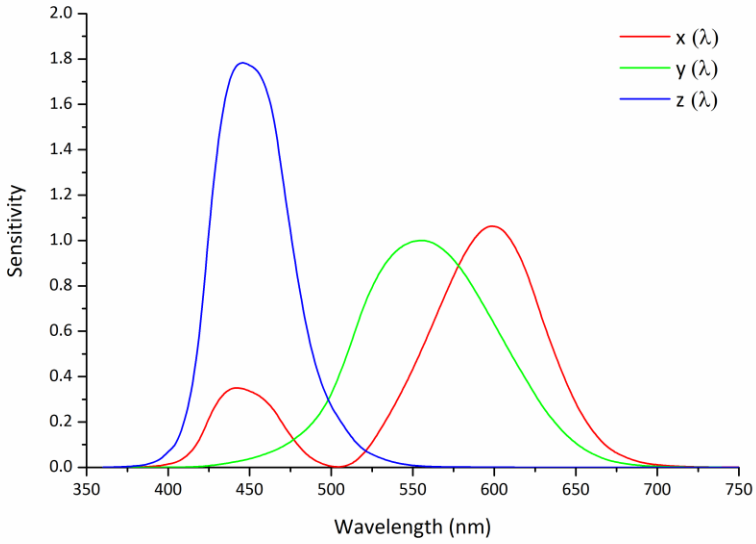

Figure 3.5 CIE (1931) colour matching functions for the 2° observer [110].

It is then possible to find tristimulus values X, Y and Z. These values represent the constituent parts of any colour and a combination of these may represent any colour observed by the human eye. The conversion of the raw spectral data to the tristimulus values is shown in equations 3.1 - 3.3 [111].

$$X = \mathrm{K}\int_{360}^{830} S(\lambda)\bar{x}(\lambda)\tau(\lambda)d\lambda \qquad (3.1)$$

$$Y = \mathrm{K}\int_{360}^{830} S(\lambda)\bar{y}(\lambda)\tau(\lambda)d\lambda \qquad (3.2)$$

$$Z = \mathrm{K}\int_{360}^{830} S(\lambda)\bar{z}(\lambda)\tau(\lambda)d\lambda \qquad (3.3)$$

Where $K = \frac{100}{\int_{360}^{830} S(\lambda)\bar{y}(\lambda)d\lambda}$

S(λ) is equal to the spectral radiance given by illuminant D65, $\bar{x}$, $\bar{y}$ and $\bar{z}$ are the colour matching functions and τ(λ) is the raw transmitted spectrum. The term K normalises the spectra to the total luminance and is performed so that the total luminance of the reference white point is equal to 100.

In practice, the spectral values are obtained at discrete intervals of 1 nm and the above integrals become summations over wavelengths from 360 nm to 830 nm. These tristimulus values are then used

in other representations of colour space. The perception of colour is not only dependent on hue, which is traditionally associated with colour, but is also dependent on chroma, or saturation, and luminance.

The most common representation of human colour perception is the CIELAB colour space which uses three coordinates L*, a* and b*. In this space L* indicates lightness, while a* and b* are antagonistic colour coordinates: a* is commonly described as the red-green colour direction and b* the blue-yellow direction. This does not necessarily mean, however, that a change in b* indicates a change in the yellowness of a sample. Conversion from the tristimulus values to the L*a*b* values is achieved using equations 3.4 - 3.6 [112].

$$L^* = 116f\left(\frac{Y}{Y_n}\right) - 16 \tag{3.4}$$

$$a^* = 500\left[f\left(\frac{X}{X_n}\right) - f\left(\frac{Y}{Y_n}\right)\right] \tag{3.5}$$

$$b^* = 200\left[f\left(\frac{Y}{Y_n}\right) - f\left(\frac{Z}{Z_n}\right)\right] \tag{3.6}$$

Where $f(t) = t^{\frac{1}{3}}$ if $t > \left(\frac{6}{29}\right)^3$

$f(t) = \frac{1}{3}\left(\frac{29}{6}\right)^2 t + \frac{4}{29}$ if $t \leq \left(\frac{6}{29}\right)^3$

X_n= 95.047, Y_n= 100 and Z_n=108.883 for D65 illuminant and are the tristimulus values for the reference white point [112].

The colour difference between two samples is given by the delta E (ΔE) function and can be calculated using several different formulae. The first formula to measure colour change, ΔE^*_{ab}, was defined in 1976 and is given by equation 3.7 [112].

$$\Delta E^*_{ab} = \sqrt{\left(L^*_2 - L^*_1\right)^2 + \left(a^*_2 - a^*_1\right)^2 + \left(b^*_2 - b^*_1\right)^2} \tag{3.7}$$

One of the limitations of the 1976 formula is that it does not correctly model colours which have a high saturation. In order to address this non-uniformity, later formulae for ΔE were refined to define ΔE in terms of lightness (L*), chroma (C*) and hue (h*), which are calculated from L*a*b* values. Figure 3.6 shows the representation of L*C*h* as a coordinate system.

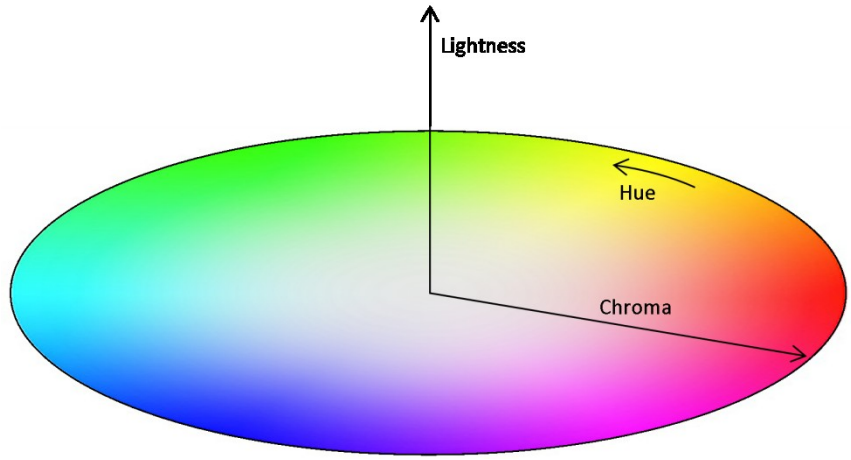

Figure 3.6 Coordinate system for the L*C*h* colour space.

The current recommended formula for ΔE is the CIEDE 2000 definition (ΔE_{00}) defined in equation 3.8 [113].

$$\Delta E_{00} = \sqrt{\left(\frac{\Delta L'}{k_L S_L}\right)^2 + \left(\frac{\Delta C'}{k_C S_C}\right)^2 + \left(\frac{\Delta H'}{k_H S_H}\right)^2 + R_T \frac{\Delta C'}{k_C S_C}\frac{\Delta H'}{k_H S_H}} \qquad (3.8)$$

Where $\Delta L'$ is the change in lightness, $\Delta C'$ is the change in chromaticity and $\Delta H'$ is the change in hue. The parametric factors k_L, k_C and k_H are related to viewing conditions and are usually equal to unity; $S_L, S_c and\ S_H$ are weighting coefficients and R_T is a rotation term.

The equations defining these values in terms of the L*a*b* values are given in Appendix C. A ΔE_{00} value of 1.0 is often said to equate to a 'just noticeable difference' (JND), although the sensitivity of the human eye to colour changes is subjective and depends on the colour in question.

An alternative measurement of colour change is given by the yellowness index. For plastics, this is commonly defined by the ASTM E313 yellowness index (YI) [114] and calculated using equation 3.9. Positive values of YI indicate yellowing of the substrate.

$$YI = 100\frac{C_x X - C_z Z}{Y} \qquad (3.9)$$

Where C_x = 1.2985 and C_z = 1.1335 for a 2° observer and D65 illuminant [114].

3.3.4 Hardness testing

The mechanical properties of plastics are affected by their composition and structure. Over the lifetime of an object these properties may change as a result of degradation. A range of mechanical properties can be measured depending on the behaviour of interest. The hardness of the materials is of particular interest for treatments affecting the surface of plastics. This may be defined as a material's

resistance to plastic deformation and is measured using an indenter. The Vickers micro-hardness of a substrate can be determined using a diamond pyramid indenter with low weight loads. This creates a diamond indentation on the surface as in figure 3.7; measurement of the diagonals is then performed to obtain a value for the Vickers Hardness Number (VHN) using equation 3.10. The 136° term relates to the angle between opposite faces of the square pyramid indenter and F is the force applied. Higher VHN values indicate a greater resistance to deformation and therefore greater hardness. This work used a Zwick Roell Indentec ZHV hardness testing machine (Zwick Roell, Germany) with a load of 100 g and a loading time of 10 s.

Figure 3.7 Schematic of the diamond indentation used to calculate the Vickers hardness.

3.4 Surface properties

The surface properties of plastics are of particular interest in this work due to their potential to be affected by the application of cleaning treatments. The characterisation techniques outlined in this section range from low magnification microscopy to highly sensitive analytical techniques, yet all provide valuable information about the sample surface. Analytical techniques for both physical and chemical properties of the surface are considered. Table 3.1 shows a comparison of the surface sensitivity of the techniques used in this work.

Table 3.1 Typical information depths and resolution limits for the techniques used in this work.

	Information depth	**Lateral resolution**	**Vertical resolution**
Optical microscopy	-	1 µm	5 µm
White light interferometry	-	1 µm	2 nm
AFM	-	1 nm	2 nm
FEG-SEM	-	1 nm	3 nm
ToF-SIMS	1 nm	1 µm	1 nm
SEM-EDX	1 µm	-	-
ATR-FTIR	1 µm	-	-

3.4.1 Light optical microscopy

Light optical microscopy is one of the most common techniques used to examine the surface of a material. It is widely used in conservation due to its ease of use, relatively low cost and the fact that it is a non-contact method. The optical microscope used in this work was an Olympus BX51 (Olympus Corporation, Japan), operated in reflected light mode.

In an optical microscope light travels through a series of lenses to illuminate the specimen under examination. Depending on the mode of operation, light is then either transmitted through the sample or reflected from the sample surface, a mode that is also known as epi-illumination. Light then passes through the objective lens to a binocular field of view or alternatively to a digital camera which records an image of the surface under investigation. The use of apertures and diaphragms refines the degree of brightness and contrast in the image.

The common limitations of light microscopy are the objective magnification and the surface roughness. Due to the relatively large convergence angle, the depth of field is of the order of several microns, and decreases with increasing magnification. This means that light microscopy is generally unsuitable for imaging rough surfaces at high magnification. In order to address this limitation, the Olympus BX51 can be operated in extended focal imaging (EFI) mode, where the topography of the surface is built up through the capture of successive images in the z direction.

The lateral resolution is commonly defined by the Rayleigh criterion which says that two point light sources can be resolved if the centre of the Airy disk from one source overlaps with the first minimum of the second source. The minimum resolvable distance between two points (r) is given by equation 3.11.

$$r = \frac{1.22\lambda}{2n\sin\theta} = \frac{0.61\lambda}{NA} \tag{3.11}$$

Where λ is the wavelength of light, n is the refractive index of the medium (n=1.00 for air), θ is the half angle of the light entering the objective and NA is the numerical aperture = $n\sin\theta$.

3.4.2 White light interferometry

White light interferometry is another non-contact technique which can be used to examine surface topography and is a very common mechanism for optical profilometry. A Zygo NewView 200 Mirau white light interferometer (Zygo Corporation, USA) was used in this work and a schematic of the principle is shown in figure 3.8. A beam of white light is collimated prior to travelling to a beam splitter, where it splits into two paths. One path is reflected by the specimen while the other is reflected by a reference surface situated at a known distance from the beam splitter. The two beams are then recombined by the beam splitter and travel to a camera. The optical path length difference

between the two waves is dependent on the distance travelled by the specimen path compared to the reference path. Due to the low coherence of white light these path lengths must be very similar to be able to observe constructive interference. Constructive interference occurs when the path length difference is zero and results in maximum contrast between the bright and dark fringes. This is the point at which the specimen is in focus; all regions in focus at the same point are therefore at the same height. Moving the specimen relative to the beam splitter results in constructive interference over the entire vertical range under evaluation, from which the relative heights of surface features can be found. The area under examination is illuminated by one or two fringes to achieve high resolution.

The limitations of white light interferometry stem from the surface roughness and reflectivity. If the angle of the surface under investigation is too high then light will not be reflected back into the lens and no data will be collected. For the interferometer used in this work the slope limit is 7.51° [115] for a ×10 objective. Similarly light absorbing materials may be difficult to image. Transparent samples can result in secondary fringes appearing from the reverse side of the sample.

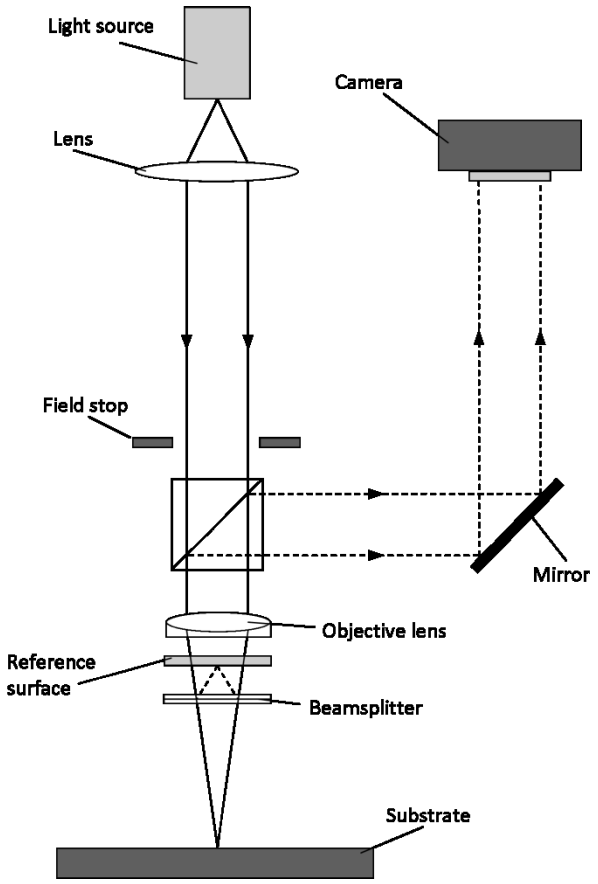

Figure 3.8 Schematic of the Zygo NewView 200 white light interferometer [115].

3.4.3 Attenuated total reflectance Fourier transform infra-red spectroscopy

Attenuated total reflectance Fourier transform infra-red spectroscopy (ATR-FTIR) is commonly used in conservation to identify the composition of many materials, including plastics. While the infra-red

region of the electromagnetic spectrum ranges from wavelengths of 700 nm to 1 mm, FTIR typically uses infra-red radiation in the mid-range of 2.5 μm - 25 μm ($1/\lambda$ = 400-4000 cm^{-1}) which is absorbed by the sample at frequencies which are characteristic of its molecular structure.

Due to the constant motion of their constituent atoms, molecules constantly vibrate at discrete frequencies which are characteristic of their composition. The number of vibrational modes for a molecule is known as the vibrational degrees of freedom and is equal to 3N - 5 for linear molecules and 3N - 6 for non-linear molecules, where N is equal to the number of atoms. These vibrations may take several configurations, shown in figure 3.9. Stretching vibrations are characterised by a change in bond length and may be symmetric or asymmetric. Bending vibrations result in a change in bond angle and may be termed as scissoring, wagging, rocking or twisting vibrations.

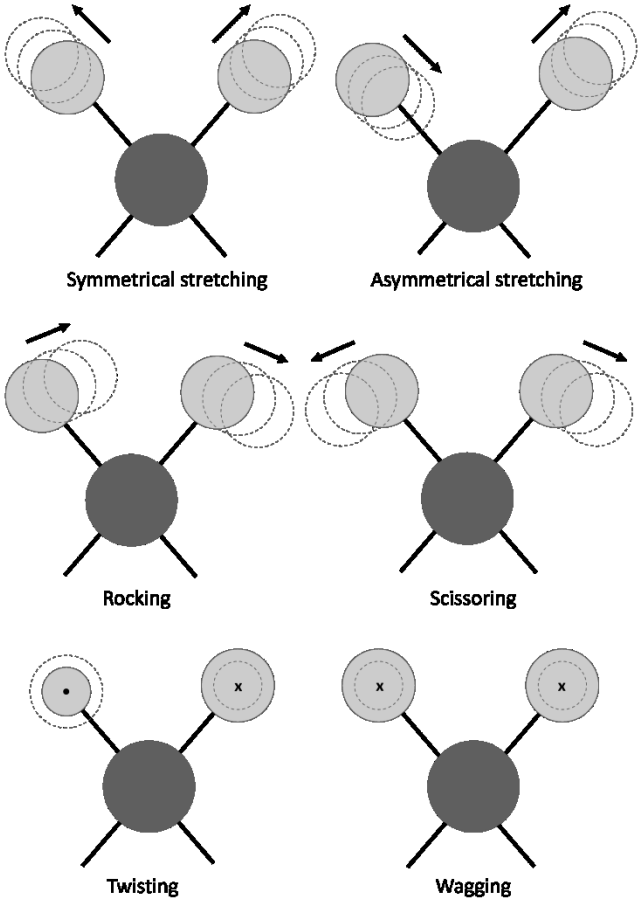

Figure 3.9 Bond vibrations for a methylene group [116]. The motion of C is not indicated here but the C atom undergoes a small displacement to conserve energy. Motion is indicated by the arrows. x indicates motion into page, • indicates motion out of page.

The absorption of infra-red radiation is only seen for molecular vibrations that cause a net change in dipole moment. If the frequency of incident radiation corresponds to the vibrational frequency of the interatomic bond, then the radiation will be absorbed and will result in a change in the amplitude of

the vibration. Diatomic molecules such as O_2 do not display characteristic absorption as their symmetry means that they do not experience a net change in dipole moment.

3.4.3.1 Factors affecting the FTIR spectrum

The frequency at which radiation is absorbed is dependent on the masses of the atoms involved. The molecular vibrations can be modelled by considering a physical system, namely that of a ball and spring model as shown in figure 3.10.

Figure 3.10 Ball and spring model for molecular vibrations.

In the case where two masses, m_1 and m_2, are connected by a lossless vibrating spring, the frequency of the vibration (υ) is given by Hooke's law, as in equation 3.12 [116].

$$\upsilon = \frac{1}{2\pi}\left(\frac{k(m_1 + m_2}{m_1 m_2}\right)^{\frac{1}{2}} \tag{3.12}$$

Where k is the force constant and m_n is the mass of atom n.

Therefore, at a constant force constant, smaller masses result in absorption at higher frequencies and shorter wavelengths (λ). The attachment of another atom can result in a change in the force constant despite the same masses being involved. Double bonds have a higher force constant and so vibrate at higher frequencies. The limitations of this model arise as Hooke's law describes simple harmonic motion which is not true at large displacements. At short interatomic distances the potential energy of the molecule rises sharply due to Coulombic repulsive forces while at long distances the bond weakens and eventually breaks.

The intensity of spectral bands is dependent on the change in dipole moment with respect to bond distance. The width of spectral bands can vary from narrow to very broad and is a result of the chemical environment. Strong intermolecular interactions such as hydrogen bonding cause broadening of the bands. The varying number and strength of hydrogen bonds in water, for example, results in a wide range of values for the force constant k, which in turn results in a broad frequency range.

One of the characteristics of an FTIR spectrum is that functional groups absorb frequencies in the same range, regardless of their chemical environment [49]. These group frequencies enable the identification of unknown samples. Figure 3.11 shows the typical bands observed in an FTIR

spectrum. By convention the x-axis of an FTIR spectrum is defined as the wavenumber ($1/\lambda$) and is numbered in order of decreasing wavenumber. The 1200-700 cm^{-1} region is known as the fingerprint region due to its ability to identify spectral bands that are uniquely characteristic of the sample under investigation.

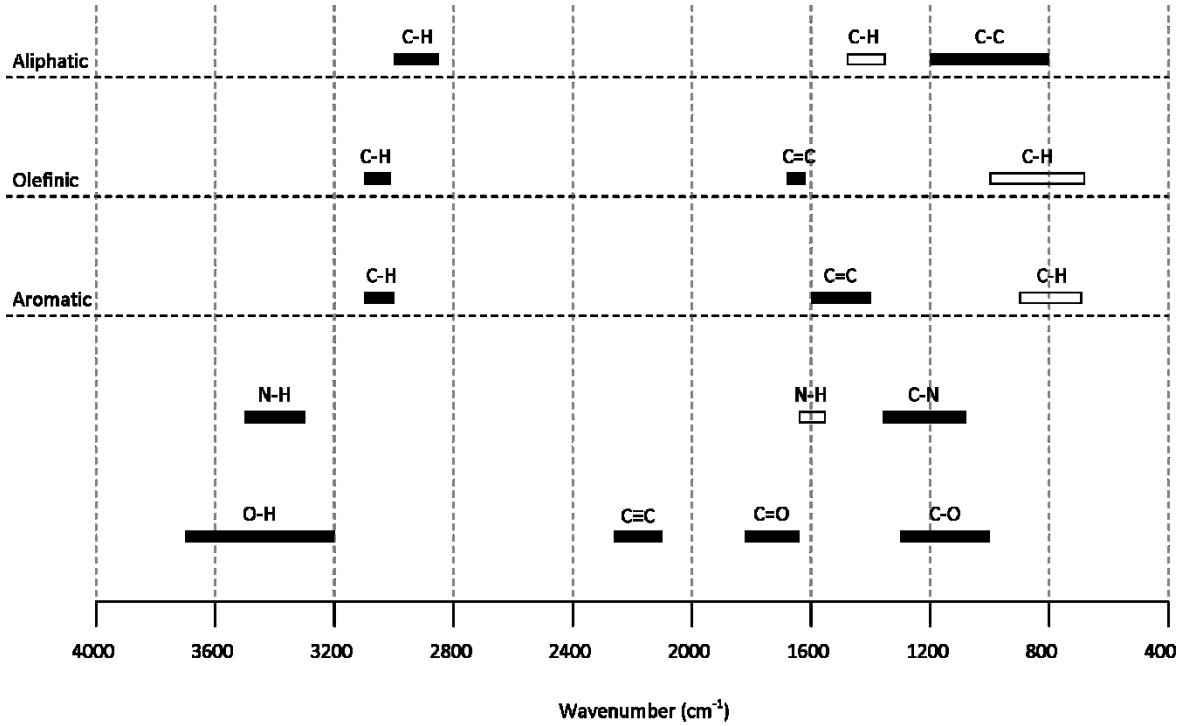

Figure 3.11 Typical FTIR bands (adapted from [49]). Filled bands represent stretching vibrations, unfilled bands represent bending vibrations.

3.4.3.2 ATR-FTIR instrumentation

The ThermoFisher Nicolet iS10 spectrometer (Thermo Fisher Scientific Inc., USA) was used in this work and a schematic of the ATR-FTIR process is shown in figure 3.12. Incident infra-red radiation is typically generated by heating a silicon carbide rod. The radiation then travels to an interferometer where it is split via a beam-splitter to produce two beams, one of which travels to a fixed mirror while the other travels to a moveable mirror. This configuration means that a changing optical path difference can be continuously created between the two beams; recombination of the beams results in the formation of a sinusoidal signal, an interferogram, that varies in intensity due to constructive and destructive interference.

The interferogram then enters an ATR crystal of high refractive index, commonly germanium or diamond, at an angle of approximately 45° and undergoes total internal reflection at the interface between the crystal and a sample of a lower refractive index. An evanescent wave is formed at the interface between the crystal and the sample which extends orthogonally into the sample and which

decays exponentially with depth. For this reason, samples must be held in close contact with the crystal; any air gap will result in a poor quality or non-existent signal. As some wavelengths of the infra-red radiation are absorbed by the sample, the wave is attenuated and the reflected radiation is returned to the detector. The infra-red radiation can undergo multiple internal reflections as shown in figure 3.12 which results in increased sensitivity. After the radiation exits the sample the detector measures the energy of the radiation as a function of time. This is then converted into a spectrum of energy as a function of frequency, and therefore wavenumber, using a Fourier transform.

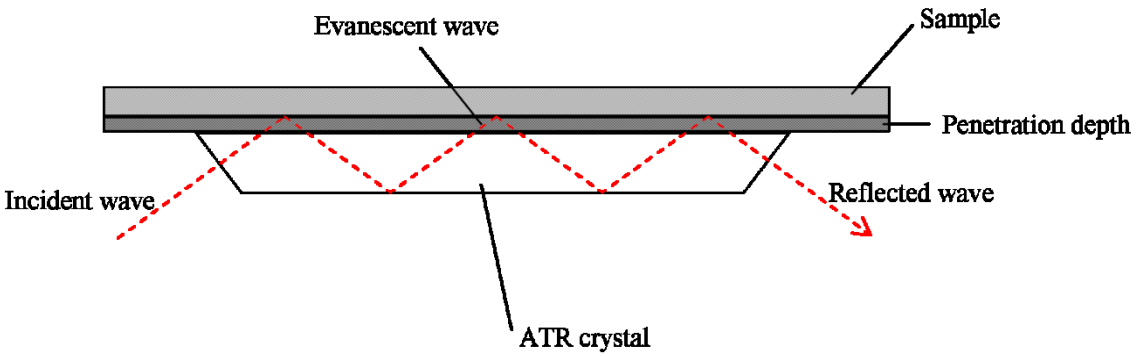

Figure 3.12 Schematic of the ATR-FTIR process.

The penetration depth (d_p) depends on the wavelength of light (λ), the angle of incidence (θ) and the refractive indices of the crystal (n_1) and sample (n_2) as shown in equation 3.13. It is defined as the distance at which the electric field amplitude has decayed to $1/e$ of its original value and is typically of the order of 0.5 µm - 5 µm [117].

$$d_p = \frac{\lambda}{2\pi\left(n_1^2 \sin^2\theta - n_2^2\right)^{\frac{1}{2}}} \tag{3.13}$$

The refractive indices of diamond and germanium at 20°C are 2.4235 and 4.0032 respectively [118]. A germanium crystal is necessary for samples having a refractive index greater than 2.4 or total internal reflection will not occur. The refractive indices of the plastics studied in this work, PMMA and polystyrene are 1.490 (20°C) and 1.590 (20°C) respectively [53] and therefore analysis is possible with a germanium crystal.

3.4.4 Scanning electron microscopy

Scanning electron microscopy (SEM) is a common high vacuum technique used to examine surface topography and composition. In a conventional SEM, electrons are thermionically generated from a tungsten or LaB_6 filament. The SEM used in this work was a LEO Gemini 1525 FEG-SEM (Carl Zeiss AG, Germany). This instrument differs from a conventional SEM in that it generates electrons

via the application of an electric field (field emission). This produces a highly coherent beam with a higher current density than conventional thermionic emitters. The main advantages of using a field emission gun (FEG) are increased spatial resolution and increased signal-to-noise ratio.

Following emission, the electrons are focused by the Wehnelt cap and accelerated towards the sample through the electron column. A series of electromagnetic lenses focus the beam and direct it towards the sample surface (figure 3.13). The electron beam is scanned over the sample in a raster pattern to build up an image of the surface.

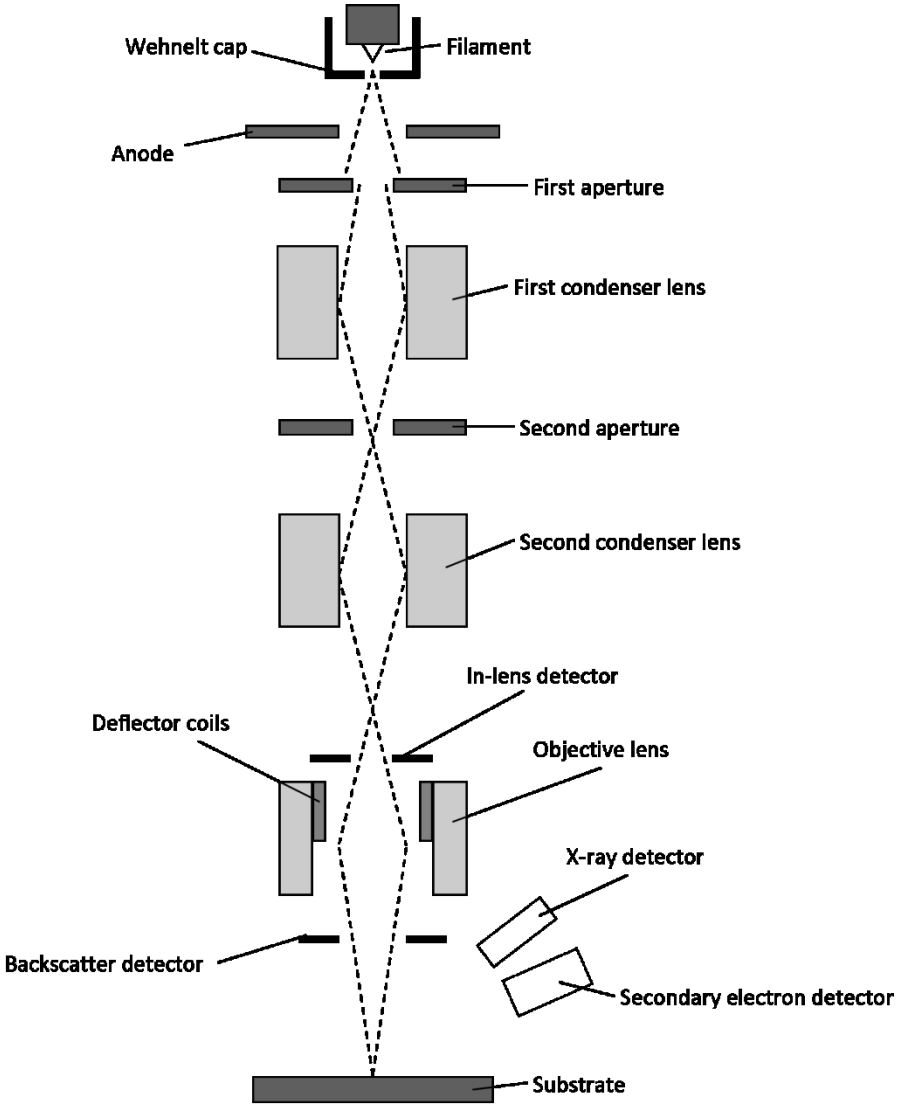

Figure 3.13 Schematic of an SEM instrument.

On impact, the incident electrons undergo elastic and inelastic interactions with atoms in the surface and subsurface layers. Inelastic collisions result in the ejection of low energy secondary electrons ($E \leq 50$ eV), which originate from electrons in the outer shell. Due to the energy required to escape the surface, only those secondary electrons from the topmost surface layers (usually 2-5 nm) will reach the detector and therefore the information provided by secondary electrons is surface specific.

Type 1 secondary electrons (SE1) are generated by the incident electrons and originate from the area close to the point of impact. Therefore they contain high resolution information about the sample surface. Type 2 secondary electrons (SE2) are generated by collisions with backscattered electrons, that is incident electrons that are elastically scattered by interactions with atoms in the sample. The SE2 electrons therefore contain both topographical and elemental information. Due to these collisions, the SE2 electrons arise from a greater volume than the SE1 electrons and therefore they provide information of lower resolution. Secondary electrons can be detected either by a conventional secondary electron detector or by an in-lens detector. The in-lens detector predominately detects SE1 electrons while both SE1 and SE2 electrons are detected by the conventional detector [119].

The in-lens detector is positioned inside the electron column, such that it detects secondary electrons that are ejected from the sample at high angles. A conventional secondary electron detector is positioned on one side of the sample chamber. A positive bias on the front of the secondary electron detector ensures that electrons from the surface and sub-surface regions are attracted towards the detector. The positioning of the detector at the side of the chamber means that electrons resulting from surfaces facing towards the detector are more likely to be collected than those facing away, resulting in the acquisition of topographical information.

Elastic scattering results in the ejection of incident electrons back out of the sample. These backscattered electrons are typically of high energy and scatter at high angles. Atoms with a higher atomic mass have a greater cross sectional area and the probability of an incident electron interacting with these larger atoms is therefore greater. Consequently a greater number of backscattered electrons are detected from heavier elements, resulting in increased brightness and enabling rudimentary elemental analysis. The backscattered electron detector is positioned above the sample, in a toroidal configuration such that it collects electrons from all areas of the sample. As well as secondary and backscattered electrons, other species are produced, including x-rays and Auger electrons. The generation and analytical value of x-rays is discussed in section 3.4.4.4.

3.4.4.1 Interaction volume

The interaction volume is the volume of the substrate which interacts either directly or indirectly with the incident electron beam and which defines the type and quality of the information received. This volume increases with accelerating voltage and decreases with increasing atomic number. Therefore the energy of the electron beam is integral to the information obtained from the surface.

A lower accelerating voltage means that the electrons do not travel very far into the sample, resulting in a small interaction volume. Therefore many of the secondary electrons are generated by the incident beam (SE1) and contain high resolution surface information. However, a very low accelerating voltage (typically <1 kV) will cause a decrease in the number of secondary electrons with

sufficient energy to escape the surface, reducing image quality. A higher energy results in the penetration of the beam further into the sample, creating a large interaction volume. Therefore many of the electrons escaping the surface are generated through collisions with backscattered electrons, resulting in the production of more SE2 electrons. These can degrade image quality and cause the loss of surface-specific information. However, the total yield of secondary electrons falls at higher incident beam energies as they are generated deep in the material and do not have sufficient energy to escape. In contrast, backscattered electrons have higher energies and can leave the material. X-rays have even higher energies and consequently contain information from greater depths. The interaction volume of the electron beam and the depths from which the different species originate are shown in figure 3.14.

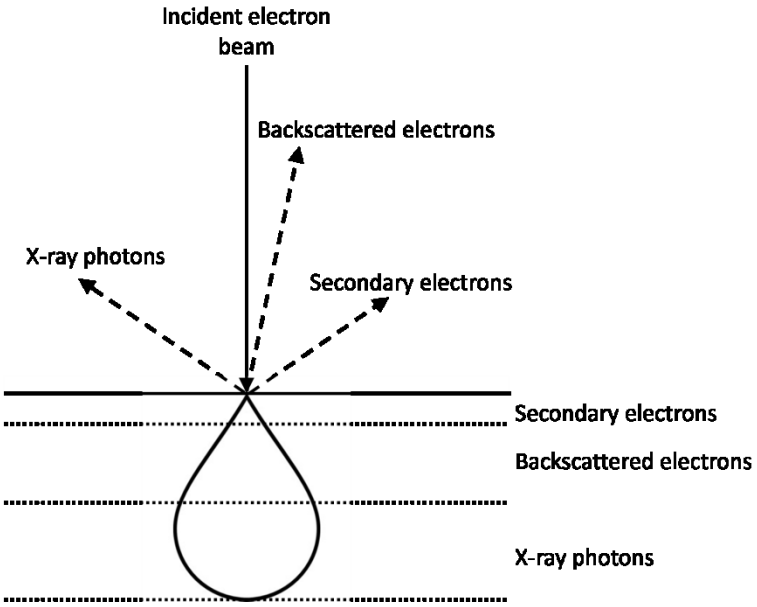

Figure 3.14 Schematic showing the interaction volume and the production of species of interest with depth.

One of the advantages of SEM is that samples can be imaged at much higher magnifications than is possible with light microscopy. The depth of field is also significantly increased and is a result of the smaller convergence angle, which is itself a result of a small aperture size. The spot size of the beam affects the size of the interaction volume and therefore the resolution of the SEM. A smaller spot size results in increased resolution but may be accompanied by a decrease in image quality.

3.4.4.2 Sample preparation

One of the most common issues encountered during SEM analysis is the build-up of charge on the sample surface. This is commonly seen for insulating materials and is due to primary electrons being deposited on the surface, resulting in an excess of negative charge. Charging can be manifested as white lines appearing across the image or the appearance of areas of high contrast. In order to minimise the build-up of charge on an insulator such as a plastic, samples are routinely coated with a

thin layer of a conductive metal such as gold or chromium. While gold is commonly used, chromium is more suited for the acquisition of higher magnification images due to the lower grain size.

Sample coating is achieved using a sputter coater. The sample is placed in a sputter chamber which is then pumped down to low vacuum. Argon gas is bled into the chamber once a sufficiently low vacuum is achieved. The application of a high potential to argon gas results in ionisation and the production of argon ions. These bombard the metal target, resulting in the ejection of metal atoms which then deposit on the substrate surface. Surface coatings are typically of the order of 10-20 nm in thickness. A Quorum Emitech K550 sputter coater (Quorum Technologies, UK) was used in this work for gold sputtering (99.99% purity) and a Quorum Q150T S sputter coater (Quorum Technologies, UK) was used for chromium (99.99% purity).

3.4.4.3 Sample damage

The exposure of polymeric materials to the electron beam can result in severe damage to the surface. This is particularly true for polymers such as PMMA, where the presence of a quaternary carbon atom in the polymer backbone renders the polymer more vulnerable to chain scission [55]. In order to minimise damage to polymeric materials, a low accelerating voltage in the region of 5 kV is commonly used. Lower accelerating voltages will result in less damage to the surface but will also decrease the intensity of the resulting image.

3.4.4.4 Energy dispersive x-ray analysis (EDX)

As well as the production of secondary electrons, the interaction of primary electrons with the surface results in the production of x-rays as shown in figure 3.14. These are produced as a result of the incident electrons undergoing inelastic atomic collisions which remove an electron from one of the inner shells. This creates a hole which is filled by an electron from an outer shell. The movement of the electron is accompanied by the emission of an x-ray which has an energy that is equal to the energy difference between the two shells. Therefore, the energy of the x-ray is directly related to both the atom from which it originates and the shells involved, allowing elemental analysis. An INCA energy dispersive spectrometer (Oxford Instruments, UK) was used in this work.

3.4.5 Atomic force microscopy

Atomic force microscopy (AFM) is a technique that can be used to gain topographical information at the nanometre scale. A schematic of the AFM technique is shown in figure 3.15.

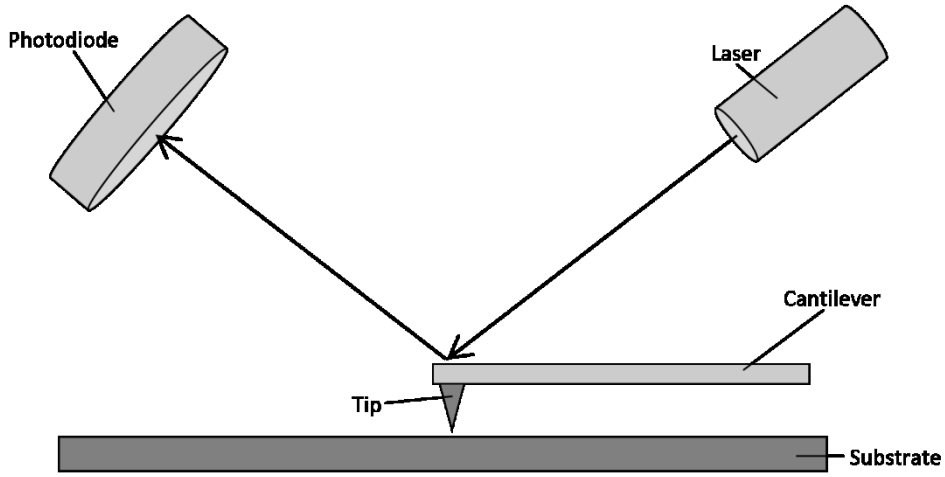

Figure 3.15 Schematic of the AFM technique. The arrows indicate the direction of the laser beam.

In contact mode the AFM operates using a cantilever that is continually in contact with the surface. As the cantilever moves over the surface, the tip follows the topography of the surface. The vertical deflection of the cantilever is measured using a laser which is reflected off the tip of the cantilever to a position-sensitive photodiode. In this work a Bruker Innova (Bruker Corporation, USA) atomic force microscope was operated in tapping mode. In this mode the cantilever vibrates at a resonant frequency and does not come into contact with the surface. The force between the tip and the sample is primarily the net result of the repulsive Coulombic force and the attractive Van der Waals forces experienced by the tip as it moves over the surface. This net force causes a change in the amplitude of the cantilever's oscillation and a feedback loop records the height adjustment required to maintain a constant amplitude of oscillation. As the tip is not in contact with the sample there is a reduced likelihood of surface damage due to the movement of the cantilever over the surface. The instrument can obtain a range of high resolution surface-specific information, but the most common are the surface topography and phase contrast.

3.4.6 Time-of-flight secondary ion mass spectrometry

Time-of-flight secondary ion mass spectrometry (ToF-SIMS) is a highly sensitive surface analysis technique used to determine the chemical composition of the surface. First developed in the late 1960s, SIMS is an ultra-high vacuum (UHV) technique which uses high energy ions to liberate atomic and molecular species from the surface of a sample under investigation. A schematic of the TOF.SIMS 5 instrument (ION-TOF GmbH, Germany) used in this work is shown in figure 3.16.

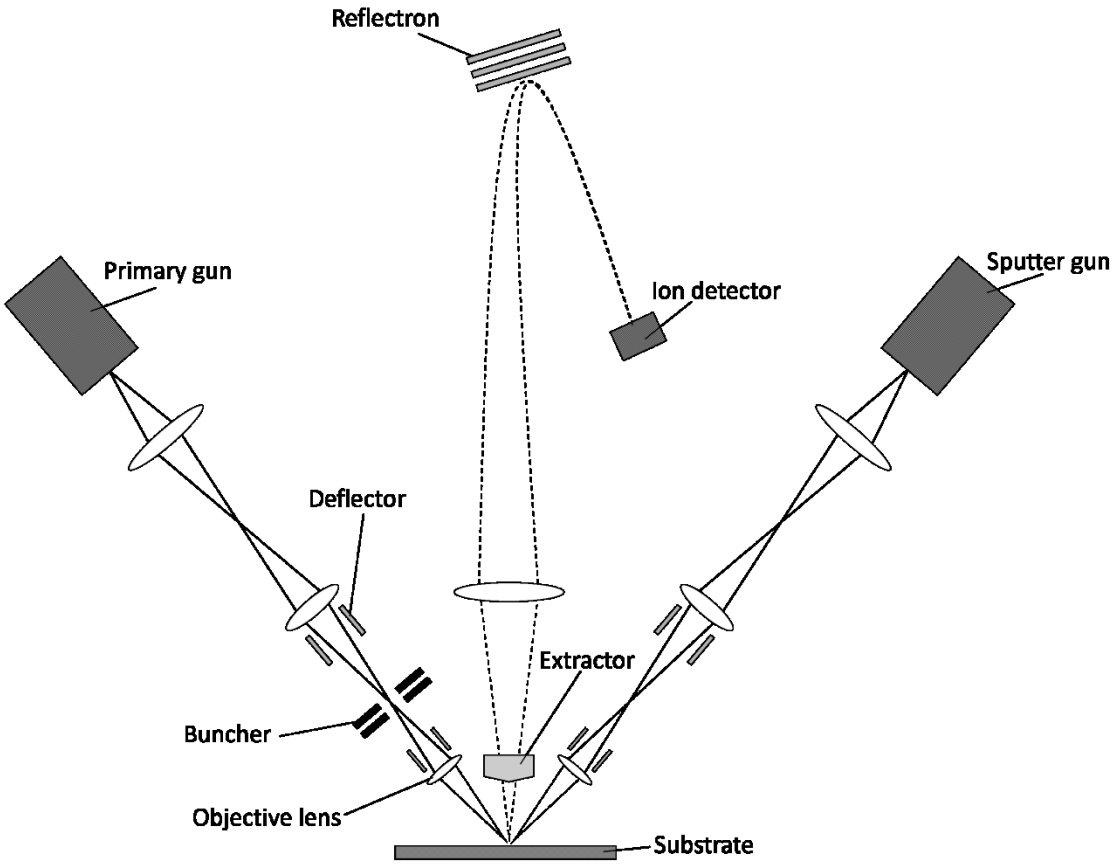

Figure 3.16 Schematic of a ToF-SIMS instrument. Dashed lines represent secondary ions from the sample.

The primary ions are liberated from a bismuth liquid metal ion gun (LMIG) by field emission and accelerated in short pulses towards the sample. The spot size of the resulting ion beam can be as small as 10 nm in diameter [120]. An arrangement of apertures and electrostatic lenses focuses the beam onto the sample. Each pulse of primary ions impinges on the sample and collides with atoms and molecules present on the surface, which in turn collide with other atomic species present, setting up a cascade. The primary ions may undergo a number of inelastic collisions which are accompanied by a transfer of energy.

When the energy of the sample species is greater than the surface binding forces they are liberated from the surface [121]. These species are ejected from the top few monolayers of the surface, which is the root of SIMS characteristic surface sensitivity. The interaction volume of the incident ions depends on the beam composition, with higher energy ions penetrating further into the material.

The sputtered species include neutral molecules, atoms, radicals, electrons and ions. The latter are created either through the initial breakage of chemical bonds or through subsequent interactions with other species and are termed secondary ions. They may be positively or negatively charged and are characteristic of the sample surface. The probability of ionisation is dependent on the atoms'

ionisation energy or electron affinity for positive and negative ions respectively [122]. Oxygen predominately forms negative ions whereas alkali metals such as Na and K have a low ionisation energy and form positive ions [122].

In this work, detection of the liberated ions is achieved by accelerating the secondary ions towards a time-of-flight (ToF) detector. All ions ejected from the surface have a kinetic energy (E_K) as in equation 3.14 [123].

$$E_K = \frac{1}{2}mv^2 = eV \tag{3.14}$$

$$t = \frac{d}{v} = d\sqrt{\frac{m}{2eV}} \tag{3.15}$$

Where m is the mass of the ion, v is its velocity, e is its charge, V is the potential difference between the surface and the detector, t is the time taken for the ion to arrive at the detector and d is the distance travelled.

It can be seen that due to the differing atomic masses of the liberated species, the travel times of ions of the same charge differ as per equation 3.15. However, secondary ions of the same mass/charge ratio are emitted from the surface with differing kinetic energies. In order to compensate for this, the instrument contains a reflectron which is set to either a negative or positive electrostatic potential, depending on the polarity of the ions of interest. Ions with a higher energy will travel a greater distance before they are deflected and therefore all ions with the same mass/charge ratio arrive at the detector at the same time [123]. This improves the mass resolution of the system.

Detection of the ions results in a spectrum of intensity as a function of atomic mass to charge ratio (m/z). The majority of species liberated from the surface are singly charged, therefore the spectrum can be considered to give the atomic masses of the fragments of interest. The intensity of the secondary ions is dependent on a number of factors. The basic SIMS equation is given by equation 3.16 and relates the intensity of the sputtered species to the incident ion beam, the material under investigation and the instrumental parameters.

$$I_s^x = I_p C_x S\gamma F \tag{3.16}$$

Where I_s^x is the secondary ion current for species x, I_p is the primary ion current, C_x is the concentration of species x, S is the sputter ion yield, γ is the ionisation efficiency and F is the transmission of the analysis system [124].

While the intensity of the species of interest is dependent on its concentration, SIMS is not a quantitative technique due to the presence of matrix effects. The chemical environment of the ions of interest can act to suppress or enhance their ionisation and can therefore affect their detection. For example, electronegative species such as oxygen can enhance the yield of positive ions. However, in some cases the use of known standards can be used to quantify the data obtained.

The sputter yield and the ionisation efficiency are influenced by both the incident ion and the material under investigation. The sputter yield is the amount of material removed from the surface during analysis. Incident ions with greater mass and energy result in a greater sputter yield [124]. However the yield also varies according to the element with which the incident ion interacts, and can vary significantly over the periodic table [124]. The impact of ions on the substrate can also damage the surface either due to implantation of the primary ions in the surface or as a result of the mixing of surface and bulk species due to secondary collisions in the subsurface layer. An energy of 25 keV is commonly used for the analysis beam.

In a similar way to SEM, the influx of ions to the sample surface can result in the build-up of charge on insulating materials. For this reason an electron flood gun is used to stabilise the surface. Charging can result in a deterioration in mass resolution [124].

3.4.6.1 Ion formation

Secondary ions are formed via a number of mechanisms: the gain or loss of an electron to form molecular ions (M^+ or M^-), via protonation or deprotonation, the loss of functional groups and catonisation [125].

Protonation and deprotonation

Protonation refers to the addition of a proton (H^+) to an atom or molecule. This commonly occurs for molecules containing basic groups [125]. Deprotonation, the loss of a proton, commonly occurs with molecules containing acidic groups such as carboxylic groups [125]. In SIMS spectra, the presence of a protonated or deprotonated molecule is detected by the presence of fragments of the form $[M+H]^+$ or $[M-H]^-$.

Loss of functional groups

Fragmentation of molecules tends to take place at weak linkages in the polymer chain. PMMA demonstrates the formation of $[M-CH_3]^-$ ions due to scission of the methyl group from the side chain [126].

Cationisation

The attachment of a cation to a molecule may result from impurities, such as Na and K or from metal ions in the substrate [125]. The resulting ion is of the form $[M+Na]^+$.

3.4.6.2 Sensitivity and resolution

Due to the emission of secondary ions from the topmost monolayers, SIMS is a highly surface sensitive technique: the vertical resolution is of the order 1 nm. The lateral resolution for organic materials can reach sub-micron values [127] but is dependent on the mode of operation. High mass resolution ($m/\Delta m$) is achieved by using very short pulse durations. This allows greater temporal separation of the secondary ions and therefore greater resolution. In a TOF.SIMS 5 instrument this is achieved by operating the instrument in the high current bunched mode (HCBM). However, the lateral resolution is reduced to a few microns in this mode [120]. SIMS may be used to either obtain chemical information from the surface or as a function of depth. These modes of operation are known as static SIMS and dynamic SIMS respectively.

3.3.6.3 Static SIMS

Static SIMS is the term given to the acquisition of spectra from the surface. Below an ion dose limit of 10^{12} ions cm^{-2} for polymer materials [121], known as the static limit, it is considered that only approximately 10% of the surface is impacted by the primary ion beam [120]. Significant damage to the substrate, excepting the sputtered layer, should not occur below this limit. In this case, the technique can be said to be essentially non-destructive.

Common issues encountered during the SIMS analysis of polymer materials include edge effects which occur when the analysis site is too close to the edge of the sample or another material. There can also be problems with uneven or excessive charging of the plastic; this may be improved by increasing the cycle time to enable charge to dissipate from the surface. Alternatively, a larger analysis area can be chosen.

3.4.6.4 Dynamic SIMS

Dynamic SIMS is used to obtain information concerning the change in the chemical composition of the sample as a function of depth. In order to achieve this a second, sputter ion beam is used in conjunction with the primary analysis ion beam. This sputter beam removes successive layers of material to expose a new surface. Alternate use of the analysis and sputter beams enables the formation of a depth profile detailing the chemical composition of the sample as successive layers are removed, as in figure 3.17.

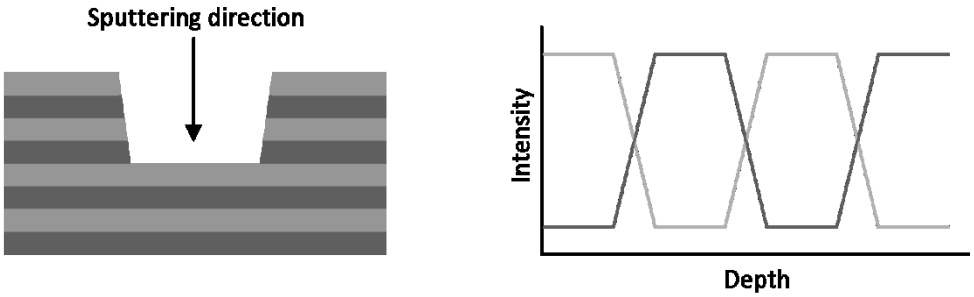

(a) (b)

Figure 3.17 Depth profiling of a substrate using a SIMS sputter beam showing a) the creation of a crater and b) the associated depth profile.

In this work an argon cluster ion source was used to sputter successive layers of material. The use of cluster sources is further detailed in section 3.4.6.5. The temporal sequencing of the sputtering and analysis ion beams can be achieved in two modes. In non-interlaced mode the sputter ion beam and the analysis ion beam alternate, while in interlaced mode sputtering and analysis of the sample occurs simultaneously. For the analysis of polymer materials it is common to use the non-interlaced mode to reduce charging and possible sample damage.

One consideration for depth profiling is that materials will undergo different sputtering rates depending on their composition. The energy of the sputter beam will also affect the rate at which material is removed. It is therefore necessary to calibrate the sputtering rate using depth profiles from homogenous samples which display uniform composition with depth.

3.4.6.5 Cluster ions

The use of high energy monoatomic primary ions enables the liberation of relatively high numbers of ions from the surface of a substrate. However, their use also results in significant damage to the surface, due to the increased number of collisions occurring in the region below the surface [128]. Cluster ions are comprised of multiple atoms of the form M_n^+ where n can range from three, in the case of Bi_3^+ to more than 2000 in the case of argon cluster beams. They can be used for both analysis and sputtering and include Bi_3^+, SF_5^+, Ar_n^+ and C_{60}^+.

Although, for a given energy, the energy of the whole ion cluster is the same as for a monoatomic ion, the energy of the individual atoms is significantly lower. Therefore, on impact, these atoms have less energy to impart to the atomic species with which they come into contact and the depth of damage to the surface is consequently reduced. Simulating the impact of cluster sources has shown that increasing the cluster size of the Ar_n^+ ion beam results in a decrease in the depth of damage as well as an increase in the lateral area sputtered by the beam, which results in less fragmentation [129]. The increase in number of atoms impacting the surface also causes an increase in secondary ion yield [128].

This work used a Bi_3^+ primary analysis beam (25 keV, I~0.3 pA) and an Ar_{1000}^+ sputter beam (5 keV, I~3.0 nA).

3.4.6.6 Considerations for the analysis of polymers

In polymers, the production of molecular fragments is thought to vary with distance from the site of impact. The high energies imparted at the point of impact are thought to result in the creation of small molecular fragments while larger macromolecular ions are produced at greater distances from the impact point [121].

As detailed in Chapter 2, polymers can be divided into two types depending on their response to high energy radiation [55]. Type I refers to those polymers that cross-link on irradiation and includes polymers such as polystyrene. Polymers which undergo chain scission when exposed to radiation are termed type II and include PMMA. This sensitivity to radiation is a challenge when considering SIMS analysis for polymers. Traditionally, it has been possible to successfully depth profile type II polymers. However, type I polymers including polystyrene have been difficult to analyse due to their tendency to cross-link on irradiation, resulting in a rapid deterioration in the depth profile intensity. In the last few years, the development of argon cluster ion beams has significantly improved the quality of depth profiles from type I polymers due to a reduction in the degree of cross-linking [130].

3.4.6.7 Data analysis

The SIMS spectrum of a polymer can be divided into three parts. The low mass ions in the fingerprint region (< 500 amu) contain molecular fragments to aid the identification of the surface under analysis and any contaminants present on the surface. The peaks in the region 500-5000 amu contain large fragment ions. The high mass region (5000-10000 amu) contains oligomers [131].

Calibration of the SIMS spectrum of a polymer may be achieved using known characteristic fragments of the polymer under investigation. In the positive polarity, fragments from hydrocarbon polymers are generally given by $C_{2x-1}H_x^+$ [129] while the number of peaks in the negative polarity tend to be fewer and the intensities decrease more rapidly than the positive polarity [121]. Here the C_xH^- peaks may be used for calibration [129]. For molecular identification it is recommended that calibration is not performed using a combination of atomic and molecular peaks [132].

Further analysis of a polymer can be difficult due to the high number of peaks present in the spectrum. In some cases the use of statistical techniques can aid identification. This topic is discussed in the next section.

3.5 Chemometrics and data processing techniques

Chemometrics is the use of statistical techniques for the interpretation of chemical data. The use of chemometrics and multivariate analysis (MVA) to interpret spectroscopic data is used widely in many fields and has gained some attention in conservation science. It has most often been applied to data obtained from Raman or infra-red spectroscopy to investigate the chemical changes occurring as pigments and paints age or degrade [133, 134]. The technique has also been applied to examine the effectiveness of anoxic storage conditions for pest control in wooden artefacts [135] and has been used with other spectroscopic techniques such as hyperspectral imaging for the identification of pigments [136]. While there is little information regarding the use of chemometrics with polymer materials in conservation, it has been used successfully with FTIR spectroscopy to determine the composition of historical plastics [96].

This work uses multivariate analysis to analyse SIMS spectra from the plastic surface. As SIMS is not a widely used technique in conservation science there is very little information about the application of chemometrics to analyse SIMS data for conservation purposes. However, Benetti et al. have used principal component analysis (PCA) to examine SIMS data relating to the composition of binders used in a 14th century wall painting [137]. The treatment of spectroscopic data using multivariate analysis (MVA) has been increasingly studied in the SIMS community.

3.5.1 Multivariate analysis and principal component analysis

The term 'multivariate analysis' (MVA) encompasses a wide range of statistical techniques used to aid the interpretation of spectral data. Although many techniques exist, the most common MVA technique used with SIMS data is principal component analysis (PCA) [138]. While a spectrum from a polymeric material contains hundreds of peaks from hydrocarbon and other molecular fragments, PCA enables the data to be reduced to significantly fewer dimensions. PCA has been used in a range of polymer studies, including to investigate the quantification of polymer additives [139], to determine the chemical composition of polymer multilayers [140] and with images to identify the spatial distribution of different polymers in polymer blends [141]. The PCA analysis of the SIMS data in this work was performed using the PLS_Toolbox, version 6.2.1 (Eigenvector Research, Inc, Manson, WA, USA) for Matlab (The Mathworks, Inc, Natick, MA, USA).

PCA works by considering the degree of covariance between variables (masses) in a data set. Spectral peaks may display a dependence on each other and therefore their intensities may increase together or be inversely related. In the case of SIMS data, this can result from different molecular fragments being produced from a sample of a specific molecular composition. For example, characteristic fragments from polystyrene include $C_7H_7^+$, $C_9H_7^+$ and $C_9H_9^+$ [121], therefore it would be expected that a strong positive correlation would exist for the intensities for these fragments. Equally, negative correlations between variables can exist. PCA therefore examines the data to determine the degree of

covariance between peaks and identifies which fragments are responsible for differences in the samples and to what extent, as manifested by the variance in the peak intensities.

Prior to PCA treatment the SIMS data undergoes a number of pre-processing steps. A scaling factor may firstly be applied to account for the instrument itself. As the detection of atomic or molecular fragments by mass spectrometry is essentially a counting exercise, the resultant data is dominated by Poisson statistics [142]. This causes peaks with higher intensities to exhibit greater variance which could bias the data. In this work a Poisson scaling is applied. In order to compare the peak ratios, the peaks in each spectrum are then 'sum normalised' so that the total ion intensity for that spectrum is equal to 1. Finally, the peak intensities for each spectrum are centred around zero by subtracting the mean value of the intensities for a particular peak from each individual value to ensure that the first principal component represents the direction of greatest variance in the data.

In a graphical representation the PCA treatment of SIMS data corresponds to a rotation of the original data around the origin, as shown for a two dimensional data set in figure 3.18 [143]. The new axes are the principal components and describe the directions of variance in the data. The first principal component (PC1) is aligned along the direction of greatest variance in the data. Each successive principal component describes the direction of next greatest variance in the data and is orthogonal to and therefore independent of the previous principal component. In this way a series of components are defined to enable the position of each spectrum in n-dimensional principal component space to be described. In practice the variance in the data set is likely to be dependent on only the first few principal components and the remainder can be disregarded as contributions from noise.

Figure 3.18 Rotation of axes for a two dimensional data set.

It is therefore of interest to find the principal components and to determine how these are related to the original data. This is done by finding the *score* for each spectrum, i.e. its position in principal component space. Each spectrum is represented by one data point. The *loadings* then give the

importance of each of the original peaks in defining the direction of the principal component of interest. This enables each spectrum to be related to the original data.

A set of raw SIMS spectra can be considered to be a matrix, with the atomic masses forming the columns and the individual spectra the rows. This matrix X therefore has dimensions n × d, where n = number of spectra and d = number of variables, in this case the variables are the peak masses. The values in matrix X are the peak intensities.

The scores and loadings are commonly found using singular value decomposition (SVD) [144]. This decomposes the matrix X into three matrices as in equation 3.17.

$$X = U\Sigma V^T \tag{3.17}$$

Where $U\Sigma$ is the scores matrix and V^T is the transpose of the loadings matrix. Therefore the matrix X can be described in terms of a finite number of principal components, where each principal component is described by a direction (given by a row of matrix V^T), a value (given by a column of matrix U) and an importance (given by the diagonal values of matrix Σ) [144]. The diagonal values of Σ are termed the singular values and are sorted in descending order, such that the first principal component describes the greatest amount of variance in the data.

The matrix X is therefore commonly represented by equation 3.18 [144, 145].

$$X = TP^T + E \tag{3.18}$$

Where T is the scores matrix, P is the loadings matrix and E represents a residual matrix which corresponds to zero if all principal components are used. This is not always the case as usually the majority of the data can be described by only a few components. The number of principal components to be used is commonly found using a scree plot, which is a graphical representation of the variance described by each principal component as in figure 3.19. The number of principal components which describe the greatest variance in the data may be estimated by locating the 'elbow' point, the point at which the plot starts to flatten out. This is only an estimate and more sophisticated methods exist to determine which principal components are of most interest [144].

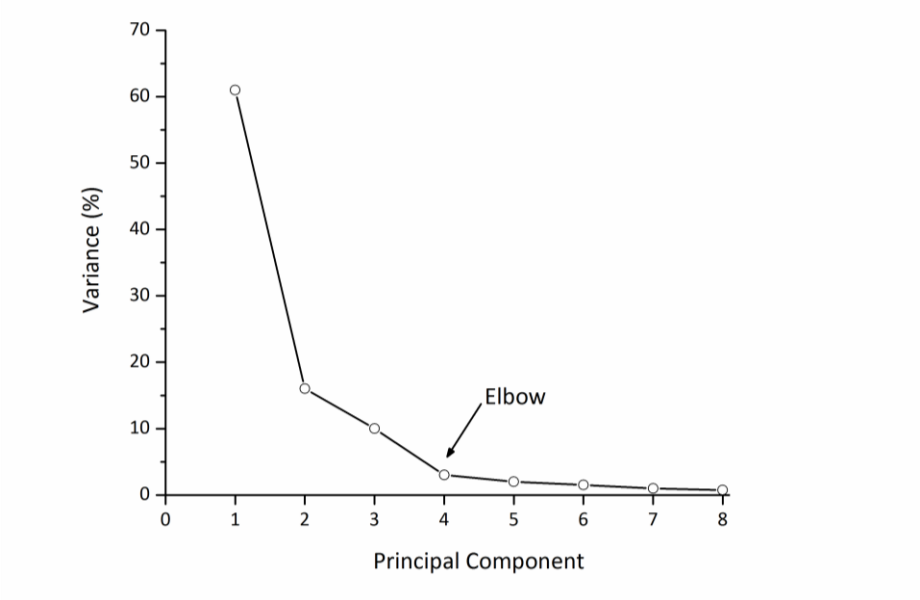

Figure 3.19 Typical scree plot showing the location of the elbow point.

PCA treatment of the data then results in two plots: the scores plot and the loadings plot. These plots should be read together: positive scores correspond to positive loadings and vice versa.

Chapter 4

Experimental detail

Many different types of plastics are found in the museum environment. These plastics have different susceptibilities to their external environments and undergo different degradation routes. As such it is unlikely that it is possible to define a cleaning procedure that is suitable for all plastic types. This chapter details the plastic substrates under investigation and the cleaning agents that were used in this work.

4.1 Substrates

This work focused on two thermoplastics, poly(methyl methacrylate) (PMMA) and polystyrene. These plastics were chosen in part due to their presence in the museum environment. In particular, a survey of the V&A's Museum of Childhood collection revealed that a significant component of the toys in the collection were thought to be comprised of polystyrene [4]. These plastics were also chosen as they are rigid sheet plastics at room temperature and do not incorporate significant quantities of plasticiser.

Among the major applications for PMMA are aircraft windows, lighting, contact lenses, signage, food packaging and furniture. Polystyrene is commonly used in the manufacture of Airfix® model kits, jewel cases, food packaging and disposable cutlery [17, 57]. The manufacture of sheet substrates for polystyrene and PMMA is commonly achieved via bulk polymerisation which is followed by casting or extrusion of the flat sheet. Following manufacture the substrate is protected by a polymer or paper sheet. This is weakly adhered to the surface as an electrostatic film or via the use of pressure sensitive adhesives [57].

4.1.1 Virgin substrates

Flat sheet substrates were used to determine the effect of cleaning on virgin substrates. PMMA was sourced from the Victoria and Albert Museum, having originally been bought in 2008 from Rias A/S (Denmark). The plastic was supplied in sheets with a thickness of 3 mm. Sheet polystyrene was

sourced directly from Plastics Direct Ltd (UK) in late 2014 and had a thickness of 1.8 mm. Both plastics were transparent to exclude the influence of pigments or dyes. The plastics were supplied with a protective polymer sheet covering both sides of the plastic sheet. In the case of PMMA this sheet was white and opaque, while the polystyrene protective sheet was transparent. The molecular structures of PMMA and polystyrene are shown in table 4.1, along with typical parameters of interest.

Table 4.1 Typical parameters for PMMA and polystyrene.

		PMMA	**Polystyrene**
Formula		$(C_5H_8O_2)_n$	$(C_8H_8)_n$
Molecular structure		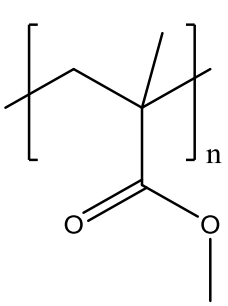	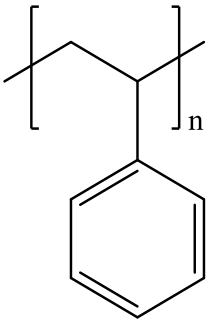
T_g (°C) [53]		105 (atactic)	80-90
T_m (°C) [53]		160 (decomposition)	240 (semi-crystalline)
Density (g/cm^3) [53]		1.19	1.04-1.065
Refractive index [53]		1.49	1.59
Surface energy at 20°C (mN/m) [53]		41.1	40.7
Hildebrand solubility parameter ($MPa^{\frac{1}{2}}$) [84]		22.6	22.5
Hansen solubility parameters ($MPa^{\frac{1}{2}}$) [84]	d_d	18.6	22.3
	d_p	10.5	5.8
	d_h	7.5	4.3
Ro [84]		8.6	12.7
Degree of crystallinity (%) [17]		0	0
Light transmission (%) [17]		92	87-92
Degradation type [55]		Type II	Type I
Degradation routes [17]		Good weathering resistance	Oxidation
Hydrogen bonding		Acceptor	None
Oxygen diffusion ($\times10^{13}$ cm^3. cm cm^{-2} s^{-1} Pa^{-1}) [53]		0.065 (at 35°C)	1.9 (at 25°C)
Water permeability ($\times10^{13}$ cm^3. cm cm^{-2} s^{-1} Pa^{-1}) [53]		480 (at 23°C)	1350 (at 25°C)

4.2 Cleaning agents and application

4.2.1 Prior work

Cleaning agents for this work were chosen with reference to those used in the POPART project [31] as this was the most extensive body of work in this area to date. During the POPART study all surfactants were applied at a 1% concentration. The cleaning process for aqueous agents consisted of five 'linear rubs', i.e. movement of the cloth in a single direction, with the cleaning agent followed by rinsing with five linear rubs of distilled water to remove residues. The process for the organic solvents again used five linear rubs but the rinsing step was not necessary.

PMMA

The least damaging cleaning tools for PMMA were found to be the microfibre cloth, synthetic spectacles cloth and cotton cloths. The microfibre and synthetic spectacles cloths were more effective in removing soil, which was attributed to their greater surface area to volume ratio. Some of the aqueous cleaning agents were observed to lubricate the surface. Orvus WA Paste was found to cause the least damage to the surface while distilled water was ineffective as a lubricant. The aqueous agents were generally unable to remove both sebum soil and organic soil from PMMA. Orvus WA Paste and one of the non-ionic surfactants were most effective in removing organic soil when used in conjunction with the microfibre cloth. The application of ethanol, isopropyl alcohol and white spirit to PMMA substrates was thought to reduce scratching again by acting as lubricants. The other solvents studied, including acetone, severely damaged the surface. Solvents were more effective than aqueous agents in removing both soils from the substrate, with ethanol and isopropyl alcohol numbering among the most effective.

Polystyrene

Polystyrene was not studied as one of the plastics in POPART, however high impact polystyrene (HIPS) was studied and its behaviour is reviewed here. As seen for PMMA, the microfibre and spectacles cloths caused the least damage to the surface and some aqueous agents were found to act as lubricants. Distilled water did not act as an effective lubricant. Dehypon LS45 was one of the least damaging agents studied and was the most effective in removing sebum soil, followed closely by Orvus WA Paste. Again the aqueous agents were generally ineffective in removing organic soil. Solvent cleaning of HIPS was found to result in scratching to the surface for all organic solvents, with the most damage being caused by acetone and the least by ethanol. Both ethanol and isopropyl alcohol were able to remove the sebum and organic soils.

4.2.2 Cleaning agents used in this work

4.2.2.1 Selection of cleaning agents

From the POPART data it is evident that the least damaging application method is via the use of the microfibre or synthetic spectacles cloth. These cloths were both comprised of polyester and polyamide. However they differed in the diameter of the fibres and the closeness of the weave. For reasons of practicality and sourcing it was decided to source a microfibre cloth from a reputable conservation supplier for this work. The microfibre cloth was used both on its own and to apply a range of cleaning agents.

Three aqueous agents were chosen on the basis of the POPART findings: Orvus WA Paste (anionic surfactant), Dehypon LS45 (non-ionic surfactant) and deionised water. The two surfactants were chosen as they caused the least damage to the PMMA and HIPS surfaces while deionised water was chosen both because of the use of water in conservation treatments and the relatively poor performance of distilled water as an aqueous agent. Deionised water was chosen over distilled water because of its higher purity. Three organic solvents were also studied: acetone, ethanol and isopropyl alcohol. Acetone was chosen due to its highly damaging performance as a cleaning agent, which would provide a 'worst case scenario' for the cleaning process. Ethanol and isopropyl alcohol were selected for study as they were found to cause the least damage to the PMMA and HIPS surfaces, and were also effective in removing surface contamination.

4.2.2.2 Sourcing of cleaning agents

A white microfibre cloth, manufactured by Stouls (France), was sourced from Conservation by Design (UK) (product no. SUWMFC7523) and is shown in figure 4.1. The composition of the cloth was 80% polyester and 20% polyamide. Prior tests with a yellow microfibre cloth had revealed leaching of the colorant with organic solvents.

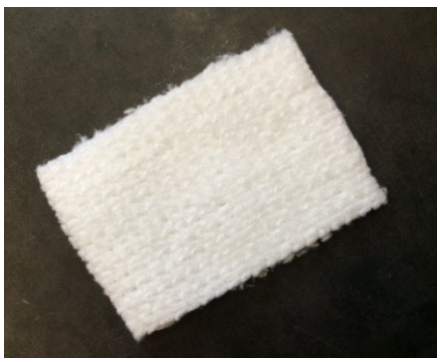

Figure 4.1 Photograph of the white microfibre cloth with dimensions 42 mm × 30 mm.

The anionic surfactant, Orvus WA Paste (Procter & Gamble, USA), was sourced from Conservation Resources UK. The exact composition of the surfactant is unknown but it contains sodium lauryl sulphate (SLS). According to the MSDS data, Orvus WA Paste has a pH of 7.8 and is completely

soluble in water [146]. Decomposition products are listed as sulphuric acid (H_2SO_4), sodium oxide (Na_2O) and hydrogen sulphide (H_2S). The non-ionic surfactant, Dehypon LS45 (BASF), was sourced from Restore Products (UK). This is an ethoxylated propoxylated fatty alcohol (C_{12}-C_{14}) which has a pH of 6.5-7.5 and is partially miscible in water [147]. Both surfactants were diluted to a 1% concentration with deionised water. Deionised water was sourced from a Merck Millipore Direct-Q® water purification system (Merck, Germany), with a resistivity of 18.2 MΩ.cm at 25°C. All the organic solvents used in this work were ACS grade and were supplied by VWR International (USA): acetone (VWRC20066, purity 99.8%), ethanol (VWRC20821, purity 99.8%) and isopropyl alcohol (VWRC20842, purity 99.7%). The cleaning agents used in this work are summarised in table 4.2.

Table 4.2 Summary of the cleaning agents used in this work.

Cleaning agent	Composition	Structure
Acetone	C_3H_6O	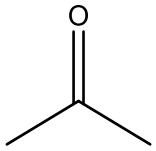
Ethanol	C_2H_6O	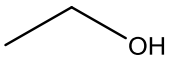
Isopropyl alcohol	C_3H_8O	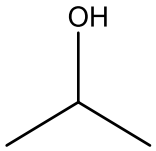
Orvus WA Paste [146]	Anionic surfactant Contains sodium lauryl sulphate (shown)	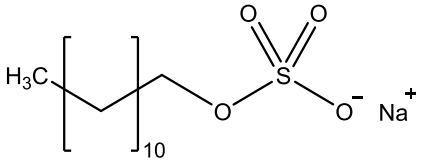
Dehypon LS45 [147]	Non-ionic surfactant Ethoxylated propoxylated fatty alcohol (C_{12}-C_{14})	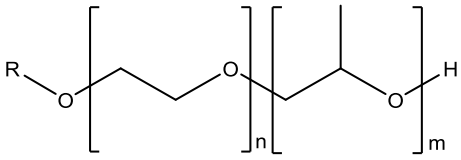
Deionised water	H_2O 18.2 MΩ.cm at 25°C	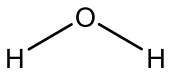
Microfibre cloth (no agent)	80% polyester, 20% polyamide	N/A

4.3 Interaction of substrates and solvents

As a contact process, cleaning has the potential to be highly damaging to the plastic surface. An estimation of the incompatibility of the cleaning agents and plastics studied in this work can be achieved by examining their solubility parameters.

4.3.1 Solubility behaviour and parameters

Table 4.3 shows the Hansen solubility parameters and interaction radii (Ro) for the plastics and cleaning agents studied in this work. The solubility parameters of the surfactants are unknown. Table 4.4 shows the Hansen distances (Ra) and RED values for the plastic-cleaning agent combinations studied.

Table 4.3 Typical solubility parameters at 25°C for the plastics and cleaning agents studied [84].

	δ_d $(MPa^{\frac{1}{2}})$	δ_p $(MPa^{\frac{1}{2}})$	δ_h $(MPa^{\frac{1}{2}})$	δ_{tot} $(MPa^{\frac{1}{2}})$	Ro
PMMA	18.6	10.5	7.5	22.6	8.6
Polystyrene	21.3	5.8	4.3	22.5	12.7
Acetone	15.5	10.4	7.0	19.9	-
Ethanol	15.8	8.8	19.4	26.5	-
Isopropyl alcohol	15.8	6.1	16.4	23.6	-
Water	15.5	16.0	42.3	47.8	-

Table 4.4 Typical Ra and RED values for the plastic-agent combinations studied.

		Acetone	Ethanol	Isopropyl alcohol	Water
PMMA	Ra	6.2	13.3	11.4	35.8
	RED	0.7	1.5	1.3	4.2
Polystyrene	Ra	12.8	18.9	16.4	41.0
	RED	1.0	1.5	1.3	3.2

4.4 Cleaning methodology

Studies investigating the cleaning of plastics have commonly replicated cleaning techniques used in the conservation environment. Therefore agents have been applied by hand, either in a linear or circular motion. Both methods were examined as part of POPART and it was found that the linear

motion was more effective in removing surface soiling [31]. Morales Muñoz used cotton swabs to clean plasticised PVC and the dampened swabs were rolled over the surface in a circular motion [34]. The linear method was used by Casella and Moore for cleaning photographs face-mounted onto sheet PMMA [148].

4.4.1 Sample preparation

Individual samples measuring 15 mm × 20 mm were cut from both plastic sheets using a bandsaw (figure 4.2).

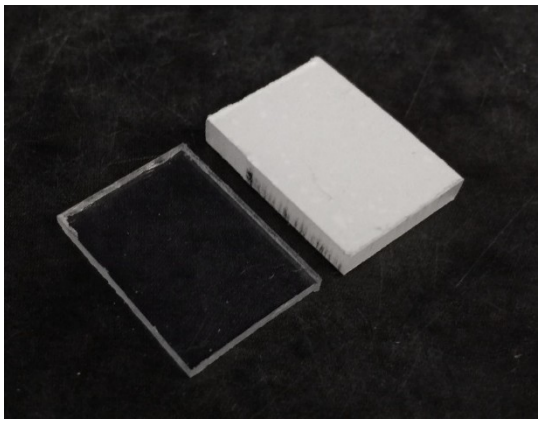

Figure 4.2 Photograph showing the cut plastic samples with the protective sheets attached. Sample dimensions = 20 mm × 15 mm.

The protective sheet was removed from both sides of the plastic samples immediately prior to preparation of the surface for cleaning. In order to be able to examine identical areas before and after cleaning, three fiducial markers were placed on the surface of the plastic samples as in figure 4.3. This was performed using a Zwick Roell Indentec ZHV micro hardness tester (Zwick Roell, Germany), which enabled the indentation of a diamond marker on the surface of the material.

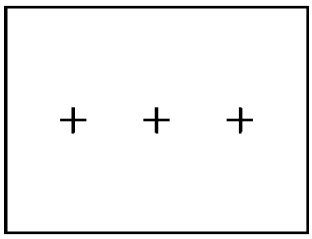

Figure 4.3 Schematic showing the positioning of the fiducial markers. Sample dimensions = 20 mm × 15 mm.

4.4.2 Cleaning procedure

Figure 4.4 shows a schematic of the cleaning procedure used in this work. This procedure uses a K control bar coater (RK Print, UK). The maximum distance between the rod and the base was equal to the thickness of the plastic sample plus 2 mm allowance for the microfibre cloth (the minimum cloth thickness when fully compressed was 0.8 mm). The rod was housed in metal holders at either end; as

the diameter of the rod was slightly smaller than the housing the rod had some freedom of movement in the vertical direction. The maximum downward force on the sample was therefore due to the weight of the rod (F = 1 N). This setup ensured that the cleaning procedure was reproducible and consistent for all samples.

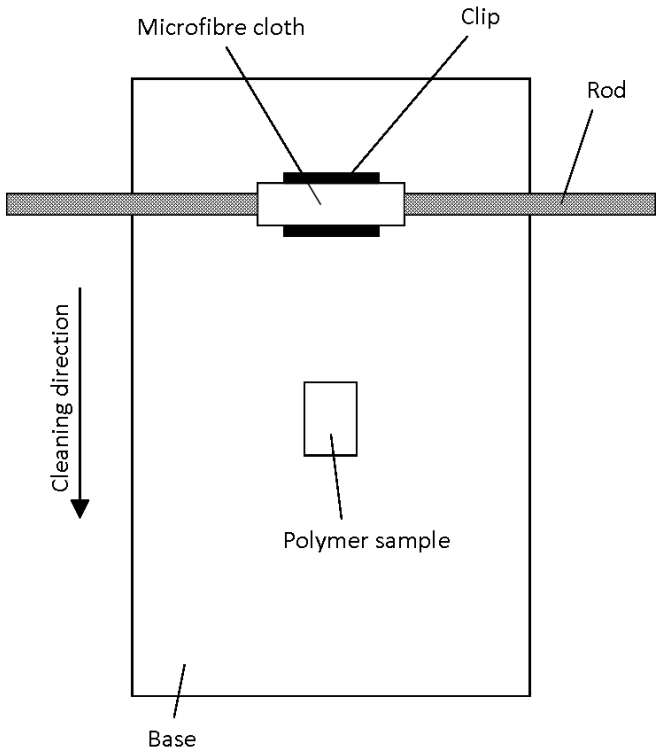

Figure 4.4 Schematic of the cleaning procedure used.

A rectangle of microfibre cloth measuring approximately 30 mm × 40 mm was used for each cleaning procedure and the mass of the dry cloth was recorded. The volume of cleaning agent applied to the cloth was 2 ml. The cloth was gently squeezed after the application of the cleaning agent to remove any excess liquid and the mass of the wetted cloth was recorded. Care was taken to ensure that the surface of the microfibre cloth did not come into contact with any potential source of contamination, including gloves, during the wetting process.

The wetted cloth was then attached to the bar coater using a clip to hold it in place and was passed over the plastic sample once in the direction indicated in figure 4.4. The velocity of the cloth over the surface was approximately 2.7×10^{-2} ms^{-1}. In the case of the surfactants, a second step was performed to remove residual surfactant from the surface. This was achieved by repeating the cleaning procedure with a cloth wetted with deionised water. The same method was used for the dry cleaning procedure except that no cleaning agent was applied to the cloth.

4.4.3 Storage

In order to limit any changes to the plastic surface before and after cleaning, samples were stored in conservation-grade cardboard boxes sourced from Conservation Resources (UK). These boxes were made from sulphur and lignin free paper; this was preferable to storing samples in a plastic container due to the potential of cross contamination from the plastic storage material. The use of cardboard also provides a more stable environment due to its moisture absorption and air permeability. Samples were stored in the enclosed box at ambient temperature and humidity.

4.5 Surface analysis considerations

Before performing analysis of the samples using ToF-SIMS it was necessary to determine which molecular fragments might be expected to be observed during analysis. This enables accurate calibration of the spectra and the ability to attribute peaks in the spectra to known fragments.

Figures 4.5 and 4.6 shows typical SIMS spectra in the positive and negative polarity for PMMA and polystyrene with the characteristic fragments indicated (m/z = 0-200 only). For PMMA notable peaks are those at 41 and 69 in the positive polarity which correspond to $C_3H_5^+$ and $C_4H_5O^+$ respectively and 41 (C_2HO^-) and 85 ($C_4H_5O_2^-$) in the negative polarity [121]. For polystyrene the peak at m/z = 91 in the positive polarity corresponds to $C_7H_7^+$ while in the negative polarity the principal peaks in the spectrum are hydrocarbon peaks of the form C_n^- and C_nH^- and peak intensities after the C_6 cluster are very weak [121]. Molecular attributions for the characteristic fragments of PMMA and polystyrene are shown in tables 4.5 and 4.6.

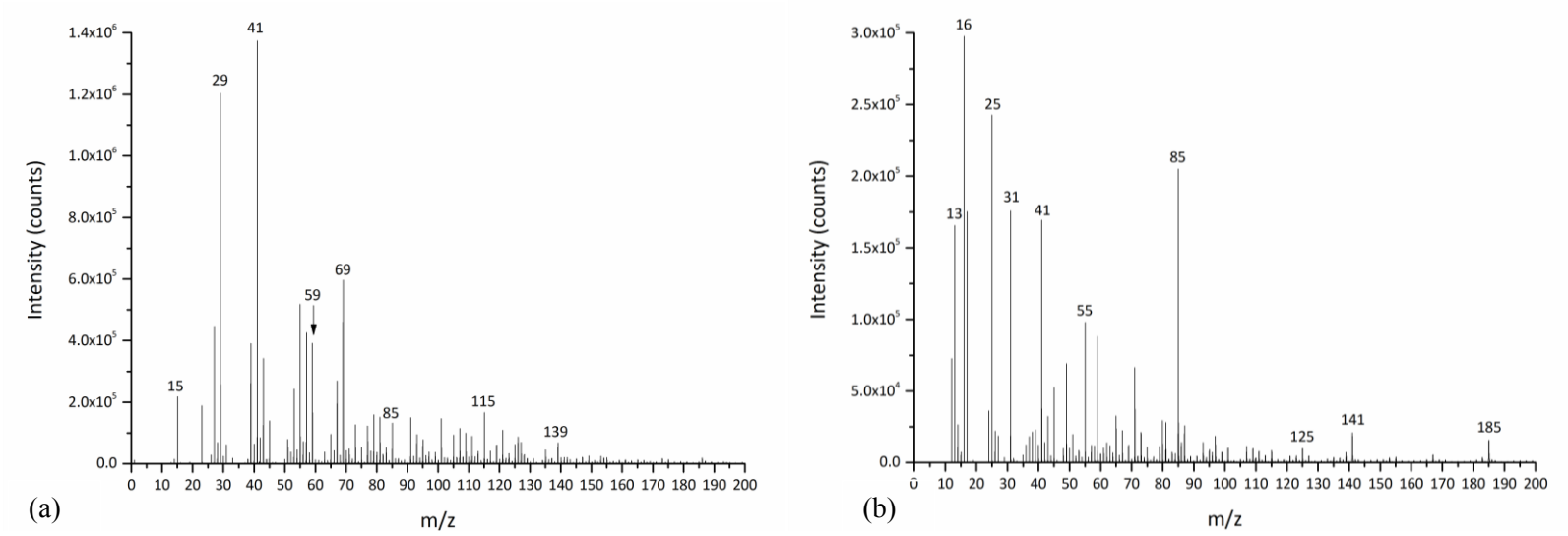

Figure 4.5 a) Positive SIMS spectrum and b) negative SIMS spectrum for PMMA with masses indicated (m/z <200).

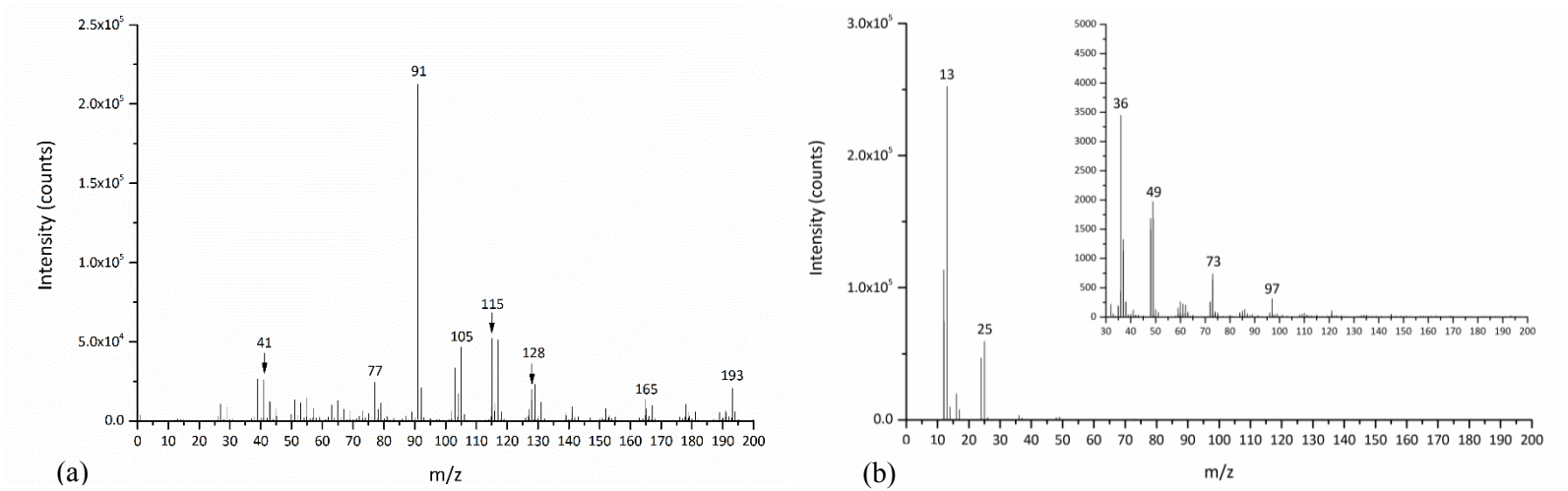

Figure 4.6 a) Positive SIMS spectrum and b) negative SIMS spectrum for polystyrene with masses indicated (m/z <200). Inset shows the negative spectrum from m/z = 30 at ×60 magnification.

Table 4.5 Characteristic positive and negative SIMS fragments for PMMA and their suggested molecular attributions [121].

Positive			Negative		
Mass	**Formula**	**Molecular structure**	**Mass**	**Formula**	**Molecular structure**
41	$C_3H_5^+$	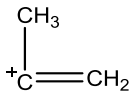	85	$C_4H_5O_2^-$	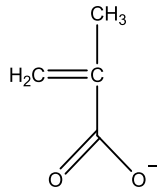
59	$C_2H_3O_2^+$	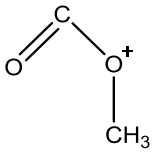	109	$C_6H_5O_2^-$	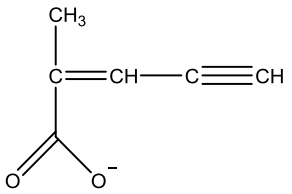
69	$C_4H_5O^+$	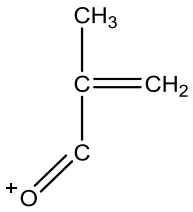	125	$C_7H_9O_2^-$	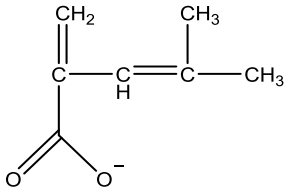
85	$C_5H_9O^+$	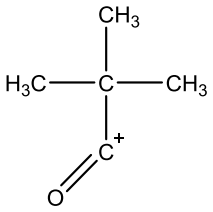	139	$C_7H_7O_3^-$	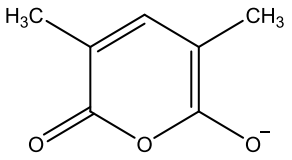
115	$C_6H_{11}O_2^+$	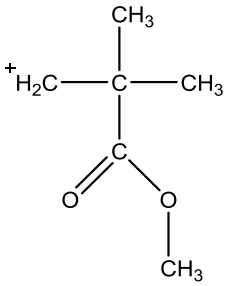			
139	$C_8H_{11}O_2^+$	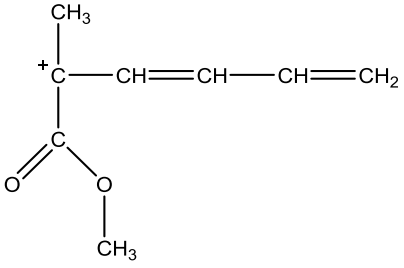			

Table 4.6 Characteristic positive and negative SIMS fragments for polystyrene and their suggested molecular attributions [121, 149].

Positive			Negative
Mass	**Formula**	**Molecular structure**	
77	$C_6H_5^+$		Fragments of the form C_n^- and C_nH^-
91	$C_7H_7^+$	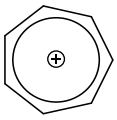	
103	$C_8H_7^+$	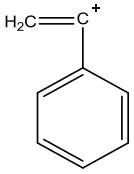	
115	$C_9H_7^+$	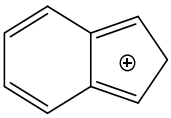	
117	$C_9H_9^+$	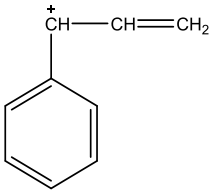	
128	$C_{10}H_8^+$	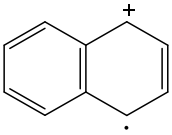	
152	$C_{12}H_8^+$	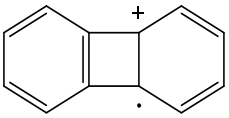	
165	$C_{13}H_9^+$	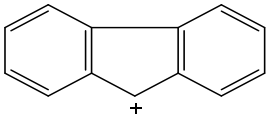	
178	$C_{14}H_{10}^+$	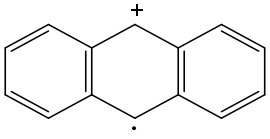	
193	$C_{15}H_{13}^+$	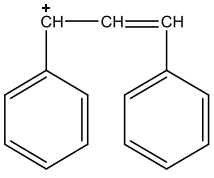	

Chapter 5

Examination of virgin substrates

The PMMA and polystyrene substrates chosen for this work were sourced from commercial suppliers and therefore little information was known about their properties prior to analysis. This chapter details the initial characterisation performed for both substrates. The effect of cleaning agents on the virgin PMMA and polystyrene substrates is also discussed in this chapter. Both the physical and chemical changes to the substrates were investigated.

5.1 Experimental

Characterisation of the bulk properties of PMMA and polystyrene was performed to determine their composition and thermal behaviour. The plastic sheets were provided with a protective polymer film present on both sides which was removed before initial characterisation was performed. No further sample preparation was undertaken before analysis of the substrates by ATR-FTIR, DSC and GPC. Micro-hardness testing of the substrates was also performed. The same side of the sheet substrate was examined in all cases.

Acquisition of the ATR-FTIR spectra was performed for both plastics, using 64 scans at a spectral resolution of 4.0 cm^{-1}. A background spectrum was captured before each sample spectrum was obtained. ATR-FTIR spectroscopy was also performed to confirm the composition of the microfibre cloth used to apply the cleaning treatments.

The glass transition temperatures of both plastics was obtained using DSC. Two runs were performed for each plastic; the first to remove any internal stresses in the sample. The T_g was calculated from the second run. Data was captured in the range of 25 °C to 200 °C at a ramp rate of 10 °C/min. The samples were allowed to cool at ambient temperature between runs.

GPC was used to obtain the molecular weight distribution of the plastics. Samples of each plastic were diluted to a 10 % concentration in tetrahydrofuran (THF) before being filtered through a mesh of 0.45 μm pore diameter and analysed.

The Vickers micro-hardness values for both plastics were obtained using a 100 g load which was applied over 10 s. Five separate indentations were made at random positions over the length of the plastic sample and repeat measurements were made for different samples of the same plastic.

Eight individual substrates were then prepared for each plastic by removing the protective sheet and creating three fiducial markers on the plastic surface as detailed in Chapter 4. Micrographs of the surface were captured at the marked areas prior to cleaning using white light interferometry. One sample was then retained as a control and each of the remaining seven substrates was treated with a different cleaning agent using the cleaning method described in Chapter 4. Surface analysis of these samples was performed using white light interferometry, SEM, AFM and ToF-SIMS. Again, the same side of the sheet substrate was cleaned and analysed in all cases.

Interferometry micrographs were captured at ×5 magnification using a 5 μm bipolar scan and a camera resolution of 640 × 480 pixels. SEM micrographs were obtained using the in-lens detector at a working distance of 7-9 mm using an EHT of 5 kV for polystyrene and 3 kV or 5 kV for PMMA. All samples were sputter coated with a 10-20 nm coating of gold or chromium prior to analysis. AFM micrographs were captured in tapping mode at a resolution of 512 × 512 pixels.

ToF-SIMS analysis was performed using a 25 keV Bi_3^+ primary ion beam in high current bunched mode (HCBM) with an emission current of 1 μA and a target current of 0.3 ± 0.1 pA. Depth profiling of the substrates was achieved in dual beam mode using a 5 keV Ar_{1000}^+ sputter ion beam with a target current of 3 ± 0.5 nA and 25 keV Bi_3^+ analysis ion beam in non-interlaced mode (sputter = 1 s, pause = 0.5 s). The dimensions of the sputter crater were 300 μm × 300 μm and analysis was performed over a 100 μm × 100 μm area in the centre of the crater. Images were captured over a 500 μm × 500 μm raster area at a resolution of 512 × 512 pixels. A low energy electron flood gun was used for charge neutralisation during the acquisition of all spectra.

Given the complexity of the resulting spectra, PCA treatment of the data was performed to aid analysis of the effect of different cleaning treatments. At least eight spectra were obtained for each surface, with their location being randomly determined but limited to the centre of the sample to avoid any edge effects. The dimensions of each analysis area measured 100 μm × 100 μm at 128 × 128 pixel resolution and the acquisition time of each spectrum was 60 s. In all cases the spectra were Poisson-scaled, sum normalised and mean centred prior to PCA.

5.2 Bulk characterisation

5.2.1 ATR-FTIR

Figure 5.1 shows the ATR-FTIR spectra for the virgin PMMA and polystyrene substrates. The bond vibrations corresponding to the principal bands are given in table 5.1. Inspection of the spectra and comparison with the HR Nicolet Sampler Library (ThermoFisher Scientific, USA) confirms the composition of the substrates.

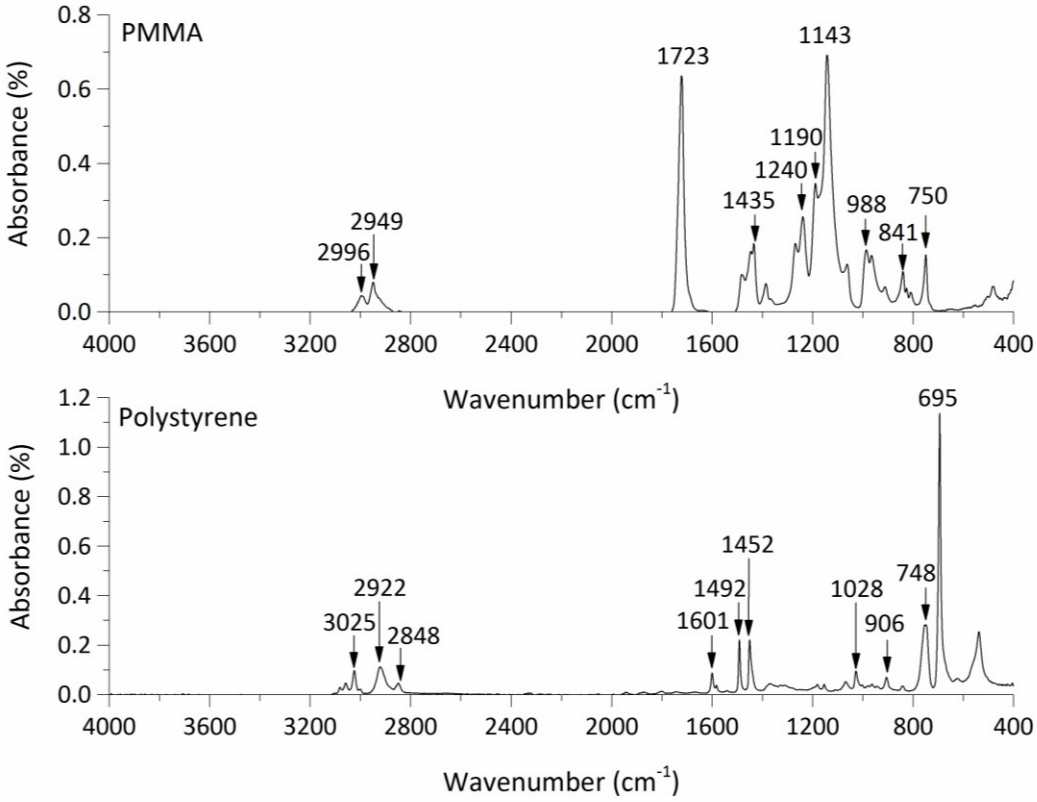

Figure 5.1 ATR-FTIR spectra for the PMMA and polystyrene substrates.

Table 5.1 Table of notable bands and suggested attributions for PMMA and polystyrene [150].

PMMA		Polystyrene	
Wavenumber (cm^{-1})	**Attribution**	**Wavenumber (cm^{-1})**	**Attribution**
2996	υ (C-H)	3025	υ (C-H)
2949	υ (C-H)	2922	υ (C-H)
1723	υ (C=O)	2848	υ (C-H)
1435	δ (C-H)	1601	υ (C=C) (benzene ring)
1240	υ (C-O-C)	1492	υ (C=C) (benzene ring)
1190	υ (C-O-C)	1452	υ (C=C) (benzene ring)
1143	υ (C-O-C)	1028	δ (C-H) (benzene ring)
988	υ (C-O-C)	906	δ (C-H) (benzene ring) (oop)
841	ρ (CH_2)	748	δ (C-H) (benzene ring) (oop)
750	υ (C-C)	695	δ (C-H) (benzene ring) (oop)

υ = stretch, δ = deformation, ρ = rock, oop = out of plane

5.2.2 DSC

The DSC data for the PMMA and polystyrene substrates is shown in figure 5.2. The T_g of both plastics was determined by using the Netzsch Proteus ® software (Netzsch, Germany) to find the mid-point of the transition region and reveals T_g values of 111.6 ± 0.5 °C and 103.6 ± 0.5 °C for the PMMA and polystyrene substrates respectively. These compare to values in the literature of 105 °C for atactic PMMA and 80-90 °C for polystyrene [53]. These greater T_g values for the substrates may be due to differences in the macromolecular structure or molecular weight of the polymers. There may also be slight differences due to the analytical methodology used. The glass transition of the PMMA substrate is broader than that of the polystyrene substrate which may be due to differences in their molecular weight distributions and may also reflect a greater degree of crosslinking in the PMMA substrate [49].

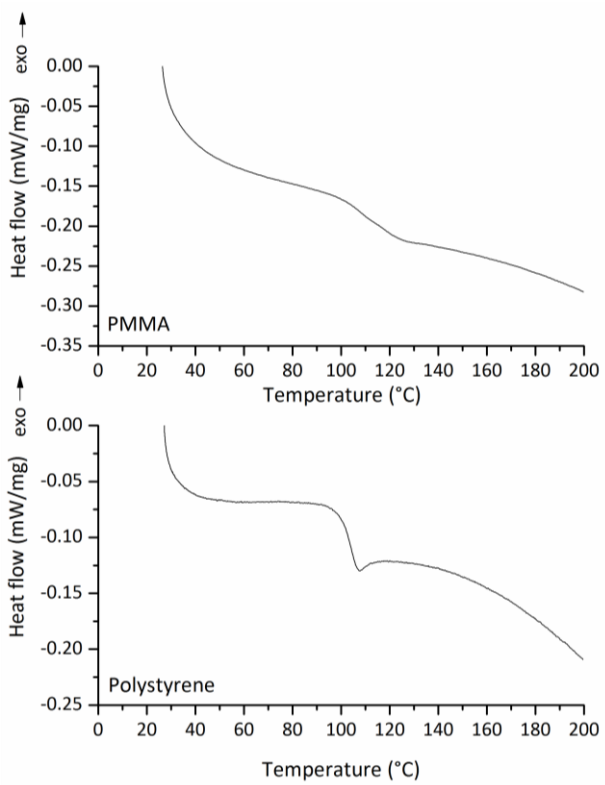

Figure 5.2 DSC graphs for PMMA and polystyrene showing the glass transition region.

5.2.3 GPC

The molecular weight distributions of both polymers were determined using GPC and are given in figure 5.3.

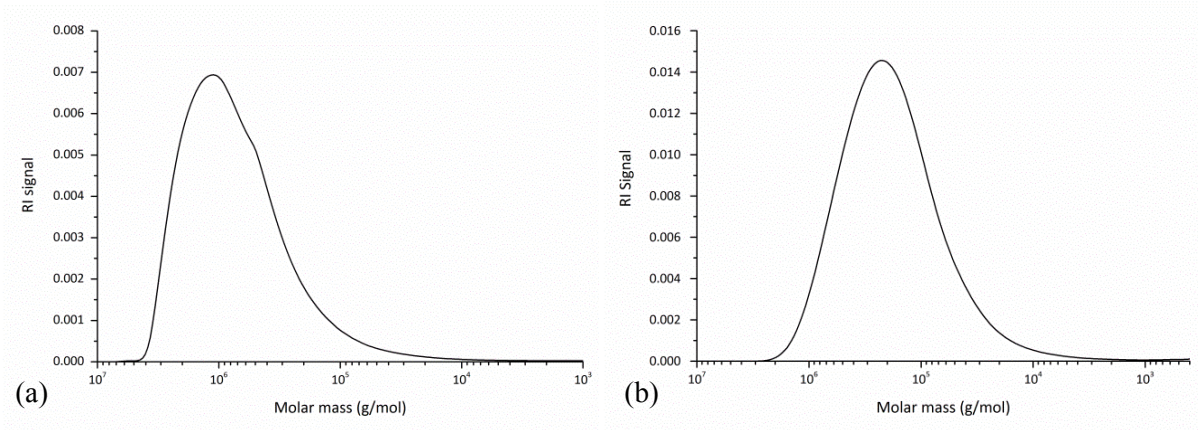

Figure 5.3 Molecular weight distributions for the a) PMMA and b) polystyrene substrates.

The average molecular weights of the polymers were $\overline{M}_n$ = 1.62×10^3 g/mol and $\overline{M}_w$ = 9.56×10^5 g/mol for PMMA and $\overline{M}_n$ = 1.88×10^3 g/mol and $\overline{M}_w$ = 2.63×10^5 g/mol for polystyrene. Figure 5.3 shows that the size distribution for the polystyrene substrate is reasonably uniform around the peak. However, the PMMA distribution has a slight shoulder around 5.0×10^5 g/mol, which indicates the presence of another peak at a lower molecular weight. The presence of two peaks may be due to

autoacceleration occurring in the polymerisation process. As the polymerisation medium becomes more viscous, the termination rate decreases and the molecular weight of the polymer chains increases [49]. The effect is more pronounced in some polymers than others, including methacrylates.

5.2.4 Hardness

The mean Vickers micro-hardness values for both plastic substrates were calculated as 21.3 VHN for PMMA and 18.4 VHN for polystyrene with standard deviations of 0.7 VHN and 0.3 VHN respectively. These reveal that the PMMA substrate had a greater hardness than the polystyrene substrate. It is also notable that the standard deviation of the values for the PMMA substrate is greater than that for the polystyrene substrate, indicating a less homogenous surface.

5.2.5 Characterisation of the microfibre cloth

Figure 5.4 shows two SEM micrographs of the white microfibre cloth. The width of the individual fibres is approximately 10 μm. Although the cloth was soft to the touch, the individual fibres are angular and many incorporate folds and crevices along their length. Examination of the fibres at high magnification revealed the presence of small particles that were adhered to the fibres. EDX analysis of these particles only revealed the presence of peaks corresponding to carbon and oxygen.

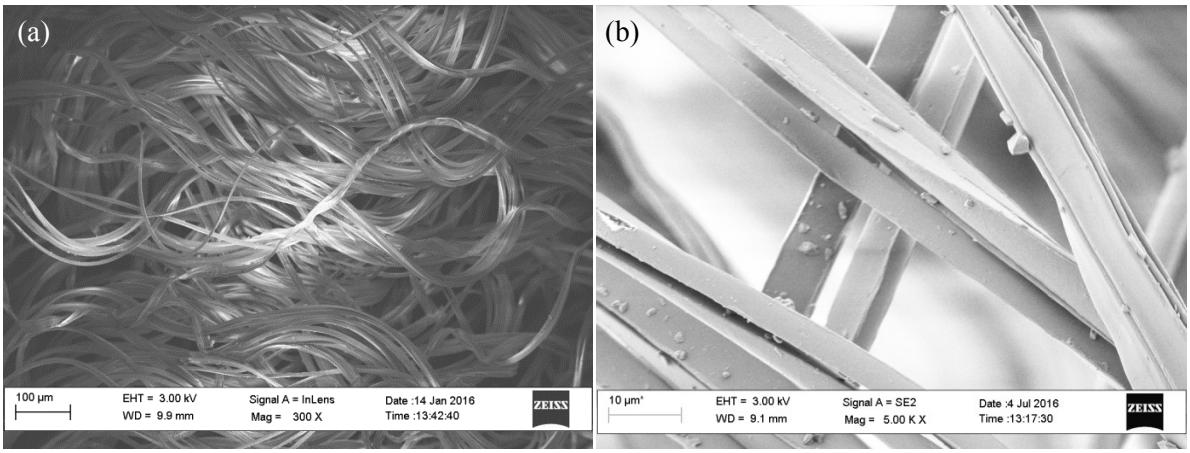

Figure 5.4 SEM micrographs of the microfibre cloth showing a) the individual fibres and b) the presence of particles on the cloth fibres.

ATR-FTIR analysis was performed to determine the composition of the microfibre cloth (figure 5.5). The product literature gives its composition as 80% polyester and 20% polyamide. Comparison of the ATR-FTIR spectrum with library spectra from the HR Nicolet Sampler Library gives a 58% agreement with polyethylene teraphthalate.

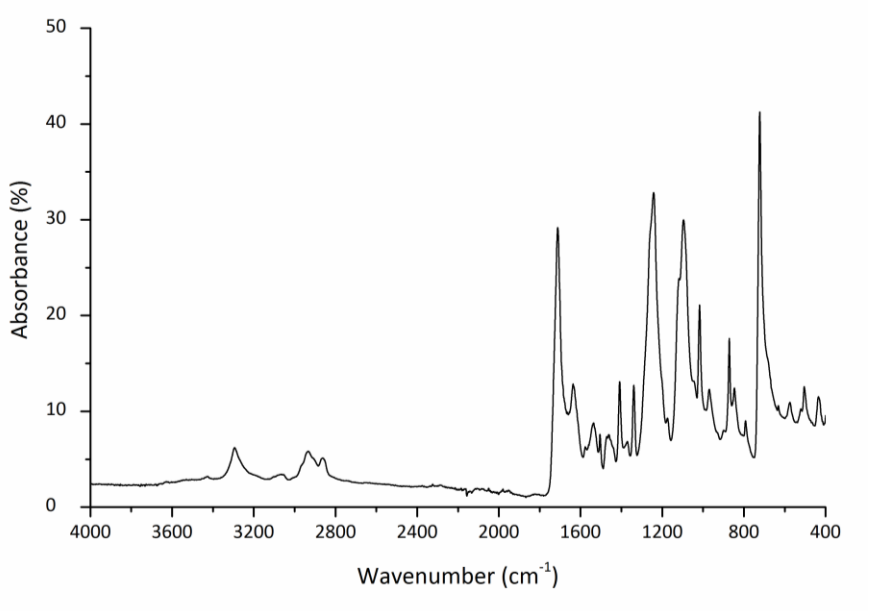

Figure 5.5 ATR-FTIR spectrum of the microfibre cloth.

5.3 Surface analysis

As detailed in Chapter 3, physical changes to the substrate were evaluated using white light interferometry, AFM and SEM. White light interferometry was used in this work to provide valuable low magnification information about the plastic surface. As a non-destructive, non-contact method, it enabled the acquisition of images before and after the application of cleaning treatments. Greater detail about the surface topography after cleaning was obtained using AFM and SEM. Chemical changes to the substrate were determined using PCA of ToF-SIMS data, as well as the use of images and depth profiles obtained using the ToF-SIMS. Findings from the PCA analysis were confirmed with reference to the original spectra.

5.3.1 Physical changes

5.3.1.1 PMMA

Figure 5.6 shows white light interferometry micrographs of all PMMA substrates before and after cleaning. This enables a direct comparison of the surface changes taking place as a result of cleaning.

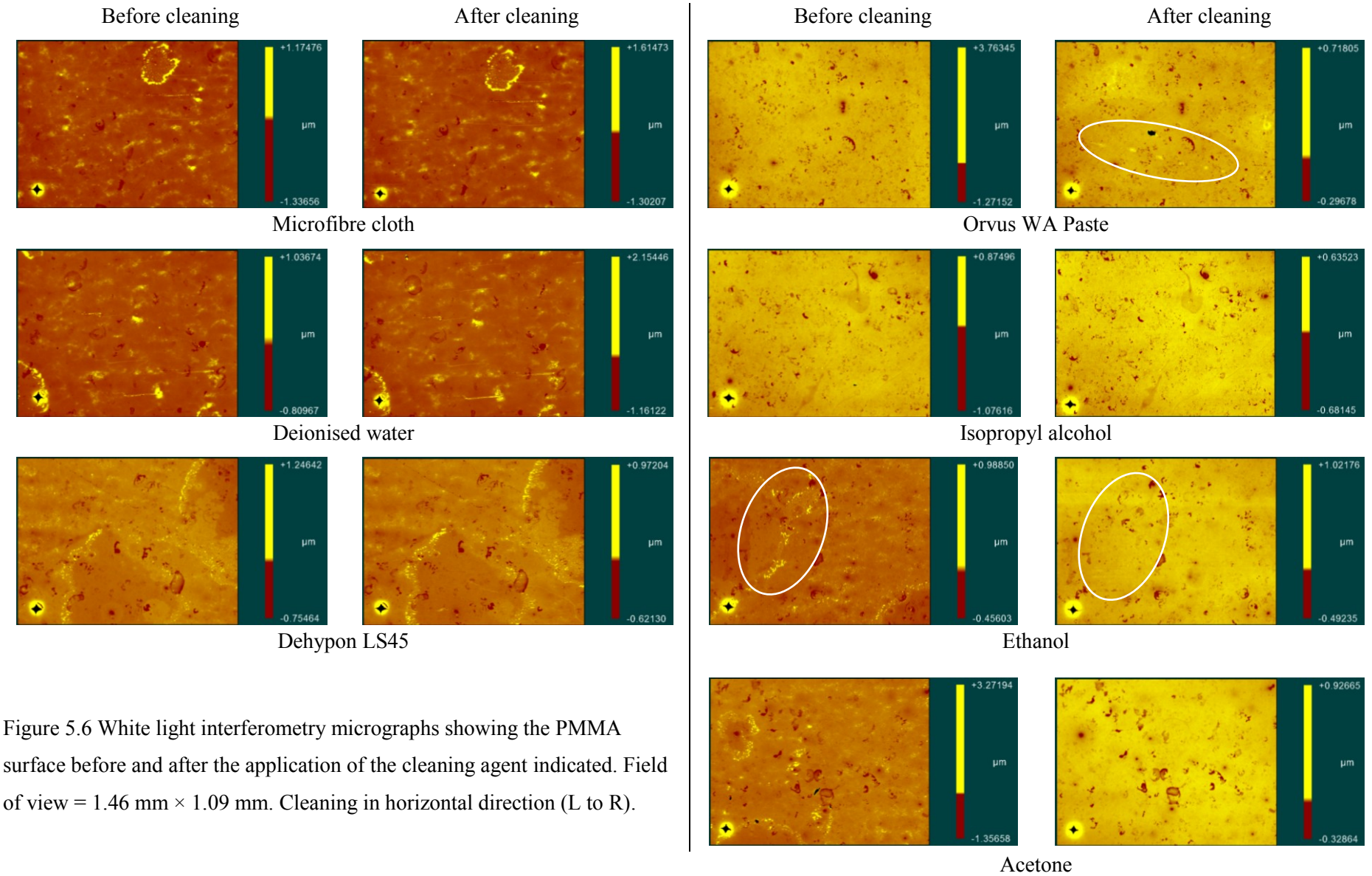

Figure 5.6 White light interferometry micrographs showing the PMMA surface before and after the application of the cleaning agent indicated. Field of view = 1.46 mm × 1.09 mm. Cleaning in horizontal direction (L to R).

It can be observed from these micrographs that elevated areas on the virgin substrate were not present after cleaning with acetone and ethanol (indicated in figure 5.6 by the white oval for ethanol). This suggests the removal of material via the use of these solvents, however the composition of the removed material is unclear. It is not possible to determine whether the same effect is true for isopropyl alcohol as there were no raised areas on the surface of the substrate prior to cleaning. Inspection of the substrates cleaned with the aqueous agents and dry cleaning procedure indicates that these raised areas were still present after cleaning. The interferometry micrograph for the PMMA substrate cleaned with the anionic surfactant (Orvus WA Paste) revealed the presence of additional raised areas after cleaning and also the re-deposition of particulate matter (indicated in figure 5.6).

An AFM micrograph of the uncleaned PMMA substrate is shown in figure 5.7a and provides further detail about the surface topography. The surface roughness is due in part to the raised areas seen in the figure 5.7b which are thought to correspond to the raised areas in the interferometry micrographs. There are a number of small depressions on the surface which were also observed using white light interferometry.

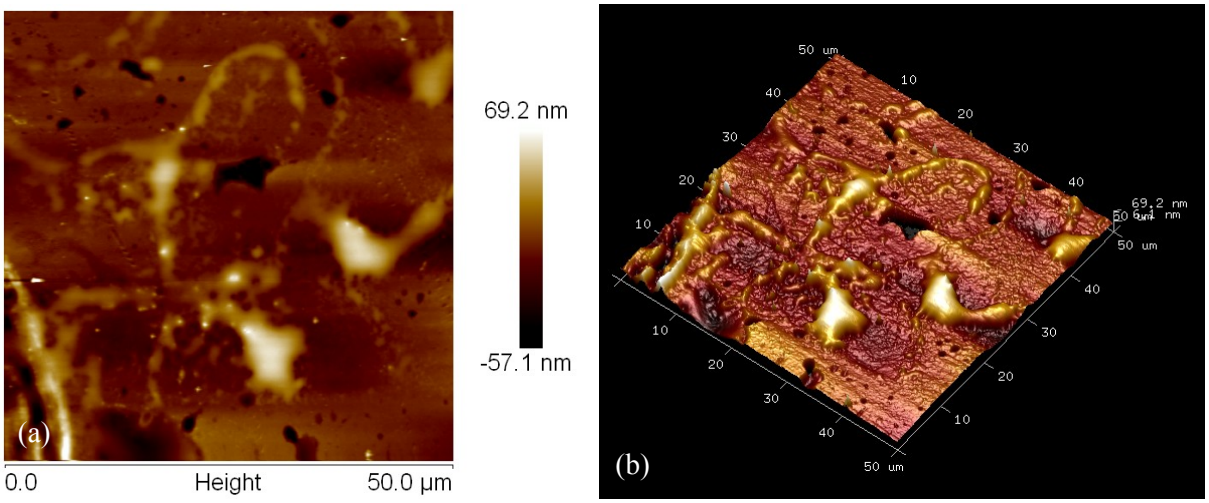

Figure 5.7 a) AFM micrograph of the uncleaned PMMA substrate and b) 3D representation of the same area.

While the interferometry micrographs do not reveal any further changes as a result of cleaning, the cleaned substrates were also examined using SEM. The SEM micrographs are shown in figure 5.8. The low magnification micrographs are shown due to the occurrence of extensive beam damage to the substrate at higher magnifications.

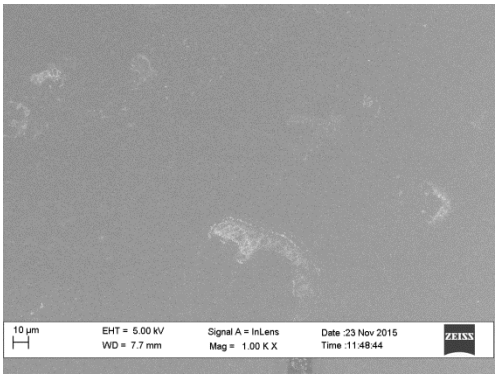

No treatment

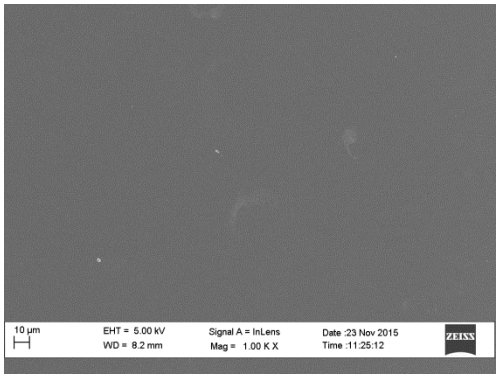

Microfibre cloth

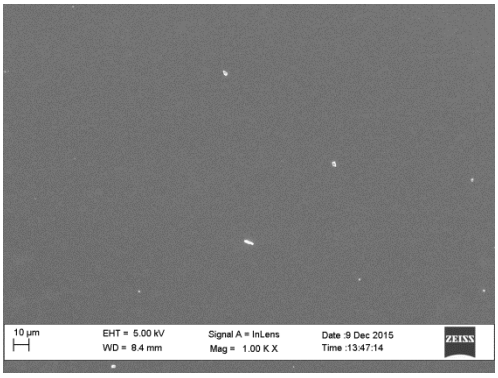

Deionised water

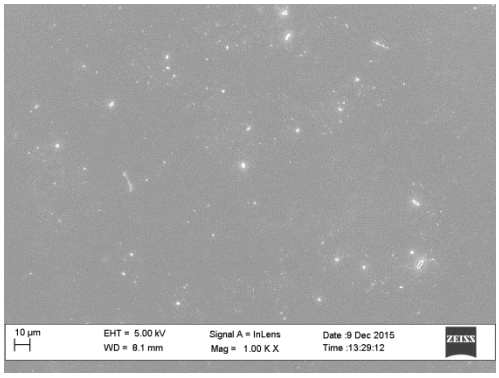

Dehypon LS45

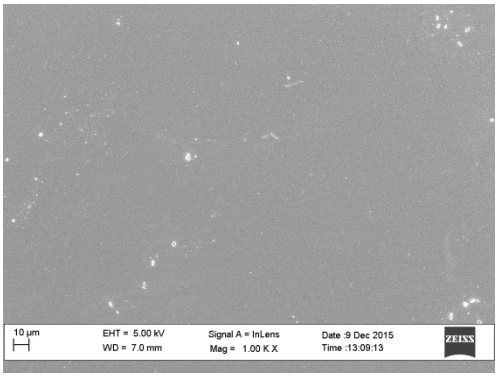

Orvus WA Paste

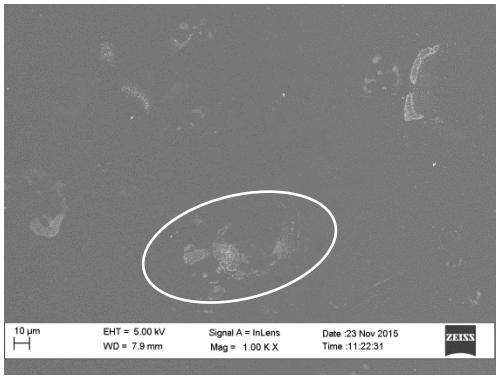

Isopropyl alcohol

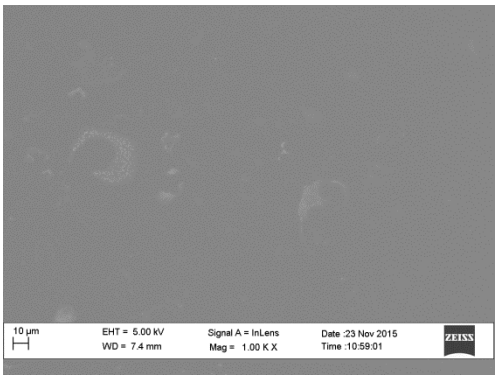

Ethanol

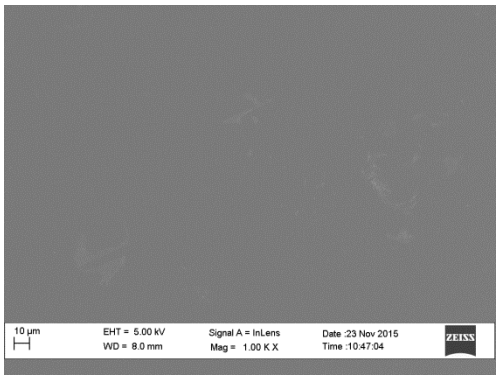

Acetone

Figure 5.8 SEM micrographs of the PMMA substrates after cleaning with the agents indicated.

Examination of the PMMA substrates did not reveal any evidence of scratching or other physical damage as a result of cleaning. It can also be observed from figure 5.8 that the two substrates cleaned with the surfactants show the presence of additional material on the surface which was not observed for the other cleaned substrates and which may be due to the presence of a residue from the surfactants. Alternatively it may result from the deionised water: particulate matter is also present to a lesser extent on the substrate cleaned with deionised water.

It is notable that a number of the micrographs in figure 5.8 show areas of topographical contrast, as indicated by the white oval for the substrate cleaned with isopropyl alcohol. These are not thought to be a result of the cleaning process due to their presence on the uncleaned substrate. Due to their presence on the substrates cleaned with organic solvents it is thought that these do not correspond to the elevated areas seen in figure 5.6 and instead may correspond to the depressed areas observed in the interferometry images. A close-up of one of these areas is shown in figure 5.9. It is suggested that these areas are due to imperfections in the sheet manufacture.

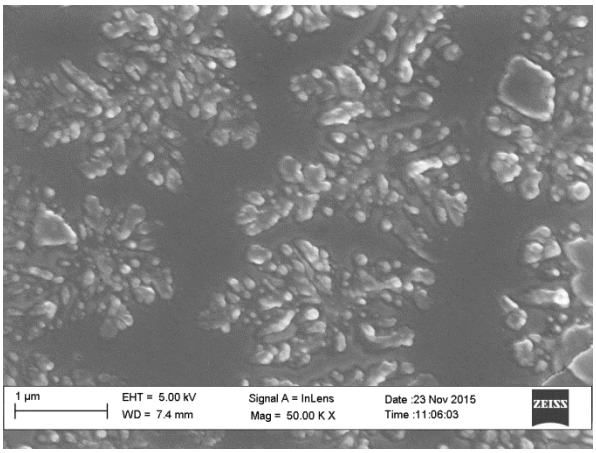

Figure 5.9 Close-up of the PMMA substrate, showing the topography of the contrasting areas.

5.3.1.2 Polystyrene

The interferometry micrographs of the polystyrene substrates before and after cleaning are shown in figure 5.10. Unlike the PMMA substrates, there is no observable contamination on the substrate prior to cleaning, with the exception of particulate matter. It can be seen from these images that the surface of polystyrene was severely damaged by the application of acetone. Aside from the removal or re-deposition of particulate matter, no notable changes were observed as a result of the application of the other cleaning agents.

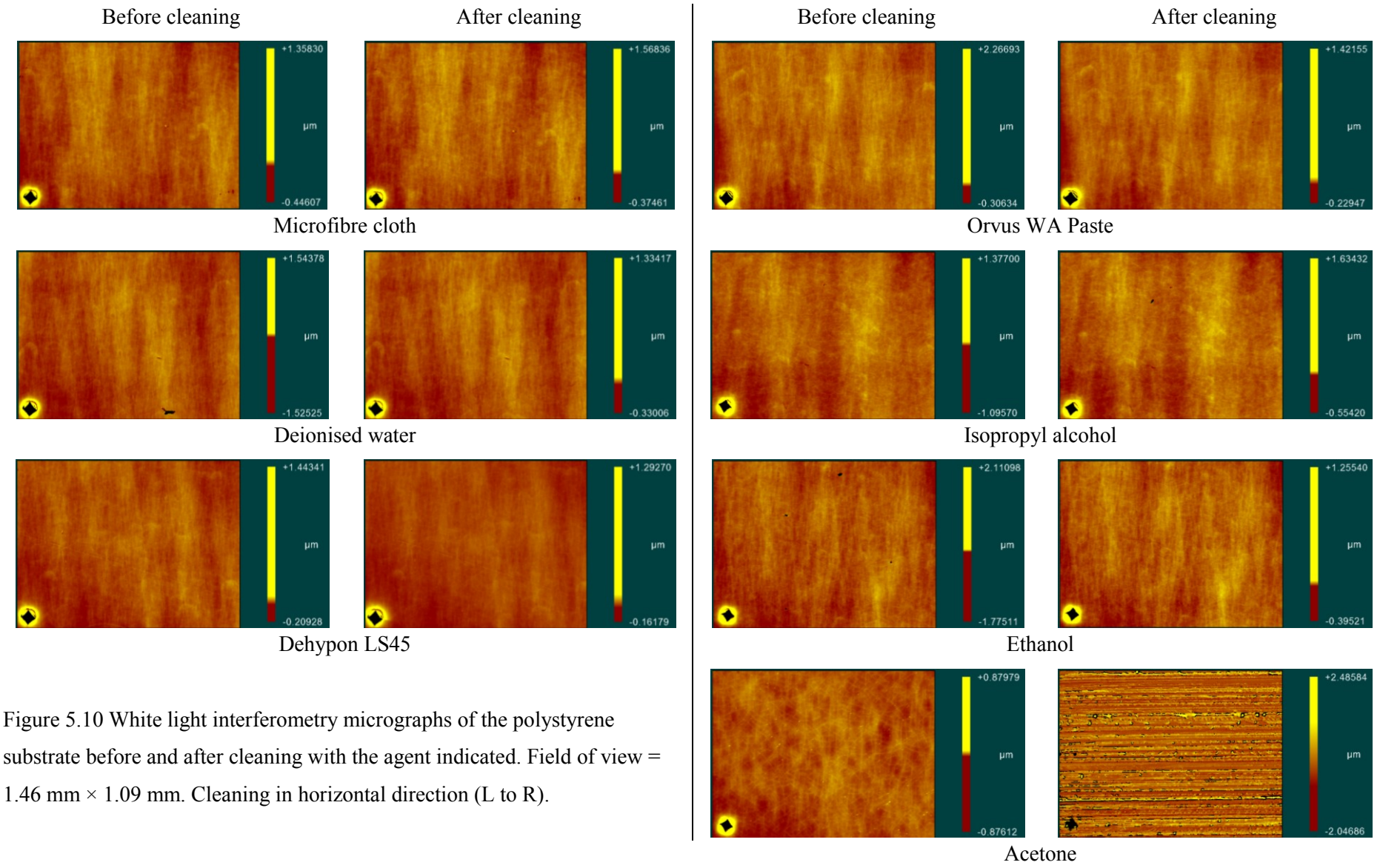

Figure 5.10 White light interferometry micrographs of the polystyrene substrate before and after cleaning with the agent indicated. Field of view = 1.46 mm × 1.09 mm. Cleaning in horizontal direction (L to R).

SEM micrographs were also obtained for all polystyrene substrates after cleaning and are shown in figure 5.11. The cracking effect observed on the surface of these micrographs is due to the gold sputter coating.

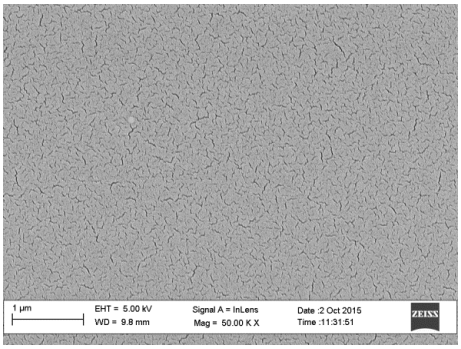

No treatment

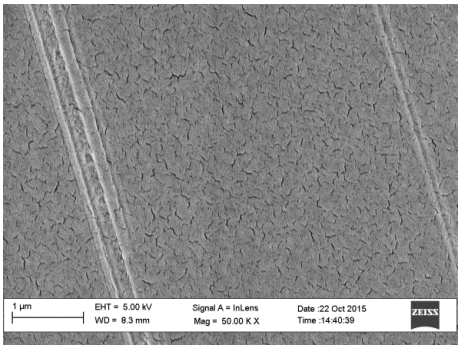

Microfibre cloth

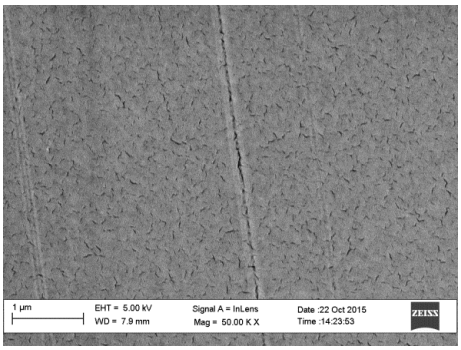

Deionised water

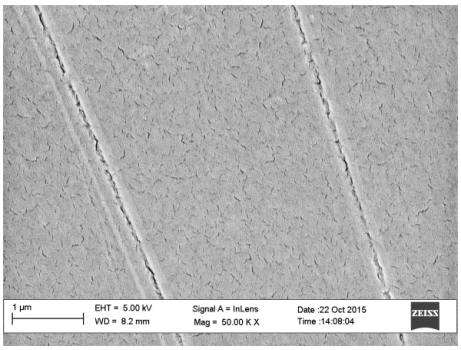

Dehypon LS45

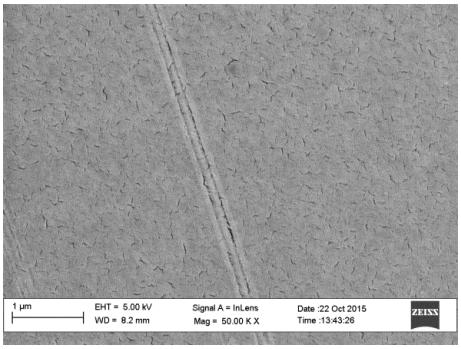

Orvus WA Paste

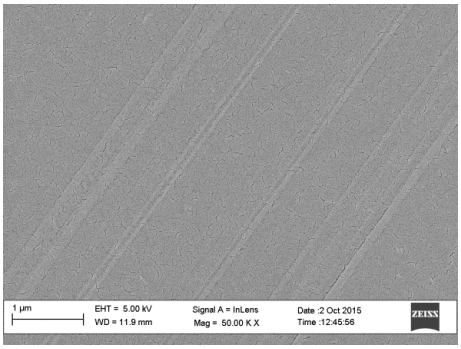

Isopropyl alcohol

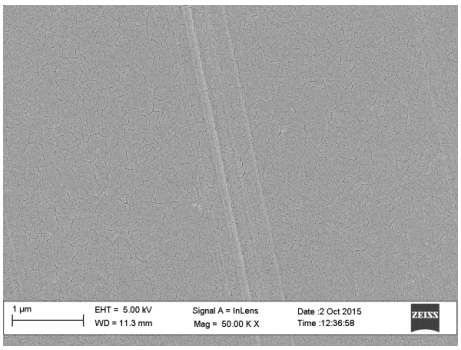

Ethanol

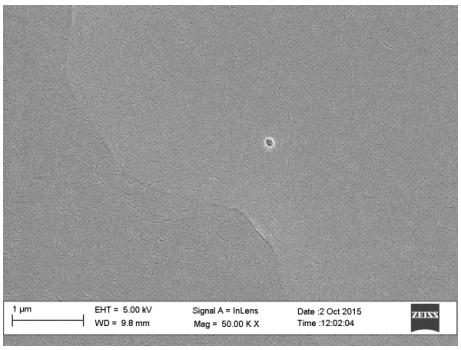

Acetone

Figure 5.11 SEM micrographs of the polystyrene substrates after cleaning with the agents indicated.

The micrographs shown in figure 5.11 were captured at a higher magnification than those captured for PMMA, however scratching was apparent even at low magnification using SEM. It can be seen from these micrographs that defined scratches were present on all of the cleaned polystyrene samples, with the exception of acetone. These scratches were formed in the direction of cleaning. The topography of the scratches appears to be very similar, regardless of the agent applied, although there is some variation in width. It was, however, noted that the scratches may be isolated or clustered, as seen in the case of isopropyl alcohol, and that this is not dependent on the cleaning agent. Defined scratches were not observed for the polystyrene substrate cleaned with acetone. In this case the surface topography varied with a shallower gradient, which is consistent with the surface being dissolved by the acetone. Some areas of the substrate cleaned with acetone also showed the formation of small crazes, as shown in figure 5.12.

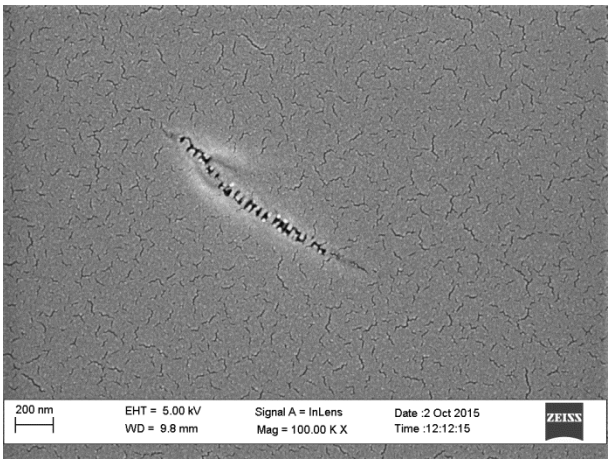

Figure 5.12 SEM micrograph of the polystyrene substrate cleaned with acetone, showing crazing.

An estimation of the topography and dimensions of the cleaned surfaces can be obtained from line profiles of the surface using AFM. Figure 5.13 shows the AFM micrographs for the polystyrene substrate after having undergone dry cleaning as well as the polystyrene substrates cleaned with isopropyl alcohol and the anionic surfactant (Orvus WA Paste).

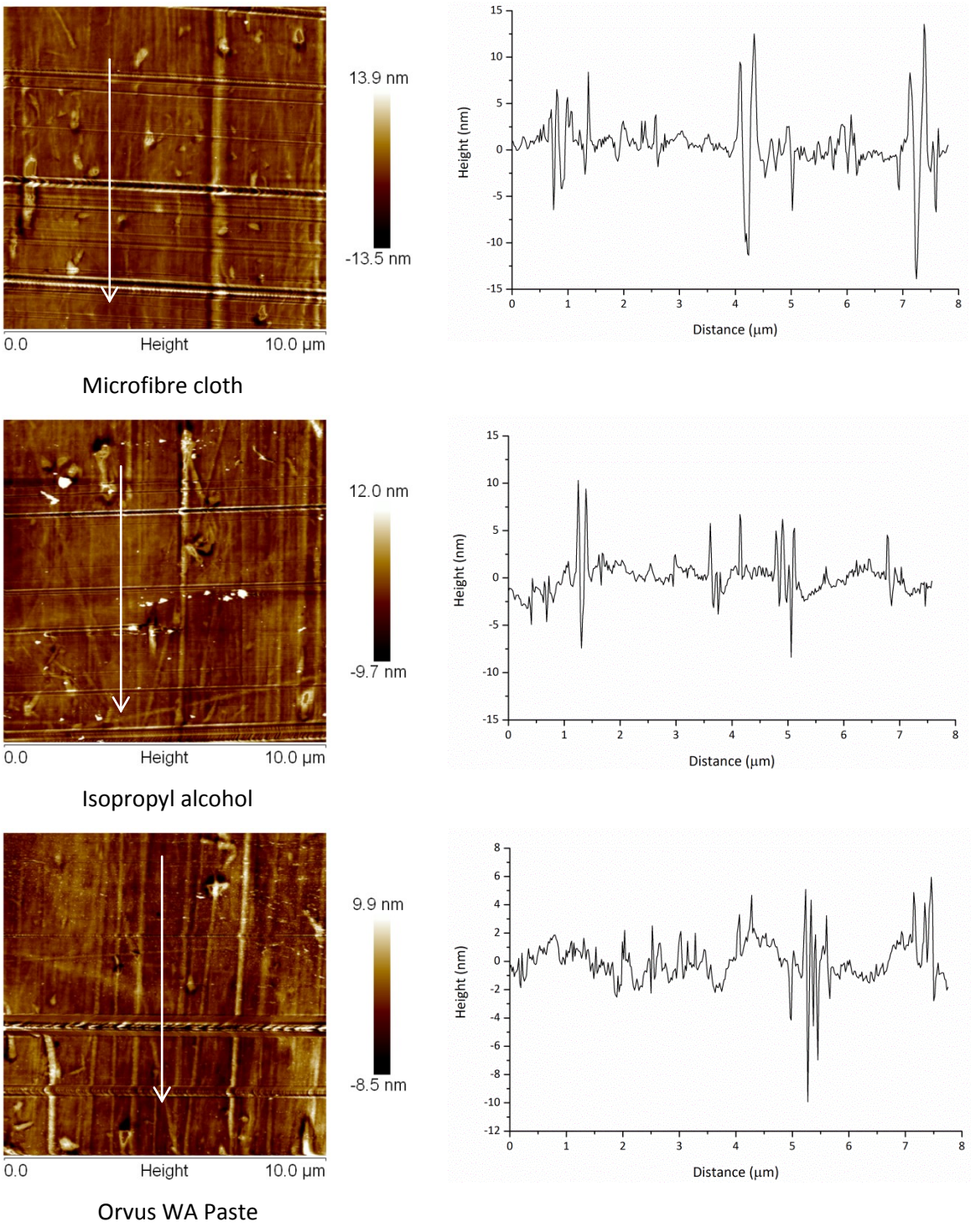

Figure 5.13 AFM micrographs of the polystyrene substrate after cleaning with the agents indicated and the associated line profiles.

These line profiles show a typical peak-to-valley height of 20 nm - 25 nm and a peak-to-peak width of around 500 nm. In all the line profiles shown in figure 5.13, the greatest variation in topography is a result of the scratches which extend across the area analysed. The scratches typically display a central trough of width 100 nm - 300 nm which is surrounded by an elevated area on both sides and which is

of the same order of magnitude as the trough. Therefore, the entire damaged area may have a width of approximately 1 µm.

5.3.2 Changes in surface chemistry

5.3.2.1 Initial substrate condition

Examination of the virgin PMMA and polystyrene substrates using ToF-SIMS reveals information about the surface composition prior to cleaning. Figure 5.14 shows an interferometry micrograph of a raised area and the corresponding SIMS maps of the PMMA substrate for the fragments at m/z = 43.05, 59.02, 69.03, 69.07 and 71.09. These masses were chosen as they show clear differences between the chemical composition of different areas of the substrate.

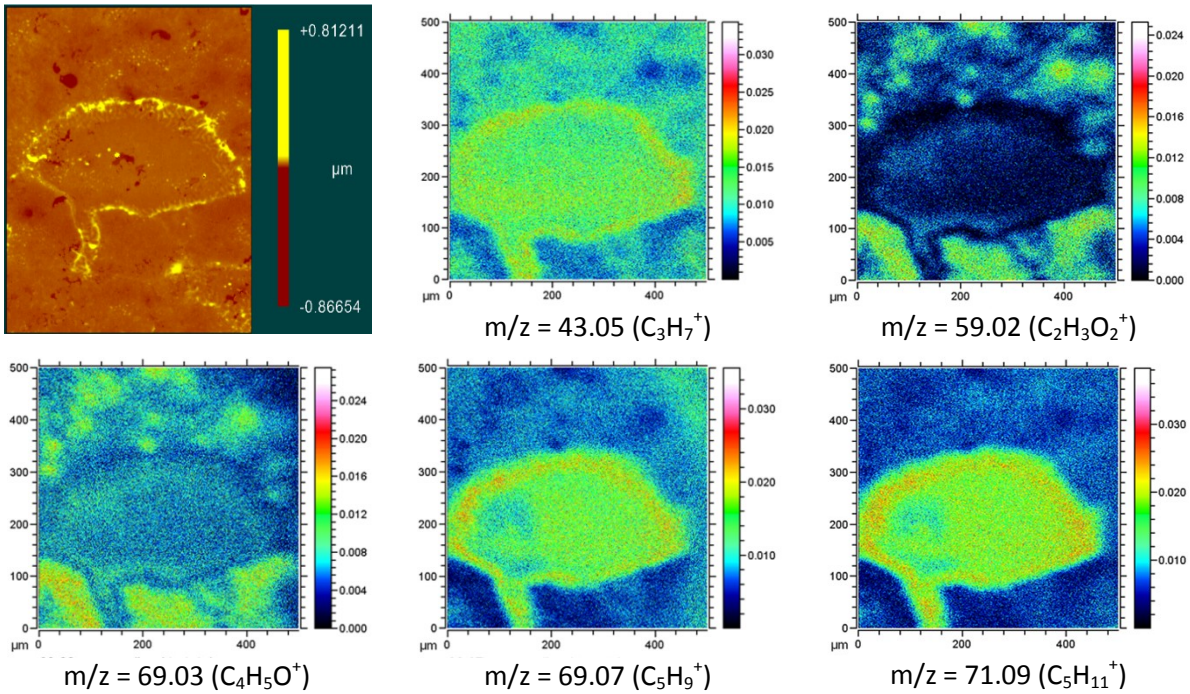

Figure 5.14 Interferometry micrographs and five SIMS maps of PMMA showing the presence of surface contamination. Interferometry micrograph field of view = 530 µm × 700 µm.

From figure 5.14 it can be seen that the raised areas observed in the interferometry images for PMMA correspond to particular molecular fragments, including $C_3H_7^+$, $C_5H_9^+$ and $C_5H_{11}^+$. The area surrounding the contamination corresponds to PMMA; the spatial distribution of the characteristic PMMA fragments $C_2H_3O_2^+$ and $C_4H_5O^+$ is shown in figure 5.14. In order to identify whether this contamination was related to the protective film, a spectrum was obtained for the side of the film facing the sheet substrate and is shown in figure 5.15. This spectrum displays peaks at m/z = 29.04, 43.05, 57.07, 69.07 and 71.09 which correspond to $[M+H]^+$ or $[M-H]^+$ and are characteristic of polyethylene $(C_2H_4)_n$ [121]. It is therefore suggested that the surface contamination is due to residue from the protective film.

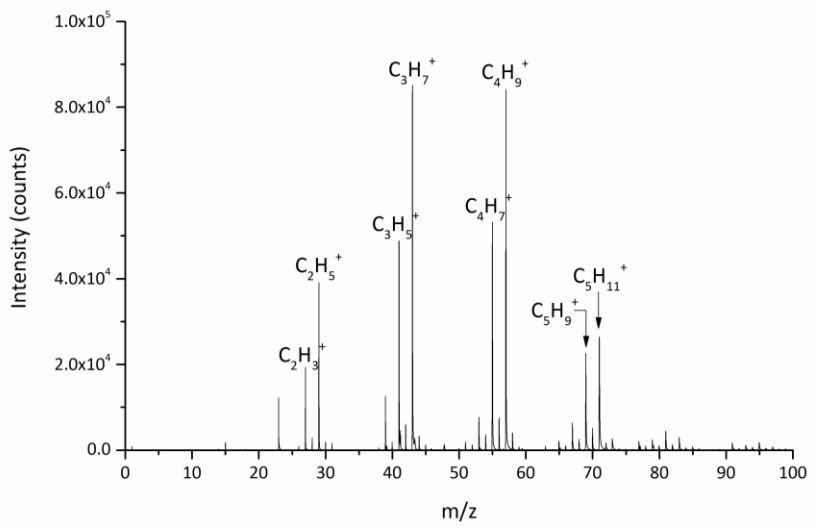

Figure 5.15 Positive ToF-SIMS spectrum for the protective film for the region m/z <100.

Further identification of the protective film was performed using ATR-FTIR spectroscopy. Figure 5.16 shows the ATR-FTIR spectra for both sides of the protective film. There is a clear difference between the spectra. The outer side of the film corresponds to polyethylene. However, a number of bands are present on the sheet-facing side which are not present on the outer side. The most notable are the bands at 1167 cm^{-1} (C-O stretch), 1237 cm^{-1} (C-O stretch), 1378 cm^{-1} (C-H bend), 1733 cm^{-1} (C=O bend) and 2958 cm^{-1} (C-H stretch). This would indicate the presence of carbonyl, carboxyl or aldehyde groups on the sheet-facing side of the film. Given that this side of the film was also sticky to the touch, these bands are attributed to the presence of an adhesive.

In contrast to the PMMA substrate, there was no contamination visible on the polystyrene substrate prior to cleaning, when viewed using white light interferometry, and no difference in the ATR-FTIR spectra from both sides of the polystyrene protective film.

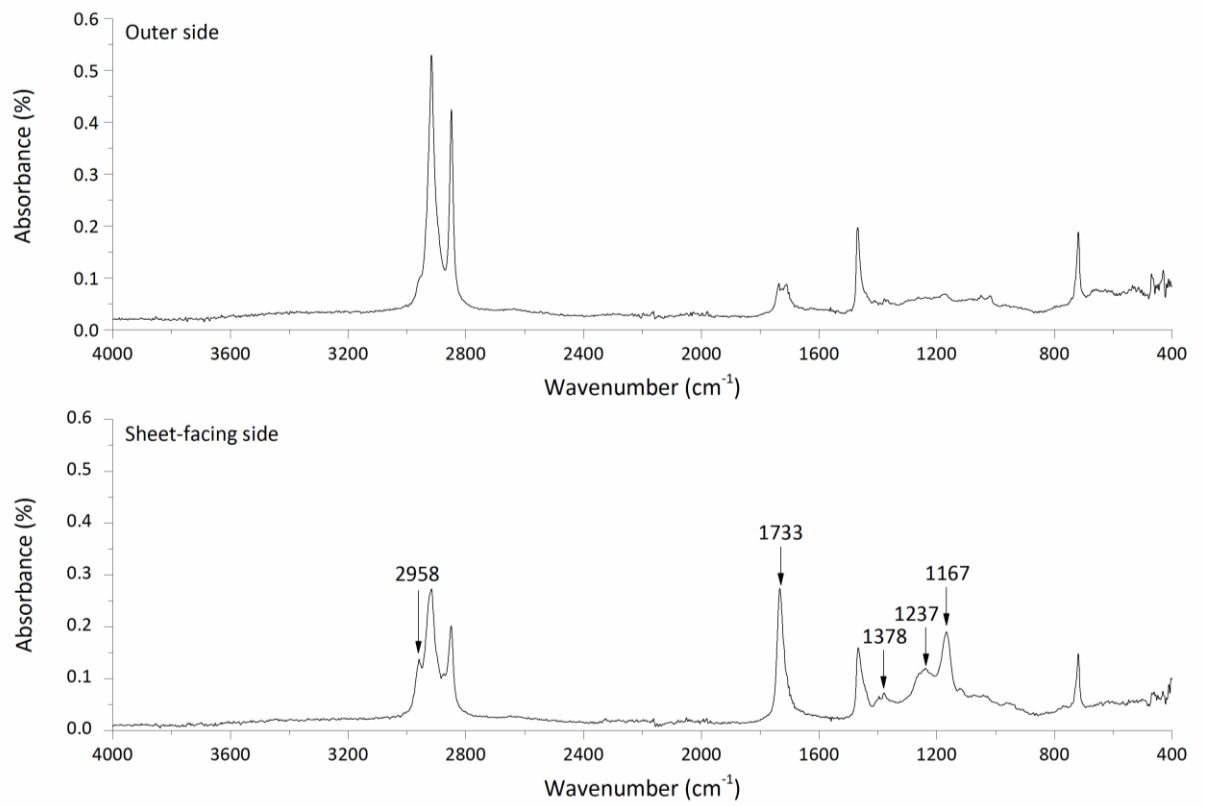

Figure 5.16 ATR-FTIR spectra from the outer side and the sheet-facing side of the protective PMMA film.

5.3.2.2 Cleaning of PMMA

PCA treatment of ToF-SIMS spectra obtained from the uncleaned and cleaned samples provides information about the changes in surface chemistry taking place due to cleaning. ToF-SIMS spectra for all cleaned substrates were obtained in the positive polarity and compared to the spectrum obtained for an uncleaned PMMA substrate. Figure 5.17 shows the PCA scores and loadings plots for PMMA substrates cleaned with organic solvents.

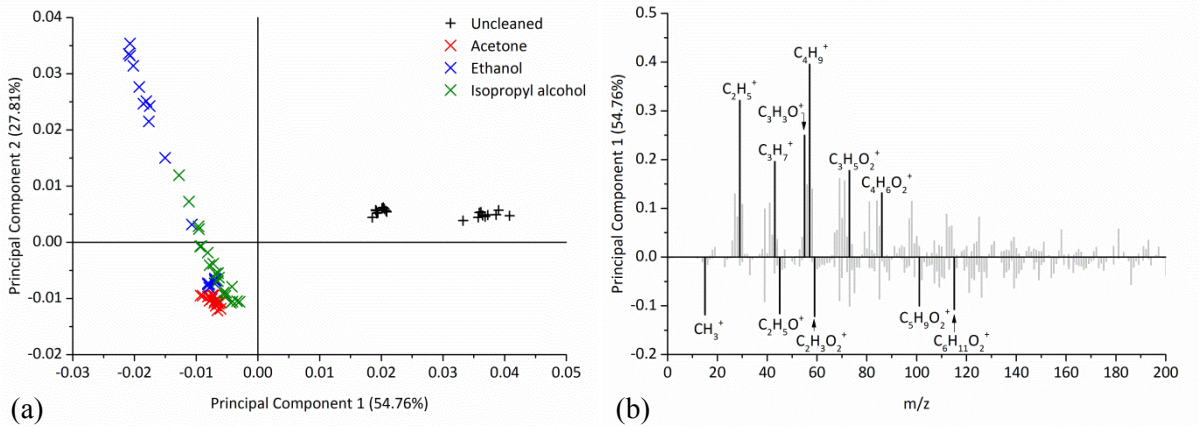

Figure 5.17 PCA a) scores and b) loadings plots for the positive polarity ToF-SIMS spectra from PMMA cleaned with organic solvents.

Figure 5.17 shows that there is a clear difference between the uncleaned substrate and all three substrates cleaned with the organic solvents. Inspection of the loadings reveals that these differences are due to the presence of fragments on the uncleaned surface which are not characteristic of PMMA (m/z = 29.04 ($C_2H_5^+$), 43.05 ($C_3H_7^+$), 57.07 ($C_4H_9^+$) and 73.03 ($C_3H_5O_2^+$)). It is notable that some of the fragments which characterise the uncleaned surface are of the form $[M+H]^+$ or $[M-H]^+$ where M = $(C_2H_4)_n$. These correspond to those fragments detected on the elevated areas of the PMMA substrate as shown in figure 5.14 and support the observation that the protective film residue is being reduced or removed via cleaning with organic solvents. The two clusters seen for the uncleaned substrate (black data points) in figure 5.17 are the result of a time difference between the acquisition of these two data sets. The loadings for the cleaned substrates are characteristic of PMMA.

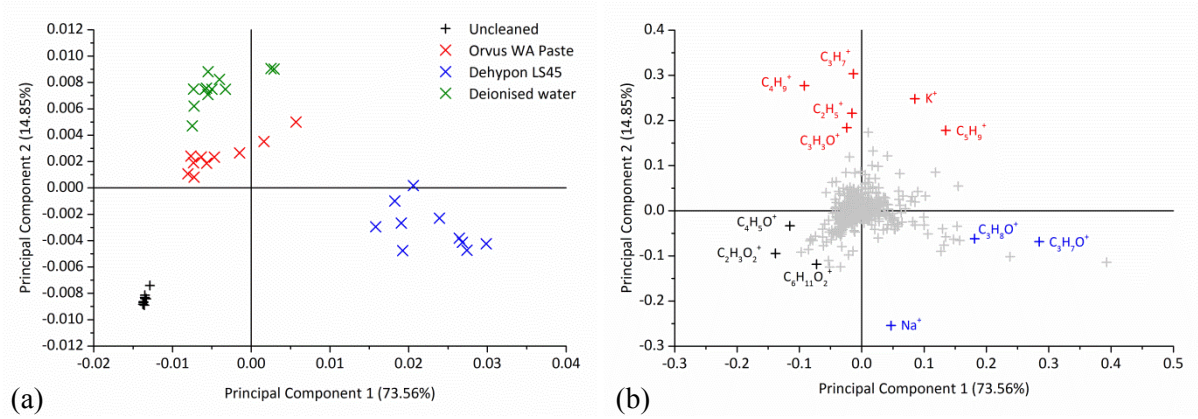

Figure 5.18 PCA biplots showing a) scores and b) loadings for the positive polarity ToF-SIMS spectra from PMMA cleaned with aqueous agents.

Figure 5.18 shows the PCA scores and loadings biplots for the PMMA substrates cleaned with aqueous agents[1]. Again there are clear differences between the substrates cleaned with different agents. The uncleaned substrates are characterised by fragments corresponding to PMMA, most notably those at m/z = 59.01 ($C_2H_3O_2^+$), 69.03 ($C_4H_5O^+$) and 115.08 ($C_6H_{11}O_2^+$). The fragments at m/z = 59.05 ($C_3H_7O^+$) and 60.06 ($C_3H_8O^+$) correspond to cleaning with the non-ionic surfactant (Dehypon LS45) and are indicative of residual surfactant on these samples[2]. Direct comparison of the uncleaned PMMA substrate with that cleaned with the non-ionic surfactant is shown in figure 5.19. Here the differences between the substrates can be clearly seen, with the positive loadings on PC1 corresponding to the non-ionic surfactant. The origin of the fragment at 284 is unclear and is not thought to correspond to the non-ionic surfactant. However, inspection of the original ToF-SIMS spectra reveals a high intensity peak at this mass for the substrate cleaned with the non-ionic surfactant.

[1] Note that all substrates cleaned with surfactants were also rinsed once with deionised water.
[2] The individual spectra for the surfactants are given in Appendix D.

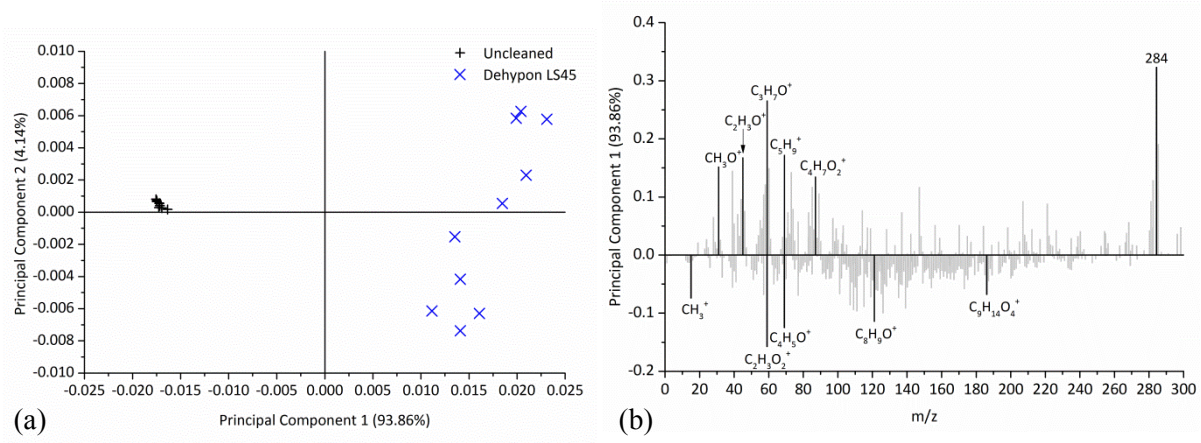

Figure 5.19 PCA a) scores and b) loadings plots for the positive polarity ToF-SIMS spectra from the PMMA substrate cleaned with the non-ionic surfactant.

The spectra from the PMMA substrates cleaned with the anionic surfactant (Orvus WA Paste) and deionised water in figure 5.18 are difficult to separate and are characterised by fragments at 29.04 ($C_2H_5^+$), 43.05 ($C_3H_7^+$), 55.02 ($C_3H_3O^+$) and 57.07 ($C_4H_9^+$) as well as the presence of K. As the hydrocarbon fragments are the same as those seen for the uncleaned substrate in figure 5.17, this suggests the presence of residue from the protective film. It might be expected that this contamination would also be seen on the uncleaned substrate, however differences between these samples may simply be due to local variations in the amount of residue present on the substrate prior to cleaning.

Alternatively these hydrocarbon fragments may be indicative of the long chain hydrocarbon tail present in SLS. However, while this could explain the fragments for the anionic surfactant, it would not explain the presence of hydrocarbon fragments as a result of cleaning with deionised water. It should be noted that the fragments characteristic of the SLS head group are more likely to be seen in the negative polarity. Figure 5.20 shows the PCA scores and loadings plots for the negative polarity SIMS spectra for the uncleaned PMMA substrate and the PMMA substrate cleaned with the anionic surfactant. Here it can be seen that the main positive loadings on PC1 are found at m/z = 78.95 and 95.95 corresponding to $[SO_3\text{-}H]^-$ and SO_4^- respectively and at m/z = 265, corresponding to the SLS hydrocarbon tail and sulphate head group ($C_{12}H_{25}SO_4^-$). It is therefore apparent that residual anionic surfactant is present on the PMMA substrate after cleaning.

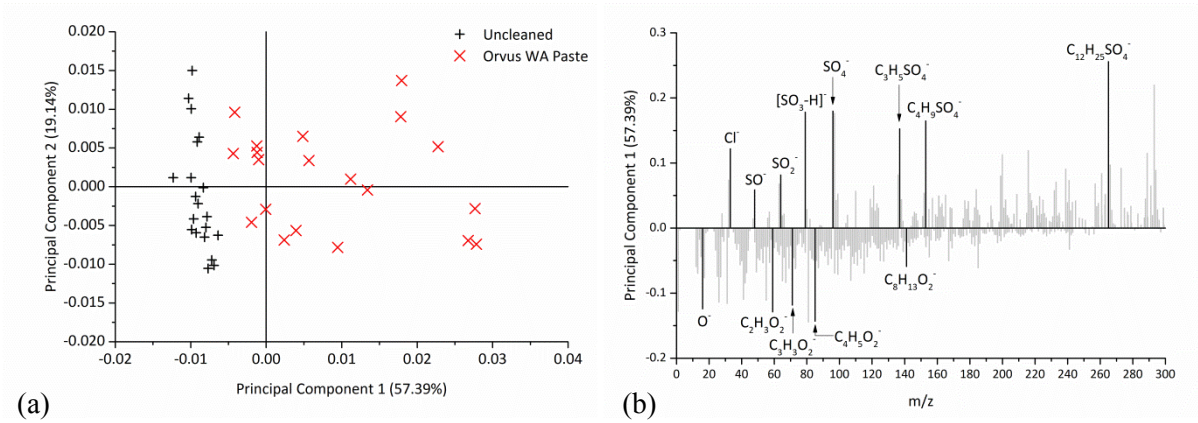

Figure 5.20 PCA a) scores and b) loadings plots for the negative polarity ToF-SIMS spectra from PMMA cleaned with the anionic surfactant.

5.3.2.3 Cleaning of polystyrene

Figure 5.21 shows the PCA scores and loadings biplots for the polystyrene substrates cleaned with organic solvents. Inspection of these plots shows clear differences between the substrates. The acetone-cleaned substrate shows fragments characteristic of polystyrene. This is most likely a result of the dissolution of the surface layer which was observed under white light interferometry. Contamination from Na and K was observed for those substrates cleaned with alcohols and there are also possible indications of residual solvent on the surface; the $C_2H_5O^+$ fragment is characteristic of both ethanol and isopropyl alcohol. The fragment $C_2H_3O^+$ is present for the uncleaned surface and is not characteristic of polystyrene, indicating that there may be some initial contamination on the polystyrene substrate prior to cleaning. Figure 5.22 provides further information about the cleaned substrates. It can be seen that the fragment at m/z = 45.03 ($C_2H_5O^+$), thought to correspond to solvent residue, and the contaminants at m/z = 22.99 (Na^+) and 38.96 (K^+) are most characteristic of the polystyrene substrate cleaned with ethanol, followed by isopropyl alcohol. The fragments characteristic of polystyrene are seen for the acetone-cleaned substrate. This suggests that ethanol and, to a lesser extent, isopropyl alcohol are likely to leave residues on the substrate after cleaning and that these residues are correlated with contamination from Na and K.

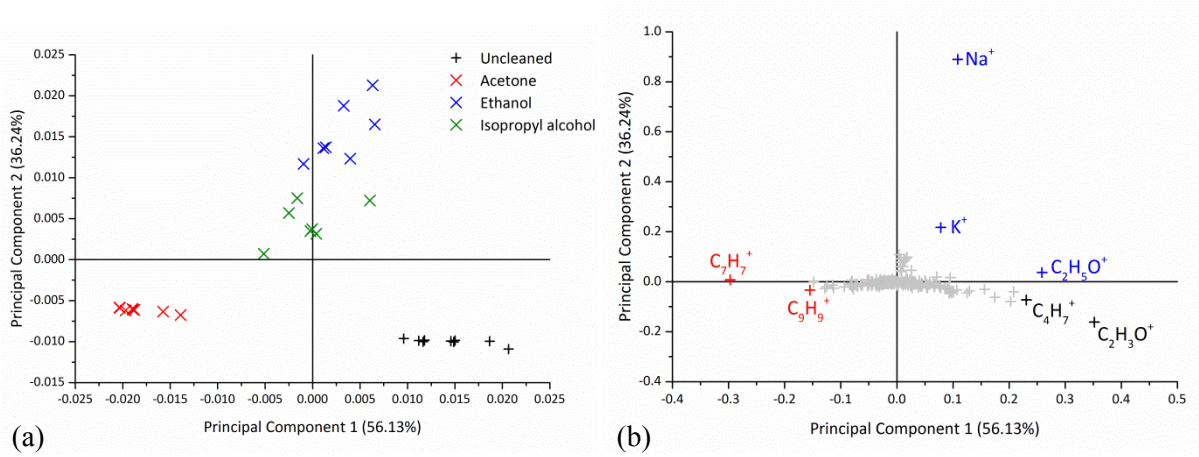

Figure 5.21 PCA biplots showing a) scores and b) loadings for the positive ToF-SIMS spectra from the polystyrene substrates cleaned with organic solvents.

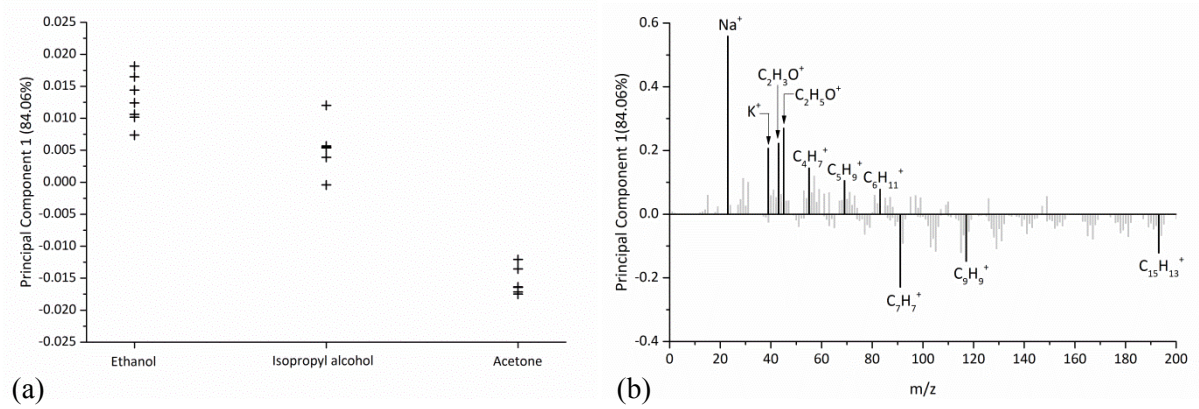

Figure 5.22 PCA a) scores and b) loadings plots for the positive ToF-SIMS spectra comparing the residues present on the polystyrene substrates cleaned with organic solvents.

The PCA scores and loadings biplots for the polystyrene substrates cleaned with aqueous agents and the dry cleaning procedure are shown in figure 5.23. These show a clear distinction between the substrates. In this case the characteristic fragments of polystyrene (m/z = 91.05 ($C_7H_7^+$) and 115.06 ($C_9H_7^+$)) are representative of the substrate that had undergone the dry cleaning procedure. This is most likely due to the presence of surface contamination on the other treated substrates. The substrates cleaned with the surfactants both suggest the presence of residual surfactant. In the case of the non-ionic surfactant this is indicated by the presence of the $C_2H_5O^+$ and $C_3H_7O^+$ fragments. The presence of the Na^+ fragment for the substrate cleaned with the anionic surfactant (Orvus WA Paste) suggests the possible presence of SLS, however inspection of the substrate in the negative polarity provides further information. It can be seen in figure 5.24 that the substrate cleaned with the anionic surfactant is characterised by the fragments at m/z = 79.96 and 96.96 which correspond to SO_3^- and SO_4H^- respectively and are indicative of SLS.

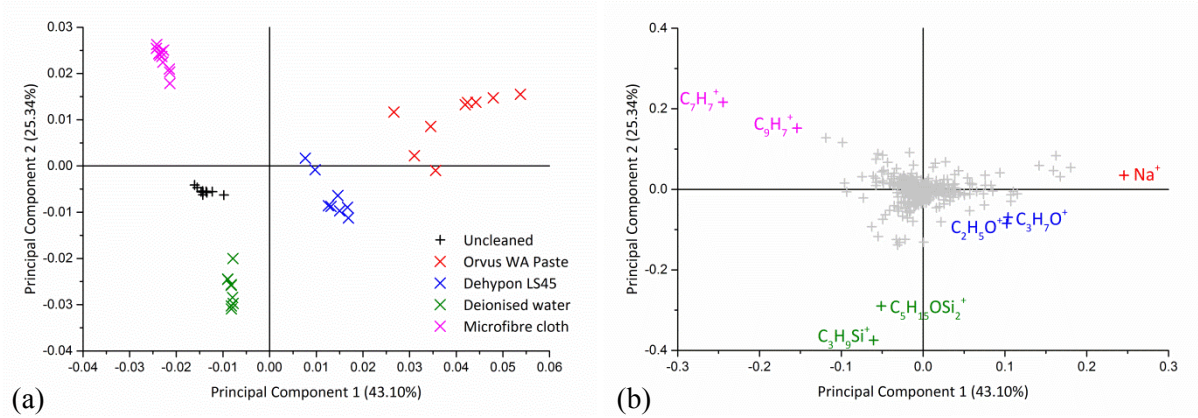

Figure 5.23 PCA biplots showing a) scores and b) loadings for the positive ToF-SIMS spectra from the polystyrene substrates cleaned with aqueous agents and the microfibre cloth.

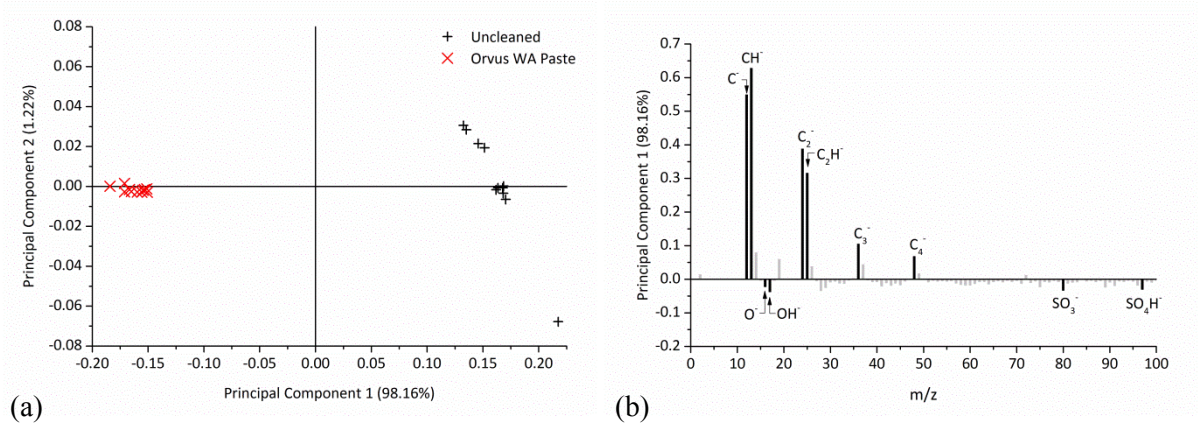

Figure 5.24 PCA a) scores and b) loadings plots for the negative SIMS spectra from the polystyrene substrate cleaned with the anionic surfactant.

In order to gain an indication of the extent of this residual surfactant layer, depth profiles were performed for the substrate cleaned with the anionic surfactant, and are shown in figure 5.25. This surfactant was chosen as the characteristic fragments of SLS are easily identifiable in the negative polarity. The fragments at m/z = 63.96 (SO_2^-), 79.96 (SO_3^-), 95.95 (SO_4^-), and 265.12 ($C_{12}H_{25}SO_4^-$) were analysed as a function of depth. The depth of the crater was calibrated using white light interferometry and a constant sputter rate assumed. It should be noted that the sputter rate of the surfactant layer is likely to be different to that of the polystyrene substrate and therefore only an estimation of the layer thickness is possible. The gradients of the depth profiles of the fragment in figure 5.25 appear to approach 0 at around 20 nm - 25 nm, indicating that a relatively thin layer of surfactant is present on the polystyrene surface after cleaning.

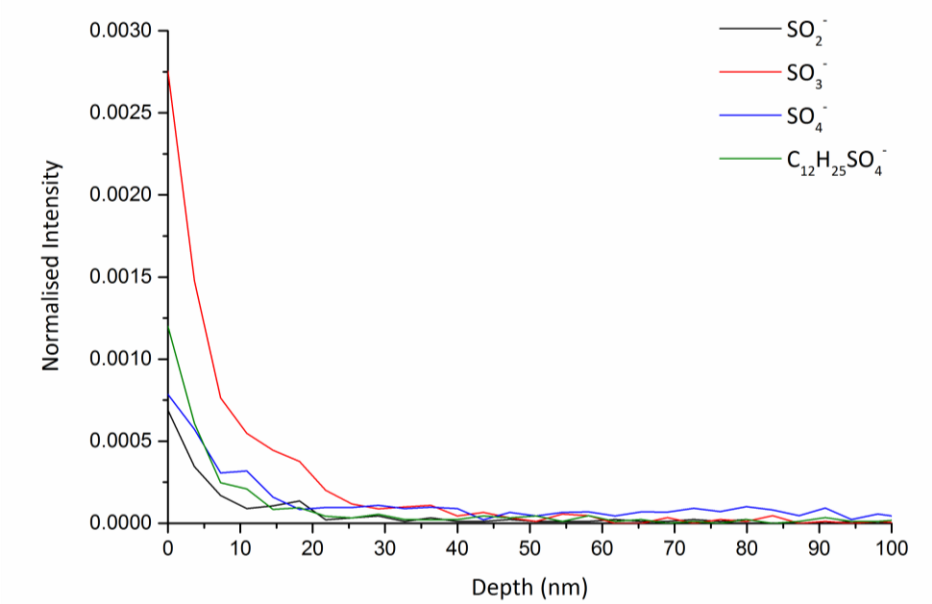

Figure 5.25 Negative polarity ToF-SIMS depth profiles for molecular fragments corresponding to the anionic surfactant.

The efficacy of additional rinsing steps as a means of surfactant removal was also explored. Figure 5.26 shows the PCA scores and loadings plots for the negative ToF-SIMS spectra from polystyrene substrates that had been cleaned with the anionic surfactant before undergoing repeated rinsing with deionised water. The number of rinsing steps ranged from 1 to 5, and a new cloth was used for each rinsing step. The PCA data reveals that an increase in the number of rinsing steps results in the surface being characterised less by the anionic surfactant and more by fragments corresponding to polydimethylsiloxane (PDMS), a highly mobile lubricant. This can be interpreted in three ways: the surfactant is being reduced or removed with additional rinsing, rinsing is resulting in greater contamination of the substrate, or a combination of these two processes is occurring. The latter is most likely, but examination of the surface that had undergone five rinsing steps was performed using ToF-SIMS to determine whether the surfactant had been entirely removed.

Figure 5.27 shows a 3D representation of the ToF-SIMS depth profile for the SO_3^- fragment for two polystyrene substrates: the first was not rinsed at all while the other underwent five separate rinsing steps. It should be noted that the extent of surfactant present is only an indication as any surfactant residue is likely to vary between samples and also between different areas on the same sample.

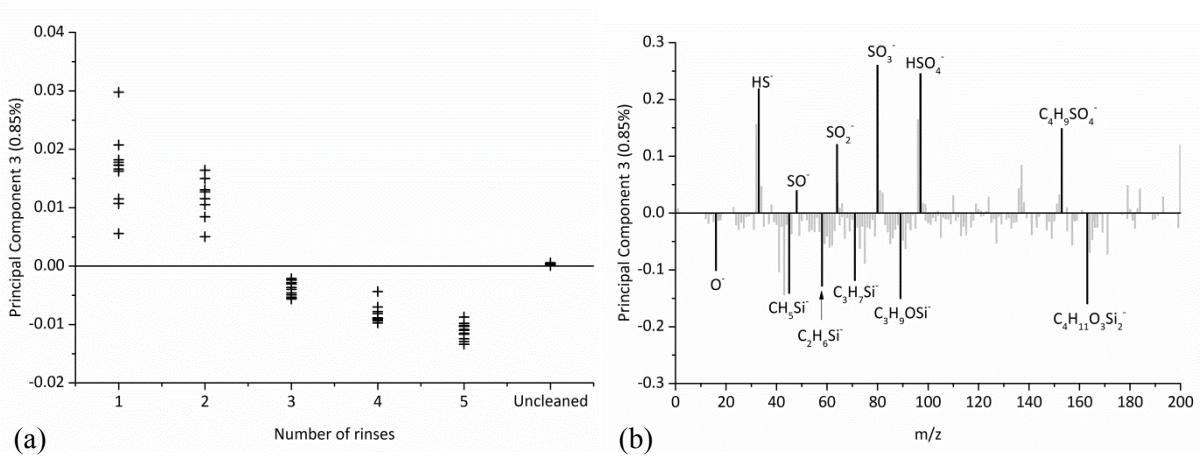

Figure 5.26 PCA a) scores and b) loadings plots for the negative polarity ToF-SIMS spectra from polystyrene cleaned with anionic surfactant showing the effect of rinsing.

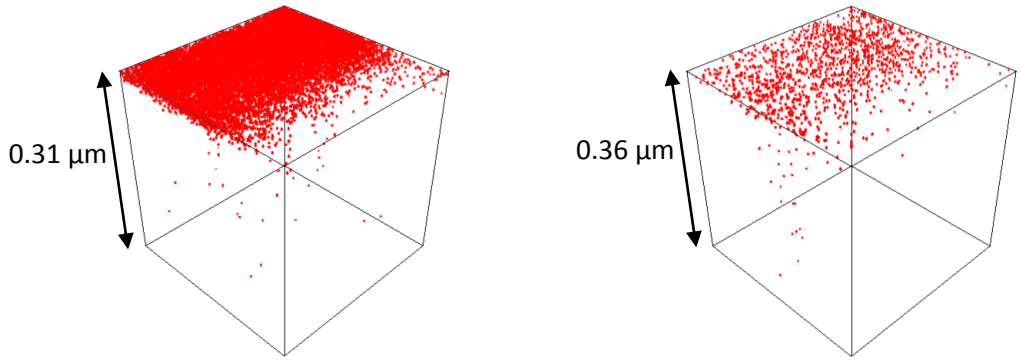

(a) No rinsing (b) After 5 rinses

Figure 5.27 3D representation showing the depth profile of the SO_3^- fragment (m/z = 79.96) for two polystyrene substrates cleaned with the anionic surfactant and having undergone a) no rinsing steps and b) five rinsing steps. Analysis area = 100 µm × 100 µm.

It is notable that the polystyrene substrate cleaned with deionised water (figure 5.23) is also characterised by fragments at m/z = 73.05 ($C_3H_9Si^+$) and 147.07 ($C_5H_{15}OSi_2^+$), which correspond to PDMS. PDMS is present in the laboratory environment, including in laboratory wash bottles and as a mould release agent for laboratory gloves. SIMS image analysis of the nitrile gloves (Kimtech, Kimberley-Clark, UK) used in this work (figure 5.28) revealed that the $C_3H_9Si^+$ fragment could be detected on the glove's surface, along with additional contamination from Na and K. However, PDMS is a well-known and ubiquitous contaminant, and other sources of contamination are possible.

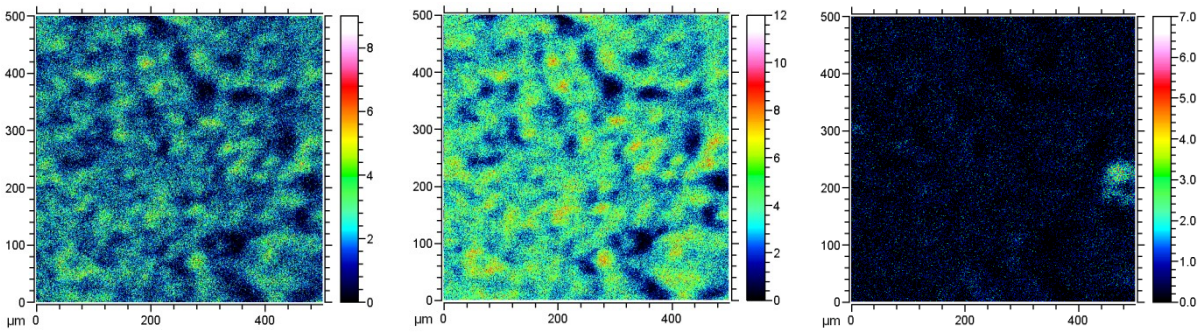

Figure 5.28 ToF-SIMS maps of the outer surface of a nitrile glove (tip of index finger) showing the presence of contaminants.

5.4 Discussion

The findings from this chapter are summarised in table 5.2.

Table 5.2 Summary of findings for the virgin substrates.

	PMMA	**Polystyrene**
Initial condition	Contamination present on the surface thought to correspond to residue from the protective film.	No notable residue from the protective film.
T_g (°C)	111.6 ± 0.5	103.6 ± 0.5
$\bar{M}_n$ (g/mol)	1.62×10^3	1.88×10^3
$\bar{M}_w$ (g/mol)	9.56×10^5	2.63×10^5
Micro-hardness (VHN)	21.3 ± 0.7	18.4 ± 0.3
Cleaning with organic solvents.	Removal of residue from protective film. No scratching observed.	Scratching observed for both alcohols. Surface dissolved with acetone. Contamination from cleaning.
Cleaning with aqueous agents.	No removal of residue from the protective film. No scratching observed. Cleaning residues from surfactants.	Scratching observed for all agents. Cleaning residues from surfactants. Contamination from cleaning. Anionic surfactant residue still present after repeated rinsing.

5.4.1 Bulk characterisation

Initial characterisation of the substrates was performed to confirm the composition of the plastics and to gain information about their properties. ATR-FTIR spectroscopy confirmed that the spectra of both plastics were consistent with the reference polymers in the HR Nicolet Sampler Library. Thermal analysis of the substrates gave values for the T_g of 112 ± 1 °C and 104 ± 1 °C for the PMMA and polystyrene substrates respectively. These are slightly higher than those reported in the literature, which are given as 105 °C for atactic PMMA and 80-90 °C for polystyrene [53]. The differences between these values may be due to differences in the polymers, such as their molecular structure and molecular weight, or the instrumentation used. The average molecular weight of both polymers was found using GPC. This gave values for PMMA of $\bar{M}_n$ = 1.62 ×10^3 g/mol, $\bar{M}_w$ = 9.56 ×10^5 g/mol and $\bar{M}_n$ = 1.88 ×10^3 g/mol, $\bar{M}_w$ = 2.63 ×10^5 g/mol for polystyrene. Micro-hardness testing was performed to find the Vickers hardness values for PMMA and polystyrene. This revealed that the PMMA substrate had a greater average hardness value than the polystyrene substrate but the surface was less homogenous. This variation may be a result of contamination on the surface of PMMA which is discussed later in this section.

5.4.2 Surface cleaning

5.4.2.1 Initial surface contamination

Analysis of the virgin PMMA substrate was performed using white light interferometry and ToF-SIMS. Most notable is the presence of existing contamination on the surface after the removal of the protective film. Analysis of the ToF-SIMS micrographs revealed that fragments corresponding to the raised areas observed under white light interferometry include those of the form $[M+H]^+$ and $[M-H]^+$, where M = $(C_2H_4)_n$. In order to determine whether these fragments were related to the protective film, the film was analysed using ToF-SIMS and ATR-FTIR. The composition of the film was found to be consistent with polyethylene and the ToF-SIMS spectrum showed characteristic fragments at $[M+H]^+$ and $[M-H]^+$, which were consistent with the hydrocarbon fragments detected on the raised areas. ATR-FTIR spectroscopy of the sheet-facing side of the protective film revealed the presence of additional bands indicating the presence of carbonyl, carboxyl or aldehyde groups which are not characteristic of polyethylene. It is thought that these may correspond to the presence of a pressure-sensitive adhesive which had been used to adhere the film to the plastic substrate. This may account for the $C_3H_3O^+$ fragment which was also detected on the PMMA surface. It is therefore suggested that the surface contamination seen on the virgin PMMA substrate is due to a residue from the protective film and/or an adhesive used to adhere the film to the substrate. This is supported by the fact that the protective film was sticky to the touch and was difficult to physically remove from the PMMA substrate with tweezers.

The use of organic solvents to clean PMMA was effective in removing the protective film residue, as seen by a change in the surface topography after cleaning with acetone and ethanol. PCA analysis of the ToF-SIMS data for these substrates also revealed that the significant differences between the uncleaned and cleaned substrates were due to the reduction or removal of the residue with cleaning: fragments corresponding to the residue were characteristic of the uncleaned surface whereas the cleaned substrates were characterised by fragments corresponding to PMMA. The use of dry cleaning and aqueous agents were not thought to be effective in removing this surface contamination as no significant changes were observed using interferometry or detected via the use of ToF-SIMS.

5.4.2.2 Scratching

Inspection of the PMMA substrates with SEM did not reveal any further physical changes to the surface as a result of cleaning. However, the effect of all cleaning agents on polystyrene was to result in noticeable scratching of the surface which could be seen using SEM. These scratches were formed in the direction of cleaning. This observation agrees in part with the POPART findings [31], which reported that scratching was observed for all plastic substrates investigated, including PMMA. Work by Nilsen et al. [151] also observed scratching and pitting on PMMA as a result of cleaning with microfibre cloths, however this study was performed using repeated strokes across the surface. It is suggested that the hardness of the substrate may affect the scratching behaviour and the greater hardness of PMMA (compared to polystyrene) may explain the lack of scratching observed in this work.

An indication of the width and depth of these scratches was obtained using AFM. The line profiles obtained indicate that the scratches consist of a central trough surrounded by raised areas on either side and appear to be of a uniform width along their length. The entire damaged area had a typical width of approximately 1 μm, while the peak-to-valley height of the troughs examined were of the order of 20-25 nm. However, it is possible that some scratches may exceed these dimensions but were not observed.

The source of these scratches is of interest. It is possible that the passage of the microfibre cloth across the substrate is responsible for their formation. However, the spacing of the scratches is not regular and the scratch width is an order of magnitude lower than the width of the individual fibres. It is suggested instead that the scratches resulted from stray dust or particulates that were picked up by the microfibre cloth and then dragged across the surface. Alternatively the SEM micrographs of the microfibre cloth show the presence of particles on the fibres which could also be a source of the scratches. It should be noted that the weave of the cloth was relatively flat and close and therefore particles might be held closer to the surface when compared to a loose-weave and fluffier cloth. POPART observed that the use of a surfactant as a cleaning agent could result in lubrication of the surface, and therefore a reduction in the extent of scratching [31]. Nilsen et al. made the same

observation in their work on PMMA [151]. However, inspection of the surfaces with SEM is inconclusive. It could not be determined whether any differences in scratching were due to a lubrication effect, the area of the surface under examination or simply differences in the initial condition of the plastic surface. It should also be taken into account that the application of the surfactants was followed by a second rinsing step and therefore these substrates were subjected to twice the mechanical contact of the other cleaning treatments.

Physical damage in the form of scratches was immediately apparent under SEM but in most cases was not visible to the naked eye. The most notable exception to this was the case of acetone, where dissolution of the surface was observed. Given the similarity of the solubility parameters for acetone and polystyrene (RED = 1.0), this is not unexpected. It might also be expected that the PMMA substrate would be dissolved by the application of acetone (RED = 0.7), however this was not observed and may be related to the higher T_g of this substrate.

Some scratching of the polystyrene substrates cleaned with alcohols was also visible to the naked eye. While the width of a scratch is not generally related to its visibility [152], the British Standard 'Test methods for surface imperfections of optical elements' (ISO 14997:2011) [153] specifies a minimum surface imperfection width of 6 μm. While the widths of the scratches formed during cleaning were typically not greater than 1 μm, many of the scratches extended across the length of the substrate and, in some cases, were clustered together, potentially increasing their visibility. The presence of scratches may not be detected by the naked eye, but can still form areas of weakness on the plastic surface and potentially result in the creation of microclimates which may adversely affect the plastic at a future point in time.

5.4.2.3 Surfactant residues and contamination

The chemical changes occurring as a result of cleaning can be divided into two categories: the removal of pre-existing surface contamination and the deposition of residues and contaminants as a result of the cleaning process. The presence and removal of the initial contamination on the PMMA substrate has already been discussed. Similar contamination was not observed for the polystyrene substrate and in this case the protective film was removed from the surface with little difficulty, indicating that an adhesive was not used.

Cleaning of both the PMMA and polystyrene substrates with solvents was effective at removing initial surface contamination. However, the polystyrene substrate cleaned with alcohols was characterised by Na and K contamination after cleaning. The source of this contamination is most likely due to contact with the microfibre cloth, which may have been itself contaminated or was contaminated by handling or the application of solvents. It should be noted that both sodium and potassium have a high ionisation probability [122] and therefore even low concentrations result in

high intensity signals. The appearance of these fragments on the cleaned surface may be related to residual solvent being present on the surface. The presence of the $C_2H_5O^+$ fragment on the polystyrene substrates indicates that residual solvent is present on the surface after cleaning. Inspection of the individual PCA data for the solvent-cleaned polystyrene substrates indicated that fragments corresponding to residual solvent and the contaminants Na and K were most characteristic of the substrates cleaned with ethanol, followed by isopropyl alcohol and finally by acetone. However, the certificates of analysis for the organic solvents indicate that the maximum contamination from sodium and potassium is very similar for all organic solvents used, being 0.5 ppm (0.2 ppm for isopropyl alcohol) and 0.1 ppm respectively. Significant contamination with Na and K was not observed for those substrates cleaned with aqueous agents.

Inspection of the PMMA substrate after cleaning with surfactants revealed the presence of small particulates on the surface and suggested the presence of residual surfactant. ToF-SIMS analysis of both plastics detected the presence of both surfactants after cleaning. This is in agreement with previous work investigating the cleaning of PVC, where surfactant residue was observed as a result of cleaning with Dehypon LS45 [34]. Inspection of the depth profiles for the polystyrene substrate cleaned with the anionic surfactant revealed that the thickness of the residual layer was of the order of 20-25 nm. However, it should be noted that the impact of primary ions on the surface can result in mixing of the surface layers and therefore this layer may be thinner than indicated by the depth profiles.

While repeated rinsing of the polystyrene substrate appeared to be effective in reducing the surfactant residue, it did not remove it entirely. PCA analysis of the SIMS data also suggests that repeated rinsing was accompanied by the deposition of contamination from PDMS. PDMS contamination was also observed for the polystyrene substrate cleaned with deionised water and is most likely a result of the surface coming into contact with the cloth during cleaning as this was the only contact with the surface during the cleaning process. However, the initial source of this contamination is unclear. While it may have been present on the microfibre cloth, it could also have resulted from transfer from the wash bottle containing the deionised water or from the nitrile gloves used to handle the cloth. ToF-SIMS inspection of the nitrile gloves used to prepare the samples detected the presence of PDMS on the glove surface and previous work on the surface composition of nitrile gloves using XPS and SIMS has also found that laboratory gloves can be a source of contamination [29, 30]. However, given that PDMS was principally detected for cleaning agents containing deionised water, the water container is also a likely source of contamination.

Conclusions

It is evident from the initial inspection of the PMMA substrate that the condition of a plastic surface may not be immediately apparent. In this case the contamination from the protective film was not visible to the naked eye, but it is likely that its presence would result in local changes in surface energy, which could change its soiling behaviour. The type of contamination would also have implications for the choice of cleaning agent.

It can be seen that the application of cleaning treatments to new, virgin substrates can result in notable physical and chemical changes to the substrate. The most notable changes observed during this work were the formation of scratches on polystyrene and the presence of residues and contamination on the cleaned substrates. The introduction of scratches and defects to the plastic surface via cleaning may result in further changes to the substrate over time and may detrimentally change the appearance of a plastic object in the future. These findings also raise questions about the effect of cleaning agents on plastic substrates which have a prior history, and which may be soiled or actively degrading. This is the focus of the next chapters.

Chapter 6

Artificially soiled substrates

It was seen in the last chapter that the cleaning of virgin plastic substrates can introduce changes to the surface in the form of scratching, residues and contamination. This chapter details the effect of cleaning agents on the surfaces of PMMA and polystyrene substrates that were artificially soiled. Analysis of the substrates was performed to determine whether the presence of soil alters the cleaning behaviour and to examine the efficacy of the cleaning agents for soil removal.

6.1 Introduction

While the examination of virgin substrates provides valuable information about the effect of cleaning on a plastic surface, real-world surfaces are rarely in pristine condition. The condition of artefacts acquired by museums can range from prototypes that originate straight from the manufacturer to items that have a lengthy and varied history. Even those items which are in good condition are not immune from dust and other contamination from the surrounding atmosphere.

As detailed in Chapter 1, dust and soiling in the museum environment may incorporate fibres, skin particles, mineral fragments, diesel particulate matter, atmospheric pollutants, adhesives and, for those items on open display, any number of foreign contaminants. Soiling also varies by location, the history and function of the object and its design. It is therefore difficult to determine the exact composition of a typical soil or contaminant. While it would be possible to naturally soil samples by leaving them exposed to the museum environment, this could be a lengthy, uncontrolled process and the precise composition of the contamination would be unknown.

The use of artificial soils to examine the efficacy of cleaning treatments is present in a number of industries and the types of soil vary widely. Pesonen-Leinonen et al. used radioactive tracers to look at soil adhesion to PVC flooring materials [154] while a similar study used palmitic acid and triolein to examine the effect of plasticiser on the soiling of PVC [155]. Much of the literature around

cleaning focuses on the decontamination of surfaces in medical applications. Therefore many of the soils employed in these studies are of a biological composition.

The British Standards BS ISO 11378-1:2000 and BS EN ISO 11378-2:2001 detail laboratory soiling tests for textile floor coverings [156, 157] and list four different standard soils. Depending on the application in question, the soil composition can range from a simple silica-based soil to one containing over 10 components. While the soils detailed in ISO 11378 are designed as model soils, the use of multiple ingredients could make it more difficult to analyse any resulting data. Galatis et al. [158] used a similar multi-component soil to investigate the removal of soiling from artificially degraded varnishes, designed to mimic aged soiled panel paintings. POPART examined two different types of soiling: a carbonaceous soil designed to imitate particulate matter from diesel engines and a sebum soil, which was used to mimic fingerprints [31]. For the purposes of this work it was decided to adapt the POPART recipe to investigate the effect of one carbonaceous soil. This was for a number of reasons, including the potential for particulate pollution due to the location of the V&A on a main thoroughfare, the visibility of carbonaceous soiling and therefore the likely aesthetic impact and the potential problems encompassed in the removal of oily, particulate matter.

6.2 Experimental

Three steps were performed in this process: the selection of an artificial soil, soil deposition and removal via cleaning.

6.2.1 Composition of artificial soil

It was decided to base the artificial soil on the recipe used in the POPART work. As this recipe consists of only two components, paraffin oil and carbon black, it was anticipated that chemical analysis would be more straightforward and it would also allow comparison with the POPART findings. The original recipe used a 95:5 paraffin oil to carbon black ratio. However, initial testing revealed that this ratio resulted in a very oily soiling layer which remained mobile for a long period of time and was not very representative of natural soiling. Adjustment of the recipe to a 70:30 paraffin oil to carbon black ratio resulted in a more viscous soil. While this still contained more oil than would be expected to be encountered in the museum environment it was sufficiently fluid to deposit via spin coating.

The paraffin oil (CAS no. 8012-95-1) and the carbon black (CAS no. 1333-86-4) were sourced from Sigma Aldrich (USA). According to the specification sheet for the carbon black, the particle sizes are in the range 2 μm - 12 μm [159]. Figure 6.1 shows an SEM image of the carbon black particles used in this work. It can be seen that the surface topography is rough and that the particles have an approximate diameter of 10 μm, in agreement with the literature value.

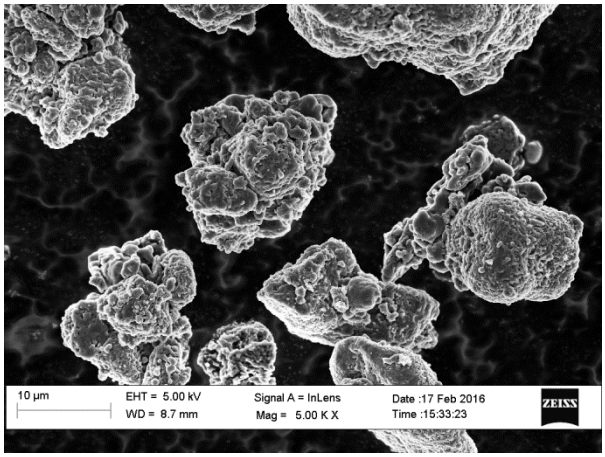

Figure 6.1 SEM micrograph of the carbon black particles.

6.2.2 Preparation of substrates and deposition of artificial soil

Prior to soiling, the protective film was removed from the substrates and fiducial markers were placed on the surface as described in Chapter 4. Based on the previous work on the virgin substrates it was decided to rinse the substrates with flowing isopropyl alcohol prior to soil deposition to remove any residue remaining from the protective films. A rinsed plastic substrate is henceforth referred to as a prepared substrate. The prepared substrates were then spin-coated with approximately 0.5 ml carbonaceous soil using a Polos Spin 150 spin coater (SPS-Europe, Germany) operating at ω=3000 rpm, a=5000 rpm/s for 60 s. Spin-coating was used as a deposition method to limit the introduction of scratching or damage to the surface; any scratching caused by the deposition of the soil would be radial and therefore possible to identify. After soiling the samples were stored at ambient temperature and humidity for two weeks to allow the soil to settle on the surface.

6.2.3 Cleaning procedure

The same cleaning procedure was used for these substrates as described in Chapter 4. For examination in high vacuum (HV), samples were repeat cleaned until they were visibly clean. For this reason separate samples were used for atmospheric microscopy and for HV analysis or AFM. Therefore it should be noted that the physical changes observed under AFM and SEM are affected by repeat cleaning. Analysis of the samples using white light interferometry, AFM, SEM and ToF-SIMS were performed using the same settings as described in Chapter 5.

6.3 Surface analysis

Samples were examined with white light interferometry after the preparation of the substrates and before subsequent soiling. Examination of the soiled and cleaned substrates was performed using optical microscopy, white light interferometry, AFM, SEM and ToF-SIMS.

6.3.1 Characterisation of soiling

Figure 6.2 shows a photograph of the soiled PMMA substrate and a composite image obtained using light microscopy in epi-brightfield mode. It can be seen that there is full coverage of the substrate and that deposition is fairly uniform although there is a slight increase in material in the centre of the sample. Inspection of the optical micrograph reveals some clumping of carbon black particles on the surface.

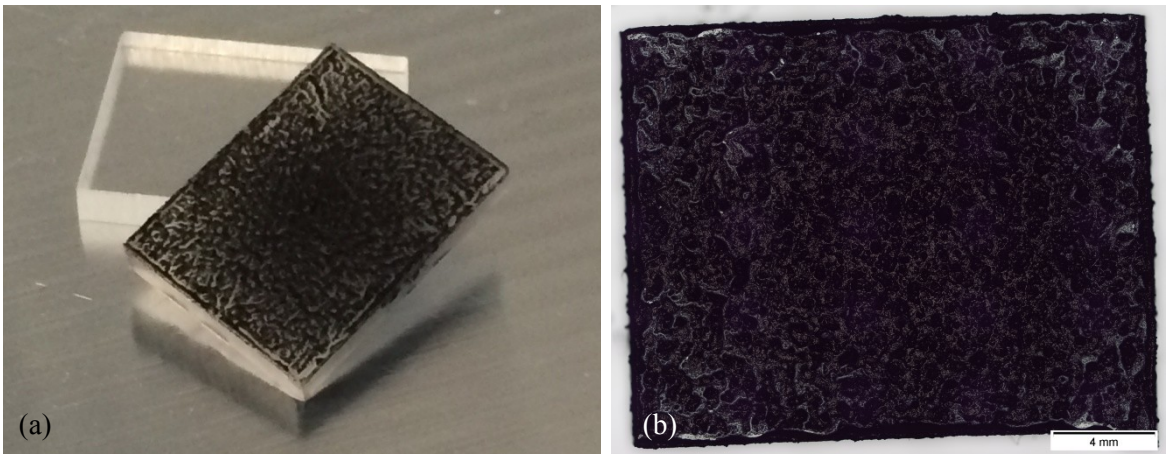

Figure 6.2 a) Photograph of the soiled PMMA substrate and b) composite light optical micrograph of the soiled PMMA substrate (scale bar = 4 mm).

6.3.2 Physical changes

6.3.2.1 PMMA

Examination of the soiled substrates after cleaning was performed using white light interferometry. Figure 6.3 shows the micrographs for all cleaning treatments for PMMA before and after cleaning. It is clear from these micrographs that the organic solvents were most effective in removing surface contamination. However, the presence of horizontal lines on all substrates cleaned with organic solvent, most apparent for acetone in figure 6.3, indicates surface damage due to the cleaning procedure. While the application of the surfactants to the PMMA substrate was effective in removing the majority of the artificial soil, it can be seen that there were still some raised areas remaining on the substrate after cleaning. Unsurprisingly, the deionised water was ineffective in removing the oily soil and the use of the microfibre cloth alone was the least effective method used. In the cases of the aqueous agents, the extent of contamination remaining on the soil means that it is difficult to determine whether there is underlying damage to the PMMA surface. SEM micrographs were therefore captured for soiled substrates that had undergone repeated cleaning steps to remove any remaining soil from the surface, and are shown in figure 6.4.

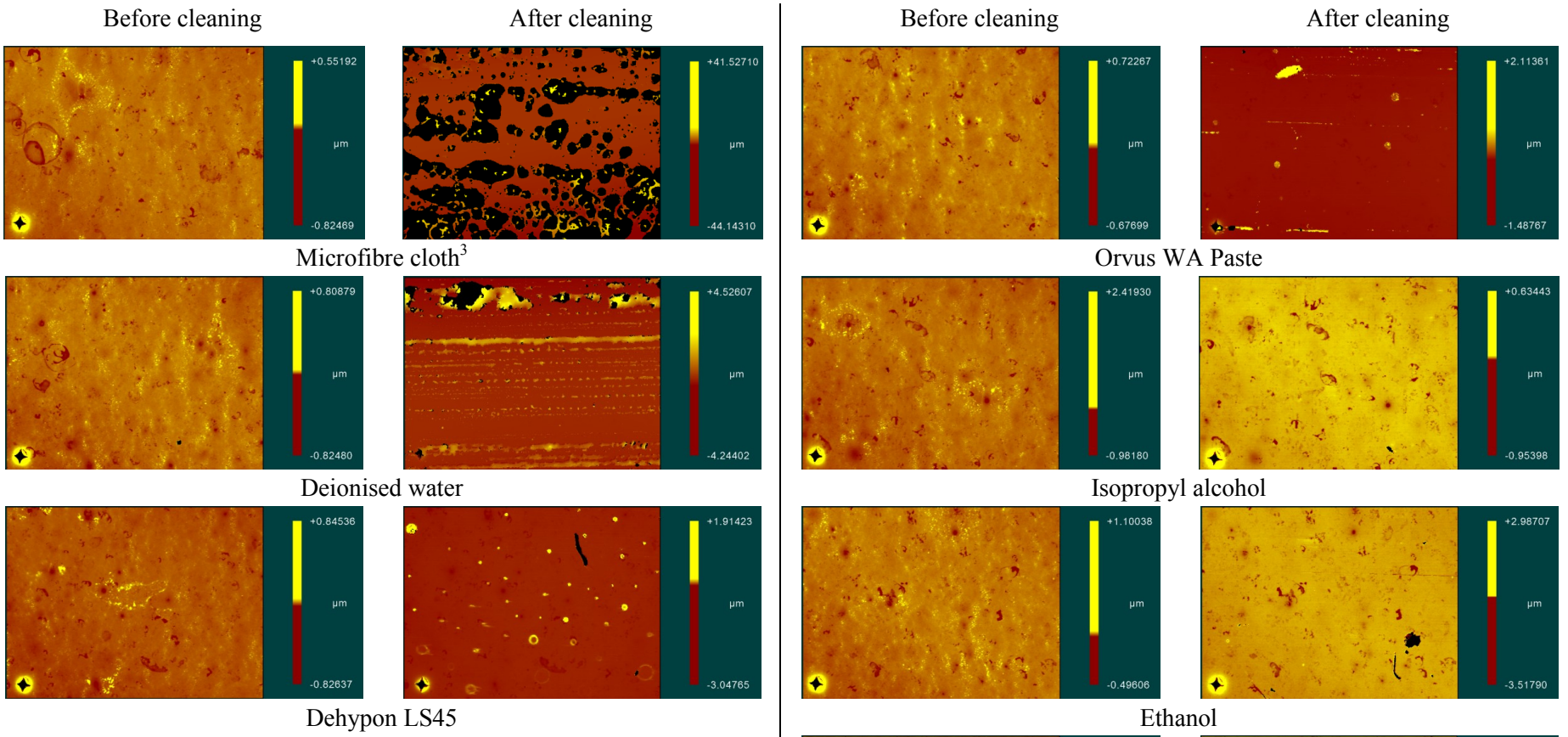

Figure 6.3 Interferometry micrographs of the PMMA substrate before soiling and after soiling and cleaning with the agent indicated. Field of view = 1.46 mm × 1.09 mm. Cleaning in horizontal direction (L to R).

[3] The image captured after cleaning does not correspond to the one captured before cleaning due to the inability to locate the marked area as it was obscured by soil.

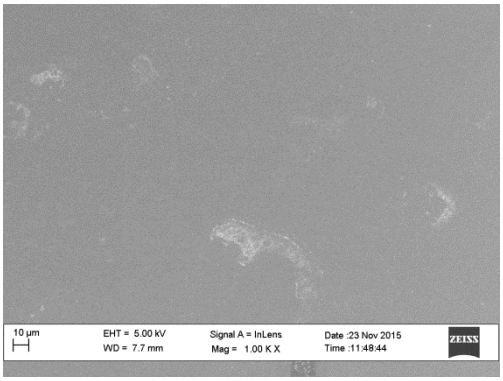

No treatment

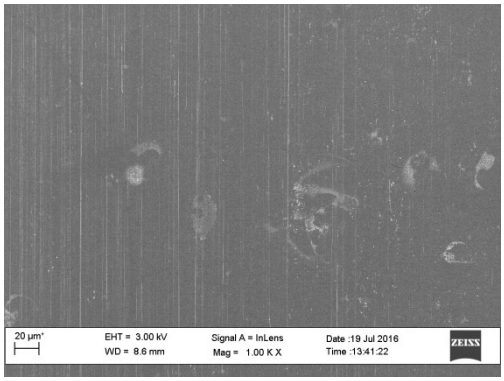

Microfibre cloth

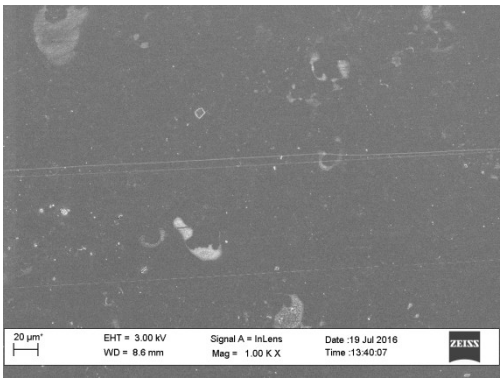

Deionised water

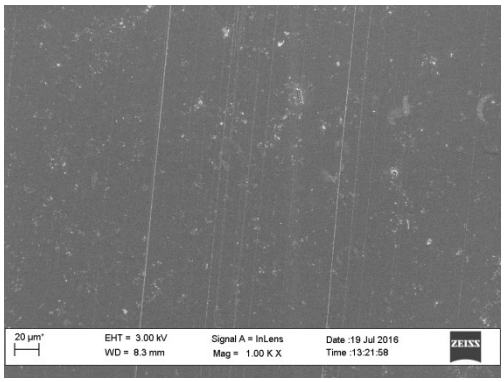

Dehypon LS45

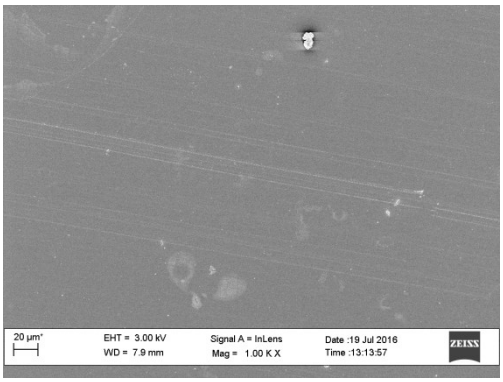

Orvus WA Paste

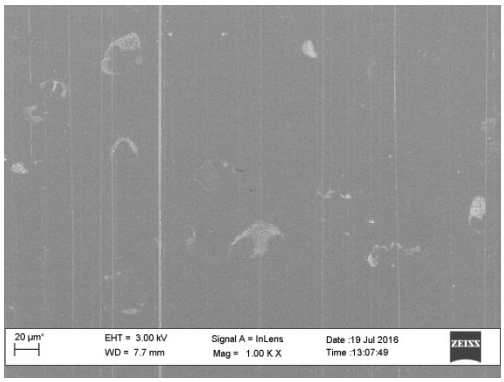

Isopropyl alcohol

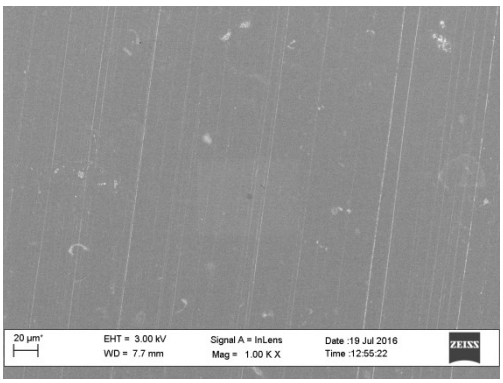

Ethanol

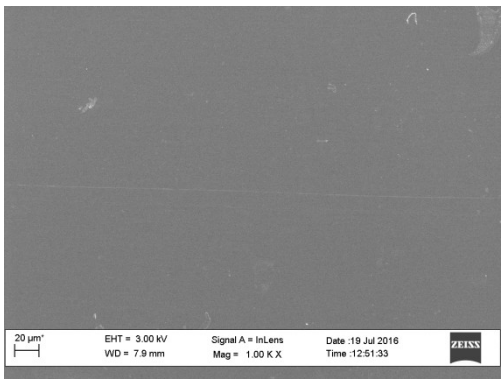

Acetone

Figure 6.4 SEM micrographs of the artificially soiled PMMA substrates after cleaning with the agent indicated.

Inspection of the SEM micrographs revealed that the PMMA substrate was scratched as a result of the application of all cleaning agents. The scratches are generally narrow, although they may be clustered and the width of the scratches may not be uniform, as seen in figure 6.5. As had been previously seen for the virgin substrates, the PMMA substrate experienced severe beam damage at high magnification. In this case there was a tendency for cracking to occur either along or in the vicinity of the scratches, indicating a possible area of weakness.

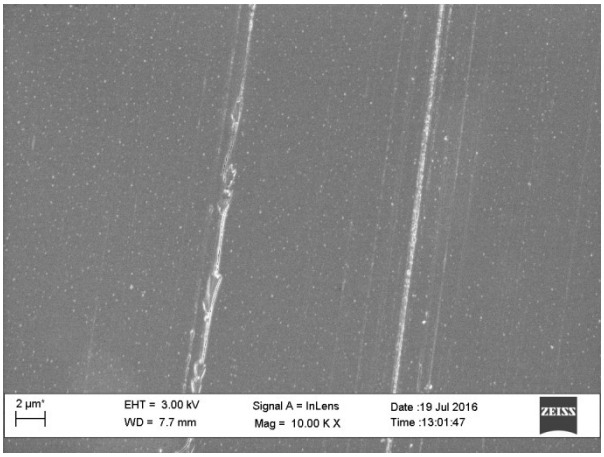

Figure 6.5 SEM micrograph showing a close-up of the soiled PMMA surface cleaned with isopropyl alcohol.

The scratch topography was investigated using AFM. Figure 6.6 shows AFM micrographs for two soiled PMMA substrates cleaned separately with acetone and the anionic surfactant (Orvus WA Paste), along with the surface profiles for the lines indicated. The peak-to-peak width of these scratches was typically in the range of 500 nm-1 µm, with a peak-to-valley height of approximately 10 nm, although deeper scratches may also be present, as seen in figure 6.6b.

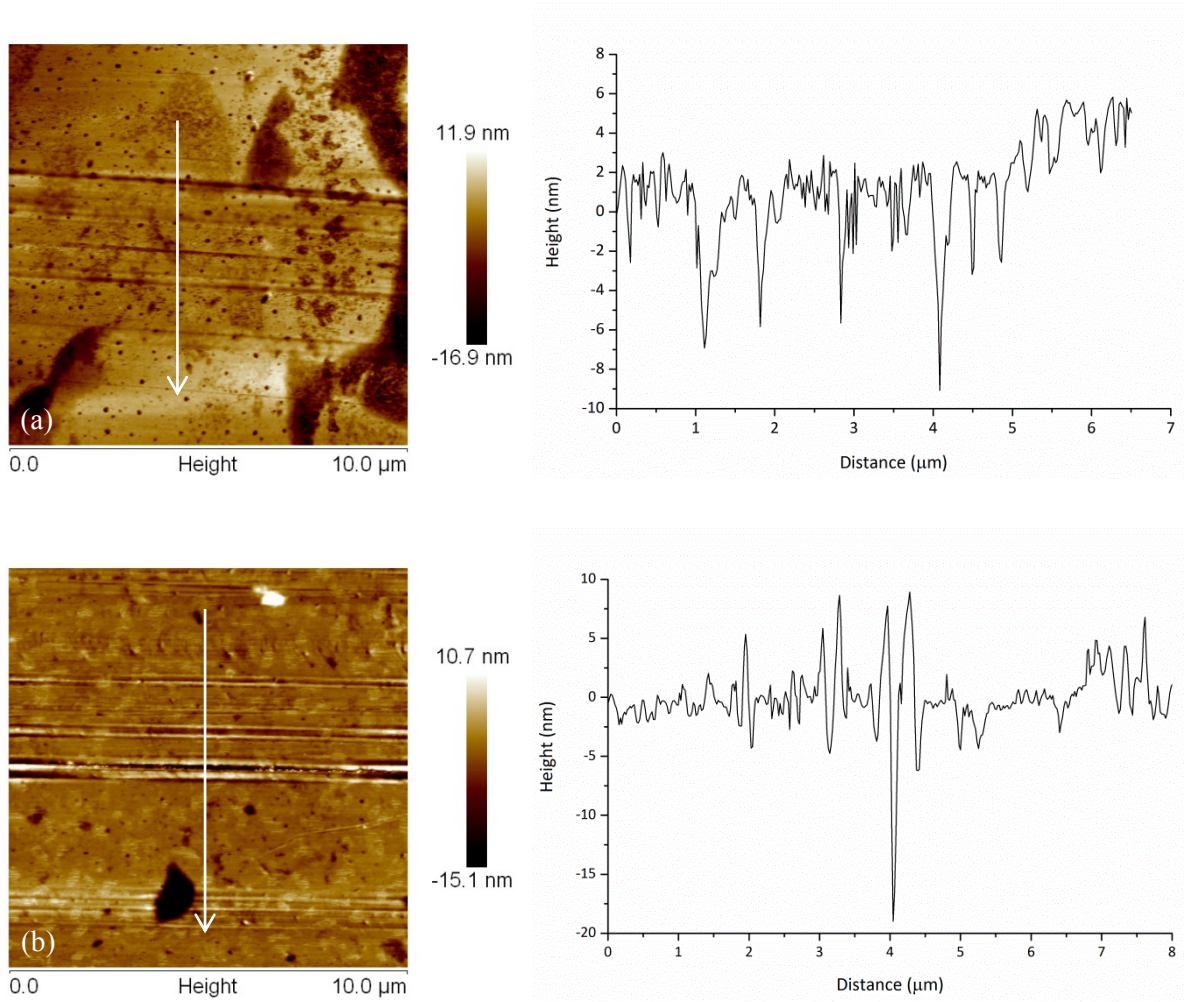

Figure 6.6 AFM micrographs and line profiles for the soiled PMMA substrate cleaned with a) acetone and b) the anionic surfactant.

6.3.2.2 Polystyrene

Interferometry micrographs of the cleaned soiled polystyrene substrates are shown in figure 6.7. The use of dry cleaning and deionised water was ineffective at removing soil from the substrate, as indicated by the raised areas in figure 6.7. However, all other cleaning agents were able to remove contamination from the surface, although this was accompanied by significant damage in the form of scratching. As previously seen the use of acetone caused severe damage to the surface.

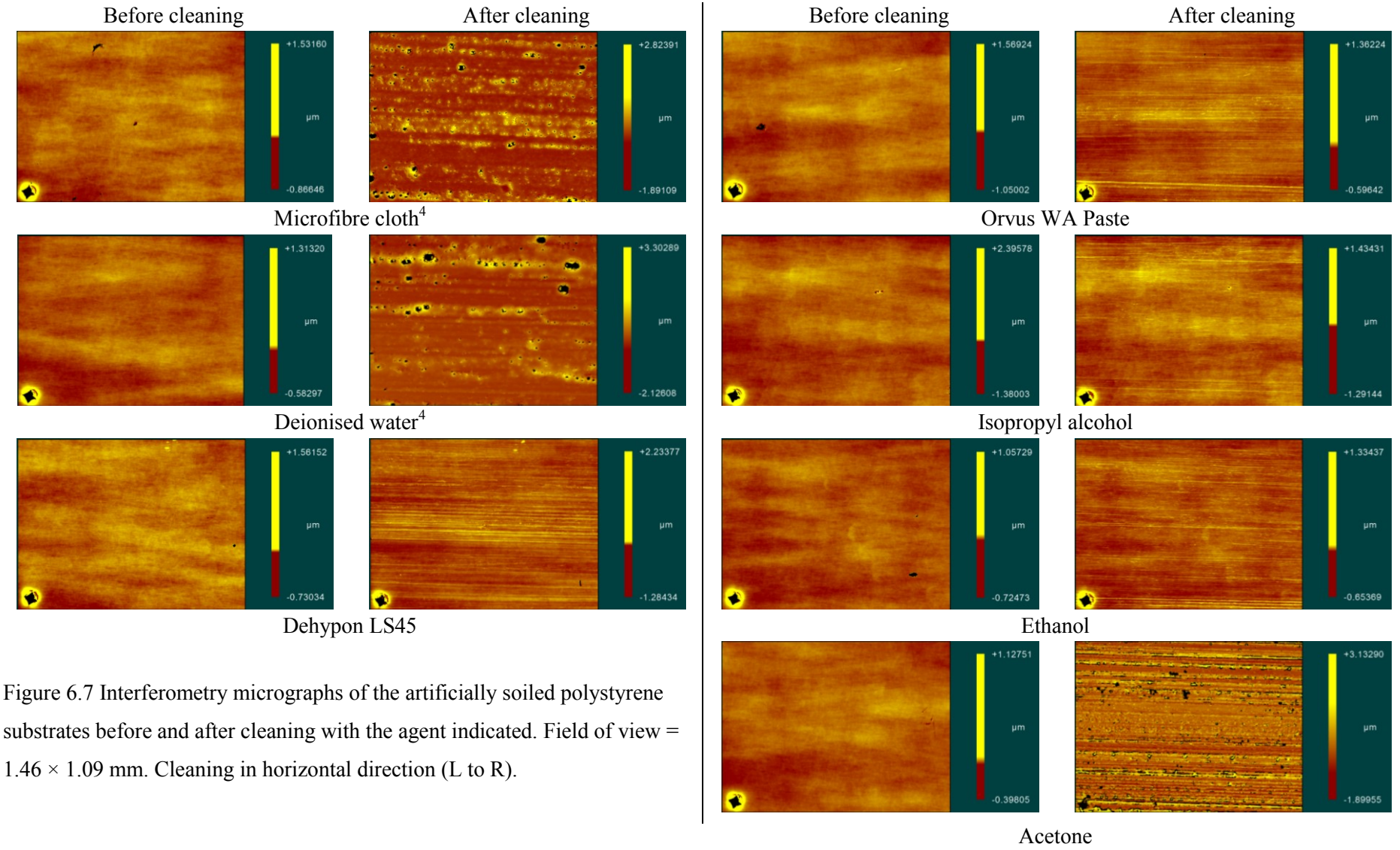

Figure 6.7 Interferometry micrographs of the artificially soiled polystyrene substrates before and after cleaning with the agent indicated. Field of view = 1.46 × 1.09 mm. Cleaning in horizontal direction (L to R).

[4] Again the image location captured after cleaning does not correspond to the one captured before cleaning

Closer examination of these surfaces with SEM revealed further detail about the scratch topography and dimensions. The SEM micrographs for all cleaned surfaces are shown in figure 6.8.

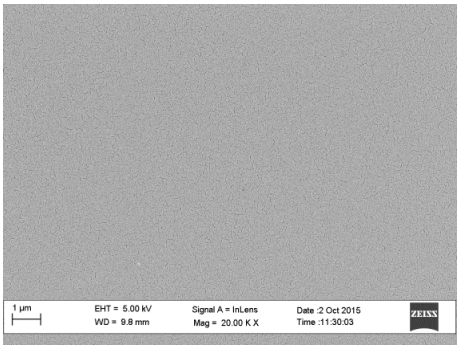

No treatment

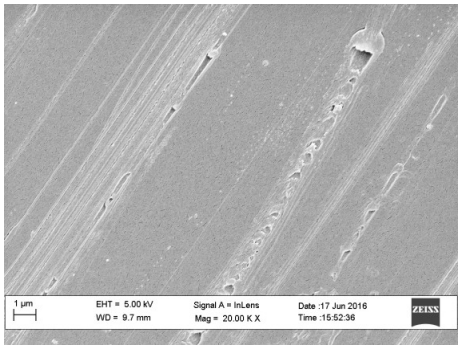

Microfibre cloth

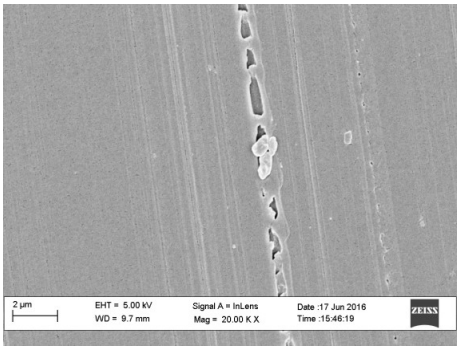

Deionised water

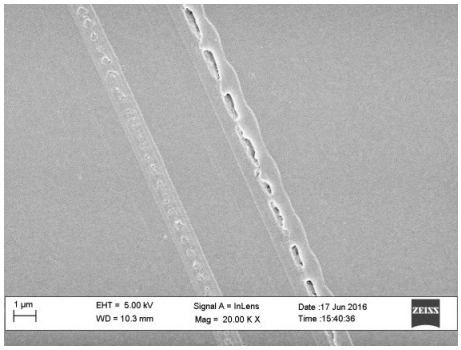

Dehypon LS45

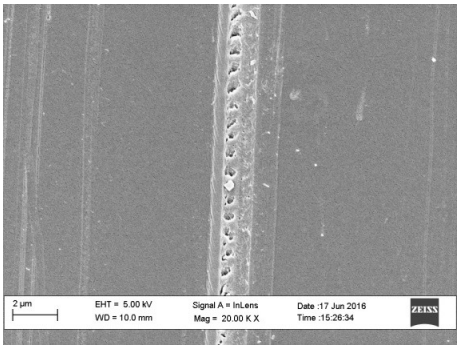

Orvus WA Paste

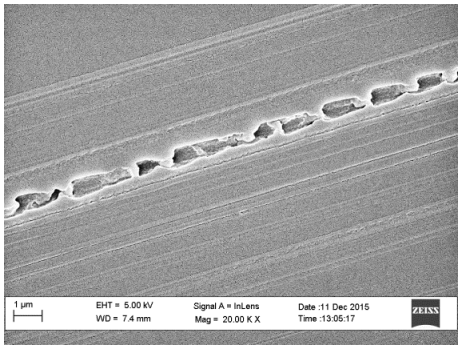

Isopropyl alcohol

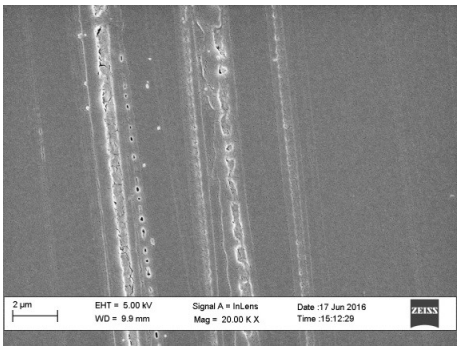

Ethanol

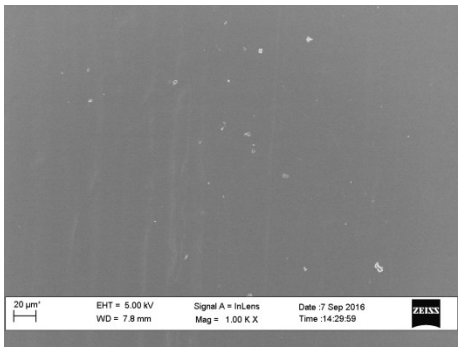

Acetone

Figure 6.8 SEM micrographs of the artificially soiled polystyrene substrates after cleaning with the agents indicated.

While the SEM micrographs show narrow uniform scratches similar to those seen for the virgin substrates, there are also other, wider scratches present. The topography of these scratches is less uniform and they are characterised by a jagged perforation of the substrate. Again, acetone dissolved the substrate as seen for the virgin polystyrene substrate. Figure 6.9 shows SEM micrographs of scratches on the polystyrene substrate cleaned with isopropyl alcohol. Inspection of the scratches reveals that the damaged area consists of an elongated narrow trough which is surrounded on either side by a raised area. Furthermore the width of the inner trough and, in some cases the outer raised section, is not uniform, and at some points narrows so as to block the centre trough. The presence of particulate matter in and around the vicinity of the scratch as in figure 6.9a indicates that these particles are instrumental in creating the observed scratches. It is thought that they are formed as a result of the particles being drawn across the surface in a rolling and dragging motion. Figure 6.9b shows the dimensions of one of the scratches and indicates that the width of the entire damaged area is of the order of 1 μm.

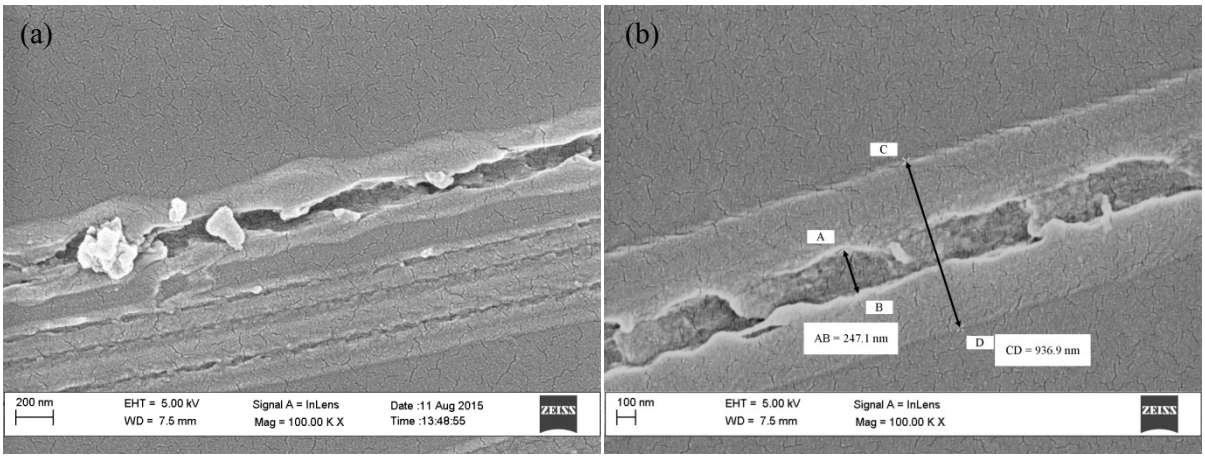

Figure 6.9 SEM micrographs of the artificially soiled polystyrene substrate after cleaning with isopropyl alcohol, showing a) the presence of particulate matter close to the scratch and b) the scratch dimensions.

The SEM-EDX analysis of fragments remaining on the surface of a gold sputter coated polystyrene substrate is shown in figure 6.10. This indicated that the composition of these particles included carbon and oxygen, which is consistent with carbon black. The presence of the calcium peak may be explained as an impurity [160].

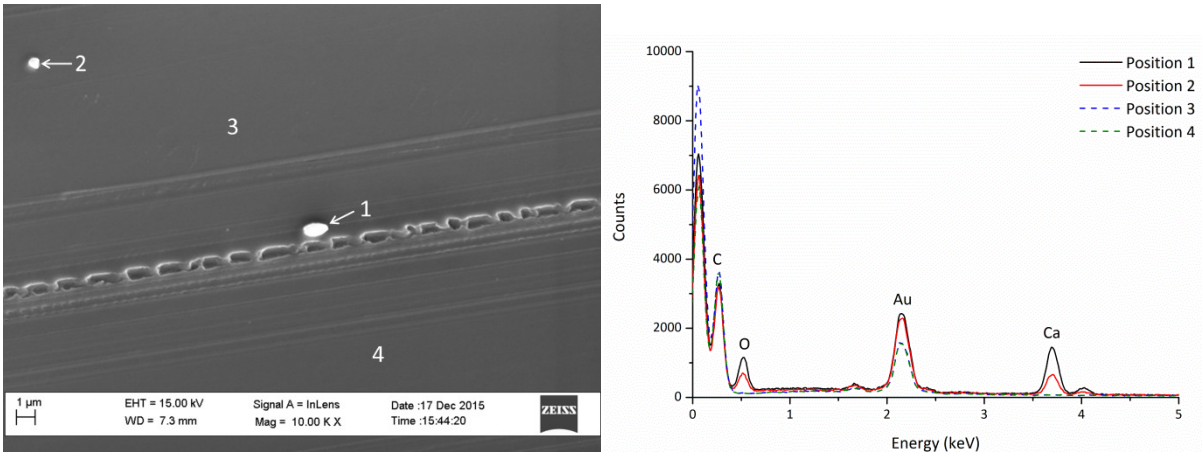

(a) (b)

Figure 6.10 SEM images of the polystyrene surface cleaned with isopropyl alcohol showing a) the presence of scratching and particulates and b) the associated EDX spectra for the positions indicated.

Measurement of the particulates seen on the surface after cleaning revealed that they had a typical diameter of 0.2-1 µm. This is significantly smaller than the diameter of the carbon black particles given by the data sheet and confirmed via SEM in figure 6.1. It is therefore suggested that the carbon black particles are breaking up due to mechanical action as the cloth is passed over the surface.

While the dimensions and topography of the observed scratches varied considerably over the surface, an estimation may be made from the AFM micrographs obtained for these substrates and shown in figure 6.11. These micrographs show two features of the cleaned substrates. Figure 6.11a shows the multiple shallow scratches present on an area of the substrate cleaned with ethanol, where it is difficult to define the individual scratches, but where the peak-to-peak width of a scratch is typically around 200 nm and the peak-to-valley height is approximately 10 nm. The topography of the substrate shown in figure 6.11b includes several scratches which are more clearly defined and have a greater peak-to-peak width of approximately 500 nm, with a peak-to-valley height of up to 40 nm. It is interesting to note that these more defined scratches have a similar width to those seen on the virgin substrates but the depth of these scratches may be greater. It should be noted that both deeper and shallow scratches were observed on all cleaned substrates.

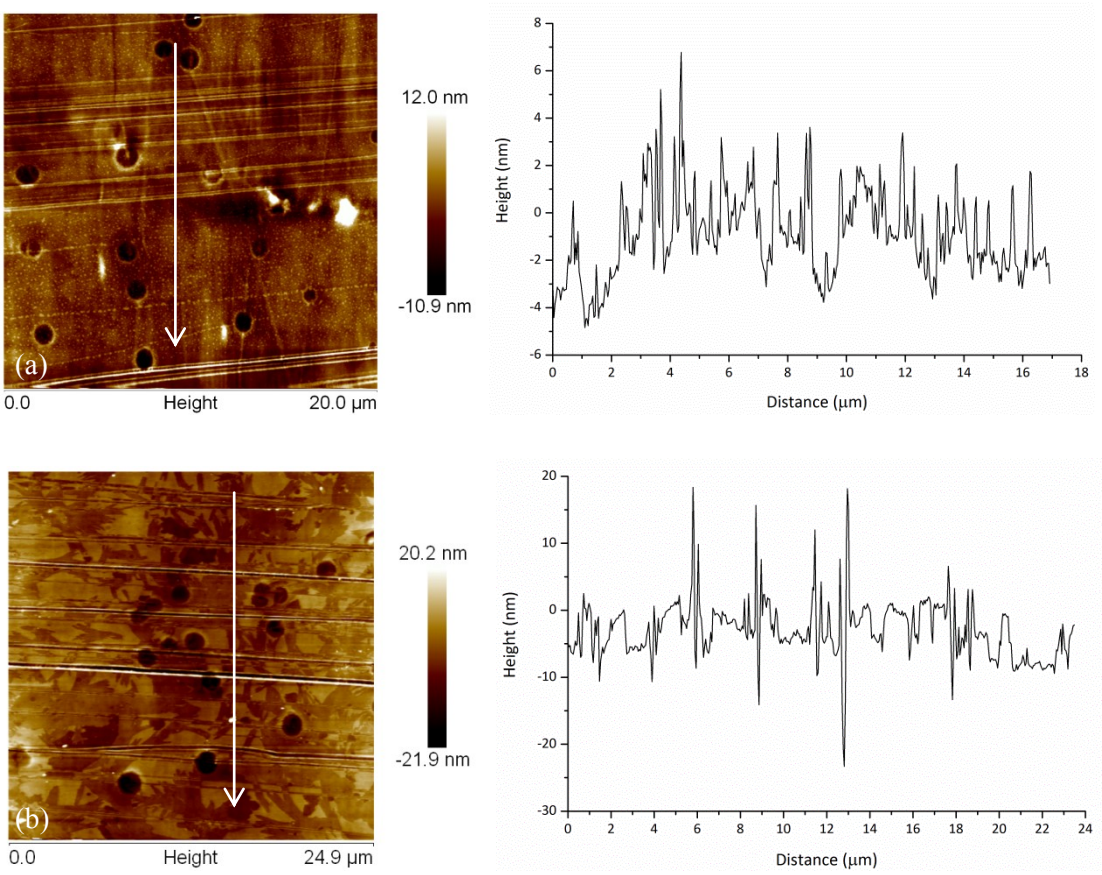

Figure 6.11 AFM micrographs of the polystyrene substrate cleaned with a) ethanol and b) anionic surfactant and the surface profiles of the lines indicated.

In order to determine whether the damage to the surface was influenced by the structure of the microfibre cloth, the cloth was inspected after cleaning. An optical micrograph of the cloth after cleaning the soiled polystyrene substrate with isopropyl alcohol is shown in figure 6.12. It can be seen that while some of the particles are distributed among the fibres, many of the soil particulates are present on the surface.

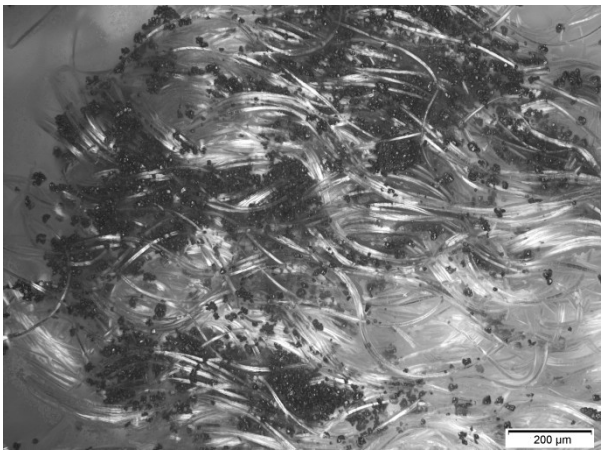

Figure 6.12 Epi-brightfield optical micrograph of the microfibre cloth after cleaning the soiled polystyrene substrate with isopropyl alcohol (scale bar = 200 µm).

6.3.3 Chemical changes

Examination of the surface chemistry was principally performed to determine whether the cleaning agents were effective in removing soil from the surface.

6.3.3.1 PMMA

Figure 6.13 shows the PCA scores and loadings biplots for the soiled PMMA substrates cleaned with acetone and ethanol. The differences between the prepared substrate (i.e. rinsed with flowing isopropyl alcohol) and the cleaned substrates are due to hydrocarbon fragments of the form $C_nH_{2n\pm1}$ on the ethanol-cleaned substrate, while fragments at m/z = 55.02 ($C_3H_3O^+$) and 73.03 ($C_3H_5O_2^+$) on the prepared substrate are characteristic of PMMA. The presence of fragments at m/z = 77.04 ($C_6H_5^+$), 79.05 ($C_6H_7^+$) and 91.05 ($C_7H_7^+$) characterise the acetone-cleaned substrates. These are indicative of an aromatic compound, which cannot be explained by either the substrate, artificial soil or the solvent and may be due to contamination with an aromatic solvent.

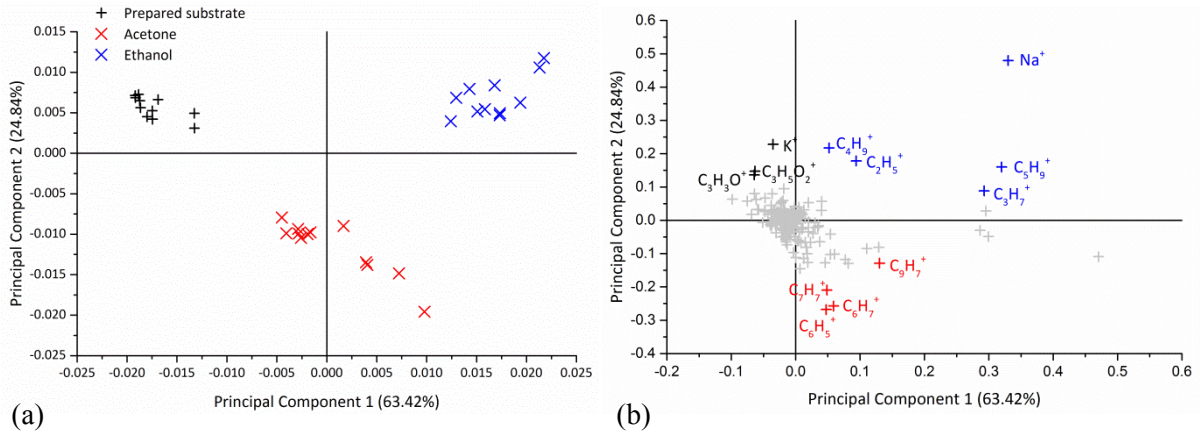

Figure 6.13 PCA biplots showing a) scores and b) loadings for the positive polarity ToF-SIMS spectra from the soiled PMMA substrates cleaned with organic solvents.

A comparison of the prepared substrate (i.e. rinsed with isopropyl alcohol prior to soiling) and the soiled substrate cleaned with isopropyl alcohol is shown in figure 6.14. In this case the major changes in the chemical composition of the surface should be due to the soiling procedure rather than solvent residues. The scores plots shows a clear difference between the two samples. The loadings show fragments characteristic of PMMA on the prepared substrate whereas hydrocarbon fragments are detected on the soiled substrate cleaned with isopropyl alcohol. This indicates the presence of residual oil on the surface of the cleaned substrate.

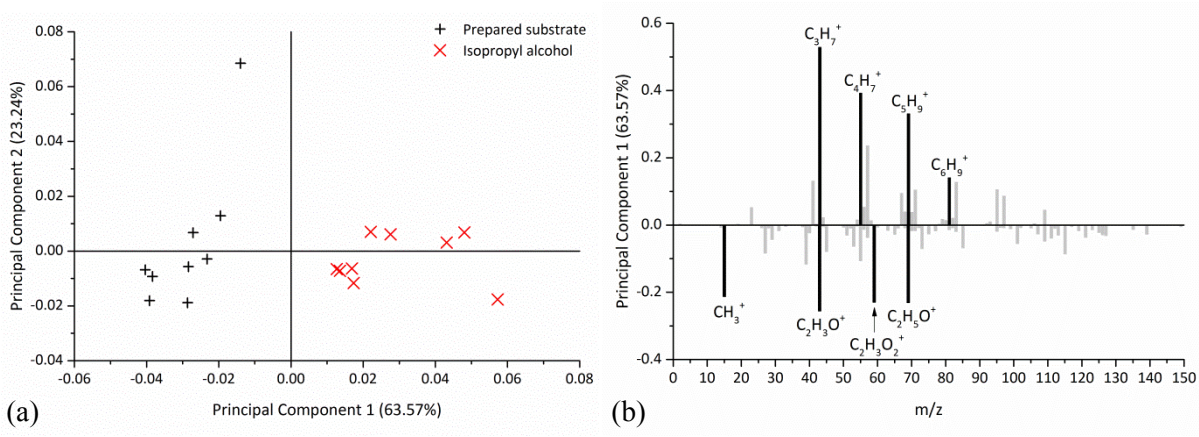

Figure 6.14 PCA a) scores and b) loadings plots for the positive polarity ToF-SIMS spectra showing the differences between the prepared PMMA substrate and the soiled PMMA substrate cleaned with isopropyl alcohol.

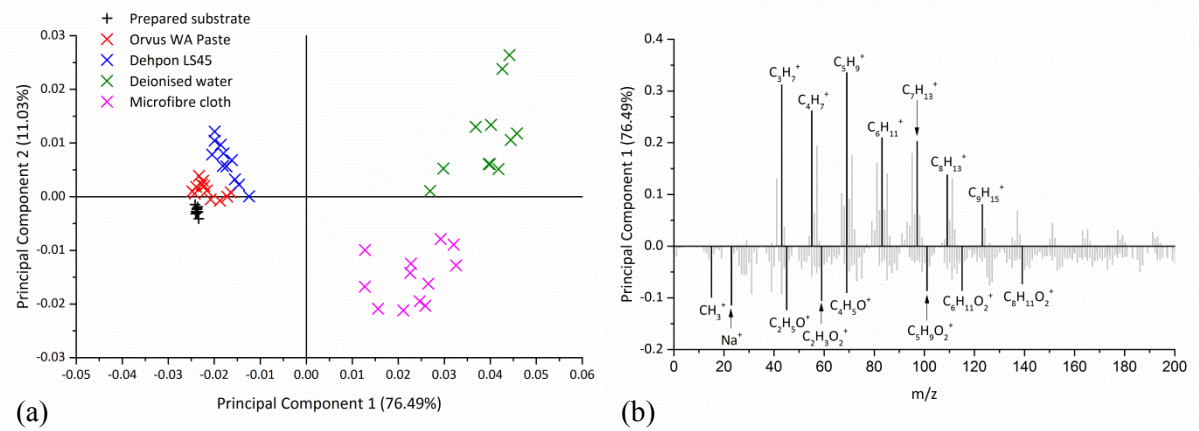

Figure 6.15 PCA a) scores and b) loadings plots for the positive polarity ToF-SIMS spectra from soiled PMMA cleaned with aqueous agents and the microfibre cloth alone.

The PCA plots for the substrates cleaned with the aqueous agents and dry cleaning procedure are shown in figure 6.15. This data confirms the findings from the interferometry micrographs in figure 6.3. The positive loadings on the first principal component are of the form $C_nH_{2n\pm1}$, indicating the presence of oil, while the negative loadings are characteristic of PMMA. There is a clear separation between the scores for the dry cleaning procedure and the use of deionised water, which have positive scores, and those for the prepared substrate and surfactant-cleaned substrates, which have negative scores. This indicates a distinctive difference in the efficacy of soil removal for these cleaning procedures. Closer inspection of the substrates cleaned with surfactants reveals that hydrocarbon fragments corresponding to residual oil were also present on these substrates, as shown in figures 6.16 and 6.17. There are also indications of residue from the non-ionic surfactant, as indicated in figure 6.16 by the $C_2H_5O^+$ and $C_3H_7O^+$ fragments on the positive PC1 loadings. Figure 6.17 shows the

presence of the Na^+ ion on loadings corresponding to the soiled substrate cleaned with the anionic surfactant, indicating residues from SLS.

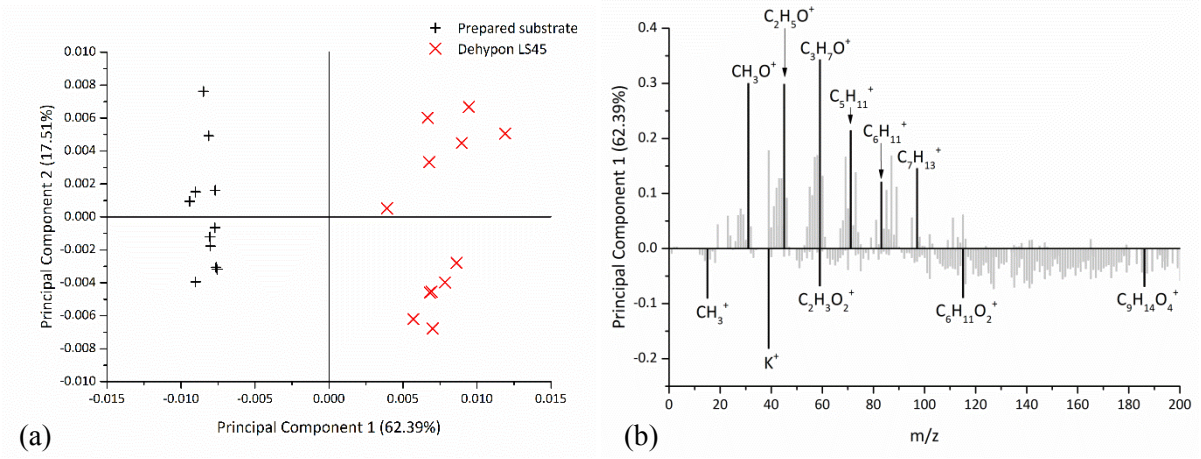

Figure 6.16 PCA a) scores and b) loadings plots for the positive polarity ToF-SIMS spectra from soiled PMMA cleaned with the non-ionic surfactant.

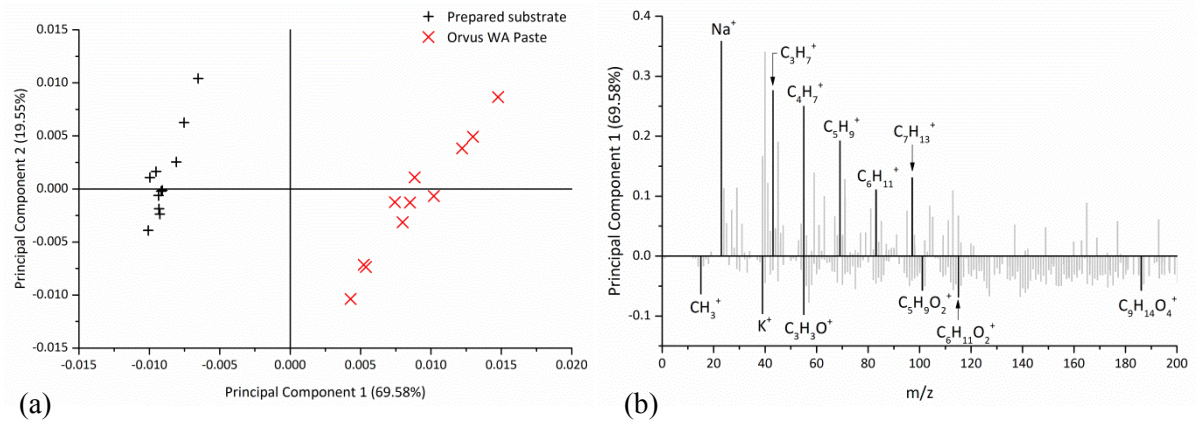

Figure 6.17 PCA a) scores and b) loadings plots for the positive polarity ToF-SIMS spectra from soiled PMMA cleaned with the anionic surfactant.

6.3.3.2 Polystyrene

The scores and loadings plots for the soiled polystyrene substrates cleaned with organic solvents are shown in figure 6.18. Again, the scores for the substrates cleaned with alcohols show fragments of the form $C_nH_{2n\pm1}$, indicating residual oil. The positive scores for some of the substrates cleaned with acetone indicate that cleaning may have been more effective for these substrates and can be explained by the dissolution and removal of the plastic as seen in section 6.3.2.2.

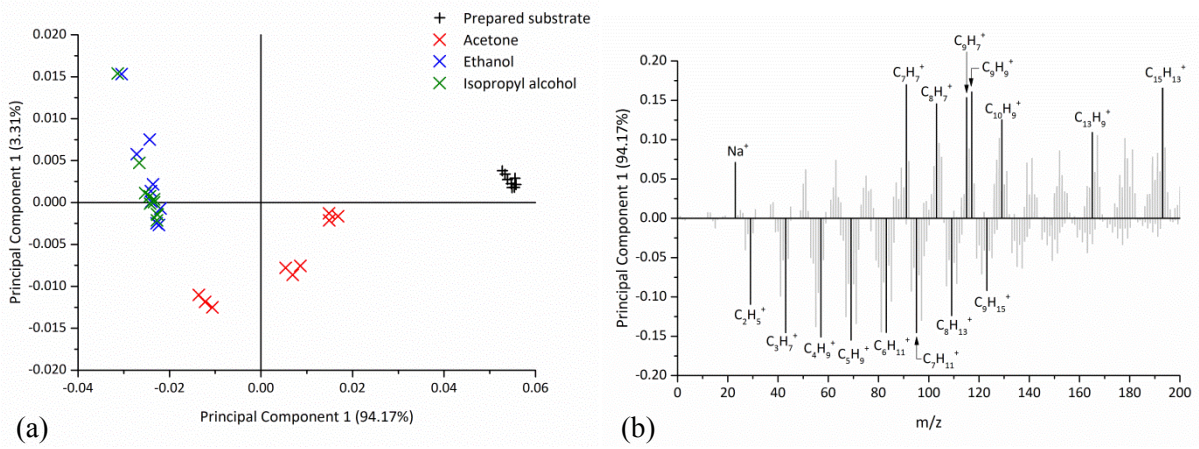

Figure 6.18 PCA a) scores and b) loadings plots for the positive polarity ToF-SIMS spectra from the soiled polystyrene substrates cleaned with organic solvents.

Figure 6.19 shows the scores and loadings biplots for the soiled polystyrene substrates cleaned with aqueous and dry cleaning methods. The clear difference between the cleaned substrates and the prepared substrate is due to the first principal component, which indicates the presence of hydrocarbon fragments on the cleaned substrates. However, it is interesting to note that the substrate cleaned with the non-ionic surfactant is also defined by positive scores for the second principal component. Inspection of the corresponding loadings reveals the fragment at m/z = 59.05 which corresponds to $C_3H_7O^+$ and is indicative of residual surfactant. It is also interesting to note that the short chain hydrocarbons at m/z = 41.04 ($C_3H_5^+$), 43.05 ($C_3H_7^+$), 55.05 ($C_4H_7^+$), 57.07 ($C_4H_9^+$) and 69.07 ($C_5H_9^+$) are also associated with the positive PC2 scores and the non-ionic surfactant.

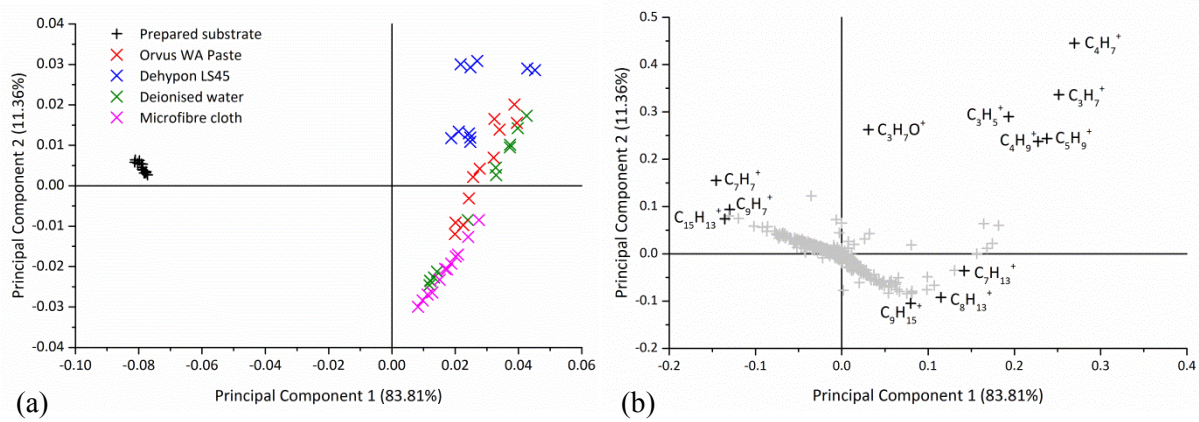

Figure 6.19 PCA biplots showing a) scores and b) loadings for the positive polarity ToF-SIMS spectra from soiled polystyrene cleaned with aqueous agents and the microfibre cloth.

The negative polarity depth profile for the soiled polystyrene substrate cleaned with the anionic surfactant is shown in figure 6.20 and reveals several points of interest. The first is the clear change in intensity that occurs at a depth of around 40 nm. The carbon peak at m/z = 12.00 increases in intensity and a corresponding decrease in hydrocarbon fragments can also be seen, which may be due to any

remaining oil or residual surfactant. It is also interesting to note the initial increase, then decrease in intensity for the fragments at m/z = 63.96 (SO_2^-) and 79.96 (SO_3^-). These fragments are indicative of the anionic surfactant and suggest that the presence of the surfactant increases at a depth of around 40 nm, indicating possible penetration of the surfactant into the residual soil.

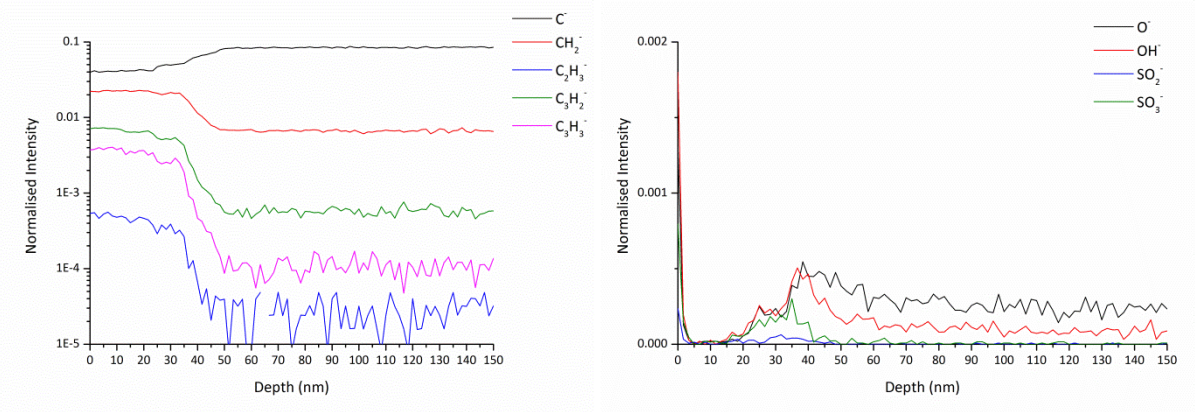

Figure 6.20 Negative polarity ToF-SIMS depth profiles for the soiled polystyrene substrate cleaned with the anionic surfactant.

6.4 Discussion

The findings from this chapter are summarised in table 6.1.

Table 6.1 Summary of findings for the artificially soiled substrates.

	PMMA	**Polystyrene**
Cleaning with organic solvents	Effective soil removal. Scratching observed for all solvents. PCA analysis indicates residual oil.	Effective soil removal. Scratching has non-uniform topography and particulates are located in scratches. PCA analysis indicates residual oil.
Cleaning with aqueous agents	Surfactants are less effective in removing soil. Deionised water and dry cleaning are ineffective for soil removal. Scratching observed for all agents. Surfactant residues detected.	Surfactants are less effective in removing soil. Deionised water and dry cleaning are ineffective for soil removal. Scratching observed for all agents. Surfactant residues detected.

6.4.1 Effect of soiling on the sample surface

The removal of soil from a surface is achieved both by the mechanical action of the cleaning tool and the presence of any cleaning agent. In this case, inspection of both plastic substrates cleaned using the microfibre cloth alone and with deionised water revealed that this was an ineffective method for soil removal, as residual soil could be seen on both plastic substrates with the naked eye. Visible improvement was noticeable with the substrates cleaned with surfactants, although residue could be seen when viewed using interferometry. However, no oil residue was observed for the substrates cleaned with the organic solvents either with the naked eye or using interferometry.

The presence of an artificial soil changes the cleaning behaviour of both plastic substrates. For PMMA, the presence of soil on the surface resulted in scratches being observed after the application of all cleaning agents. As scratching was not observed for the virgin substrates this was most likely due to abrasion from the carbon black particles which were dragged across the surface during cleaning. For the polystyrene substrates, the presence of a soil resulted in the presence of deeper scratches than were seen for the virgin substrates. The topography of these scratches was also less uniform than was previously observed, with both the width and depth of the scratch varying across the surface. Inspection of the SEM micrographs revealed the presence of particulate matter in, or close to, the scratches and SEM-EDX analysis of these particles indicated that the composition of these particles was consistent with that of carbon black. This indicates that the observed scratching is most likely due to the soil particles being dragged and rolled across the surface. However, the diameter of the particles and the width of the corresponding scratches are an order of magnitude smaller than the diameter of the original carbon black particles, suggesting that the particles are breaking up during cleaning.

It is interesting to note that the scratches observed for both the PMMA and polystyrene substrates had a typical width of 500 nm-1 μm, and that this is consistent with the width of the scratches observed for the virgin polystyrene substrates. It is likely that this width is related to the diameter of the soil particulates. It is also possible that it may be influenced by the structure of the microfibre cloth; the SEM micrograph of the cloth fibres in Chapter 5 showed possible folds and crevices of the order of 2 μm in width that could trap particles of a similar diameter. Inspection of the microfibre cloth after cleaning also indicated that the particulates were held close to the cloth surface in contact with the substrate. The scratch depth appears to increase with the addition of a particulate soil; in the case of polystyrene, scratches were measured as reaching 40 nm in depth, compared to around 20 nm for the virgin substrates. The lateral distribution of the scratches over the surface appeared to be random and did not appear to be related to the density of the carbon particles on the surface.

6.4.2 Cleaning efficacy

Analysis of the surface chemistry revealed that oil residues were present on all cleaned substrates. However, there was no evidence of oil absorbance as was seen for some substrates in the POPART study [31]. These residues were most characteristic of the substrates cleaned with the microfibre cloth and deionised water, again indicating their ineffectiveness. In addition to oil residues, analysis of the surfactant-cleaned substrates revealed residual surfactant. Fragments corresponding to residual oil were also indicated by PCA analysis of the ToF-SIMS spectra from soiled substrates cleaned with organic solvents. Inspection of the PCA data for the polystyrene substrates indicated that acetone was the most effective in removing the soil, although this was likely due to the dissolution of the plastic surface.

The mechanical effect of the microfibre cloth is also instrumental in soil removal. Microfibre cloths consist of numerous fibres, in this case a blend of polyester and polyamide, which have a diameter of around 10 μm. There is therefore a large surface area available to interact with soil particulates and contaminants. Attractive Van der Waals forces between the fibres and the soil result in adhesion of soil particulates to the fibres. While the findings from this work revealed that the microfibre cloth was less effective in removing soil on its own, this may be related to the type of soil present. Many microfibre cloths are marketed as being able to remove dust and soiling via electrostatic attraction, meaning that there is no requirement for a cleaning agent. While this may be the case for dry soils or dust, the presence of an oil component increases the adhesion between the substrate and the soil, potentially making it more difficult to remove.

The efficacy of microfibre cloths to physically remove organic soil from stainless steel surfaces has been studied in the healthcare sector and found that their performance depended on the type of cloth as well as whether it was dry or wet. The cloths have also been found to have the potential to redeposit contamination on the surface [161]. A study by Pociut et al. [162] found that polyester cloths used in surgical applications exhibit 'self-cleaning' behaviour when wetted with water due to their high hydrophobicity. This was observed to increase with the number of individual filaments present in a given area of the cloth. It has been suggested by Moore and Griffith [161] that this may be detrimental for cleaning applications due to the potential for re-deposition. While the use of water as a cleaning agent is unlikely to aid the removal of oily soil, it is possible that the presence of water on the cloth fibres resulted in some re-deposition of soil on the substrates cleaned with deionised water.

The three-dimensional structure of the cloth is also a consideration. The cloth used in this work had a close flat weave, meaning that any soil transferred to the cloth would remain on or close to its surface, limiting its effectiveness. Inspection of the cloth after cleaning revealed that the soil particulates were located close to the surface. A cloth with a looser weave might be expected to have longer fibres

available to interact with the substrate and therefore a greater surface area capable of trapping and removing soil particulates from the surface.

The addition of a surfactant to water reduces the surface tension, thus increasing the wetting behaviour of the cleaning agent. Surfactants act to reduce the interfacial tension between a soil and water. They therefore consist of a hydrophilic and a hydrophobic component; the hydrophilic component is attracted to the water molecules while the hydrophobic component attracts the oils or soil particulates. In the case of an anionic surfactant such as SLS, the hydrophobic component consists of a long hydrocarbon tail while the negatively charged head group is hydrophilic. Non-ionic surfactants are generally ethoxylated fatty alcohols; the presence of oxygen atoms in the molecule provides the hydrophilic component as these are able to form hydrogen bonds.

The mechanism of oily soil removal depends on its composition but may be achieved by one or a combination of three processes: roll-up, emulsification or solubilisation [163]. The roll-up process occurs when the surfactant acts to reduce the interfacial tension between the soil and the substrate, resulting in the soil forming a sphere which can then be removed via mechanical means. However, this relies on wetting of the substrate, and is less effective for plastic substrates due to their hydrophobicity [163]. Removal of oily soil is therefore more likely to occur via solubilisation and emulsification. Solubilisation occurs above a critical micelle concentration (CMC), when surfactants arrange themselves into small spherical structures such that the hydrophobic component of each surfactant molecule is positioned in the centre of the structure and the hydrophilic head group is associated with the water phase. The oil molecules are then contained within the micelles, forming a micro-emulsion. The final process, emulsification, occurs when the surfactant reduces the interfacial tension between the oil and the water. In this case drops of oil are released from the surface surrounded by a layer of surfactant. Solubilisation and emulsification require the penetration of surfactant into the soil layer. In this work, depth profiling of the polystyrene substrate cleaned with the anionic surfactant suggested that the surfactant was present at a depth of around 40 nm, indicating possible penetration of the surfactant into the soil. However, this may also be due to mixing of the oil and the surfactant due to the mechanical cleaning motion.

It is known that the short chain hydrocarbons in oily soils tend to mix with the hydrocarbon tail of the surfactants while larger molecules do not [163]. This is suggested by the surfactant data for the polystyrene substrates. When the dry cleaning and aqueous cleaning systems are compared, both surfactant residue and short chain hydrocarbons were characteristic of the substrate cleaned with the non-ionic surfactant, while long chain hydrocarbons were more characteristic of the substrate cleaned with the dry microfibre cloth.

It is difficult to say which of the surfactants was more effective in removing soil as removal is not only dependent on the agent but also on the mechanical action. Non-ionic surfactants are generally

considered to be more effective in removing oily soils [164], however this could not be conclusively confirmed in this work. The quantity of soil on the surface is also a factor when considering cleaning efficacy. While all the substrates in this work were soiled with the same volume of soil, it is likely that there are small variations in soil coverage. The resulting soil was also of a greater thickness and had a greater oil component than might be expected to occur naturally. The pressure and speed at which cleaning took place is also likely to affect the cleaning efficacy.

Organic solvents dissolve oily soils to facilitate their removal. Acetone was detected to be the most effective at removing oil from the polystyrene substrate, although this may be due to the removal of the surface layer. Polar solvents, including alcohols, are less effective in dissolving non-polar oils and residual oils were detected for both alcohols used in this work. The dielectric constants (ε) of isopropyl alcohol and ethanol are 20.18 and 25.30 respectively at 20 °C [165]. Isopropyl alcohol should therefore be more effective in removing oily soil than ethanol, however this could not be confirmed from the PCA data. The use of non-polar solvents such as hexane or heptane might be more effective in removing the oily component of the soil.

It is worth noting that the roughness of a surface increases the adhesion of soils. All the substrates used in this work had a low roughness value and were rinsed to remove any film residue before the application of soil. There were therefore no cracks, defects or surface contamination which could trap the soil and affect the cleaning behaviour.

Conclusions

The addition of an artificial soil to the plastic substrates changed the cleaning behaviour in two main ways. The first was the formation of scratches on PMMA, which were observed following the use of all cleaning agents. The scratches observed on polystyrene were found to include deeper scratches than had been observed on the virgin substrates. Inspection of the polystyrene substrates after cleaning found particulate matter in and around the scratches, indicating that these were instrumental in their formation. EDX measurements of these particles was consistent with carbon black and suggests that these particles were being fragmented and dragged across the surface during cleaning.

Soil residues were observed on all substrates after cleaning. These were immediately apparent for the substrates cleaned via dry cleaning and with the use of deionised water. The use of surfactants improved soil removal, however residues were still visible under interferometry. While the substrates cleaned with organic solvents appeared clean when viewed with the naked eye and interferometry, ToF-SIMS analysis of the substrates revealed fragments corresponding to residual soil. It is therefore apparent that while the organic solvents were most effective in removing the soil, some oil residues remain after cleaning.

Chapter 7

Accelerated ageing of virgin substrates

It has been seen in the previous two chapters that the act of cleaning can have a notable impact on the plastic surface and that changes to the surface can be immediately apparent with the aid of sophisticated high-resolution analytical equipment. However, one of the concerns with any interventive treatment is that damage to the substrate may only become visible over a period of time. The typical timescales involved in natural ageing are relatively long, and it is therefore difficult to acquire meaningful data in a short time period. For this reason, accelerated ageing techniques are often used to simulate the effect of ageing over a far shorter time period. This chapter details the experimental work performed to investigate the effect of light exposure on cleaned plastic substrates, using accelerated light ageing techniques. The effect of cleaning on artificially aged virgin polystyrene substrates was also investigated.

7.1 Introduction

Accelerated ageing has historically been used in conservation to gain information about the behaviour of an object or material in a shorter time span than would be achievable via natural ageing. It is usually achieved by exposing the sample of interest to conditions of elevated temperature, relative humidity, light exposure, or a combination of these three. Daily or seasonal variations may also be simulated by cycling one or more of the aforementioned variables. Some ageing tests also use a water-spray to simulate the effect of precipitation. It is important to note that accelerated ageing experiments assume that the changes that take place during accelerated ageing are the same that would take place during natural ageing, except over a shorter period of time.

While plastics may degrade via multiple routes, the principal degradation route for many plastics is photo-oxidation via exposure to light and UV radiation. Museum lighting is a combination of natural and artificial light. In the case of natural light, efforts are made to prevent the exposure of artefacts to direct sunlight and window glass typically filters radiation below 315 nm [166]. UV filters or films

can also be applied to windows; a cut-off midpoint of between 390 nm – 410 nm has been proposed as being acceptable for these films [167]. Artificial lighting in museums has historically been achieved via the use of UV-filtered tungsten-halogen or fluorescent lamps although more recently there has been a move towards using LED lighting [168, 169]. These do not emit ultraviolet radiation although some LEDs have a peak in the blue region of the spectrum. There are also additional considerations concerning colour, appearance and visibility which are taken into account when considering the illumination of objects.

Plastic artefacts displayed and stored in museums with controlled environmental conditions will usually not be exposed to UV radiation. The illumination of materials in the museum environment is commonly specified in terms of the eye's sensitivity to light, and is therefore usually given in lux. The light exposure guidelines for the V&A's FuturePlan strategy [43] specify a limit of 50 lux illumination for light sensitive objects, assuming an exposure of 10 hours per day for 365 days per year. They also specify that these objects should undergo rotation. Objects defined as 'light durable' may be exposed to a maximum illumination of 250 lux. All illumination should exclude radiation in the UV part of the spectrum. Plastics are categorised under light sensitive objects.

These guidelines are in agreement with those presented elsewhere. The luminance guidelines for plastics in museum collections broadly agree that that illumination levels should not exceed 50 lux for light-sensitive polymers, although more light-stable objects may be exposed to levels up to 250 lux [23, 170, 171]. However, not all artefacts are housed in environmentally controlled conditions. Those artworks which are designed to be displayed outdoors, such as sculptures, may well experience illumination levels which are in excess of recommended guidelines for plastics and which also contain damaging UV radiation. Artefacts with a prior history before acquisition may have been exposed to UV radiation in the past. This may be due to outdoor exposure or from artificial sources such as flash photography, particularly if these artefacts were photographed in the first half of the twentieth century [166].

An extensive review of accelerated ageing in the museum environment is given by Feller [166]. There have also been several studies on polymeric materials using a range of ageing parameters. Korenberg studied the effect of accelerated ageing on the tensile properties of polyester fabrics [172] using a fluorescent lamp over a period of 69 days. Mitchell used accelerated light ageing to investigate the effect of light on polyurethane foam [96]. In this case a xenon lamp was used with a 300 nm cut-off and samples were aged for a maximum period of 144 hours. Cucci et al. [173] performed accelerated ageing tests on expanded polystyrene (EPS) with the aim of replicating the degradation of an EPS artwork. A halogen lamp was used due to its similarity to museum lighting conditions and the samples were exposed for 1540 hours. There was also a UV component to the spectrum. Researchers in the POPART project performed accelerated light ageing tests on cleaned plastic samples using a xenon

lamp, though it is unclear whether the spectrum included a UV component. Samples were exposed for a total of 160 hours. It was reported that the PMMA substrates exhibited a reduction in gloss and surface energy, however any residues present on the substrate did not worsen [31].

There are three main light sources that are commonly used for accelerated light ageing: fluorescent, carbon-arc and xenon-arc [174]. Of these, the spectrum of the xenon lamp bears the greatest similarity to that of natural daylight. However, xenon lamps are typically more expensive and are therefore not always used for accelerated testing. They also contain a UV component that is not present in solar radiation, however this can be removed via the use of filters. Similarly, filters may be used to remove the infra-red part of the spectrum. Figure 7.1 shows the spectral power distribution for the Q-Sun xenon lamp used in this work compared to noon summer sunlight in North America.

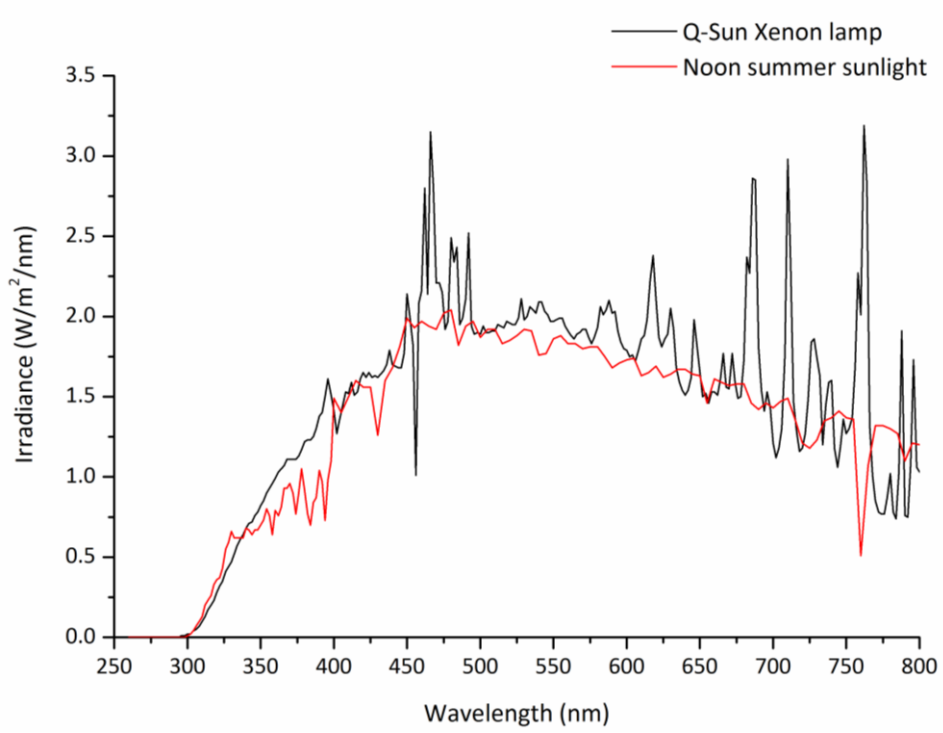

Figure 7.1 Spectral power distribution of the Q-Sun xenon lamp compared to noon summer sunlight in the visible and UV region [175, 176].

Museum illumination guidelines are commonly given in terms of illuminance (ϕ_v), which may be found from the irradiance using equation 7.1 [177].

$$\phi_v = K_m \int_0^\infty \phi_{e\lambda} V(\lambda) d\lambda \tag{7.1}$$

Where $\phi_{e\lambda}$ is the incident irradiance, $V(\lambda)$ is the luminous efficiency, which is dependent on the wavelength of light and K_m is the maximum spectral luminous efficiency and is equal to 683 lmW^{-1} at λ = 555 nm [166, 177].

The British Standard BS EN ISO 4892-2:2013 details the methodology for the light ageing of plastics via exposure to xenon-arc lamps [178] and the recommended parameters for daylight exposure contained within the standard were used in this work. The American Society for Testing and Materials (ASTM International) provides a standard for accelerated light ageing using xenon lamps and gives a list of common exposure conditions used [179]. The National Physical Laboratory (NPL) has also performed an extensive review of accelerated ageing techniques for polymer materials [174], with a view to being able to predict the lifetime of plastics in industrial and engineering applications.

Accelerated ageing is normally performed using model samples and has the advantage that it can be undertaken under controlled and reproducible conditions. However, one of the questions surrounding accelerated ageing is its correlation to the natural ageing of plastics. In accelerated light ageing tests it is assumed that the reciprocity principle is applicable. The reciprocity principle states that the total energy absorbed by an object is equal to the product of the illumination and the exposure period [166]. Therefore, an object exposed to an illumination of 50 lux for 100 hours would absorb the same amount of energy as one that had been exposed to 500 lux illumination for 10 hours. However, the use of illuminance to predict photo-degradation based on the reciprocity principle has been criticised as being misleading [180] as it is not only radiation in the visible part of the spectrum that leads to degradation, and a material's sensitivity to radiation has a poor correlation with the eye's perception of light.

Given the length of the timescales involved in natural ageing, it is unclear whether accelerated ageing accurately replicates the changes that would be seen in natural ageing. It is also important to note that polymers have different spectral sensitivities and will behave differently under the same conditions [180]. Light ageing can also raise the temperature and decrease the moisture content of the environment [166]. Finally, the degradation of objects is usually not a result of only one variable but a complex combination of many, and accelerated ageing can be limited in its ability to accurately reflect the natural environment.

7.2 Experimental

7.2.1 Preparation of samples

This work examined the effect of accelerated light ageing on uncleaned and cleaned virgin PMMA and polystyrene substrates. For each plastic, two sets of cleaned samples were made according to the procedure described in Chapter 4. In this case only virgin, unsoiled substrates were cleaned to limit the potential effect of other contaminants from the soiling procedure on the ageing behaviour. In

addition a set of eight uncleaned polystyrene samples were also placed in the ageing chamber to examine their cleaning behaviour after ageing. All samples were analysed with white light interferometry before and after cleaning and prior to ageing.

7.2.2 Accelerated light ageing

The plastic samples were affixed to a black cardboard backing to hold them in place in the ageing chamber and to enable easy removal for periodic analysis. The samples were mounted at a 10° tilt to the horizontal as in figure 7.2.

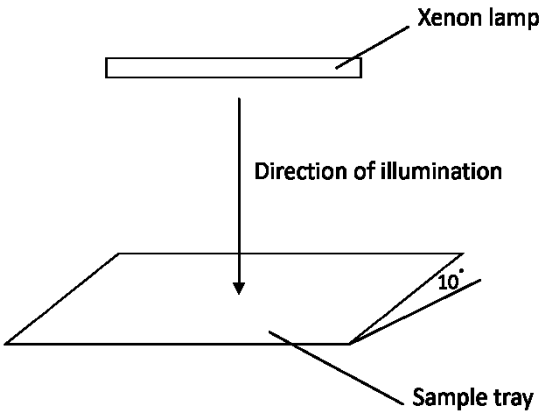

Figure 7.2 Schematic showing the positioning of samples in the ageing chamber.

Accelerated light ageing was performed using a Q-Sun Xe-1 xenon test chamber (Q-Lab Corporation, USA) which was equipped with one xenon lamp. A new lamp was installed prior to ageing and, in accordance with the manufacturer's guidelines, the lamp underwent a 168 hour burn-in period prior to use. This was to limit any fluctuations in irradiance which may occur at the start of the lamp's lifetime. A Q-Lab Daylight-Q filter was used which has a cut-off below 295 nm and is recommended for the simulation of natural outdoor light exposure [181]. It was decided to include the UV component to simulate the worst-case scenario for light exposure. In accordance with ISO 4892-2:2013 for exposure using daylight filters, the irradiance was set to 0.51 $W/m^2.nm$ at 340 nm at a black panel thermometer (BPT) temperature of 63 °C. The relative humidity of the chamber was uncontrolled. The chamber also contained a fan to assist air circulation and the air temperature of the chamber was measured to be 44 °C ± 1 °C after 40 minutes operation.

The total energy absorbed over a period of 1344 hours was calculated to be 7.17×10^7 lux-hours. Note that this illumination includes UV radiation, which would not be present in the museum environment. Assuming that the reciprocity principle is valid, at an exposure of 50 lux for 3650 hours per year, this would be equal to 393 years in the museum environment. However, at the higher illumination level of 250 lux, this would be equal to 79 years. At an outdoor illumination of 10000 lux for 3650 hours per year, the equivalent natural ageing time is significantly shorter, and corresponds to 2 years. It is

unlikely that artworks would be exposed to this illumination level continuously throughout the year, but gives an indication of the type of timescales that could be possible.

The samples were removed from the light ageing chamber at 1, 2, 4, 6 and 8 week intervals and analysed using white light interferometry. As a non-contact, atmospheric technique, this enabled periodic analysis without potentially changing the ageing behaviour of the substrates. The samples' positions in the chamber were rotated at 2 week intervals to enable an even exposure to all samples. The 1, 2, 4, 6 and 8 week exposure periods corresponded to 168, 336, 672, 1008 and 1344 hours respectively.

Bulk characterisation of the aged samples was performed using ATR-FTIR, GPC, DSC and micro-hardness testing. All parameters used were the same as detailed in Chapter 5. Spectrophotometry was also performed using a Hitachi U-4000 spectrophotometer (Hitachi, Japan) with a deuterium lamp at wavelengths 250 nm - 340 nm and a tungsten lamp for wavelengths in the range 340 nm - 2500 nm. The ΔE_{00} values were calculated using the CIEDE 2000 formula [113] and the yellowness indices were calculated according to the ASTM International E313 standard [114].

The plastic samples were analysed after 8 weeks accelerated ageing using SEM, AFM, white light interferometry and ToF-SIMS. Due to extensive charging on the aged polystyrene substrates, the ToF-SIMS spectra for these samples were obtained using a 300 μs cycle time. Otherwise the same parameters were used as detailed in Chapter 5. A separate set of uncleaned polystyrene substrates were placed in the chamber and removed after 1, 2 or 4 weeks to examine the physical and chemical characteristics of the surface at these intervals. These were analysed using ToF-SIMS, SEM and AFM. ATR-FTIR, micro-hardness and colorimetric measurements were also made for these samples.

7.2.3 Heat ageing

As the temperature of the Q-Sun chamber increased during ageing, heat ageing was performed for PMMA and polystyrene samples to enable comparison with the light-aged samples. In this case the protective film was removed from the plastic surface but the samples were not cleaned before ageing. The samples were affixed to black cardboard and placed in a Lenton 1100C chamber furnace (Lenton Furnaces, UK) at a temperature of 63 °C ± 3 °C. This temperature was chosen to correspond to the BPT temperature used during light ageing. Samples were removed from the chamber at 1, 2, 4, 6 and 8 week intervals.

7.3 Bulk characterisation

Bulk characterisation of the artificially light-aged substrates was performed to determine the changes taking place as a result of treatment.

7.3.1 ATR-FTIR

The ATR-FTIR spectra of the PMMA substrate before ageing and after 8 weeks accelerated light ageing are shown in figure 7.3. No notable changes were detected as a result of the accelerated ageing treatment.

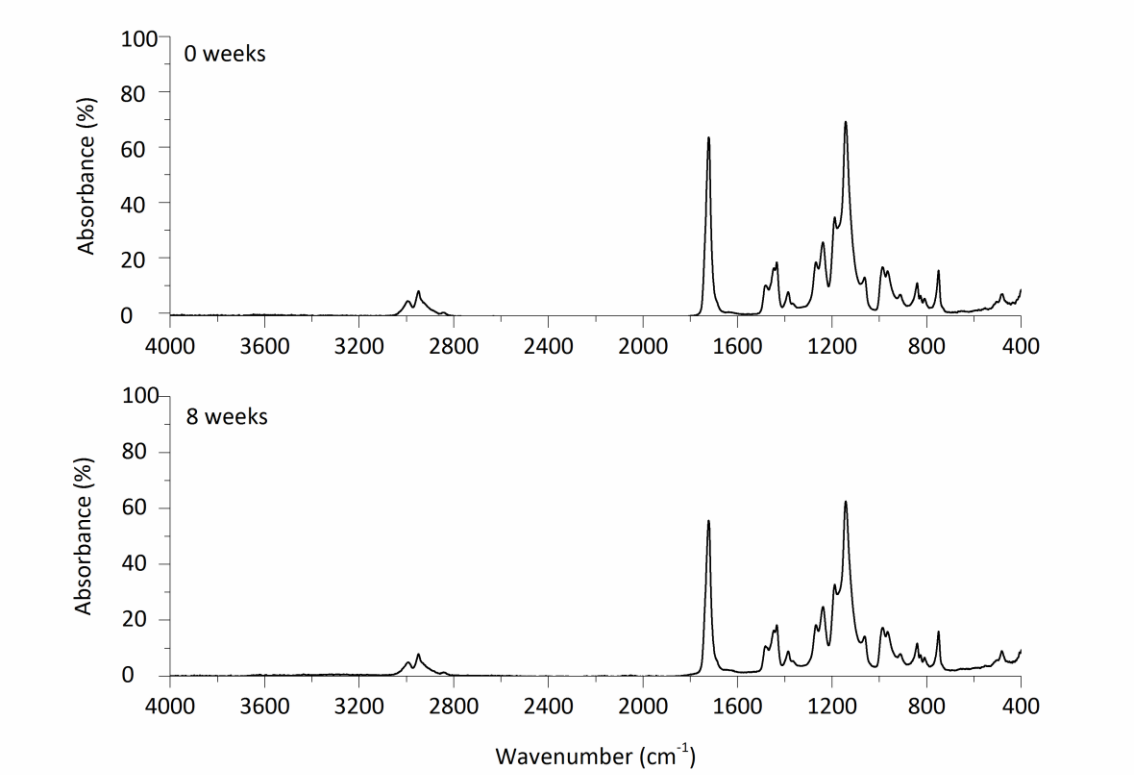

Figure 7.3 ATR-FTIR spectra of the unaged PMMA substrate and the PMMA substrate after 8 weeks accelerated light ageing.

Figure 7.4 shows the ATR-FTIR spectra for the polystyrene substrate before ageing and after 1, 2, 4 and 8 weeks accelerated light ageing. It is apparent from this data that there were chemical changes taking place as a result of accelerated ageing. The most noticeable change in the spectra occurs at 4 weeks, where the development of two bands of interest can be seen. These consist of a broad band around 1750 cm^{-1} and another broad band around 1250 cm^{-1}. These correspond to a C=O stretch and a C-O stretch respectively, and are indicative of oxidation of the polymer. The very broad band from 3100 cm^{-1} to 3600 cm^{-1} corresponds to an O-H stretch and the broadness of this band is indicative of hydrogen bonding.

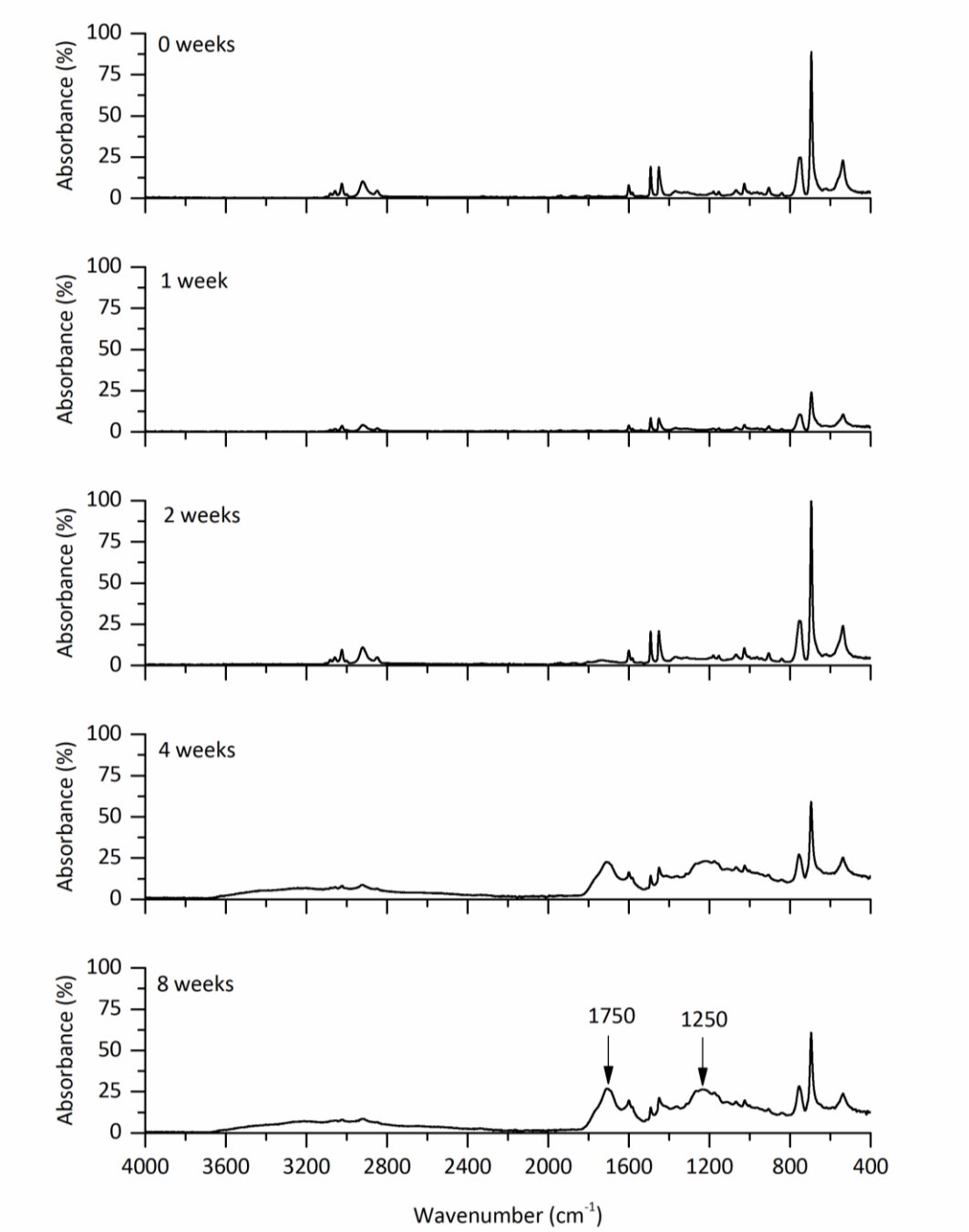

Figure 7.4 Comparison of the ATR-FTIR spectra for the polystyrene substrate before and after 1, 2, 4 and 8 weeks accelerated light ageing.

7.3.2 DSC

The thermal behaviour of PMMA before and after 8 weeks accelerated light ageing is shown in figure 7.5. The T_g of the PMMA substrate aged for 8 weeks was 118.1°C ± 0.5 °C compared to a T_g of 111.6 °C ± 0.5 °C for the unaged PMMA substrate. Figure 7.6 shows the DSC plot for polystyrene before and after 8 weeks accelerated ageing. There is a slight decrease in the T_g of the aged polystyrene

substrate, which was found to be 101.3 °C ± 0.5 °C compared to 103.5 °C ± 0.5 °C for the unaged substrate.

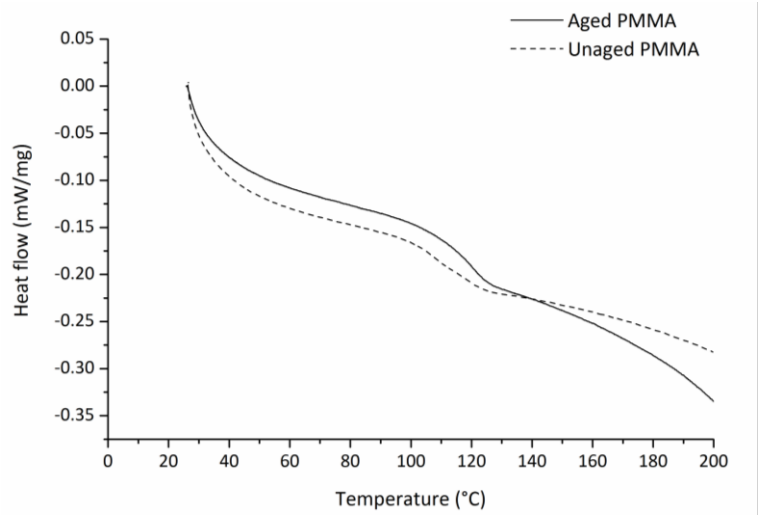

Figure 7.5 DSC plots for the PMMA substrate before and after 8 weeks accelerated light ageing.

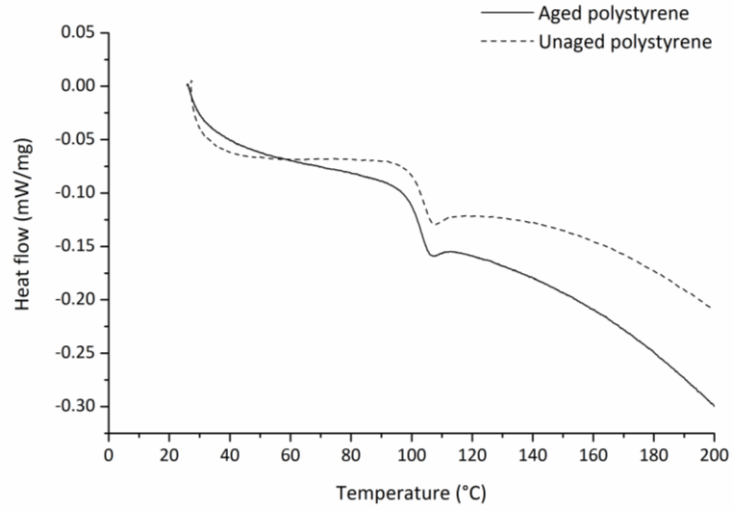

Figure 7.6 DSC plots for the polystyrene substrate before and after 8 weeks accelerated light ageing.

7.3.3 GPC

Figure 7.7 shows the molecular weight distributions for PMMA before and after 8 weeks ageing. It can be seen that there is a shift in the peak position from 1.1×10^6 g/mol to 5.6×10^5 g/mol for the sample that had been aged for 8 weeks. This shift is most likely due to chain scission with ageing, although the presence of a small peak around 5.5×10^6 g/mol suggests that there is also some cross-linking taking place.

The molecular weight distributions for the polystyrene substrate before and after 8 weeks ageing are shown in figure 7.8. Again, a shift in the peak position towards a lower molecular weight was observed, from 2.1×10^5 g/mol to 1.3×10^5 g/mol and represents almost a halving of the molecular

weight. However, the polystyrene substrate also shows a small shoulder around 3.0×10^6 g/mol after ageing which is suggestive of cross-linking.

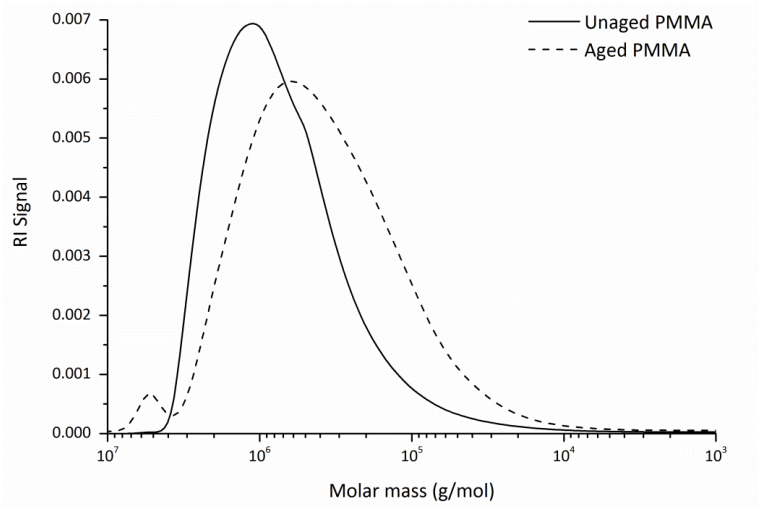

Figure 7.7 Molecular weight distributions for the PMMA substrate before and after 8 weeks accelerated light ageing.

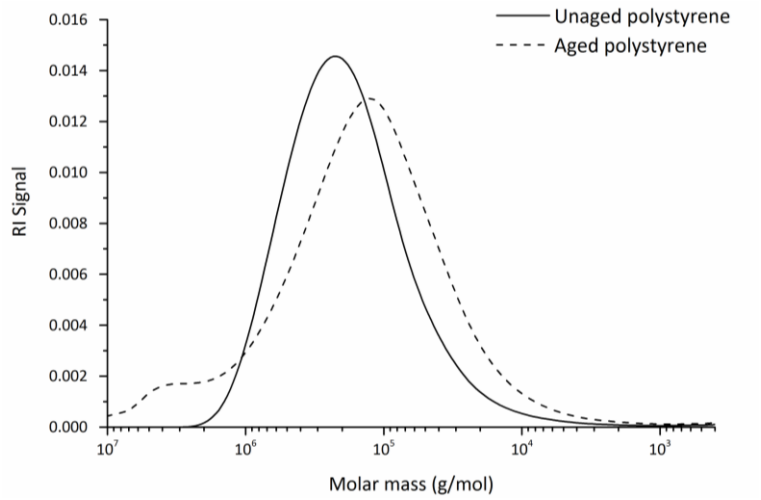

Figure 7.8 Molecular weight distributions for the polystyrene substrate before and after 8 weeks accelerated light ageing.

7.3.4 Hardness

Figure 7.9 shows the mean micro-hardness values for the polystyrene substrate after 0, 1, 2, 4 and 8 weeks ageing and shows a significant increase in the hardness of the substrate with accelerated light ageing. The micro-hardness values for PMMA were only measured at 0 and 8 weeks ageing. There was a slight increase in the mean Vickers micro-hardness for PMMA, from 21.6 VHN for the unaged substrate to 22.3 VHN after 8 weeks ageing. The standard deviation decreased from 0.9 VHN to 0.3 VHN.

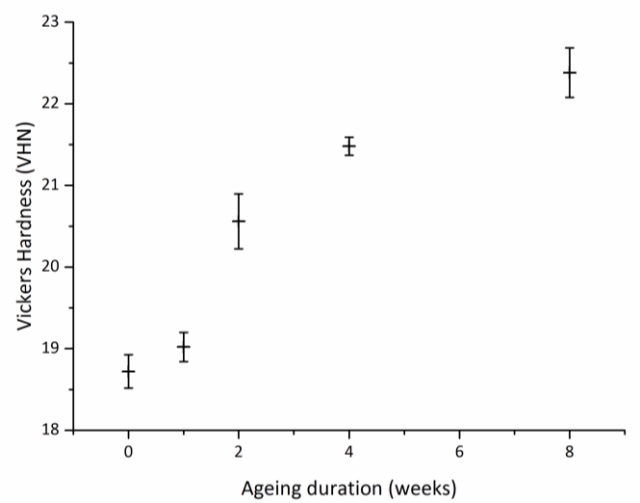

Figure 7.9 Mean micro-hardness values for the polystyrene substrate after 0, 1, 2, 4 and 8 weeks accelerated light ageing.

7.3.5 Spectral response and colorimetry

Figure 7.10 shows the transmission spectra in the wavelength range 250 nm - 830 nm for the polystyrene substrates that had been aged for 0, 1, 2, 4 and 8 weeks. As the polystyrene aged, it absorbed light at longer wavelengths and after 2 weeks accelerated light ageing was starting to absorb radiation in the visible part of the spectrum. This was manifested as a visible yellowing of the polystyrene substrate. Figure 7.11 shows the transmission spectra in the same wavelength range for the PMMA substrates that had been aged for 0 and 8 weeks.

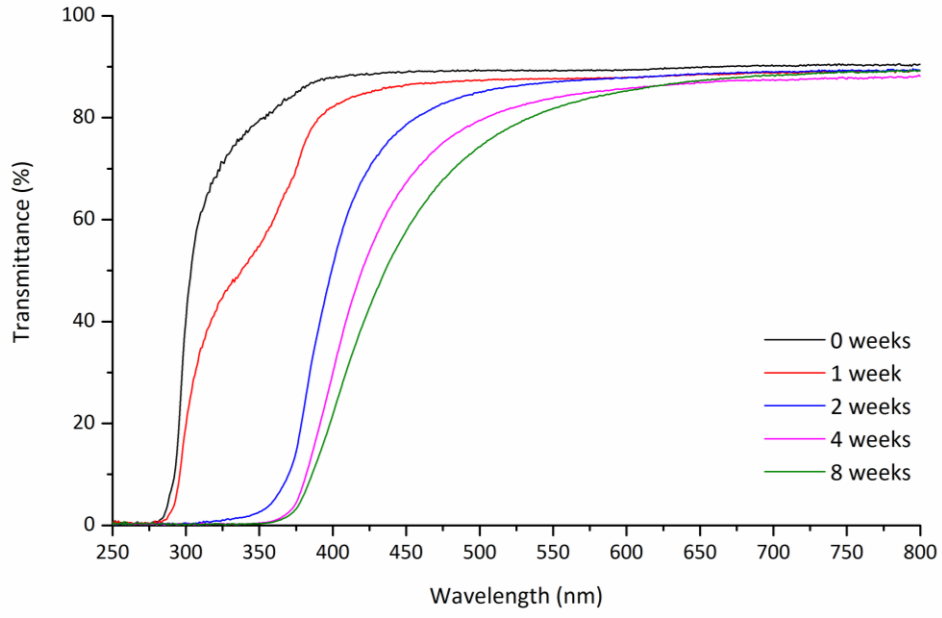

Figure 7.10 Transmission spectra for the polystyrene substrates in the UV and visible region after 0, 1, 2, 4 and 8 weeks accelerated light ageing.

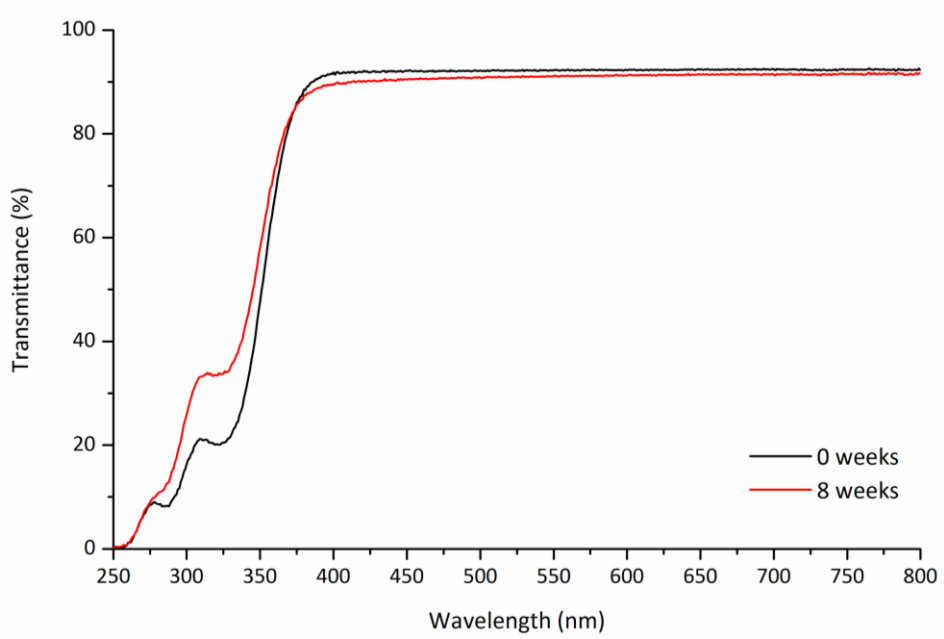

Figure 7.11 Transmission spectra for the PMMA substrates in the UV and visible region after 0 and 8 weeks accelerated light ageing.

Calculation of the ΔE_{00} values and yellowness indices (YI) was performed for the polystyrene substrate after 0, 1, 2, 4 and 8 weeks ageing and are shown in figure 7.12. Both values show an increase over time. While a slight yellowing of the substrate is discernible with the naked eye after 1 week, after 2 weeks the change in colour is immediately apparent. The ΔE_{00} value for PMMA after 8 weeks ageing was found to be $\Delta E_{00} = 0.4$. The yellowness index for PMMA was calculated as YI = 0.25 at 0 weeks and YI = 0.78 after 8 weeks accelerated light ageing.

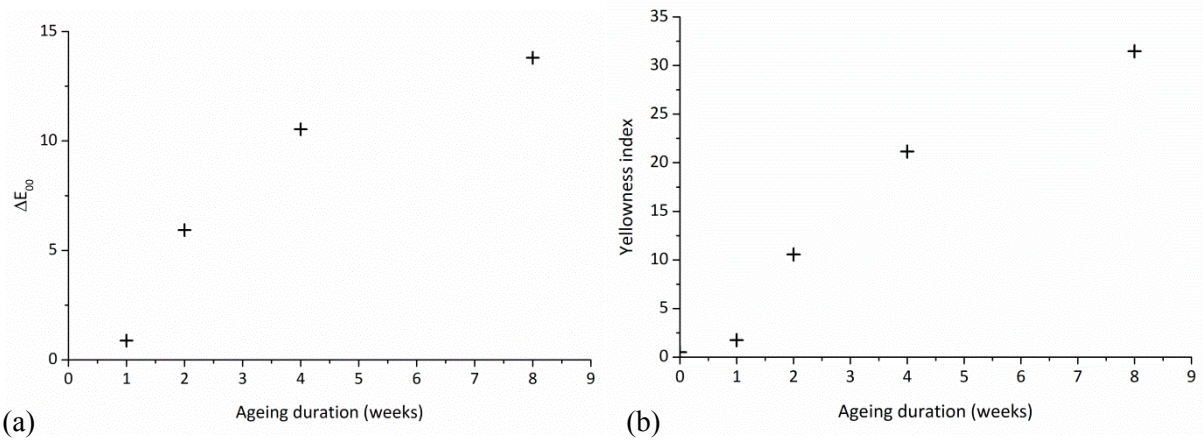

Figure 7.12 a) ΔE_{00} values and b) yellowness indices for polystyrene after 0, 1, 2, 4 and 8 weeks accelerated light ageing.

7.4 Results from ageing of cleaned substrates

This section examines the virgin substrates that were cleaned *before* accelerated ageing.

7.4.1 Physical changes

7.4.1.1 PMMA

Examination of the interferometry and SEM micrographs for PMMA did not reveal any significant changes after 8 weeks ageing. Some deposition of particulates on the surface of the PMMA was observed over the course of ageing.

7.4.1.2 Polystyrene

Interferometry micrographs of the polystyrene substrates were captured before and after cleaning and after 1, 2, 4, 6 and 8 weeks accelerated aging. The changes to the substrates are illustrated by the polystyrene substrate cleaned with deionised water, shown in figure 7.13. There are several points of interest in these micrographs. The first is the appearance of a line across the substrate after 4 weeks accelerated light ageing and indicated by the arrows in figure 7.13. This was formed in the direction of cleaning and is also present in the micrographs captured at 6 and 8 weeks. At 4 weeks this line has a peak-to-peak width of around 2.5 μm and a peak-to-valley height of around 5 nm. The 4 week micrograph also shows the appearance of what appear to be dust particulates on the surface, which may indicate a change in the surface energy of the substrate. The extent of dust redeposition on the polystyrene substrates was noticeably greater than that observed for the PMMA substrates. The interferometry micrographs after 6 weeks and 8 weeks accelerated ageing show that these particulates sink into the polystyrene substrate over time. This was not observed for the dust particles on the PMMA substrates.

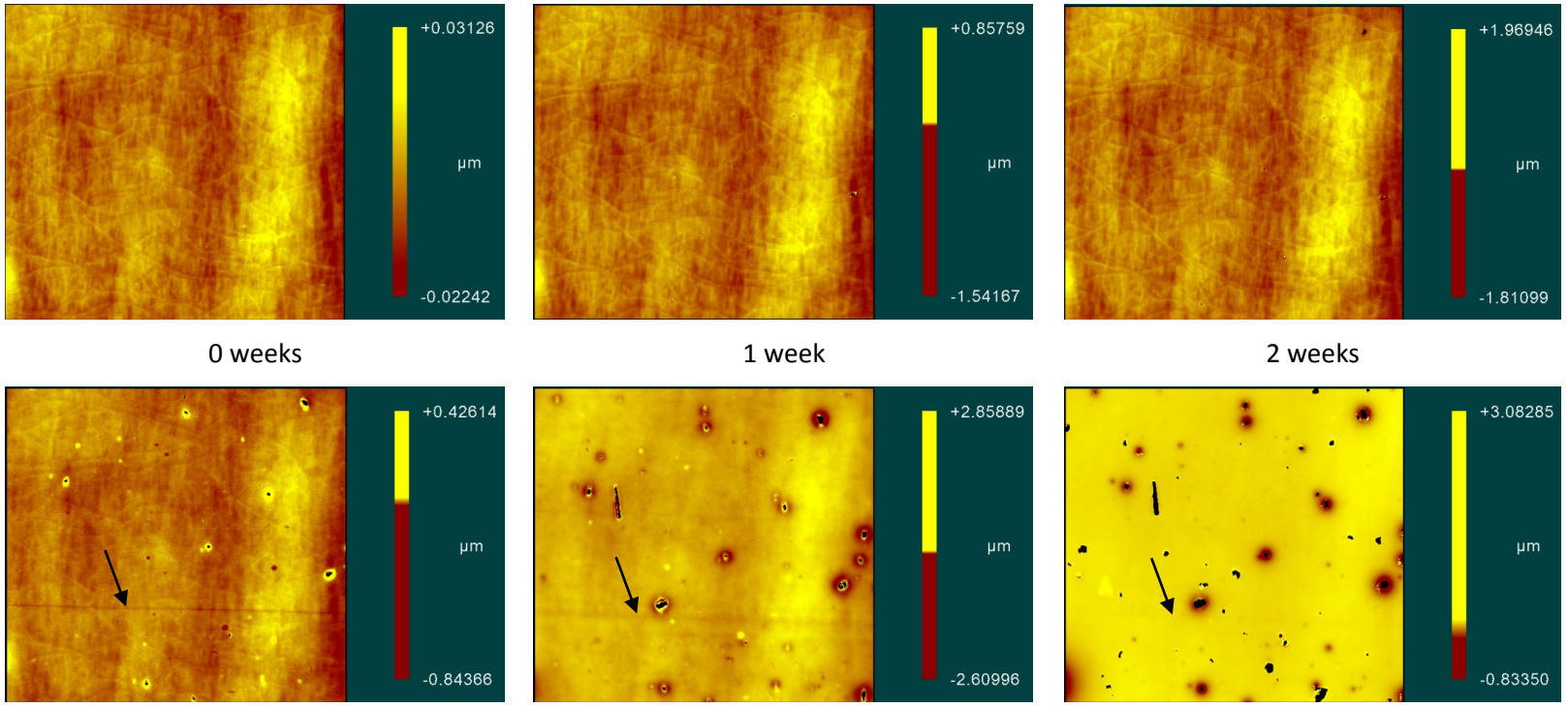

Figure 7.13 Interferometry micrographs of the polystyrene substrate cleaned with deionised water which then underwent accelerated light ageing for the durations indicated. Field of view = 0.57 mm × 0.53 mm. Cleaning in horizontal direction (L to R). The black arrows indicate the location of the line that developed during accelerated light ageing.

At wavelengths above 800 nm, the xenon lamp spectrum displays several intense peaks in the 800 nm – 1000 nm region. It is therefore thought that the absorption of infra-red radiation by the particulates results in a localised increase in temperature which causes softening of the polystyrene and enables the particles to sink into the substrate. As the solar spectrum does not contain these peaks, it is thought that this sinking of particulates would not be observed in natural ageing.

Dust measurements were performed for the inside of the chamber after operation using an Aerocet 531S particle mass monitor (Met One Instruments, USA) and the distribution of the detected particulates is shown in figure 7.14. The PM classification includes all particles smaller than that diameter in microns, e.g. PM10 includes all particles with a diameter of 10 μm or less. The total suspended particles (TSP) value includes all particles detected. These particle sizes are consistent with the particles observed on the polystyrene surface using both interferometry and SEM, and suggest that they are a result of dust deposition.

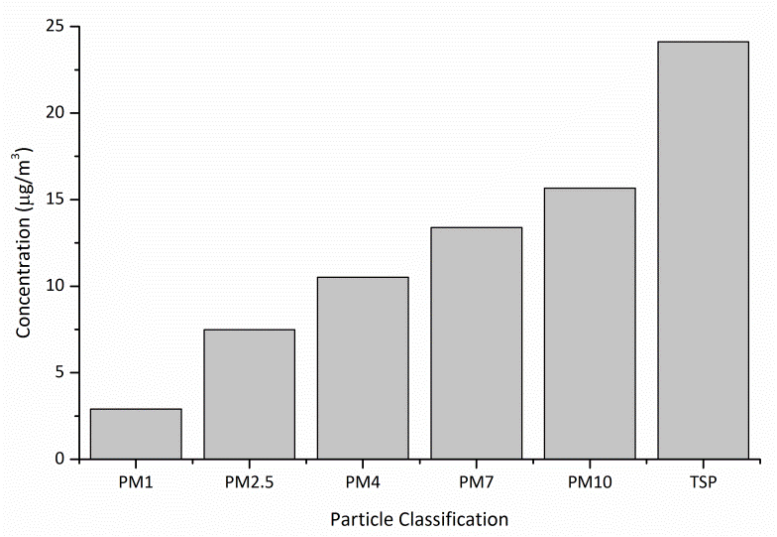

Figure 7.14 Particle size distribution of dust particulates from the ageing chamber after operation.

SEM micrographs of the polystyrene substrates were captured after 8 weeks accelerated light ageing. Examination of the polystyrene substrates after 8 weeks ageing revealed the presence of small formations on the surface as shown in figure 7.15. These formations were present on all substrates and did not depend on the cleaning agent applied. They were not observed on the polystyrene samples that had been aged for 4 weeks or less.

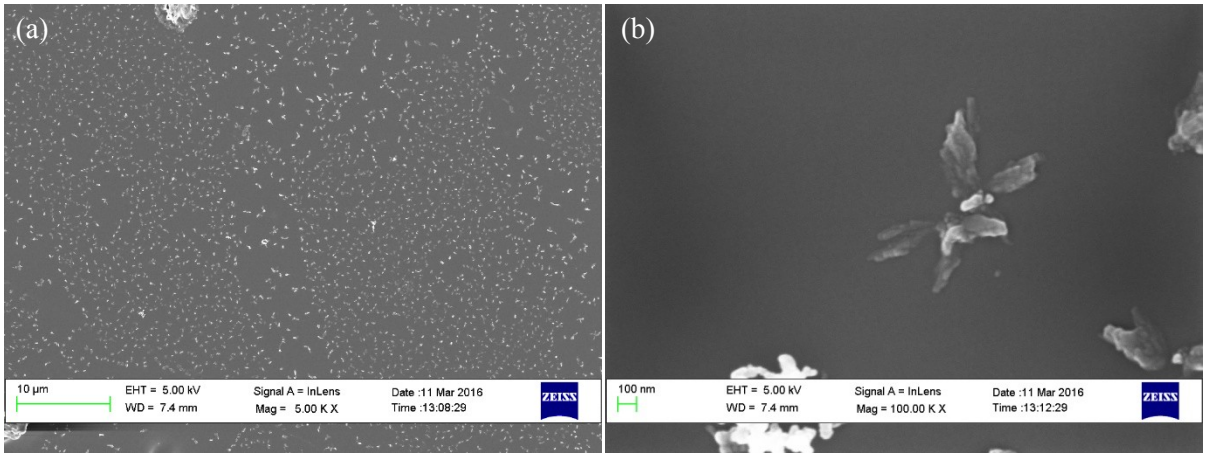

Figure 7.15 SEM micrographs of the uncleaned polystyrene substrate after 8 weeks accelerated light ageing at a) 5k magnification and b) 100k magnification showing the presence of formations on the surface.

However, it was noted that some of the formations aligned to form lines on the cleaned substrates, as indicated by the arrow in figure 7.16a. It is possible that these were preferentially occurring in regions which were already scratched, however by 8 weeks ageing these scratches were not evident. These micrographs also show that some of the dust particles which have been deposited on the substrate are surrounded by an area which is devoid of formations. It is thought that these dust particulates have deposited early in the ageing process and have therefore acted to shield the local area from incident light. The formation of cracks in the vicinity of some dust particulates was also observed and can be seen in figure 7.16b. This may be due to the preferential cracking of the substrate around these particulates, possibly by the same localised increase in temperature that was thought to result in the sinking of these dust particulates. Alternatively, the aged substrate was noticeably more brittle than the unaged substrate and these cracks may have been formed by the deposition of the particles themselves.

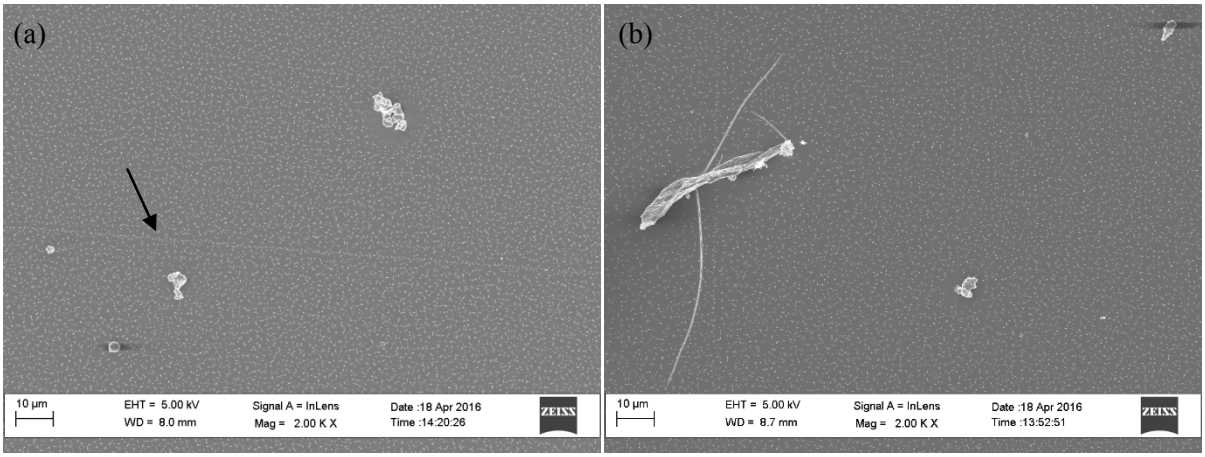

Figure 7.16 SEM micrographs of the isopropyl alcohol-cleaned polystyrene substrate after 8 weeks accelerated light ageing showing a) the presence of a line of formations (indicated by the black arrow) and clear areas around the dust particulates and b) cracking of the substrate in the vicinity of the deposited particles.

AFM examination of the aged uncleaned polystyrene substrate was performed to further characterise these formations (figure 7.17). The formations are approximately 200 nm in height and are irregular in their topography. Figure 7.17b appears to show that the formations are in close contact with the surface, suggesting that these are not depositions but have instead originated from the bulk plastic. It is also notable that the circular depressions seen in previous AFM images for the unaged polystyrene substrate are not present on the aged substrate. Note the horizontal lines in both images are an artefact of the AFM analysis. EDX and ToF-SIMS analysis of the aged substrate did not reveal any significant difference in composition for these formations when compared to the rest of the polystyrene substrate.

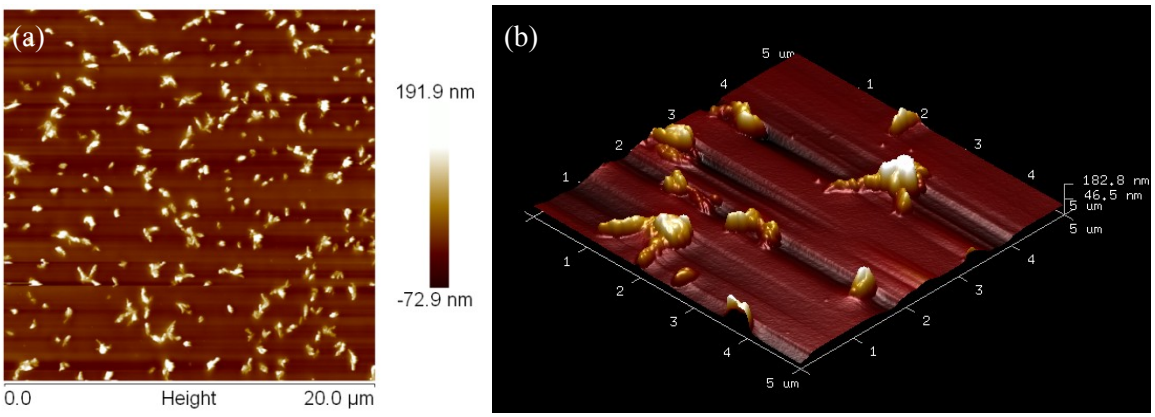

Figure 7.17 a) AFM micrograph of the uncleaned polystyrene substrate after 8 weeks accelerated light ageing and b) 3D representation showing the formations present on the surface.

In order to ascertain whether these formations were due to the elevated temperature in the ageing chamber, a set of heat-aged polystyrene samples were examined after 8 weeks ageing at a temperature of 63 °C ± 3 °C. The heat-aged samples did not exhibit the formations seen on the light-aged samples.

Further detail about the formations is given by the AFM micrographs shown in figure 7.18. The tapping amplitude micrograph (figure 7.18b) shows that the larger formations appear to be formed from multiple parts and have the appearance of bubbles which have joined together, creating a common boundary where they have come into contact. It can also be seen that there is a clear difference in the contrast of areas corresponding to the formations in the phase micrograph (figure 7.18c). Changes in contrast in AFM phase micrographs correspond to a change in the oscillation phase of the cantilever, which in turn indicates a change in the adhesion properties of the substrate.

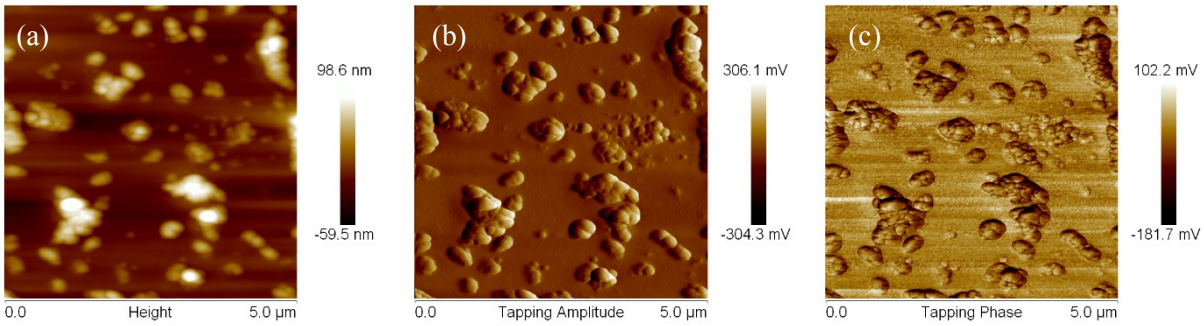

Figure 7.18 AFM micrographs showing the presence of the formations in a) topography, b) amplitude and c) phase mode.

7.4.2 Chemical changes

Most of the work in this section was performed on polystyrene as this showed the most noticeable changes due to ageing. However, the PMMA substrates were examined to determine whether they showed chemical changes which might be indicative of degradation and which were not yet visibly apparent.

7.4.2.1 PMMA

Figure 7.19 shows the PCA plots for the positive polarity ToF-SIMS data from the unaged and the aged PMMA substrates. The differences between these samples are due in part to the presence of the protective film residue on the unaged substrate, as indicated by the presence of fragments at 29.04 ($C_2H_5^+$), 43.05 ($C_3H_7^+$), 56.06 ($C_4H_8^+$) and 71.09 ($C_5H_{11}^+$). However, the PCA data also reveals the presence of fragments at m/z = 18.04 (NH_4^+), 30.03 (CH_4N^+), 44.05 ($C_2H_6N^+$), 58.07 ($C_3H_8N^+$) and 88.08 ($C_4H_{10}NO^+$) which are characteristic of the aged substrate.

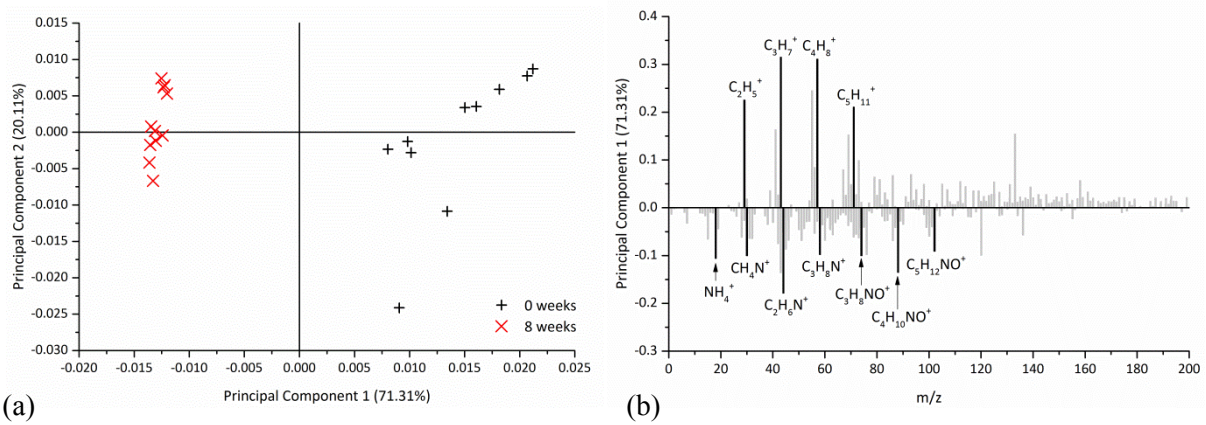

(a) (b)

Figure 7.19 PCA a) scores and b) loadings plots for the positive polarity ToF-SIMS data comparing the unaged PMMA substrate and the PMMA substrate that had undergone 8 weeks accelerated light ageing.

The PCA scores and loadings data for the PMMA substrates cleaned with organic solvents prior to ageing is shown in figure 7.20. There are several contributions to the differences between the cleaned and the uncleaned substrates. The uncleaned substrate shows the presence of fragments at m/z = 29.04 ($C_2H_5^+$) and 57.07 ($C_4H_9^+$), corresponding to the film residue that was detected on the unaged substrates and which is still present after ageing. The uncleaned substrate is also characterised by fragments containing nitrogen at m/z = 44.05 ($C_2H_6N^+$) and 58.07 ($C_3H_8N^+$). In contrast the cleaned substrates are characterised by fragments at m/z = 59.01 ($C_2H_3O_2^+$), 85.07 ($C_5H_9O^+$), 101.06 ($C_5H_9O_2^+$) and 115.08 ($C_6H_{11}O_2^+$) which correspond to PMMA, as well as fragments corresponding to PDMS contamination.

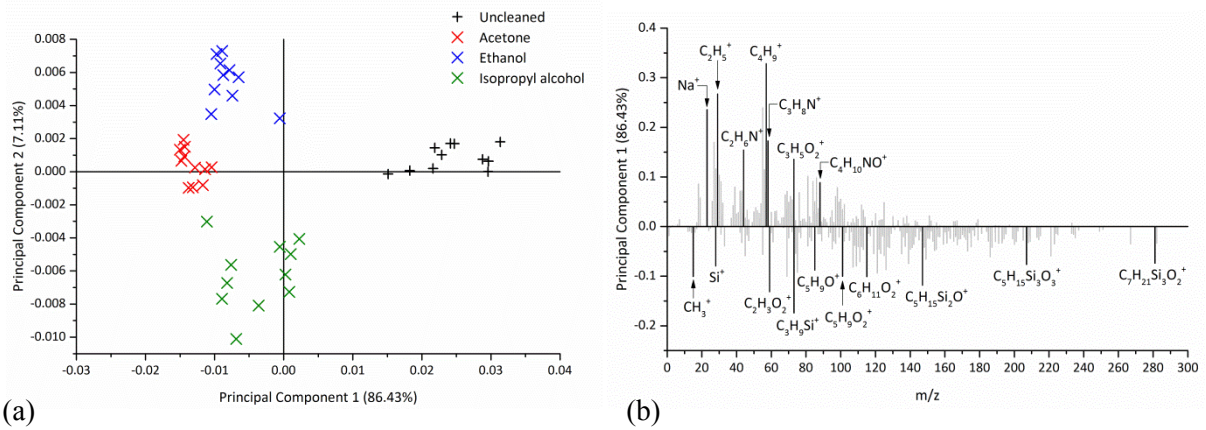

(a) (b)

Figure 7.20 PCA a) scores and b) loadings plots for the positive polarity ToF-SIMS spectra from the PMMA substrates cleaned with organic solvents which then underwent 8 weeks accelerated light ageing.

Figure 7.21 shows the PCA scores and loadings data for the aged PMMA substrates that had been cleaned with aqueous agents and the dry cleaning procedure prior to ageing. The differences between the cleaning procedures are less distinct than for the unaged PMMA substrates. The main differences

between the cleaned and uncleaned samples are due to the nitrogen fragments which are characteristic of the uncleaned sample.

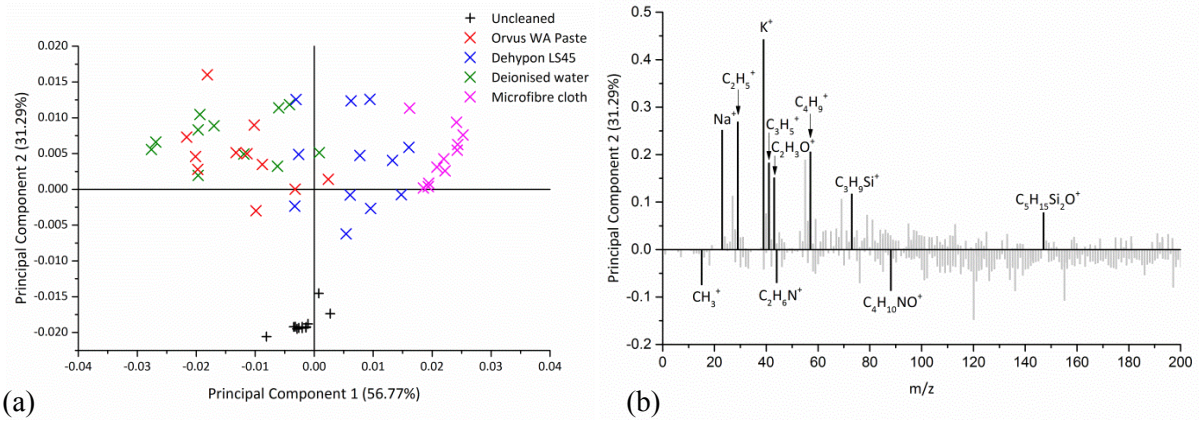

Figure 7.21 PCA a) scores and b) loadings plots for the positive polarity ToF-SIMS spectra from the PMMA substrates cleaned with aqueous agents and dry cleaning which then underwent 8 weeks accelerated light ageing.

7.4.2.2 Polystyrene

Initial characterisation of the aged polystyrene substrate was performed to determine the chemical changes taking place on the surface due to accelerated light ageing. Figure 7.22 shows the PCA scores and loadings plots for the positive polarity ToF-SIMS spectra from the uncleaned polystyrene substrates before ageing and after 1, 2 4 and 8 weeks accelerated ageing. It can be seen that the trend of the scores on PC1 is towards the negative values as the substrate is aged. The positive loadings on PC1 correspond to polystyrene, as indicated by fragments at m/z = 91.05 ($C_7H_7^+$), 105.07 ($C_8H_9^+$), 117.07 ($C_9H_9^+$) and 193.10 ($C_{15}H_{13}^+$). These are characteristic of the unaged substrate and, to a lesser extent, the substrate that had undergone 1 week accelerated ageing. However, from 2 weeks onwards, the substrates are increasingly defined by the negative loadings on PC1. These loadings are attributed to fragments that contain nitrogen, as seen by those at m/z = 18.03 (NH_4^+), 30.03 (CH_4N^+), 44.05 ($C_2H_6N^+$) and 58.07 ($C_3H_8N^+$) and indicate a change in composition of the surface.

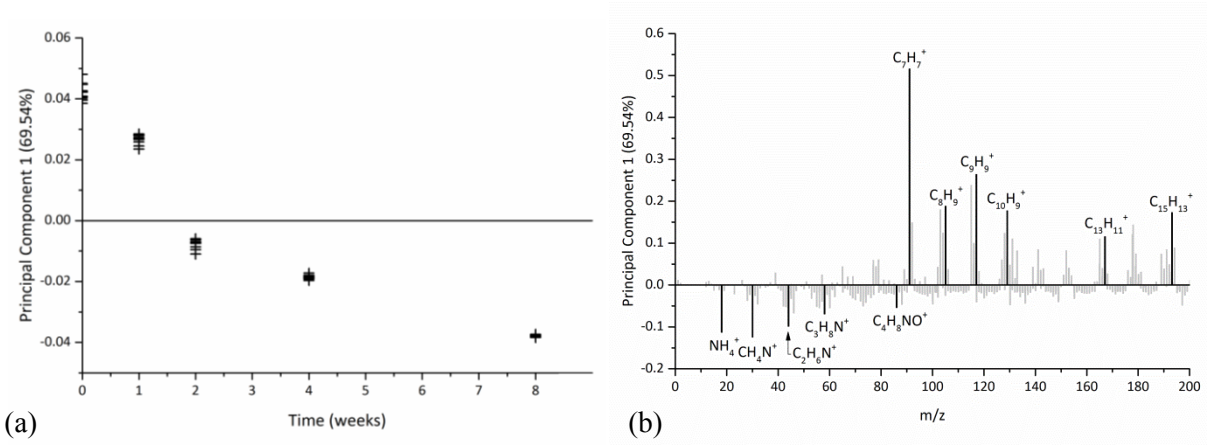

Figure 7.22 PCA a) scores and b) loadings plots for the positive polarity ToF-SIMS data from the uncleaned polystyrene substrates that had undergone 0, 1, 2, 4 and 8 weeks accelerated light ageing.

In order to gain further information about the changes occurring in the surface region, depth profiles were performed for the fragments at m/z = 18.03 (NH_4^+) and 91.05 ($C_7H_7^+$), and are shown in figure 7.23. It can be seen from these profiles that there is a change in the profile of the $C_7H_7^+$ fragment with ageing, most notably at 4 and 8 weeks. The difference between the intensity at the surface and sub-surface region also increases with ageing, indicating an accumulation at the surface of fragments that are not characteristic of polystyrene. Inspection of the NH_4^+ fragment reveals that while detection of this fragment at 0 and 1 week is very low, there is a slight change in the profile after 2 weeks, which becomes more significant after 4 and 8 weeks accelerated ageing. Again, the gradient of the profile close to the surface changes, becoming steeper for the samples aged for 8 weeks and suggesting an accumulation of the NH_4^+ fragment at the surface.

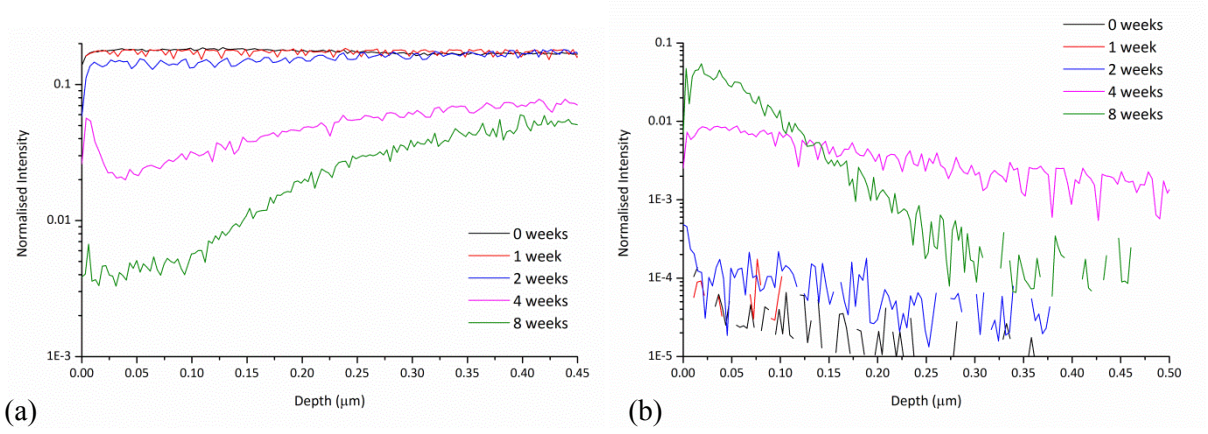

Figure 7.23 Depth profiles of the aged uncleaned polystyrene substrate for the fragments a) m/z = 91.05 ($C_7H_7^+$) and b) m/z = 18.03 (NH_4^+).

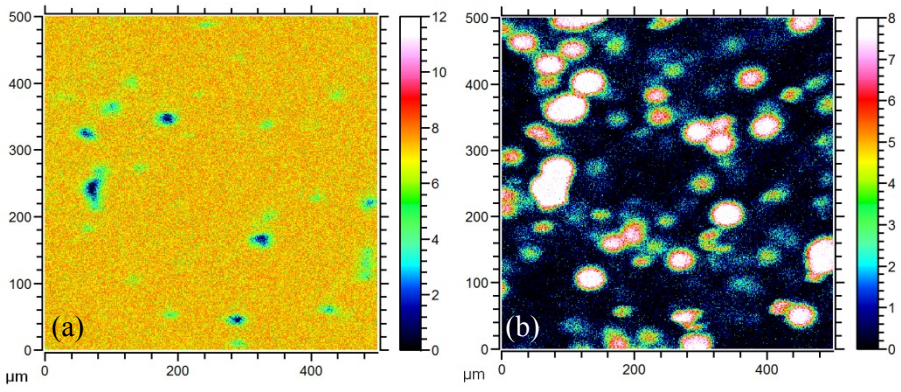

Figure 7.24 SIMS maps showing the spatial distribution of the a) NH_4^+ and b) Na^+ fragments on the uncleaned polystyrene substrate after 8 weeks accelerated light ageing.

Figure 7.24a shows the spatial distribution of the NH_4^+ fragment on the surface of the uncleaned polystyrene substrate that had been aged for 8 weeks. It can be seen that the fragment is detected uniformly over the surface. The only local variations are due to the presence of dust particulates on the surface, as indicated by the presence of sodium in figure 7.24b. In order to determine whether the presence of these fragments is a result of exposure to elevated temperature rather than light, the spectra from the heat-aged samples were also analysed and compared to an unaged substrate. The PCA scores and loadings plots for these substrates are shown in figure 7.25.

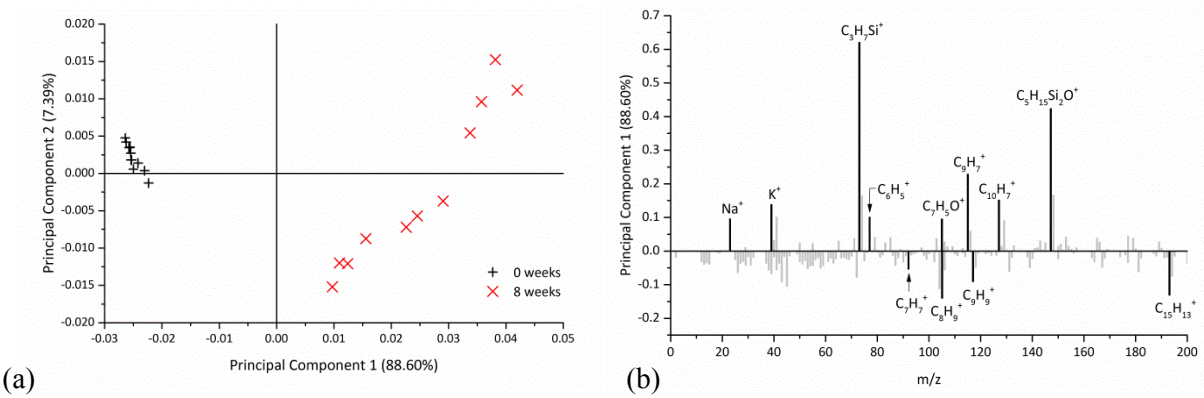

Figure 7.25 PCA a) scores and b) loadings plots for the positive polarity ToF-SIMS spectra from the uncleaned polystyrene substrates that had undergone heat ageing at 63 °C ± 3 °C for 0 and 8 weeks.

The loadings for the heat-aged substrate shows the presence of Na^+ and K^+, most likely from contamination in the form of dust depositing on the surface. There is also evidence of oxidation, as indicated by fragment at m/z = 105.03 ($C_7H_5O^+$). However, fragments corresponding to polystyrene are detected on both the aged and the unaged substrate. Inspection of these fragments reveals that those characteristic of the unaged substrate at m/z = 105.07 ($C_8H_9^+$), 117.07 ($C_9H_9^+$) and 193.10 ($C_{15}H_{13}^+$) originate from the main chain, while the fragments at m/z = 77.04 ($C_6H_5^+$), 115.05 ($C_9H_7^+$) and 127.05 ($C_{10}H_7^+$) are cyclic fragments and are characteristic of the heat-aged substrate. It is notable

that the heat-aged substrate is not characterised by loadings corresponding to NH_4^+ or other nitrogen fragments, which indicates that the presence of these fragments on the artificially light-aged substrates is not due to the elevated temperature.

Figure 7.26 shows the PCA data for the polystyrene substrates cleaned with solvents prior to ageing. Inspection of the PC2 loadings indicates that the substrates cleaned with alcohols are characterised by nitrogen fragments. The loadings on PC2 for the uncleaned substrates (shown in red) correspond to contamination, while the substrate cleaned with acetone is characterised by the fragments at m/z = 105.05 ($C_7H_5O^+$) and 147.09 ($C_{10}H_{11}O^+$) (shown in blue) which are attributed to oxidation of the substrate.

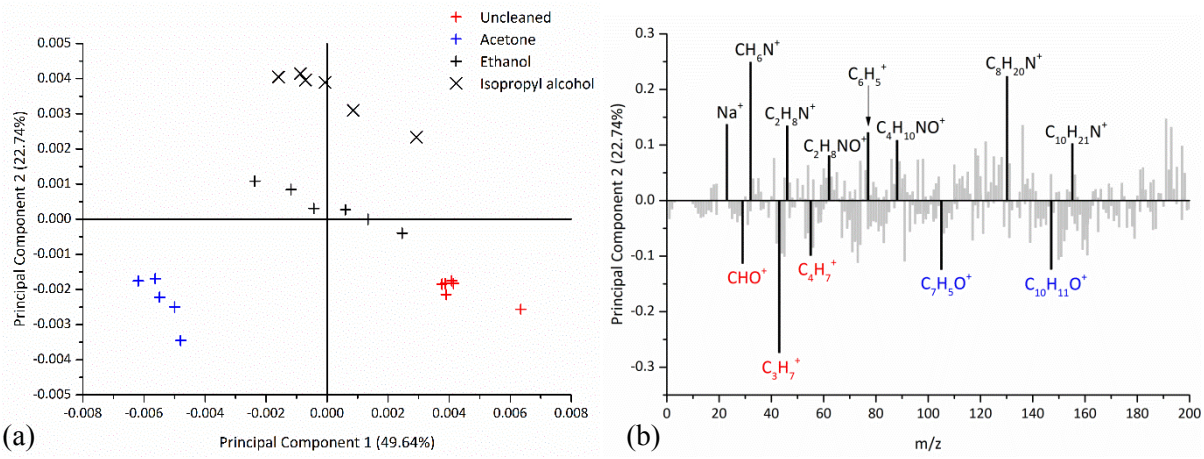

Figure 7.26 PCA a) scores and b) loadings plots for the positive ToF-SIMS spectra from the polystyrene substrates cleaned with organic solvents which then underwent 8 weeks accelerated light ageing.

The PCA scores and loadings plots for the polystyrene substrates cleaned with aqueous agents and the dry cleaning procedure prior to ageing are shown in figure 7.27. The uncleaned polystyrene surface and that cleaned with the dry cleaning procedure are characterised by the negative PC2 fragments, which mainly correspond to hydrocarbon contamination. To a lesser extent, fragments containing nitrogen also characterise these surfaces. The fragment at m/z = 91.05 ($C_7H_7^+$) corresponding to polystyrene is more characteristic of the substrates cleaned with aqueous agents, as is the fragment at m/z = 105.05 ($C_7H_5O^+$) corresponding to oxidation of the polystyrene. Contamination of the substrate due to cleaning is also indicated for the aqueous agents.

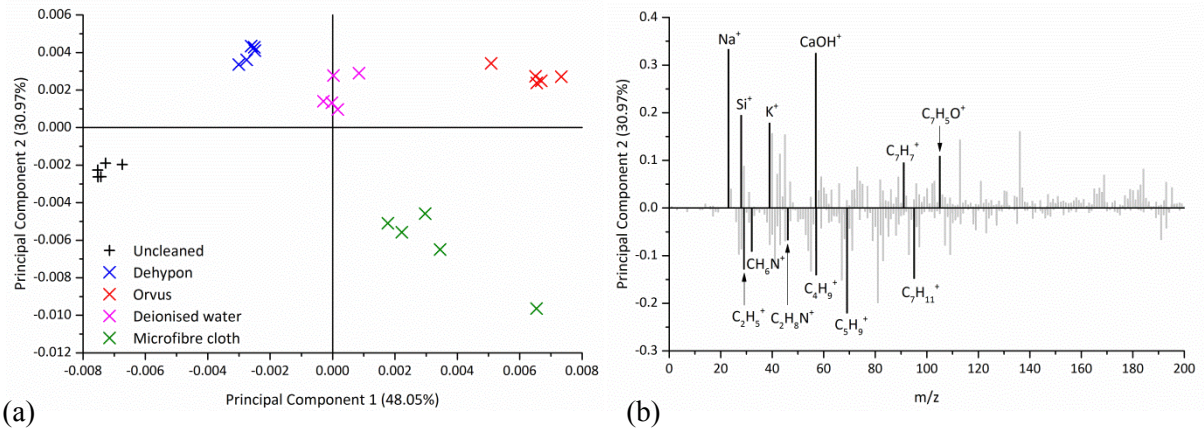

(a) (b)

Figure 7.27 PCA a) scores and b) loadings plots for the positive polarity ToF-SIMS spectra from the polystyrene substrates cleaned with the aqueous agents or the dry cleaning procedure which then underwent 8 weeks accelerated light ageing.

Further information was obtained regarding the presence of the surfactant residues after ageing. Figure 7.28 shows the PCA scores and loadings for the positive polarity ToF-SIMS spectra from the polystyrene substrate cleaned with the non-ionic surfactant prior to ageing compared to the aged uncleaned substrate. The uncleaned substrate shows the presence of nitrogen fragments but the positive loadings, which correspond to the cleaned surface, are less conclusive. Fragments corresponding to contamination are characteristic of the cleaned substrate as is the fragment at m/z = 91.05 ($C_7H_7^+$) which corresponds to polystyrene. The fragment at m/z = 59.05 ($C_3H_7O^+$) which is characteristic of the non-ionic surfactant is not prominent in the loadings. However, inspection of the raw SIMS spectrum does reveal the presence of this fragment as well as the fragment at m/z = 45.03 corresponding to $C_2H_5O^+$. Depth profiles were performed in order to determine the distribution of the $C_3H_7O^+$ fragment in the surface region and are shown in figure 7.29. These reveal that the $C_3H_7O^+$ fragment is present on the surface and starts to flatten out at a depth of around 0.4 µm.

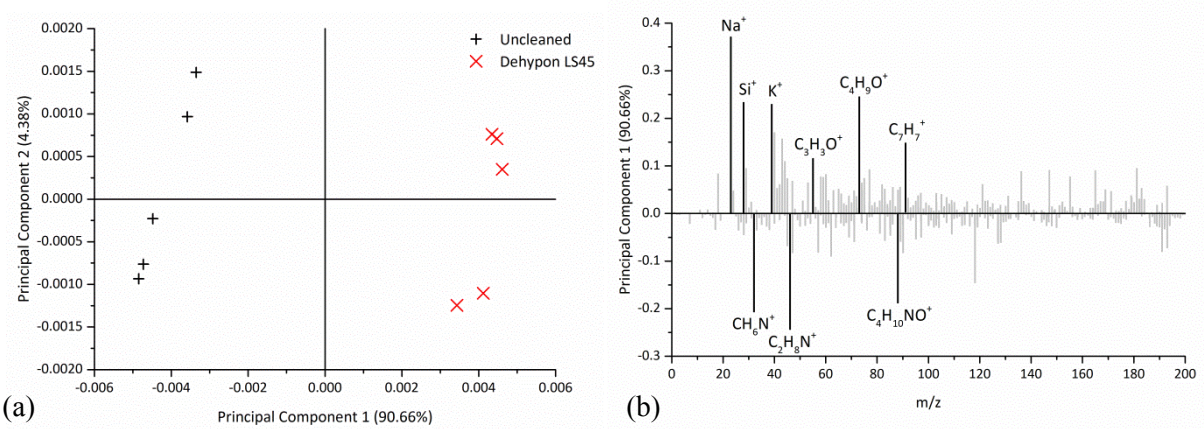

(a) (b)

Figure 7.28 PCA a) scores and b) loadings plots for the positive polarity ToF-SIMS spectra from the polystyrene substrate cleaned with the non-ionic surfactant which then underwent 8 weeks accelerated light ageing.

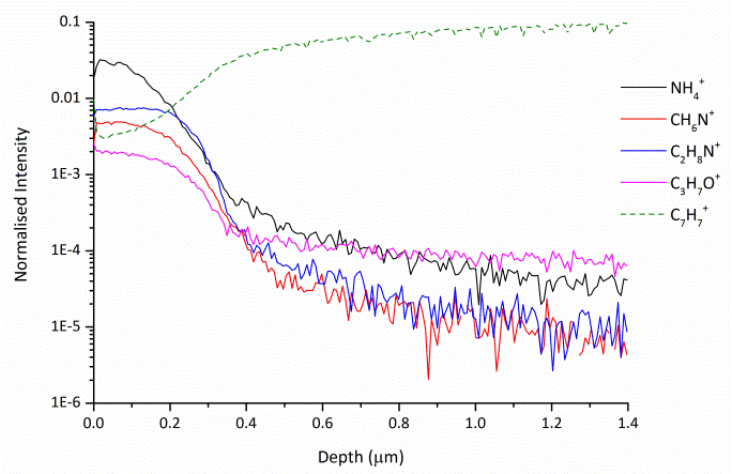

Figure 7.29 Depth profiles of the ToF-SIMS fragments indicated for the polystyrene substrate cleaned with the non-ionic surfactant which then underwent 8 weeks accelerated light ageing.

The PCA scores and loadings for the negative polarity ToF-SIMS spectra from the anionic surfactant are shown in figure 7.30 and show that the major differences between the substrates are due to the presence of oxygen and hydroxyl ions on the cleaned substrate. The SO_4H^- fragment indicates that there are traces of the anionic surfactant present on the cleaned substrate and this is supported by the raw spectrum, which also displays peaks at m/z = 63.96 (SO_2^-), 79.96 (SO_3^-) and 95.95 (SO_4^-). However, the absence of loadings at SO_3^- and SO_2^- indicate that the contribution of fragments corresponding to surfactant residue to the differences between the substrates is much less than for the unaged substrates.

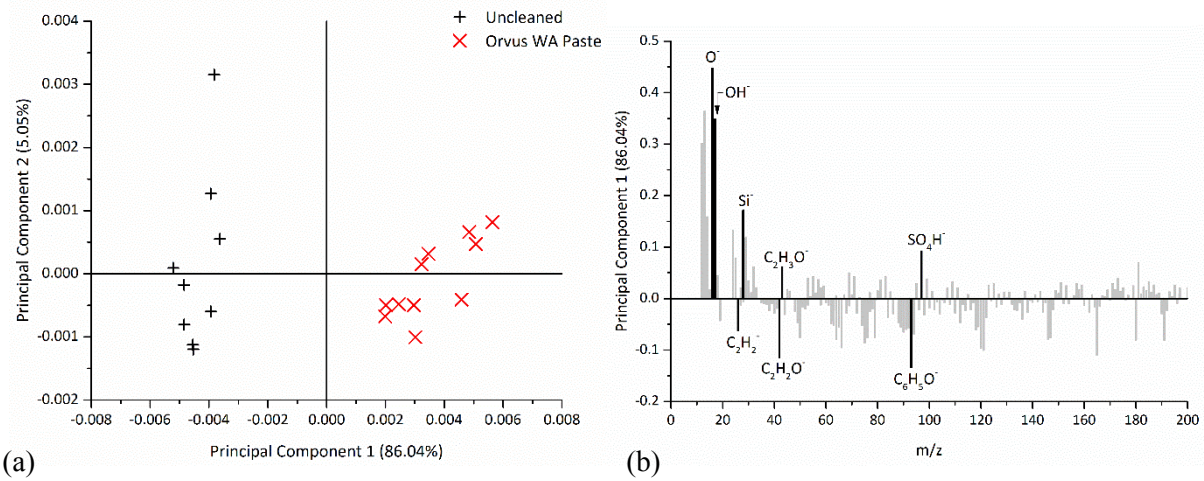

(a) (b)

Figure 7.30 PCA a) scores and b) loadings plots for the negative polarity ToF-SIMS spectra from the polystyrene substrate cleaned with the anionic surfactant which then underwent 8 weeks accelerated light ageing.

7.5 Results from the cleaning of aged substrates

This section focuses on the physical changes occurring to the aged virgin polystyrene substrate as a result of cleaning. These samples were cleaned *after* undergoing 8 weeks accelerated light ageing. As no significant changes had been seen for the PMMA substrate due to ageing, this substrate was not investigated.

7.5.1 Physical changes

Interferometry micrographs of the aged polystyrene substrate before and after cleaning are shown in figure 7.31. There are two notable differences in the behaviour of these substrates when compared to the cleaning behaviour of the unaged polystyrene substrates. The first is that the application of acetone to the substrate does not result in dissolution of the plastic surface and that there is no significant scratching occurring. Secondly, the use of surfactants has resulted in notable roughening of the aged polystyrene surface. It can also be seen that all the cleaning agents applied are ineffective at removing the dust particulates when they have sunk into the surface, as they did not come into contact with the microfibre cloth during cleaning.

SEM micrographs of the cleaned aged polystyrene substrates are shown in figure 7.32. It can be seen that the dry cleaning procedure is the least damaging to the aged surface, although there is evidence of some lines being formed in the direction of cleaning. The application of deionised water resulted in the removal of some of the formations. The use of surfactants caused scratching to the surface and there are indications that the formations have been spread over the surface in the direction of cleaning. This scratching was significantly more severe than was seen for the unaged virgin polystyrene substrate.

All the organic solvents result in the removal of the formations to a greater or lesser extent: ethanol is the least effective. However, scratches were also observed on the substrates cleaned with isopropyl alcohol and ethanol. The application of acetone results in the removal of the formations and very little scratching, and is consistent with the interferometry observations. In addition, the acetone micrograph shows the presence of a dust particle that has been pressed into the substrate during cleaning. This was also observed on other cleaned substrates. Comparison of these micrographs to those obtained for the unaged virgin polystyrene substrate indicates that the application of solvents to the aged substrates did not result in scratching to the same extent as that seen for the unaged substrate.

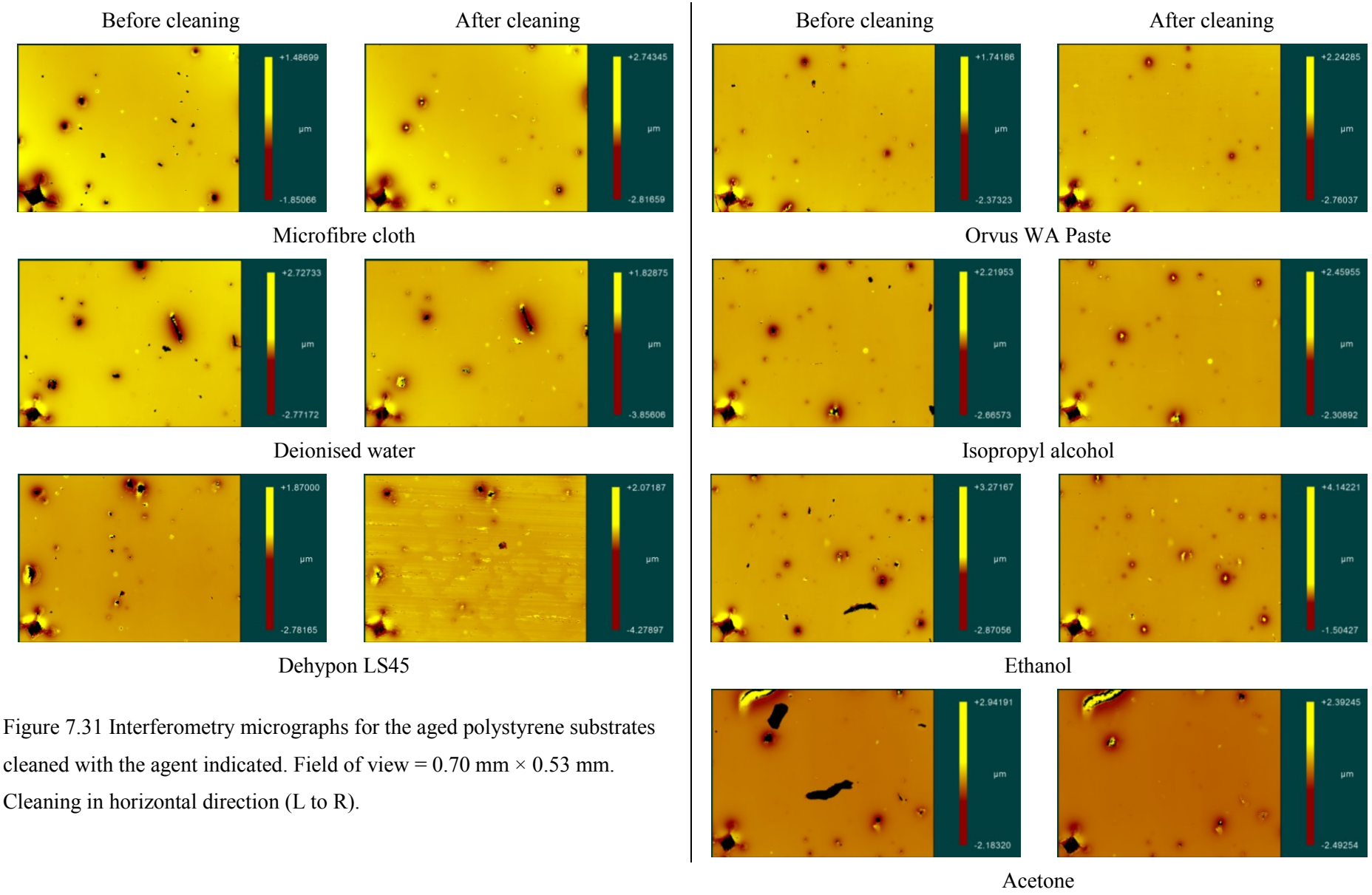

Figure 7.31 Interferometry micrographs for the aged polystyrene substrates cleaned with the agent indicated. Field of view = 0.70 mm × 0.53 mm. Cleaning in horizontal direction (L to R).

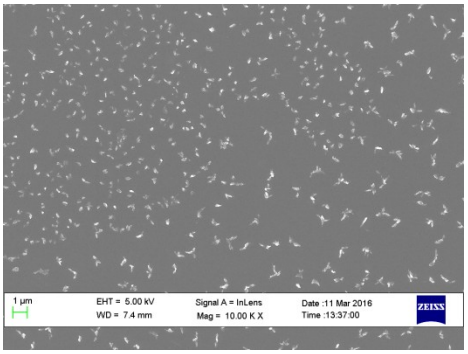

No treatment

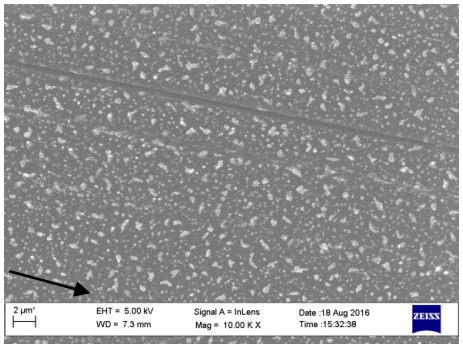

Microfibre cloth

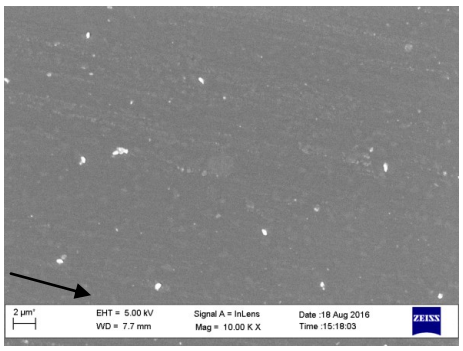

Deionised water

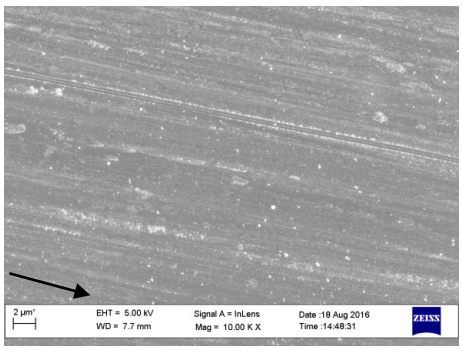

Dehypon LS45

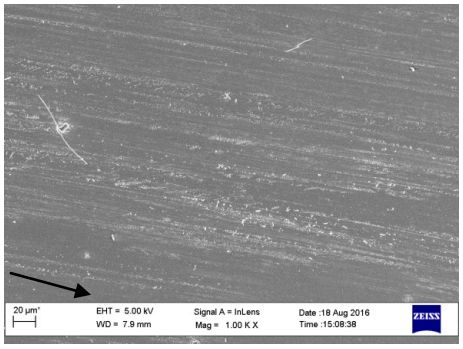

Orvus WA Paste

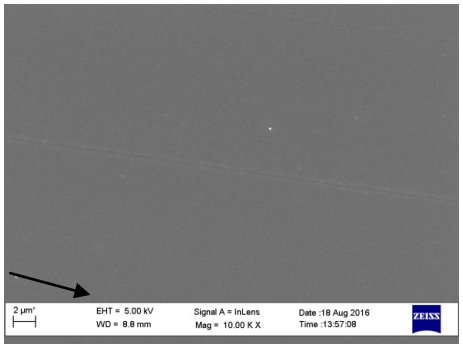

Isopropyl alcohol

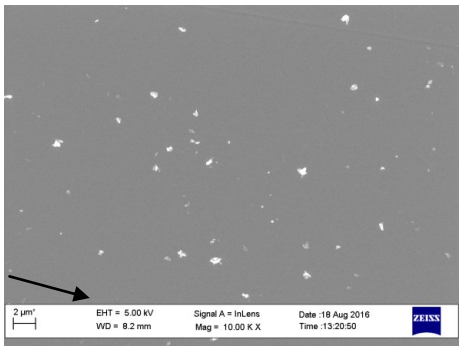

Ethanol

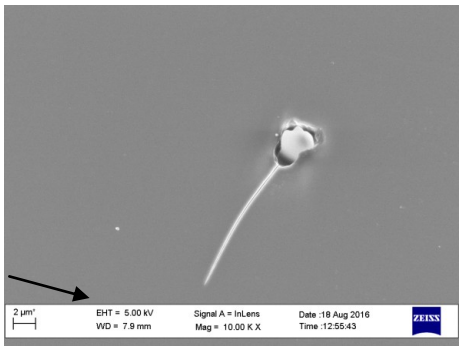

Acetone

Figure 7.32 SEM micrographs for the aged polystyrene substrates cleaned with the agent indicated. The cleaning direction is indicated by the black arrow.

AFM micrographs for the aged polystyrene substrate cleaned with the anionic surfactant and deionised water are shown in figure 7.33. It can be seen that the formations are no longer intact on the

substrate cleaned with the surfactant and that the surface is instead characterised by much smaller debris. This supports the previous observation that the formations have been broken up and distributed across the surface by mechanical action during cleaning. The substrate cleaned with the deionised water also showed some evidence of smearing, however discrete raised areas corresponding to the formations were still present.

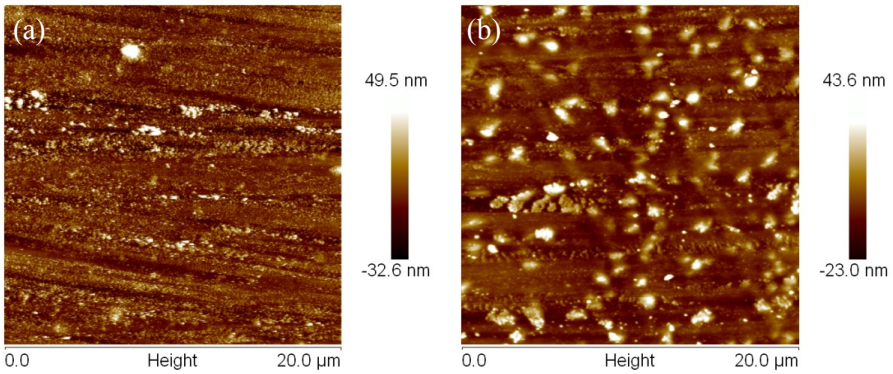

Figure 7.33 AFM micrographs showing the aged polystyrene substrate after cleaning with a) the anionic surfactant and b) deionised water.

The presence of scratches on the aged polystyrene substrate cleaned with alcohols were observed in the SEM micrographs. Figure 7.34 shows the AFM micrograph from the aged polystyrene substrate cleaned with isopropyl alcohol; scratches in the direction of cleaning can be clearly seen on the substrate. The corresponding surface profile of the white line is shown in figure 7.34b. This shows that the peak-to-valley height of the scratches can be of the order of 40 nm, with peak-to-peak widths of around 0.5 µm. These are comparable to the scratches observed for the unaged virgin polystyrene substrate. The topography of these scratches is also interesting as they are uniform in width, unlike the scratches observed on the soiled substrates. Similarly to those seen on the unaged virgin substrates, they are thought to be a result of the passage of stray dust or particles over the surface.

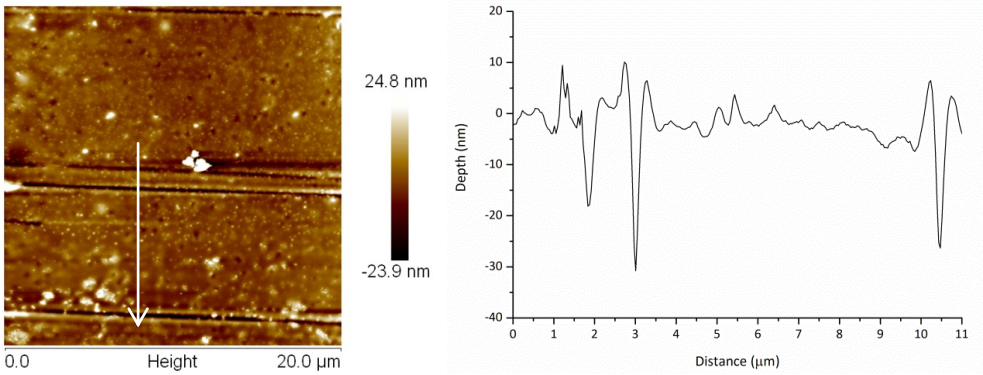

Figure 7.34 AFM micrograph of the aged polystyrene substrate cleaned with isopropyl alcohol and the corresponding surface profile of the white line.

7.5.2 Chemical changes

Due to the severe damage observed for the polystyrene substrates cleaned with the surfactants, both of these substrates were analysed using ToF-SIMS to determine whether there were any chemical changes occurring to the substrate. Figure 7.35 shows the PCA scores and loadings plots for the aged polystyrene substrate cleaned with the anionic and the non-ionic surfactants. These show that the major differences between the uncleaned and cleaned substrates are due to the presence of residual surfactant on the cleaned surfaces as indicated by fragments at m/z = 31.02 (CH_3O^+), 45.03 ($C_2H_5O^+$) and 59.05 ($C_3H_7O^+$) for the substrate cleaned with the non-ionic surfactant (indicated in blue) as well as PDMS contamination for the substrate cleaned with the anionic surfactant (indicated in red). The uncleaned substrate is characterised by the nitrogen fragments.

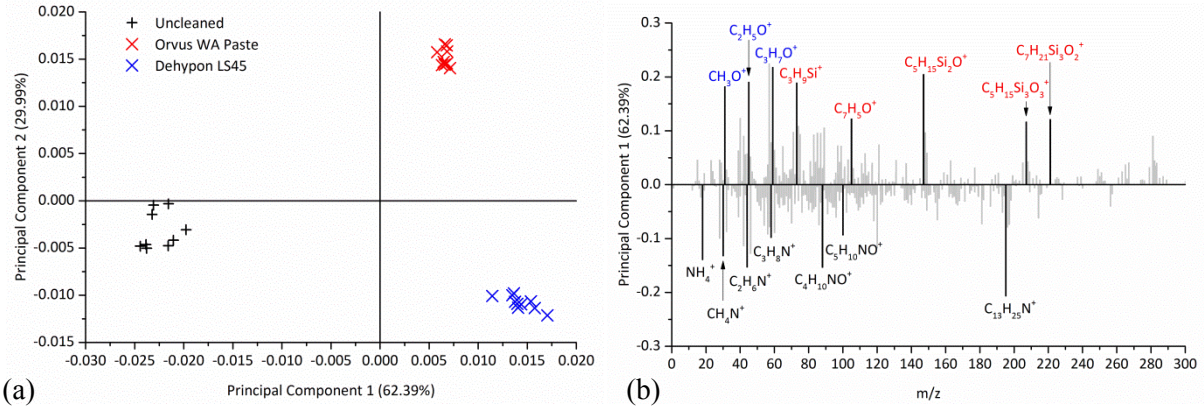

Figure 7.35 PCA a) scores and b) loadings plots for the positive polarity ToF-SIMS spectra from the aged polystyrene substrate cleaned with the anionic and non-ionic surfactants.

In order to determine whether the differences between the uncleaned and the cleaned substrates were due to the removal of the nitrogen compounds from the surface or whether these were simply obscured by residual surfactant, depth profiles of the substrate cleaned with the non-ionic surfactant were performed and are shown in figure 7.36. These indicate that the fragments at m/z = 32.05 (CH_6N^+), 46.07 ($C_2H_8N^+$) and 60.08 ($C_3H_{10}N^+$) are still present, but are obscured by a layer of surfactant residue on the surface, as indicated by the fragments at m/z = 31.02 (CH_3O^+), 45.03 ($C_2H_5O^+$) and 59.05 ($C_3H_7O^+$).

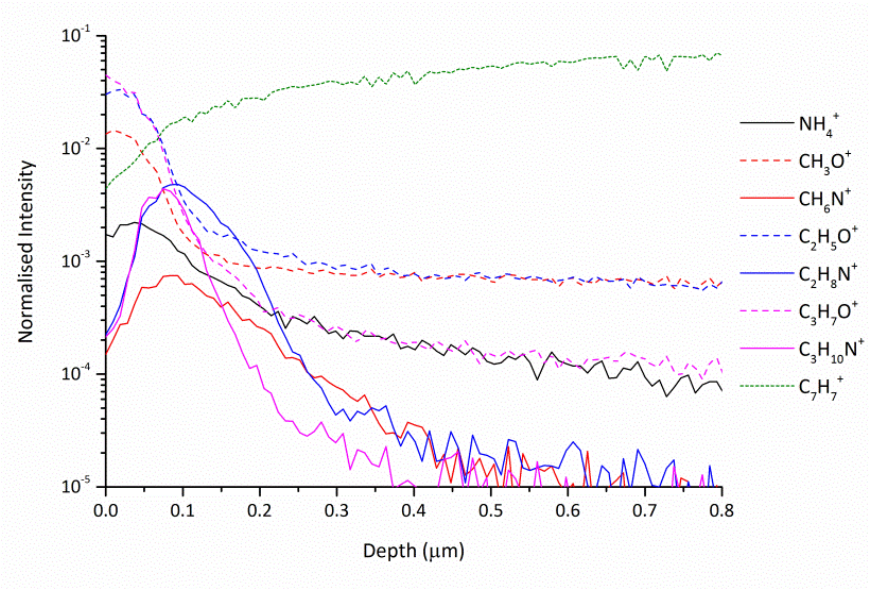

Figure 7.36 Depth profiles of the aged polystyrene substrate cleaned with the non-ionic surfactant.

Figure 7.37 shows the PCA data for the aged substrate cleaned with the anionic surfactant. The differences in the substrates are due to the residual surfactant on the cleaned substrate. The uncleaned substrate shows evidence of oxidation, as indicated by the fragment at m/z = 93.03 ($C_6H_5O^-$) and also shows the presence of contamination, as indicated by the presence of the F^- ion. There are no indications of other chemical changes taking place as a result of cleaning.

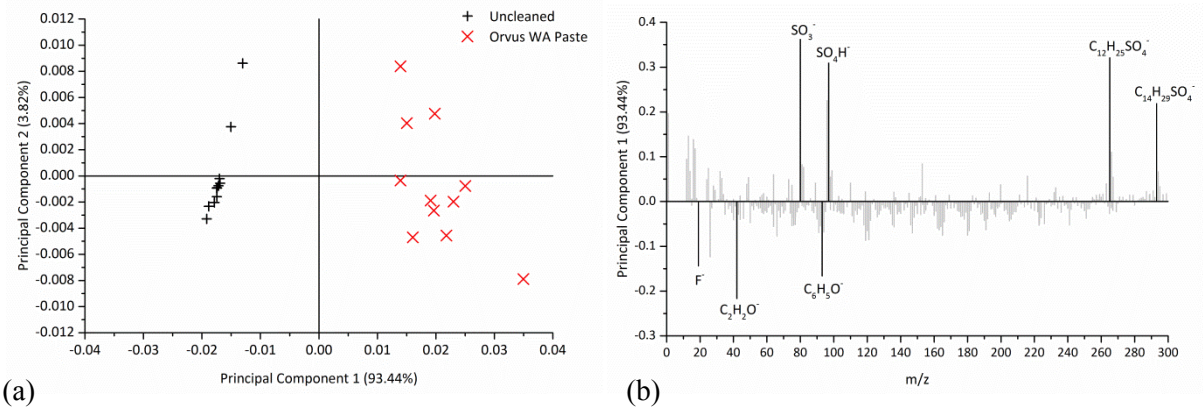

(a) (b)

Figure 7.37 PCA a) scores and b) loadings plots for the negative polarity ToF-SIMS spectra from the aged polystyrene substrate cleaned with the anionic surfactant.

7.6 Discussion

The findings from this chapter are summarised in table 7.1

Table 7.1 Summary of findings from the accelerated ageing of plastic substrates.

	PMMA	**Polystyrene**
ATR-FTIR	No change after 8 weeks ageing.	Formation of bands corresponding to oxidation after 8 weeks ageing.
T_g (°C) (8 weeks)	118.1 ± 0.5	101.3 ± 0.5
GPC	Molecular weight distributions suggest chain scission and some cross-linking.	Molecular weight distributions suggest chain scission and some cross-linking.
Micro-hardness (VHN) (8 weeks)	22.3 ± 0.3	22.4 ± 0.3
ΔE_{00} (8 weeks)	0.4	13.8
Yellowness index (0 weeks)	0.25	0.50
Yellowness index (8 weeks)	0.78	31.46
Surface changes with ageing	Deposition of dust on the surface. Detection of nitrogen fragments on aged substrates.	Deposition of dust and sinking of dust into the surface over time. Detection of nitrogen fragments on aged substrates. Detection of formations on the polystyrene surface. Appearance of lines on cleaned substrates after ageing. Surfactant residues were less readily distinguished compared to the unaged substrate.
Cleaning of aged substrate	Not examined.	Dissolution not observed for cleaning with acetone. Surface damage observed with surfactants. Some scratching observed for alcohols, deionised water and dry cleaning. Organic solvents were effective in removing formations. PCA indicates the presence of surfactant residues.

7.6.1 Bulk characterisation

The ATR-FTIR spectra from the PMMA substrates did not show any significant changes as a result of accelerated light ageing. However, the polystyrene substrates showed the development of two bands at 1750 cm^{-1} and 1250 cm^{-1} after 4 weeks ageing, which were attributed to a C=O stretch and a C-O stretch respectively. The oxidation of polystyrene results in the formation of both carboxyl and carbonyl groups on the polymer backbone [69] which would explain the presence of these bands. In addition the very broad band between 3100 cm^{-1} and 3600 cm^{-1} that develops after 4 weeks accelerated light ageing corresponds to an O-H stretch and is attributed to hydrogen bonding [182].

Thermal analysis of the aged plastic substrates did not reveal a significant change in the T_g of the plastics after ageing. There was a slight increase in the T_g for PMMA and a slight decrease in the T_g for polystyrene. An increase in T_g for the PMMA substrate could indicate cross-linking, while a decrease for polystyrene could indicate chain scission. However, they do not represent a significant change in the T_g with ageing. It is also worth noting that the DSC analysis was performed on samples taken from the entire depth of the substrate and not just the surface region. Therefore local variations in the T_g at the surface would not necessarily affect the measured T_g to a significant extent. The molecular size distribution of the aged polymer substrates indicated that chain scission occurred for both polymers with ageing, with peak shifts towards a lower molecular weight. For the polystyrene substrate, this decrease in molecular weight corresponded to an observed increase in brittleness. However both polymers also showed the development of an additional peak at a higher molecular weight, indicating that some cross-linking was also taking place.

The micro-hardness values of both plastic substrates were found to increase with accelerated light ageing, although the increase in hardness was significantly greater for the polystyrene substrate. This was thought to be due to the oxidation of the plastic surface. A previous study on the plasma treatment of polyethylene recorded a change in the micro-hardness of this plastic which was attributed to oxidation of the substrate [183].

The yellowing of the polystyrene substrate was just noticeable after 1 week accelerated light ageing and apparent after 2 weeks ageing. This was reflected in the ΔE_{00} values and yellowness indices for the polystyrene substrate. The spectrophotometry results also revealed that the polystyrene substrate absorbs light in the visible region as it ages, in agreement with Feller [166]. This is explained by chain scission of the polymer which results in an increasingly conjugated backbone and absorbance at longer wavelengths as described in Chapter 2. While a colour change for the PMMA substrate was not noticeable, the values for ΔE_{00} and the yellowness index after 8 weeks ageing indicated that there was also a slight change occurring for this substrate.

7.6.2 Aged cleaned substrates

Inspection of the aged polystyrene substrates revealed several points of interest. Firstly redeposition of dust on the substrates was observed over the 8 week ageing period. The most significant redeposition occurred between 2 and 4 weeks ageing. This is most likely due to an increase in the surface energy of the substrate due to oxidation and resulting in increased attraction between the dust particulates and the surface. There may also be an electrostatic component due to the loss of water content during ageing.

The spatial distribution of the redeposited dust was observed to be random and was not localised close to areas damaged by the cleaning process. The diameter of the particles observed on the surface is in agreement with the airborne particle distribution measured in the chamber after operation. These dust particles were observed to sink into the polystyrene substrate in the weeks after deposition. It is thought that this was due to the absorbance of infra-red radiation by the particles which results in a local change in temperature and causes softening of the polystyrene substrate. Therefore this dust sinking is thought to be an artefact of the accelerated light ageing process and would not necessarily happen in a natural ageing scenario. Cracking was also observed in the region of some, but not all, of the dust particulates that had deposited on the surface. In addition there was a lack of formations in the areas around some of the dust particles which may be a result of local shielding from the xenon light source.

The interferometry micrographs also revealed the appearance of lines across some of the cleaned polystyrene substrates over the course of the ageing period. These are thought to correspond to scratches that were too shallow to be detected by interferometry immediately after cleaning but which became apparent as the substrates were aged. At 4 weeks ageing, the line observed on the substrate cleaned with deionised water had a peak-to-peak width of approximately 2.5 μm and a peak-to-valley height of approximately 5 nm; these dimensions are comparable with some of the scratches formed on the unaged virgin polystyrene samples. However, measurement of the width is limited by the lateral resolution of the interferometer and may be smaller. The interferometry micrographs of the substrates appeared to suggest that these scratches became less defined over time. In addition the SEM micrographs showed no obvious evidence of scratching on the surface of the cleaned polystyrene substrates after 8 weeks ageing. It is unclear as to why this is the case. It may be that the loss of moisture content has resulted in shrinkage of the plastic which has revealed an already weakened line on the substrate and the sides of which move further apart as the ageing process continues, eventually becoming less defined. It would be worth examining the surface of the cleaned polystyrene substrate with SEM after 4 weeks accelerated light ageing to determine whether scratching can be observed at this stage.

The SEM micrographs of the polystyrene substrates that had been aged for 8 weeks showed the presence of small irregular formations on the surface. These were present on all substrates, regardless of the cleaning procedure used. AFM micrographs of the aged polystyrene substrates revealed that the formations were in close contact with the surface and therefore they are thought to originate from the plastic itself, rather than being the result of deposition on the surface. Variations in the AFM phase micrograph were observed to correspond to the formations and indicate a change in the adhesive properties of the surface. However, examination of the surface chemistry using ToF-SIMS did not reveal any local variations in composition, which indicates that these formations are more likely to originate from the plastic itself rather than the migration of additives. Heat-ageing tests did not result in the appearance of these formations and it is therefore indicated that these are a result of the light ageing process. However, it was observed that some of the aforementioned formations were arranged in lines on the cleaned substrates and may indicate that they preferentially form in locations which have been damaged by scratching.

The chemical changes occurring to the surface as a result of ageing were analysed using ToF-SIMS. Both plastics showed the presence of fragments containing nitrogen on the aged substrates. Depth profiles of fragments corresponding to polystyrene ($C_7H_7^+$) and NH_4^+ indicated that there was a change in the distribution of these fragments in the surface region with ageing. This indicated an increase in the presence of these fragments at the surface which could be explained either by migration from the bulk or from the surrounding atmosphere.

It was hypothesised that these nitrogen fragments might be related to the formations on the surface. However, inspection of the ToF-SIMS images from the substrate does not reveal any localised variations in the surface chemistry which would correspond to the formations. Moreover, similar fragments were detected for the aged PMMA substrate, which does not display the presence of formations. It is therefore thought that the nitrogen fragments may originate from two sources, either from the surrounding atmosphere or as a result of migration of additives from the bulk plastic. Awaja and Pigram [184] detected the increased presence of nitrogen on the surface of epoxy resin composites when subjected to UV irradiation and elevated temperatures. This was attributed to the creation of reactive sites on the polymer chain via chain scission and it is possible that a similar mechanism is occurring here. Alternatively, both plastic substrates may contain additives such as hindered amine light stabilisers (HALS) which contain an amine functional group, and which may be migrating to the surface.

Analysis of the heat-aged polystyrene substrates was performed in order to check whether these fragments were a result of the elevated temperatures experienced during light ageing. The PCA analysis of the substrates did not reveal the presence of nitrogen fragments on the surface of the heat-aged substrate, indicating that these fragments are a result of exposure to light or UV radiation.

However it was noted that different fragments corresponding to polystyrene were detected on both the heat-aged and the unaged substrates. Inspection of the ToF-SIMS spectra revealed that these differences resulted from the origin of the polystyrene fragments. While the fragments that are characteristic of the unaged substrate originate from the main chain, the fragments that are characteristic of the heat-aged substrate are cyclic fragments [149]. This difference in fragmentation is thought to indicate the thermal degradation of the polymer as a result of heat ageing.

The differences in the aged PMMA substrates due to the cleaning procedures broadly agreed with those seen for the unaged substrates: the organic solvents were effective in removing the film residue from the PMMA substrate and contamination was seen for both the solvent and aqueous cleaning methods. Contamination from cleaning was also detected on the aged cleaned polystyrene substrates. The PCA treatment of the ToF-SIMS spectra from the polystyrene substrates cleaned with surfactants prior to ageing was not conclusive regarding the presence of residues on the cleaned substrates. While there were indications of residual surfactant, the contribution of fragments characteristic of the surfactants to these samples were less significant than for the unaged polystyrene substrates. However, inspection of the raw SIMS data indicated that surfactant residues were still present after ageing.

In the majority of cases the nitrogen fragments were more representative of the uncleaned substrates. The exception to this was the polystyrene substrates that were cleaned with organic solvents prior to ageing where nitrogen fragments were more representative of the substrates cleaned with alcohols. It is unclear whether this is a true characteristic of the uncleaned substrate or whether the difference is due to residues on the cleaned substrates obscuring these fragments. If the presence of nitrogen is due to the surrounding atmosphere it may be that the uncleaned substrates have more reactive sites available due to contamination on the surface.

7.6.3 Cleaned aged substrates

Cleaning of the aged polystyrene substrates was performed to assess the differences in cleaning behaviour after artificial ageing. Examination of the surface after cleaning revealed some significant differences with the unaged substrate. Due to the sinking of dust particulates into the plastic surface, cleaning was generally ineffective in removing particle contamination from the surface. However, the cleaning procedures had a notable effect on the formations that had developed on the surface after 8 weeks ageing. In the case of the deionised water and the surfactants, cleaning resulted in the appearance of multiple smaller raised areas on the polystyrene surface. This was thought to be due to the redistribution of the formations over the surface. The AFM micrographs revealed a difference in the adhesion properties of the formations compared to the plastic surface. It is therefore thought that the formations may be softer and more adhesive than the surrounding substrate. This would explain their redistribution over the surface as a result of the application of the cleaning agents. However, as

this was not seen for the case when the microfibre cloth was used on its own, it is suggested that the surfactants also aided in their redistribution. While the use of the microfibre cloth did not have a significant effect on the formations, some scratching was observed.

The application of acetone to the aged polystyrene surface did not result in the dissolution observed for the unaged polystyrene substrate. This suggests a change in the solubility of the substrate due to oxidation of the surface. It is suggested that the formation of hydroxyl groups on the backbone of the polymer chain results in increased hydrogen bonding between individual chains, as indicated by the broad band around 3200 cm^{-1} in the ATR-FTIR spectra. This would change the hydrogen bonding component of the Hansen solubility parameter for polystyrene and would therefore affect its solubility in acetone. The application of alcohols to the substrate resulted in some scratching, which was of a similar width and depth to that observed for the unaged virgin polystyrene substrate.

The application of organic solvents was observed to result in the removal of the formations to a greater or lesser extent. Acetone was the most effective solvent used, while ethanol was the least effective. It is suggested that the formations therefore have a solubility similar to the unaged substrate which would enable their preferential removal. This could be explained by the formations originating from the bulk of the substrate as they would not be oxidised to the same extent as the material on the surface.

Due to the surface damage observed for the surfactant cleaning procedure on aged polystyrene, ToF-SIMS analysis was performed for these substrates. Both non-ionic and anionic surfactant residues were detected. Depth profiles of the aged polystyrene substrate cleaned with the non-ionic surfactant revealed that cleaning did not remove the nitrogen fragments from the surface. This may be due to two reasons: the chemical bonding of nitrogen to the polymer or the inability of the surfactant to remove additives that have migrated to the surface.

Conclusions

The accelerated light ageing tests performed on the PMMA and polystyrene substrates revealed some interesting data about the potential surface changes occurring both as a result of ageing and cleaning. The appearance of small formations on the polystyrene substrate is of interest as it suggests possible movement of the polymer or additives from the bulk to the surface. However, as these were only formed between 4 and 8 weeks ageing it is likely that an object would have to be severely degraded before a similar phenomenon would be seen. The composition of the plastic is also likely to influence their formation. The presence of nitrogen fragments on the surface of all the samples investigated is also of interest. While these do not appear to affect the substrate, they may provide a useful indication of degradation as changes were detected after only 1 week accelerated ageing for the polystyrene samples. Finally the spectrophotometry results indicated that radiation was absorbed at longer

wavelengths as the polystyrene aged. It is therefore apparent that an aged polystyrene substrate that has been exposed to light or UV radiation in its past may be more susceptible to radiation in the visible region, particularly at shorter wavelengths in the blue part of the spectrum. This could potentially affect the choice of lighting for these objects in the future.

The accelerated light ageing of the cleaned polystyrene samples indicated that areas of weakness may become more apparent with ageing. This was seen in the appearance of lines across some of the cleaned substrates. The presence of formations in lines across the cleaned substrates indicates that these may be preferentially occurring in weakened areas of the plastic surface. While there were indications that residues from surfactants were still present on the surfactant-cleaned surfaces after ageing, this was not as conclusive as for the unaged substrates. Finally, the differences in the cleaning behaviour of the aged polystyrene substrates is of interest. This was particularly noticeable for the substrates cleaned with acetone or the surfactants, and indicates the potential issues involved with cleaning aged plastic objects.

It has already been noted that accelerated ageing tests may not accurately replicate the processes occurring in natural ageing. It is worth mentioning that this work was performed using a xenon lamp which emits radiation in the UV and infra-red parts of the electromagnetic spectrum as well as the visible region. It is likely that many of the changes reported in this chapter are a result of exposure to UV radiation. Further work using filters to remove these parts of the spectrum would be valuable to determine whether these changes would still occur without the UV component. It is also worth mentioning that the samples examined in this work were transparent. It is anticipated that the addition of colorants to a plastic object would change the observed ageing behaviour and could also result in a change in the appearance of the object, such as colour fade.

Chapter 8

Case study: Business card box

While the use of model substrates is useful to determine the cleaning behaviour of plastics under controlled conditions, in reality an object made from a single type of polymer may differ in its molecular structure, types of additives and prior history. This chapter considers a specific case study to examine whether the cleaning behaviour previously described is applicable to a real-world polystyrene object.

8.1 Introduction and history

The object chosen for investigation was a small business card holder, consisting of a base and lid, with dimensions 58 mm × 94 mm × 21 mm, as shown in figure 8.1. The box was translucent, smokey grey-brown in colour and originated from Japan in the early 2000s, although the exact date of manufacture is unknown. For the purposes of this work, only the lid of the box was used and the outer face of the lid was examined as this was expected to have undergone the most wear and tear and would therefore have experienced the most damage and contamination.

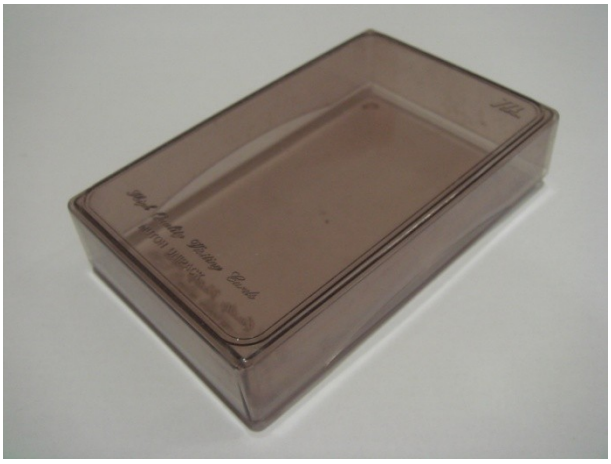

Figure 8.1 Photograph of the polystyrene business card box. Dimensions 58 mm × 94 mm × 21 mm.

There were several notable differences between the box and the sheet polystyrene subject. The most obvious was the colour, however closer inspection revealed that the box was also noticeably scratched and marked. The box was also at least ten years older than the sheet polystyrene and had been naturally aged. Bulk characterisation was performed to determine whether there were any other major difference between the two substrates.

8.2 Experimental

Samples measuring 15 mm × 20 mm × 1mm were cut from the base of the box lid using a bandsaw. The individual samples were marked with fiducial markers prior to any analysis work taking place. All samples were marked on the side corresponding to the outer side of the box as this was thought to be where most contamination would be present. The samples were imaged using white light interferometry then cleaned using the cleaning procedure outlined in Chapter 4.

Characterisation of the box was performed using ATR-FTIR to determine its composition as well as DSC and GPC to find the T_g and molecular weight of the polymer. The hardness of the substrate was also determined via micro-hardness testing. The initial physical and chemical condition of the box was characterised using white light interferometry, AFM, SEM and ToF-SIMS, using the parameters described in the previous chapters unless indicated. Surface analysis of the substrate was performed before and after cleaning using white light interferometry. Interferometry and SEM micrographs of the surface were captured after cleaning, while ToF-SIMS spectra were also acquired to look for changes in the chemical composition of the surface.

8.3 Bulk characterisation

8.3.1 ATR-FTIR

The ATR-FTIR spectrum of the box is shown in figure 8.2, and compared to the ATR-FTIR spectrum from the sheet polystyrene. The spectra are very similar and confirm the composition of the box as polystyrene. The only notable difference between the spectra is the presence of a small band at 1740 cm^{-1} (indicated in figure 8.2) which corresponds to a C=O stretch. The presence of this band at a similar wavenumber to that seen for the artificially aged polystyrene substrates suggests that this is due to oxidation of the polymer.

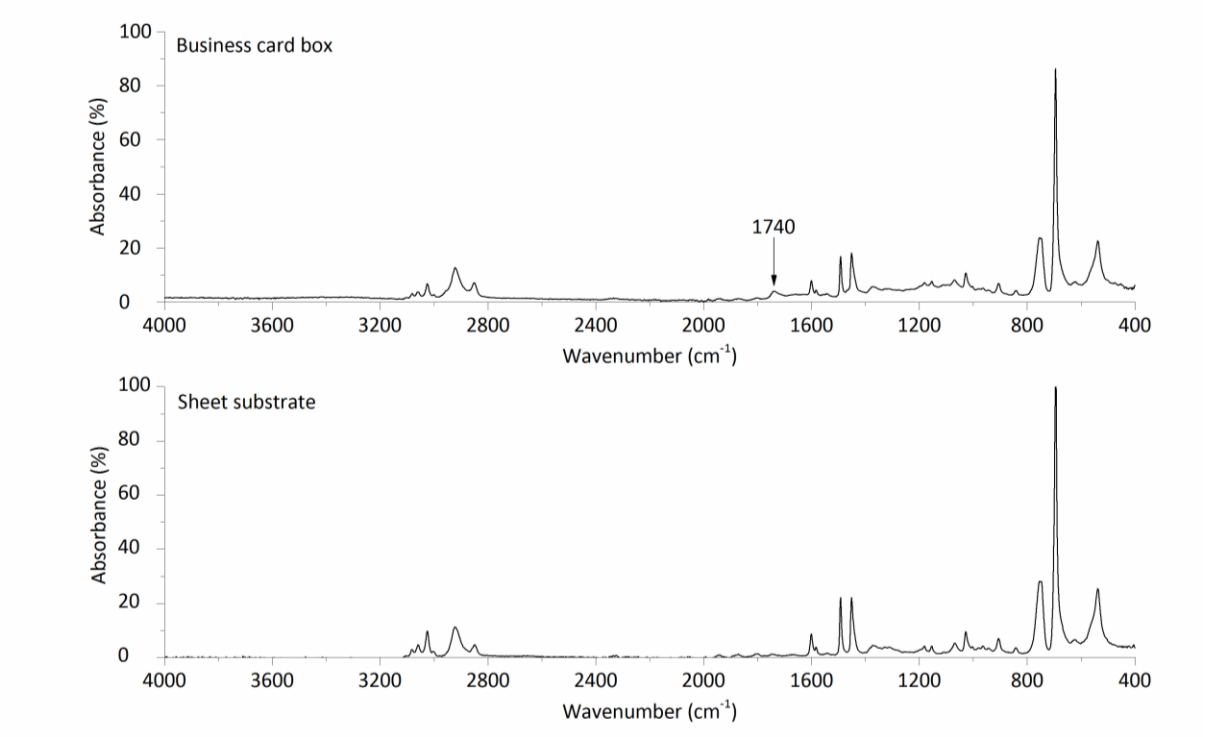

Figure 8.2 ATR-FTIR spectra of the business card box and the polystyrene sheet substrate.

8.3.2 DSC

The DSC plot for the box is shown in figure 8.3 and compared to the DSC plot for the sheet polystyrene substrate. The T_g of the card box was found to be 89.3 ± 0.5 °C, which is in agreement with the literature values for polystyrene [53]. However, this is significantly lower than the T_g of the sheet polystyrene (103.6 ± 0.5 °C) and indicates a possible difference in the molecular weight or a lowering of the T_g via the presence of additives.

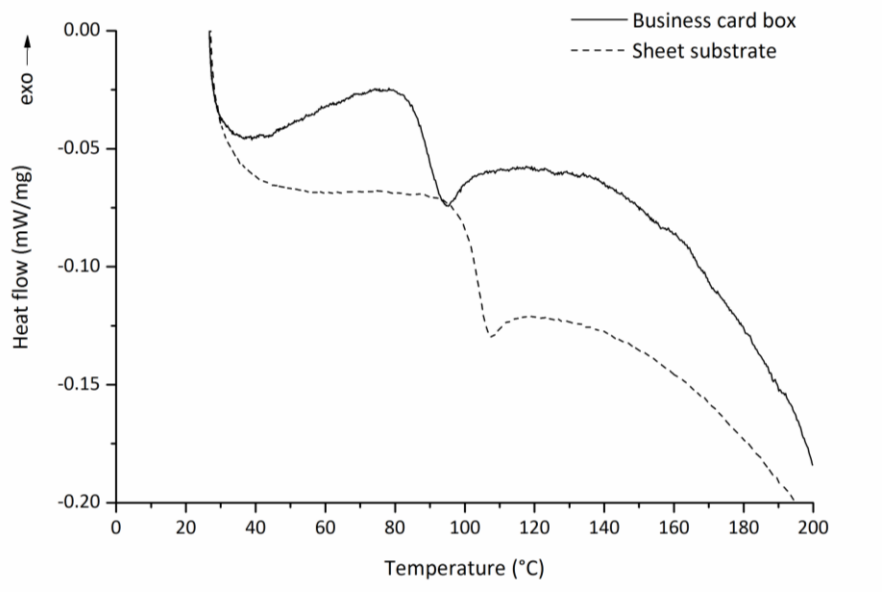

Figure 8.3 DSC plots for the business card box and the polystyrene sheet substrate.

8.3.3 GPC

Figure 8.4 shows the molecular weight distributions for the business card box and the polystyrene sheet substrate.

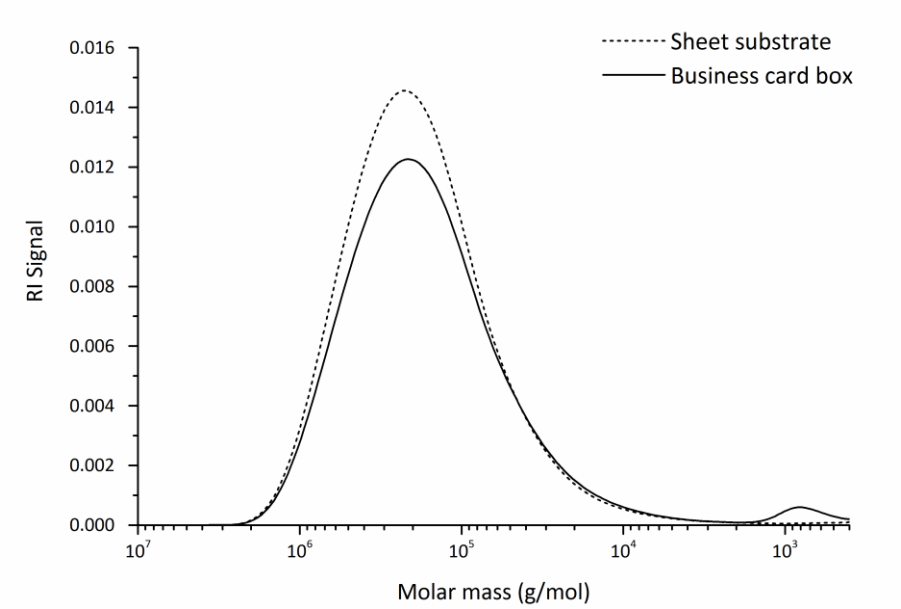

Figure 8.4 Molecular weight distributions of the business card box and the polystyrene sheet substrate.

The average molecular weights of the box were $\bar{M}_n$ = 1.68 ×10^3 g/mol and $\bar{M}_w$ = 2.48 ×10^5 g/mol compared to $\bar{M}_n$ = 1.88×10^3 g/mol and $\bar{M}_w$ = 2.63×10^5 g/mol for the sheet polystyrene. These values are slightly lower for the polystyrene box, which may be due to the composition of the plastic or some degradation. The molecular weight distribution of the box shows an additional peak around a mass of 828 ± 30 g/mol indicating the presence of some molecules of lower molecular weight. Given the age of the box, this may be due to scission of the polymer or the presence of additives.

8.3.4 Hardness

Micro-hardness values were captured at random locations on the substrate surface. The mean hardness value was found to be 20.5 VHN with a standard deviation of 0.6 VHN compared to 18.4 VHN with a standard deviation of 0.3 VHN for the sheet polystyrene substrate. The greater hardness of the box substrate may be a result of the initial composition or the age of the box.

8.4 Surface characterisation

8.4.1 Physical changes

8.4.1.1 Initial condition

An indication of the initial condition of the box is given by the optical and interferometry micrographs shown in figure 8.5. It can be seen that there are a notable number of scratches, lines and defects that are typical of the entire surface. These scratches can extend into the bulk of the material as seen in the interferometry micrograph. There is significant variation in both the depth and width of scratches on the surface, but the larger scratches are of the order of 50 μm in width and 5 μm in depth.

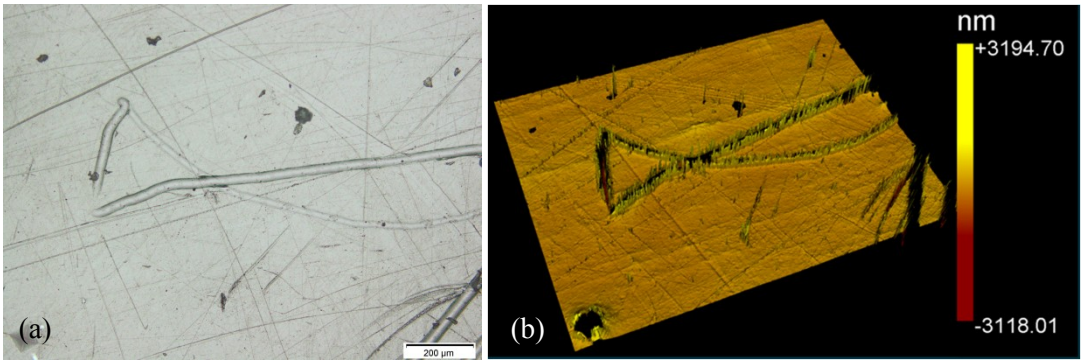

Figure 8.5 a) Optical micrograph (scale bar = 200 μm) and b) 3D interferometry micrograph of the box substrate.

Additional information regarding the topography of the plastic surface was obtained using SEM and AFM. Micrographs of the surface are shown in figure 8.6. Again, the roughness of the surface is significantly greater than that of the sheet polystyrene and is indicative of the object's prior history. Figure 8.6b shows the AFM micrograph for a section of the surface which is relatively undamaged and which has a peak-to-valley height of approximately 0.3 μm.

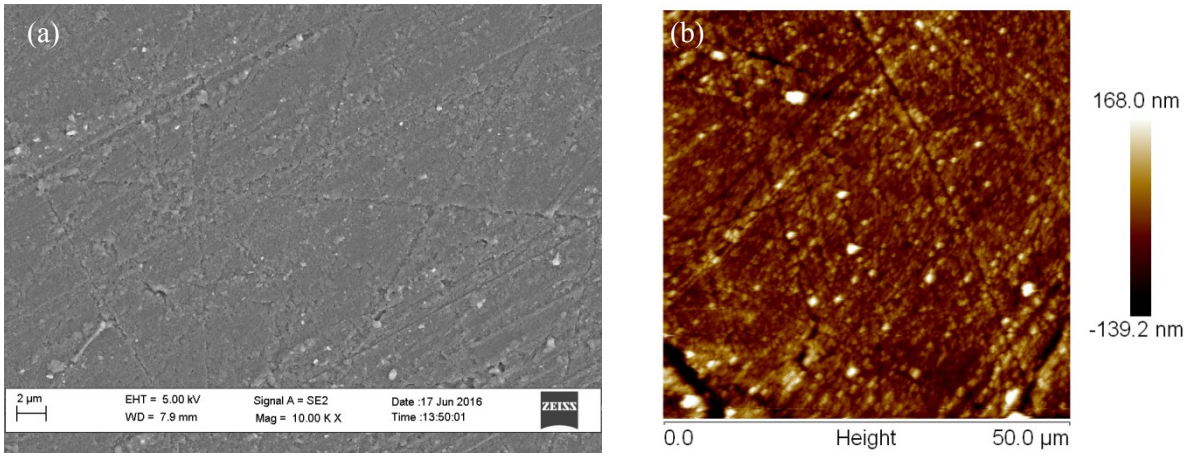

Figure 8.6 a) SEM and b) AFM micrographs of the uncleaned box substrate.

8.4.1.2 Cleaning

Given the surface changes observed for the sheet polystyrene substrate, white light interferometry was performed using a 10 µm bipolar scan to examine the surface for changes due to cleaning. Figure 8.7 shows interferometry micrographs for sections of the box substrate before and after cleaning with the agent indicated. The micrographs captured before cleaning illustrate the type and range of damage present on the surface.

Comparison of the same areas before and after cleaning reveals the removal of some particulate matter from the surface. However, the micrographs do not show any notable damage as a result of the application of cleaning agents with the exception of acetone. Similarly to the polystyrene sheet substrates, the application of acetone results in dissolution of the plastic.

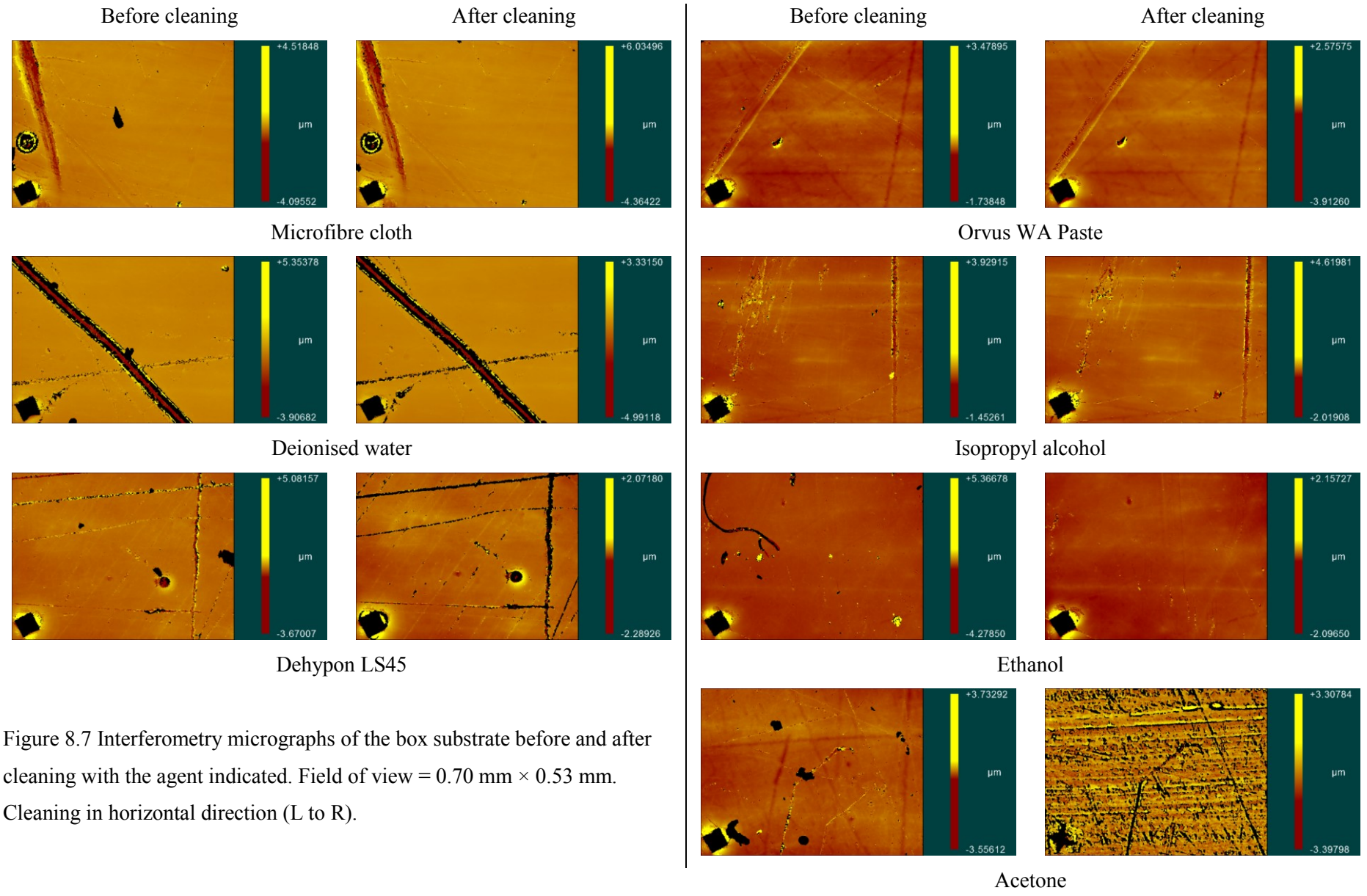

Figure 8.7 Interferometry micrographs of the box substrate before and after cleaning with the agent indicated. Field of view = 0.70 mm × 0.53 mm. Cleaning in horizontal direction (L to R).

SEM micrographs were captured to examine the surface at high magnification. While the dissolution of the surface can be seen for the substrate cleaned with acetone (figure 8.8), damage due to cleaning is not immediately apparent for the other cleaning agents. This is illustrated in figure 8.8b by the SEM micrograph of the surface cleaned with the microfibre cloth. While there are scratches in the cleaning direction, it is difficult to distinguish these from the existing surface damage. This suggests that the scratches are too shallow to be identified and may not be visible if the roughness of the surface exceeds or is comparable to the scratch depth.

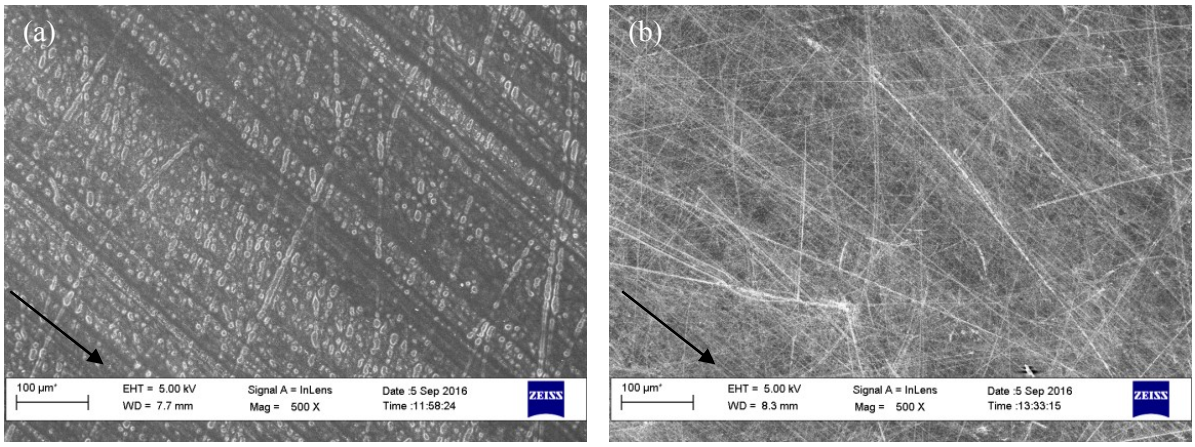

Figure 8.8 SEM micrographs of the substrate cleaned with a) acetone and b) the dry microfibre cloth. The arrows indicate the cleaning direction.

8.4.2 Chemical changes

8.4.2.1 Initial condition

The positive polarity ToF-SIMS spectrum for the substrate is shown in figure 8.9. Note the change in scale for the y axis at higher masses. The lower mass region of the spectrum is dominated by fragments of the form ($C_nH_{2n\pm1}$) which are indicative of hydrocarbon contamination in the form of oils, as well as contamination from Na and K. The characteristic peak for polystyrene, at m/z = 91.05 ($C_7H_7^+$), is of relatively low intensity. Fragments at m/z = 73.05 ($C_3H_9Si^+$), 147.07 ($C_5H_{15}OSi_2^+$) and 207.03 ($C_5H_{15}O_3Si_3^+$) correspond to PDMS, which may have originated from numerous sources, including cosmetics and soaps. There are also other indications of contamination from handling. The spectrum shows peaks at m/z = 283.26 ($C_{18}H_{35}O_2^+$) attributed to stearic acid, m/z = 313.27 ($C_{19}H_{37}O_3^+$) attributed to monoacylglycerol, m/z = 430.38 ($C_{29}H_{50}O_2^+$), attributed to vitamin E, and m/z = 551.50 ($C_{35}H_{67}O_4^+$) attributed to diacylglycerol [185]. The ToF-SIMS spectrum in the negative polarity is shown in figure 8.10. This spectrum also shows the presence of fragments corresponding to SLS, most likely from soaps or other toiletries and the presence of a peak at m/z = 255.23 ($C_{16}H_{31}O_2^-$), attributed to palmitic acid.

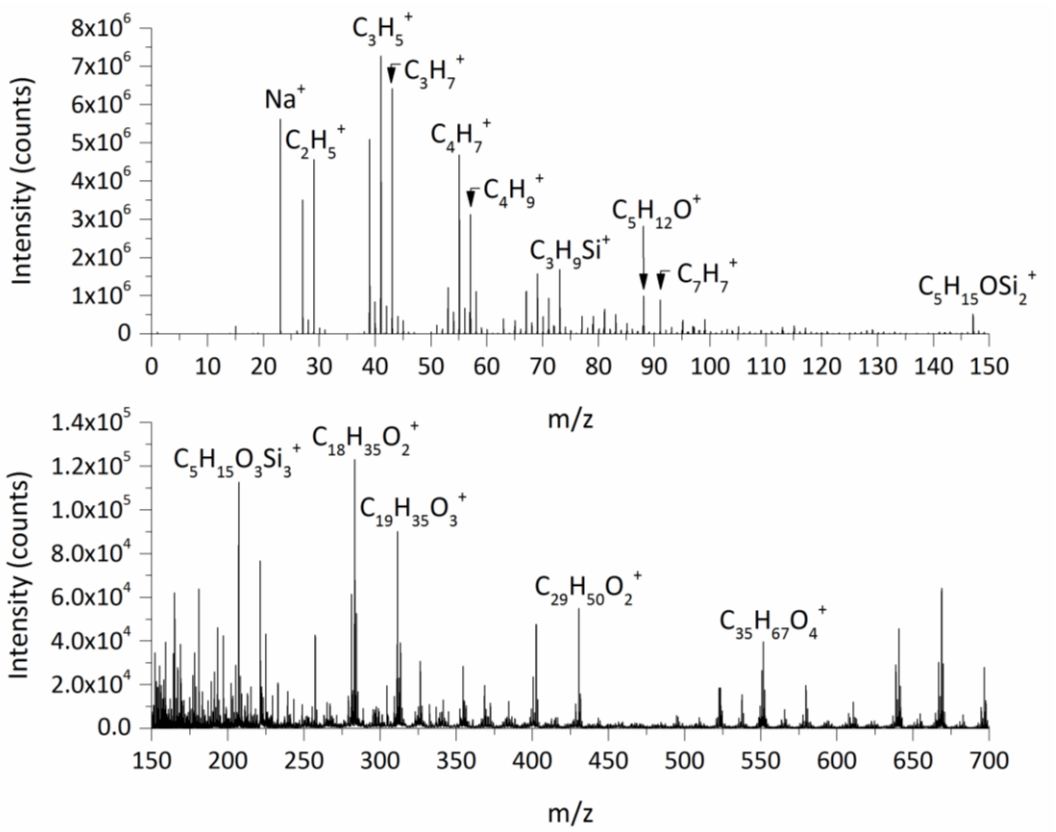

Figure 8.9 Positive polarity ToF-SIMS spectrum of the polystyrene box (m/z < 700).

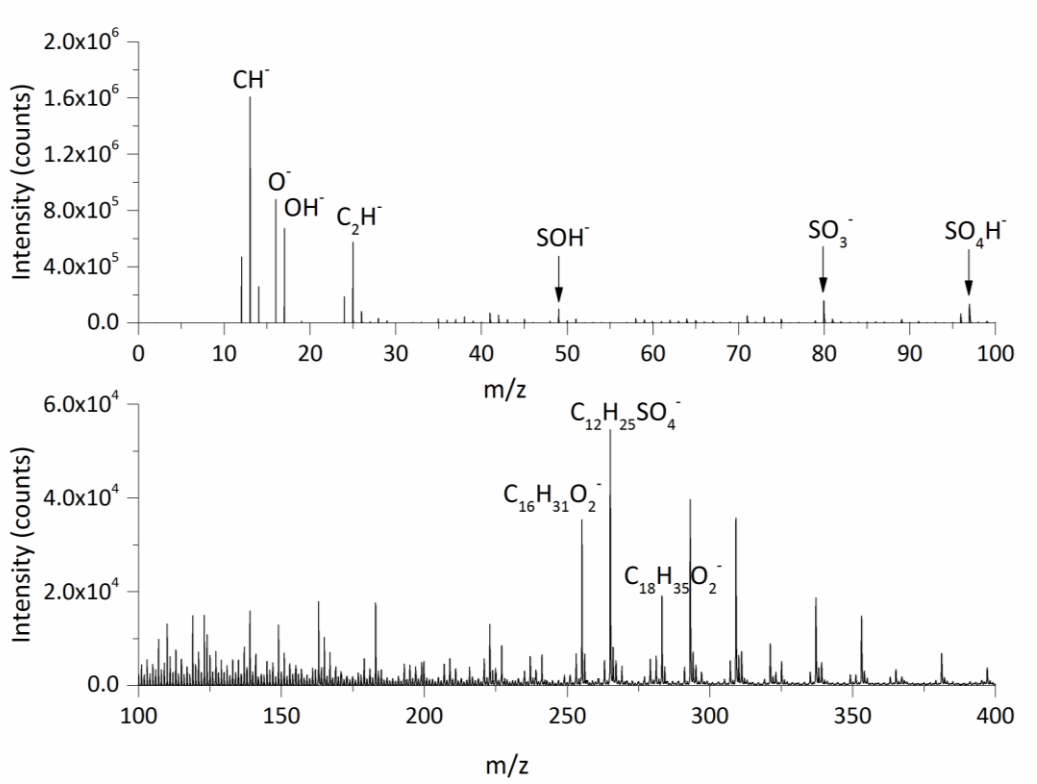

Figure 8.10 Negative polarity ToF-SIMS spectrum of the polystyrene box (m/z < 400).

The spatial location of these fragments was examined by obtaining SIMS maps for the substrate. Figure 8.11 shows a section of the box surface imaged using interferometry and the same section when analysed with ToF-SIMS. It can be seen that the K^+ fragment is uniformly distributed over the analysis area, indicating that contamination is present over the majority of the surface. The $C_7H_7^+$ fragment corresponding to polystyrene is noticeably greater in intensity from a number of randomly positioned lines, suggesting that scratching has revealed the bulk. However, fragments corresponding to PDMS, such as m/z = 147.07 ($C_5H_{15}OSi_2^+$), also display a greater intensity in these lines, indicating additional contamination in the scratches. There are also two raised areas on the interferometry image, whose location correspond to fragments at m/z = 313.27 ($C_{19}H_{37}O_3^+$) and 551.50 ($C_{35}H_{67}O_4^+$), attributed to monoacylglycerol and diacylglycerol respectively and which may have originated from foodstuffs or cosmetics, among other possibilities.

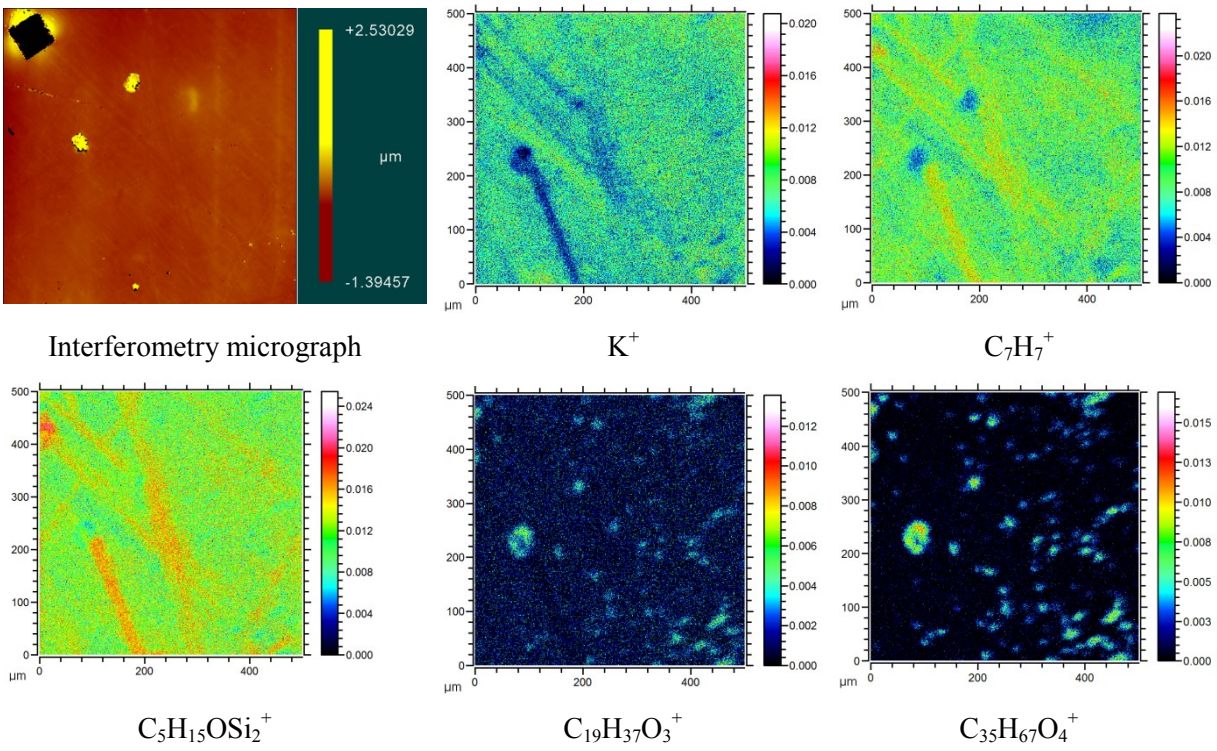

Figure 8.11 Interferometry micrograph of the substrate and SIMS maps of the same area showing the normalised intensity for the positive ions and fragments indicated.

Depth profiles of the substrate were obtained to gain more information about the surface region and are shown in figure 8.12. It is interesting to note the presence of the NH_4^+ fragment, which is present here to a depth of around 0.6 µm. A similar depth profile for NH_4^+ was obtained for the substrate cleaned with isopropyl alcohol, suggesting that this fragment is not due to surface contamination. It is suggested that the NH_4^+ fragment is a result of ageing, as this fragment was previously detected for the artificially aged substrates. The fragments corresponding to SLS contamination are also present to a depth of around 0.6 µm. It is suggested that this is related to the roughness of the surface as well as the presence of scratches and other defects which could trap contamination.

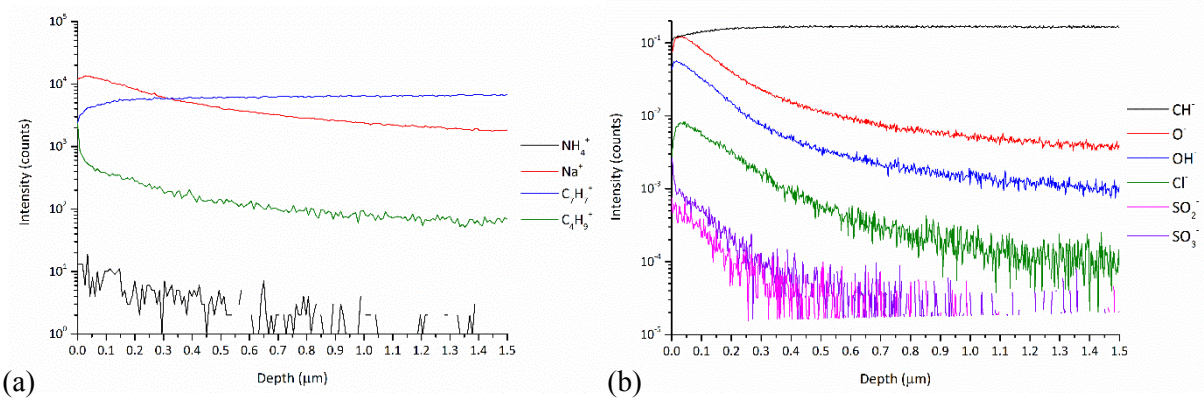

Figure 8.12 a) Positive polarity and b) negative polarity ToF-SIMS depth profiles of the uncleaned box substrate.

8.4.2.2 Cleaning

Figure 8.13 shows the PCA scores and loadings plots for the positive polarity ToF-SIMS spectra for the solvent-cleaned samples. It can be seen that the main difference between the uncleaned and the cleaned samples lies in the first principal component. The characteristic fragments of polystyrene are present in the positive PC1 values and indicate the effectiveness of cleaning on the plastic surface. The negative PC1 values provide information regarding the type of contamination which has been removed: the fragments previously described as being due to handling and those corresponding to PDMS are more representative of the uncleaned surface. The negative polarity PCA data provides little additional information about the surface after cleaning.

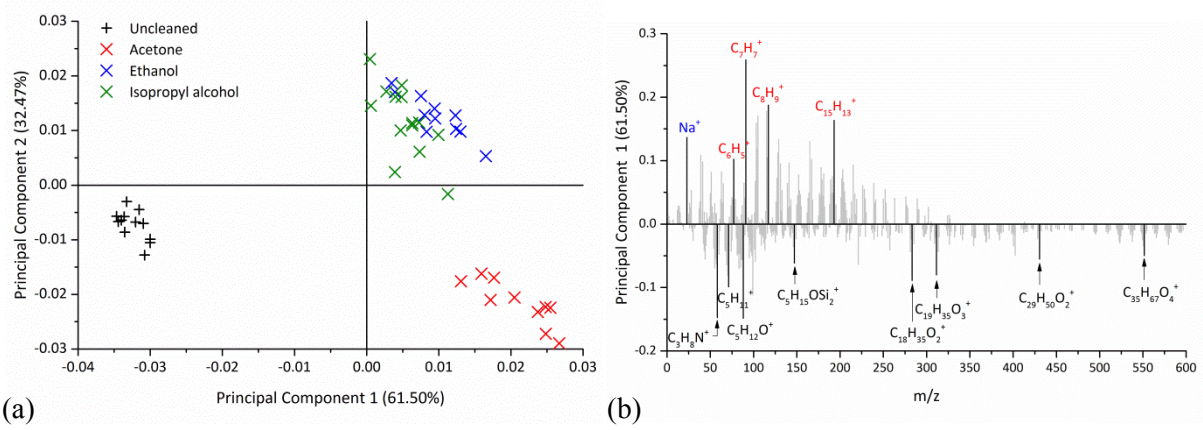

Figure 8.13 PCA a) scores and b) loadings plots for the positive polarity ToF-SIMS spectra from the substrates cleaned with the organic solvents.

Figure 8.14 shows the PCA scores and loadings biplots for the positive polarity ToF-SIMS spectra from the substrates cleaned with the aqueous agents and the dry microfibre cloth. The uncleaned substrate and the substrate cleaned with the dry microfibre cloth show the presence of fragments corresponding to the initial contamination present on the surface. Residual surfactant is indicated by the fragments at m/z = ($C_3H_7O^+$) and ($C_4H_9O^+$) for the substrates cleaned with the non-ionic

surfactant. The substrates cleaned with the anionic surfactant and deionised water are contaminated with PDMS. It is possible that this contamination does not arise from the cleaning procedure but is due to PDMS already on the surface.

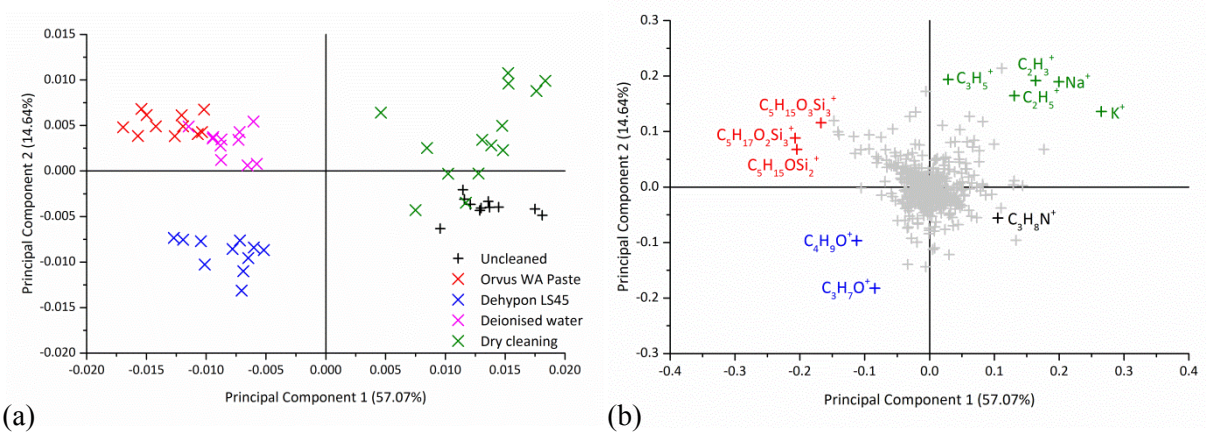

Figure 8.14 PCA biplots showing a) scores and b) loadings for the positive polarity ToF-SIMS spectra from the substrates cleaned with the aqueous agents and the dry microfibre cloth.

Further information about the behaviour of the surfactants is given by the PCA plots in figure 8.15, which compare the surfactant-cleaned surfaces to the uncleaned surface. The positive PC1 loadings reveal that the PDMS contamination can be detected on the substrate cleaned with the anionic surfactant, however the presence of the $C_7H_7^+$ peak for this substrate indicates that cleaning has been effective. The substrate cleaned with the non-ionic surfactant is characterised by fragments corresponding to residual surfactant. Inspection of the negative PC1 values provides information as to the type of soiling that has been removed, and includes fragments at m/z = 58.06 ($C_3H_8N^+$), 87.96 ($NaKCN^+$) and 196.87 ($Na_4Cl_3^+$) [185], as well as those fragments previously described as being due to handling.

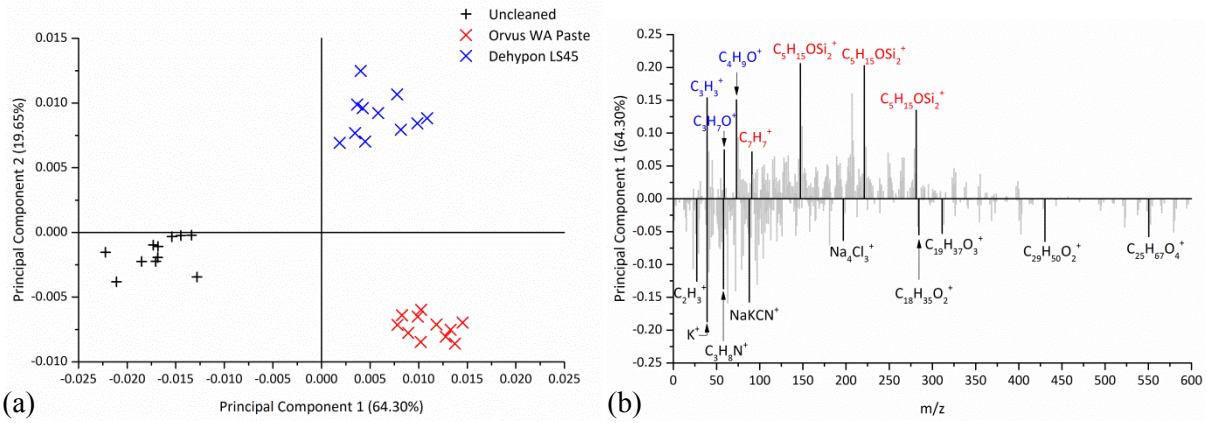

Figure 8.15 PCA a) scores and b) loadings plots for the positive polarity ToF-SIMS spectra from the substrates cleaned with the surfactants.

The PCA scores and loadings biplots for the negative polarity ToF-SIMS spectra from the aqueous cleaning agents are shown in figure 8.16 and provide further information about differences between these cleaning procedures. The difference between the substrate cleaned with deionised water and that cleaned with the anionic surfactant is notable. In this case it is the substrate cleaned with deionised water that is most characterised by fragments corresponding to SLS and indicates both its original presence on the surface and the ineffectiveness of deionised water in its removal. The PCA data also reveals that the substrate cleaned with the anionic surfactant is contaminated with PDMS while fragments corresponding to the polystyrene substrate are most characteristic of the substrate cleaned with the non-ionic surfactant.

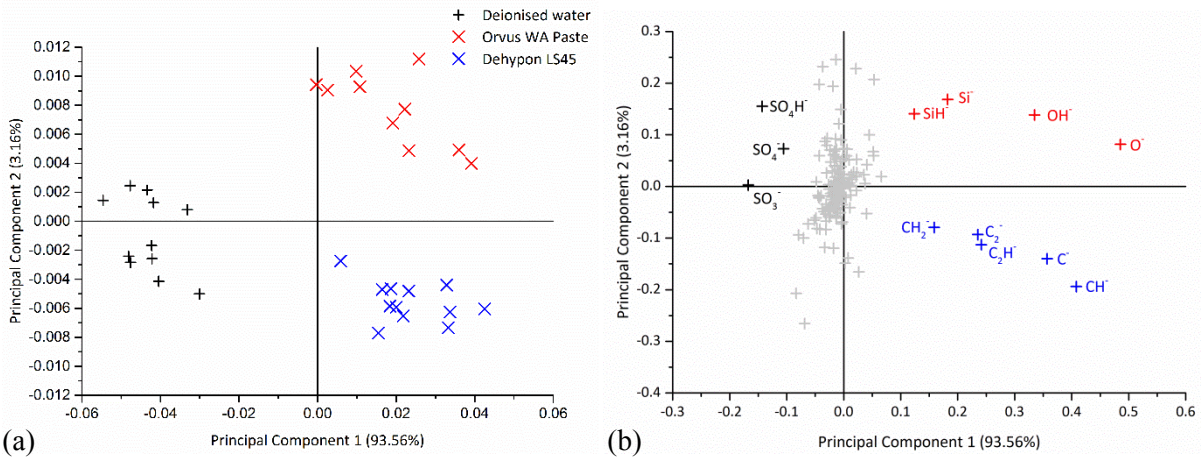

Figure 8.16 PCA biplots showing a) scores and b) loadings for the negative polarity ToF-SIMS spectra from the substrates cleaned with the aqueous agents.

8.5 Discussion

The findings from this chapter are summarised in table 8.1

Table 8.1 Summary of findings from the business card box.

	Business card box
Initial condition	Extensive scratching and physical defects on surface. Significant surface contamination thought to result from handling.
ATR-FTIR	Presence of band corresponding to oxidation.
T_g (°C)	89.3 ± 0.5
$\bar{M}_n$ (g/mol)	1.68×10^3
$\bar{M}_w$ (g/mol)	2.48×10^5
Micro-hardness (VHN)	20.5 ± 0.6
Cleaning with organic solvents	Dissolution of surface observed with acetone. Physical damage due to cleaning for alcohols not distinguishable from pre-existing surface damage. Removal of original contamination from surface. Contamination from cleaning detected.
Cleaning with aqueous agents	Physical damage due to cleaning not distinguishable from pre-existing surface damage. Removal of original contamination from surface. Surfactant residue detected for the non-ionic surfactant. Contamination from cleaning detected.

8.5.1 Bulk characterisation

Initial bulk characterisation of the polystyrene substrate revealed notable differences with the commercial sheet substrate. ATR-FTIR spectroscopy confirmed the composition of the box as polystyrene. However, comparison with the commercial sheet substrate revealed an additional band at 1740 cm^{-1} corresponding to a C=O stretch, which indicated possible oxidation of the polymer. Given that the box was over 10 years old, this would not be unreasonable. While the T_g of the substrate was significantly lower than that of the sheet substrate, it was in agreement with literature values. This difference in the T_g does not appear to be due to a difference in the molecular weight as the values for $\bar{M}_n$ and $\bar{M}_w$ were in agreement with those obtained for the sheet substrate. Another possible explanation for the lower T_g is the presence of additives, such as the colorant, or plasticisers in the polystyrene box. The hardness of the substrate was greater than that measured for the sheet substrate

and may be due to the composition of the box. However, it is also possible that the increased hardness is due to ageing, as was seen in the previous chapter.

8.5.2 Initial surface characterisation

Initial inspection of the box revealed it to be in good condition, with no obvious cracks, breakages or abrasions. However, a number of scratches were visible when viewed with the naked eye and closer inspection with microscopy and interferometry revealed the presence of numerous scratches, indentations and contaminants on the surface. These can measure tens of microns in width with a peak-to-valley height of around 5 μm and are therefore significantly greater than the limit of 6 μm width for optical imperfections described in ISO 14997:2011 [153]. The roughness of the surface is also an indication of the object's history; in areas that were not significantly scratched the peak-to-valley height was of the order of 0.3 μm.

Analysis of the chemical composition of the surface prior to cleaning revealed a number of points of interest. The ToF-SIMS spectrum was dominated by hydrocarbon fragments of the form $C_nH_{2n\pm1}$, which indicated the presence of oils on the substrate and most likely resulted from skin contact. There were also other indications of handling, such as the presence of fragments attributed to fatty acids and vitamin E. Other contamination on the surface included PDMS and SLS which could both be a result of contact with soaps or cosmetics, among other possibilities.

Inspection of the ToF-SIMS images for the substrate indicated the spatial distribution of contamination on the surface. While some contamination was uniformly distributed over the surface, localised contamination was also observed in the form of raised areas on the surface, which was indicative of contamination from handling. Interestingly, the scratches present on the surface were most clearly defined by fragments corresponding to polystyrene. However, fragments corresponding to PDMS were also present in these scratches. This indicates that either the PDMS contamination occurred at the same time that the scratches were made or afterwards. PDMS is a very mobile lubricant and can spread over a surface over time [186]; it is therefore possible that contamination migrated to the scratches at some point after their formation. The absence of contamination from other sources in the scratched areas indicates that not all contamination was necessarily preferentially collecting in the scratches. This may be due to the narrow width of the scratches and it is also possible that the raised edges of the scratches provide some protection.

Depth profiles of the substrate provided further information about the surface region. Of most interest was the presence of the NH_4^+ fragment, which was present to a depth of around 0.6 μm. This would suggest a similar ageing behaviour to that detected for the artificially aged substrates. Depth profiles also gave information regarding the presence of sodium, chlorine and hydrocarbon contamination, as well as SLS, which was present on the surface as a layer approximately 0.6 μm in thickness.

However, the measured depths of these layers may be affected by both mixing effects and the roughness of the substrate surface.

One of most notable features of the uncleaned surface was the absence of particulate matter. This may be explained by the fact that the object was not on display prior to analysis and had also been handled regularly meaning that dust was not able to accumulate on the surface. Therefore, examination of the cleaning behaviour was of interest due to the potential for the agents to remove contamination resulting from handling rather than exposure to atmospheric dust. The age of the substrate also provided an opportunity to evaluate its cleaning behaviour.

8.5.3 Cleaning behaviour

The physical damage imparted to the polystyrene sheet substrate by cleaning was not observed on the box substrate when viewed using interferometry. However, given the extensive damage already present on the surface, the surface roughness is an order of magnitude greater than the depth of the scratches observed on the sheet substrate (around 20 nm), and therefore it is likely that shallow scratches could not be easily resolved. SEM micrographs of the cleaned substrates were also inconclusive as scratches in the direction of cleaning could not be easily distinguished from other surface damage. The one exception to this was that the application of acetone to the polystyrene surface caused severe damage in agreement with that observed for the sheet substrate. This suggests that despite the evidence of some oxidation, the cleaning behaviour of the box substrate is more in agreement with the unaged polystyrene sheet substrate than the artificially aged substrate. The hardness of the surface may also affect the scratching behaviour. The mean micro-hardness value for the polystyrene box was greater than for the sheet polystyrene substrate and was close to that measured for the sheet PMMA substrate. It is notable that the latter did not exhibit scratching in the absence of an artificial soil.

The contamination present on the surface prior to cleaning might be considered to have similarities with sebum soiling. Sebum is an oily substance present on the surface of the skin, which can easily be transferred to objects via touch. Artificial sebum soils have been designed to mimic natural sebum; a standard recipe is given in the American Society of Testing and Materials (ASTM) D4265-14 [187], which consists of ten components, including oils and fatty acids. A simplified recipe was used in the POPART study and consisted of a 20% concentration of palmitic acid dissolved in 1-propanol [31]. The cleaning behaviour of substrates soiled with this artificial sebum soil was studied; ethanol and isopropyl alcohol were both able to remove the soil from the PMMA and HIPS substrates. The most effective surfactant for both plastics was Dehypon LS45, followed by Orvus WA Paste. However, both surfactants were found to be unable to remove the artificial sebum soil entirely, and distilled water was found to be ineffective. However, there was no oil component to the POPART recipe, which could affect the removal of a sebum soil. The use of surfactants to remove sebum soil similar to

that described by ASTM D4265-14 has been studied by Cox et al. [188]. The removal process of solid sebum soil from a hard textile surface was found to be similar to that of other oily soils and was principally removed by a roll-up process facilitated by the penetration of surfactant into the soil.

In this work, cleaning of the substrate with solvents was found to be effective in reducing or removing the surface contamination due to handling. However, additional contamination from the cleaning process was also detected in the form of Na^+ and K^+ ions on the cleaned substrate, particularly those cleaned with ethanol and isopropyl alcohol. The PCA data from the substrates cleaned with the aqueous agents and dry cleaning revealed that contamination could be removed via the application of the aqueous cleaning agents, while the dry cleaning procedure was ineffective. Surfactant residue was also detected for the non-ionic surfactant, however all substrates cleaned with aqueous agents showed evidence of PDMS contamination, which may have been present prior to cleaning. Further inspection of the surfactant data indicates that both surfactants are able to reduce or remove existing contamination in the form of salts, fatty acids and other fragments from handling. Analysis of the PCA data for the negative polarity spectra revealed that residue from the anionic surfactant could not be distinguished from the SLS on the surface prior to cleaning.

Conclusions

The findings from this case study illustrate some of the difficulties associated with the analysis of a non-model substrate. Nevertheless, there are some valuable conclusions which can be drawn from this study. Significant physical damage and chemical contamination was present on the initial substrate. The extensive physical damage, in the form of scratching, pitting and other defects meant that, with the exception of acetone, any scratching imparted to the surface by the cleaning process was not easily distinguished from the pre-existing topography.

The wide range of contamination present on the substrate prior to cleaning illustrates the type of soiling that it might be desirable to remove, much of which appears to result from contact with human skin. The distribution of the contamination varies: while some contaminants are uniformly distributed over the surface, other fragments corresponding to lipids are present as discrete drops. It was also seen that that contamination from PDMS was preferentially present in existing scratches. In this case, the presence of multiple contaminants on the surface prior to cleaning complicated the analysis of the ToF-SIMS data. However, PCA analysis of the data indicated that the organic solvents were effective in removing contamination from handling, as was the use of surfactants. Similarities to the cleaning behaviour of the polystyrene sheet substrate could also be made. Surfactant residues were detected on the surface cleaned with the non-ionic surfactant though inspection of the substrates cleaned with anionic surfactant was inconclusive due to the existing SLS contamination on the surface.

One of the limitations of this work lies in the unknown nature of the surface prior to cleaning. Analysis of the data has assumed that soiling was uniformly distributed over the surface, which was not always the case. However, by capturing multiple spectra from random locations for each sample, it is anticipated that the combined spectra are representative of the substrate in question. Further work on the artificial soiling of substrates with sebum soil would provide a valuable comparison to these findings.

Chapter 9

Conclusions and future work

In recent years there has been increasing interest in the stability of plastic artefacts in the museum environment. This has led to research activity on polymer degradation mechanisms, polymer identification and a number of case studies on different plastic artefacts. To date, the most extensive work on the conservation of plastic artefacts was performed as part of the collaborative POPART project [31].

The preventive and interventive conservation of polymer materials is critical to retard or prevent degradation. As an interventive treatment commonly employed to improve the stability of the surface, cleaning also has the potential to introduce undesirable changes to the plastic surface. While studies such as POPART have examined the effect of cleaning on multiple plastics, previous work has been performed using low magnification and macroscopic techniques.

This work was performed with the aim of providing insight into the physical and chemical changes occurring to the surface of two plastics, PMMA and polystyrene, as a result of the application of conventional cleaning treatments. The originality of this work lies in the use of sensitive surface analysis techniques combined with chemometric techniques to evaluate the microscopic changes occurring to the surface. A number of results have been identified that could have implications for the care of plastic artefacts in the future.

9.1 Conclusions

One of the important questions addressed in this work regarded the effect of cleaning agents on new, virgin plastic substrates, which were unaffected by any variables such as soiling or degradation. The work on these samples is described in Chapter 5. Initial characterisation of the PMMA substrate revealed localised raised areas on the surface which were not evident to the naked eye. These areas were attributed to residue from the protective film which was removed from the surface prior to analysis. While this residue could be removed with organic solvents, the application of aqueous

agents was ineffective. This emphasises the fact that the condition of the surface prior to cleaning may not be immediately apparent and that there may be localised variations in the surface composition which can affect both the soiling behaviour and the choice of cleaning agent to remove them.

The application of cleaning treatments was shown to cause damage to a clean, virgin plastic surface, as seen in the case of polystyrene. Cleaning with acetone resulted in the dissolution of the plastic surface but scratching was observed to occur following the application of all cleaning treatments. Scratches were typically of the order of 1 μm in width with a peak-to-valley height of approximately 20 nm. The hardness of the substrate was thought to play a role in the formation of scratches as no scratching was observed for the PMMA substrate. While POPART indicated that the use of aqueous agents had a lubricating effect on the plastic surface, it was difficult to draw this conclusion from the findings in this work due to the potential variations in the cleaning methodology as well as local variations in scratching on the substrates.

PCA analysis of the ToF-SIMS spectra revealed that surfactant residues were present on the surfaces of both plastic substrates. Depth profiles of the polystyrene substrate cleaned with the anionic surfactant revealed that these residues can form a layer approximately 20 nm in thickness on the surface of the plastic. However, mixing of the surface layers may result from primary ion impact and it is possible that this layer is thinner than indicated by the depth profiles. Repeated rinsing of the polystyrene substrate with deionised water was ineffective in removing the residue entirely. However, PCA treatment of the data indicated that substrates that had undergone repeated rinsing were characterised by a decrease in fragments corresponding to the anionic surfactant and a corresponding increase in those attributed to PDMS contamination. The potential for contamination from the cleaning process was also apparent for other cleaned substrates. This was thought to result from the cleaning agent or the microfibre cloth.

In reality, not all plastic artefacts are received in a pristine, unsoiled condition. Indeed, many have a prior history before acquisition, which may affect their future degradation behaviour and response to cleaning treatments. Furthermore, artefacts are likely to become naturally soiled via the deposition of dust during display and storage. Chapter 6 details the effect of cleaning substrates soiled with an artificial oily carbonaceous soil, chosen to simulate the type of soiling that might originate from airborne pollution. The effect of applying cleaning treatments to these soiled substrates resulted in some marked differences to the virgin substrates.

Physical damage in the form of scratching was observed for both plastic substrates when soiled. Scratching was observed for all cleaning agents and the dry microfibre cloth. The scratches formed on the soiled polystyrene substrate were noticeably different to those observed for the virgin substrate. The non-uniform width and depth of these scratches was attributed to the mechanical movement of soil particulates over the plastic surface. This was supported by SEM-EDX analysis of particulates in

the vicinity of the scratches, which revealed that their composition was consistent with carbon black. Inspection of the cleaned soiled substrates revealed that the organic solvents were most effective in removing the soil. Residual soil was clearly visible at low magnification for the substrates cleaned with the aqueous cleaning agents and the dry microfibre cloth. However, PCA treatment of the ToF-SIMS data from the soiled substrates indicated the presence of hydrocarbon fragments on all cleaned soiled substrates, which was attributed to soil residue.

One of the concerns surrounding any interventive treatment is that its effects may only be seen or detected at some point in the future and this is addressed in Chapter 7. Accelerated ageing is a technique that is commonly used in conservation to assess an object's or material's stability at timescales which are shorter than natural ageing processes. Accelerated light ageing of the plastic substrates revealed a number of points of interest, particularly for the polystyrene substrate, although it should be noted that the radiation included both an ultraviolet and infra-red component in addition to the visible region.

The bulk characterisation of both aged plastic substrates revealed changes in their T_g values. The PMMA substrate showed an increase in the T_g while a decrease in the T_g was detected for the polystyrene substrate. The micro-hardness values were found to increase for both plastic substrates, although the increase was greater for the polystyrene substrate. The use of GPC revealed that both polymers displayed a shift in their peak molecular weight to a lower molar mass, indicating chain scission, however a small peak at a higher molar mass was also observed and attributed to cross-linking. ATR-FTIR analysis of the plastics did not reveal any notable changes for PMMA over the course of 8 weeks accelerated light ageing. Analysis of the polystyrene substrates showed the development of two bands corresponding to oxidation as well as a broad peak corresponding to hydrogen bonding.

While the polystyrene substrates visibly yellowed with ageing, no discernible changes were observed for the PMMA substrate. However, spectrophotometry measurements revealed an increase in the yellowness index after 8 weeks ageing and a slight colour change as represented by ΔE_{00}. In the case of the polystyrene substrate, both the yellowness index and the ΔE_{00} values increased significantly over the 8 week ageing period. Changes in the transmission spectra were also evident and after 2 weeks ageing, the polystyrene substrate was absorbing radiation in the visible region. This could have an effect on the future stability of the plastic.

The chemical composition of the surface of both plastics changed after 8 weeks ageing, as indicated by the appearance of peaks in the ToF-SIMS spectra that corresponded to fragments containing nitrogen. These was thought to originate from one of two sources: the migration of additives from the bulk or from nitrogen in the surrounding atmosphere. However, it was not possible to determine

which mechanism was responsible. SEM and AFM examination of the aged polystyrene substrate revealed the presence of small formations on the surface after 8 weeks accelerated light ageing. The AFM micrographs suggested that these originated from the bulk of the plastic and that their adhesive properties were different to those of the polystyrene surface. However, examination of the surface using ToF-SIMS did not reveal any localised changes in chemistry that would correspond to the formations.

Heat ageing of the plastic substrates did not reveal the presence of nitrogen fragments or formations on the surface of the polystyrene substrate, indicating that these changes were due to exposure to light or UV radiation. However, PCA analysis of the heat-aged polystyrene substrates did reveal different fragments were characteristic of the heat-aged substrates when compared to the unaged polystyrene substrate. As the heat-aged substrates were characterised more by cyclic fragments this was thought to be a result of thermal degradation.

Further surface changes were observed for the substrates after ageing. Dust deposition was visible on both plastic substrates over the course of the 8 week ageing period; however, the extent of dust deposition was greater for the polystyrene substrate. This is explained by a change in the surface energy of the substrate due to oxidation. There may also be an electrostatic component as a result of loss of moisture content. The dust particulates were observed to sink into the substrate over the ageing period; however, this is not thought to be a phenomenon that would be seen in natural ageing. Instead it is thought to be a result of localised absorption of infra-red radiation by the dust particulates which results in a local increase in temperature and softening of the plastic.

In addition, some of the polystyrene substrates that had been cleaned before ageing showed the appearance of lines across the surface after 4 weeks accelerated light ageing. These were not visible immediately after cleaning and became less defined as ageing progressed to 8 weeks. It was thought that these lines developed due to localised areas of weakness which widened as the plastic experienced loss of moisture and shrinkage. In addition, inspection of the SEM images revealed that some of the formations created lines on the surface. It is suggested that in this case the formations had preferentially formed in a weakened area.

Cleaning of the aged polystyrene substrate was also performed and showed some notable differences to the unaged substrates. This was principally seen in the physical changes that occurred after the application of acetone and both surfactants as cleaning agents. In contrast to the behaviour of the unaged substrate, acetone did not dissolve the aged substrates. This was attributed to an increase in hydrogen bonding between polymer chains. Furthermore, the organic solvents were effective in reducing or removing the formations from the surface. Additionally, severe scratching was observed after cleaning the aged substrates with both surfactants, which was not seen for the unaged substrates. The application of the surfactants to the aged substrates also resulted in the smearing of the

formations over the surface. The inability of all cleaning agents to remove sunken particles from the substrate illustrated potential issues with the removal of dirt and soiling from crevices or depressions in the plastic surface.

The final part of the work investigated the cleaning of a polystyrene business card box and is described in Chapter 8. This provided a valuable opportunity to assess the cleaning behaviour of a real-world object. Initial examination of the box revealed that the surface was significantly scratched and pitted. In addition, analysis of the surface chemistry revealed contamination from handling, with fragments corresponding to hydrocarbon contamination, fatty acids, vitamin E and salts among others. In this respect the soiling present on the substrate differed from the artificial soil in Chapter 6 and bore more similarities with an artificial sebum soil designed to mimic fingerprints.

Bulk characterisation of the box substrate also revealed differences with the sheet polystyrene substrate. The T_g of the box substrate was significantly lower than that of sheet polystyrene, which may indicate the presence of additives. However, the micro-hardness of the box substrate was greater than that of the sheet substrate. Examination of the ATR-FTIR spectra revealed a small peak corresponding to a C=O stretch which was indicative of some oxidation and which may partially explain the increased hardness. There were also indications that nitrogen fragments were present in the surface region of the cleaned box substrate, indicating a possible agreement with the data from the aged polystyrene substrate.

Despite the evidence of oxidation, the cleaning behaviour of the box substrate most closely correlated to that of the unaged sheet polystyrene in that severe damage was observed following the application of acetone. The fact that any scratching from the cleaning treatments could not be distinguished from scratching already present on the surface prior to cleaning illustrated the difficulties in assessing the changes caused to real-world objects. It also indicated that while scratching might be detrimental to a glossy or reflective substrate, it is less likely to affect the aesthetic qualities of an object in a less pristine condition and therefore acceptable changes to the surface may be dependent on the initial condition of the object.

Analysis of the surface chemistry revealed that the cleaning agents were effective in removing much of the surface contamination from handling. In agreement with the findings from the sheet plastic substrates, residue from the non-ionic surfactant was detected. However, the presence of SLS on the substrate prior to cleaning meant that it was not possible to determine the presence or extent of the anionic surfactant residue.

9.2 Implications for cleaning protocols

This work has a number of potential implications for current cleaning protocols. One of the most visible findings was the potential for mechanical damage to occur with the use of microfibre cloths, even though these are commonly recommended and have previously been found to cause minimal damage to the surface [31]. Moreover, the use of dry microfibre cloths can be damaging to the surface. Scratching is more severe where there is significant soiling on the plastic surface, due to the abrasion of the soil particulates as they are dragged over the surface. It is anticipated however that any cleaning method that involves the mechanical movement of a cleaning tool over a substrate could potentially cause scratching.

The use of gels as cleaning agents is a current focus of study in the conservation sector, and is one of the areas addressed by the Nanorestart project [189]. One of the concerns around the use of these gels is their potential to leave residues on the surface. While it has been seen in this work that surfactants leave residues, these do not appear to affect the stability of the surface with ageing. Indeed, the findings from this work indicated that the aged substrates were less characterised by surfactant residues, although inspection of the raw SIMS data revealed that they were still present. It is the damage caused to the plastic substrate via mechanical action which appears to be more detrimental. However the findings from cleaning the aged polystyrene substrate indicate that all cleaning agents should be used with caution on aged materials due to their potentially detrimental effect when compared to unaged substrates.

One of the points raised by this work was the potential for contamination from the cleaning process. This was commonly seen in the presence of sodium and potassium on the substrates cleaned with alcohols. In addition PDMS contamination was detected for those substrates cleaned with surfactants or deionised water. These contaminants could originate from multiple sources, including the cleaning agent, the microfibre cloth or a result of the cloth coming into contact with nitrile gloves.

The accelerated ageing of the polystyrene substrates indicates that though damage might not be visible on the substrate immediately after cleaning, it can potentially create areas of weakness which become apparent with ageing. This was observed in the case of the polystyrene substrate cleaned with deionised water. The findings from the aged substrates also indicated that differences in dust redeposition could be dependent on the ageing behaviour of the object. This has implications for both storage and display as aged substrates may be more sensitive to the airborne particles in their local environment. Finally, the cleaning of aged substrates illustrated that appropriate cleaning protocols are dependent on the history and age of the object. This was most clearly seen in the different behaviour exhibited by the aged and unaged polystyrene substrates cleaned with acetone.

9.3 Future work

This work has revealed several areas which would warrant further investigation. One of the most detrimental findings from this work was the formation of scratches caused by the mechanical action of the cloth over the substrate. It was thought that this might be affected by the texture and weave of the cloth due to the particles being located close to the interface between the cloth and the substrate. Further investigation with cloths of a different texture and weave would therefore be of interest.

While the cleaning agents were chosen with reference to previous work, the findings indicate that it would be valuable to explore additional solvents. While the use of alcohols has been generally avoided in the cleaning of plastics the application of ethanol and isopropyl alcohol to the plastic substrates did not result in greater surface damage than that seen with the other cleaning methods. An aliphatic solvent such as hexane might be more effective in enabling the removal of oil residues, however, the solvent may cause damage to the substrate. It would also be worthwhile to examine different solvent-water mixtures to assess their cleaning effectiveness and effect on the plastic surface.

As previously mentioned, the photo-degradation and photo-oxidation of polystyrene principally occurs as a result of exposure to radiation in the ultraviolet part of the spectrum. Both ultraviolet and infra-red radiation were present within the spectrum of the irradiation used for accelerated ageing in this work. It would therefore be worthwhile to explore any changes occurring to the plastics investigated here as a result of exposure to light in the visible part of the spectrum only.

One of the interesting findings from the accelerated ageing work was the development of nitrogen fragments on the surface of both plastics. These fragments were thought to be either due to migration from the bulk of the material or from the surrounding atmosphere. While it was possible to profile the change in intensity with depth, it was not possible to distinguish whether this was due to movement in or out of the substrate. The accelerated ageing of samples in a ^{15}N rich atmosphere would provide a valuable method to determine which mechanism is responsible for the presence of these nitrogen fragments. The cleaning behaviour of the aged polystyrene substrates also illustrated the validity in examining cleaning treatments for substrates that have been aged to different extents. This would provide valuable information about the potential changing solubility and behaviour of plastic substrates over time.

Appendices

A Glossary

Additive	A material added to a plastic to obtain desired physical or chemical properties.
Amorphous	Not having an ordered or regular molecular structure.
Artefact	An object that is of cultural or historical importance.
Bloom	A whitish film on the plastic surface due to the migration of additives.
Chain scission	The cleavage of molecular bonds in polymer chains.
Chemometrics	The application of statistical techniques to the analysis of chemical data.
Cleaning	The act of reducing or removing soil, dirt or alien matter from a surface.
Clearing	The application of distilled or deionised water to remove cleaning agent residues.
Conservation	The act of preserving, protecting and restoring objects of cultural and historical value.
Interventive	Conserving an object via direct action.
Preventive	Controlling external conditions for an object's protection.
Crazing	The formation of fine cracks which are bridged by fibrils.
Cross-linking	The creation of new intermolecular bonds between polymer chains.
Crystalline	Having an ordered or regular molecular structure.
Degradation	A change, usually undesirable, in an object's chemical or physical properties.
Dynamic SIMS	Data acquisition of surface and subsurface chemical data via the sputtering and analysis of successive layers.
Fatty acid	A long chain hydrocarbon with a carboxyl end group.
Free volume	The volume in a polymer that is not occupied by polymer chains.
Functional group	A group of atoms in a molecule involved in characteristic chemical reactions.
Hardness	The resistance of a material to surface deformation.
Hydrolysis	The breaking of chemical bonds due to the presence of water.
Illuminance	Luminous flux per unit area.
Irradiance	Radiant flux per unit area.

Lipid	Organic compound that is insoluble in water.
Loadings	Weightings which relate the principal components to the original data.
Macromolecule	Long chain molecule comprised of many repeating monomer units.
Microfibre cloth	A cloth comprised of many narrow synthetic filaments woven together.
Oxidation	The interaction of oxygen molecules with other substances, resulting in the increased presence of oxygen.
Plastic	A material formed of a polymer and additives that impart desired physical or chemical properties.
Plasticiser	An additive that facilitates the movement of polymer chains relative to one another. Used to increase flexibility.
Polymer	A substance which is comprised of many macromolecular chains.
Scores	Values which describe a spectrum's position in principal component space.
Scratch	A surface defect typically consisting of a long trough usually but not always bounded along its length by a raised region.
Side group	Group of molecules extending from the backbone.
Soil	Particulate matter that has been deposited on a surface. Usually undesired.
Solubility parameter	Numerical value that may be used to predict whether two materials will be miscible.
Static limit	Ion dose below which SIMS analysis of a surface is deemed non-destructive. Static limit = 10^{12} ions/cm^2 for polymer materials.
Static SIMS	Data acquisition of a surface's chemical composition via the interaction of primary ions with surface atoms.
Surfactant	A compound that acts to reduce surface tension, commonly used to reduce the interfacial tension between water and oil.
Anionic	Containing a negatively charged head-group.
Non-ionic	Containing a polar, uncharged, head-group.
Tacticity	The positioning of a molecule's side groups relative to its backbone.
Atactic	Side groups are randomly positioned.
Isotactic	All side groups are on one side.
Syndiotactic	Side groups are positioned on alternate sides.
Teas chart	A visual representation of solubility parameters often used in conservation.
Thermolysis	The breaking of chemical bonds due to heat.
Thermoplastic	Plastic that can be remoulded with the application of heat.
Thermoset	Plastic that cross-links on curing and cannot be remoulded.
Weeping	The appearance of droplets on the plastic surface, usually a result of plasticiser migration.

B Symbols and constants

a	Acceleration
c	Speed of light in a vacuum $= 2.998 \times 10^8$ ms^{-1}
E	Energy
ΔE_{00}	Colour difference (according to CIEDE 2000)
h	Planck's constant $= 6.63 \times 10^{-34}$ m^{2}kgs^{-1}
H_v	Latent heat of vaporisation
m	Mass
m/Δm	Mass resolution
$\bar{M}_n$	Mean number molecular weight
$\bar{M}_w$	Mean weight molecular weight
R	Gas constant $= 8.31$ J K^{-1} mol^{-1}
Ra	Solubility distance
RED	Relative energy difference
RH	Relative humidity
Ro	Interaction radius
T	Temperature
T_g	Glass transition temperature
V_m	Molar volume
δ	Hildebrand solubility parameter
δ_D	Dispersion solubility parameter
δ_P	Dipolar solubility parameter
δ_H	Hydrogen bonding solubility parameter
λ	Wavelength
ν	Frequency
ω	Rotational speed

C Calculation of CIEDE Delta E

From BS ISO CIE 11664-6:2014 [113].

$$\Delta E_{00}^{*} = \sqrt{\left(\frac{\Delta L'}{k_L S_L}\right)^2 + \left(\frac{\Delta C'}{k_C S_C}\right)^2 + \left(\frac{\Delta H'}{k_H S_H}\right)^2 + R_T \frac{\Delta C'}{k_C S_C}\frac{\Delta H'}{k_H S_H}}$$

Where

$\Delta L' = L_2^* - L_1^*$

$\bar{L} = \frac{L_1^* + L_2^*}{2}$

$\bar{C} = \frac{C_1^* + C_2^*}{2}$

$a_n' = a_n^*\left(1 + \frac{1}{2}\left(1 - \sqrt{\frac{\bar{C}^7}{\bar{C}^7 + 25^7}}\right)\right)$ n=1,2

$\overline{C'} = \frac{C_1' + C_2'}{2}$

$\Delta C = C_2' - C_1'$

$C_1' = \sqrt{a_1'^2 + b_1^{*2}}$ $C_2' = \sqrt{a_2'^2 + b_2^{*2}}$

$h_1' = tan^{-1}(b_1^*, a_1')$

$\Delta h' = h_2' - h_1'$ if $|h_1' - h_2'| \leq 180°$

$\Delta h' = h_2' - h_1' + 360°$ if $|h_1' - h_2'| > 180°, h_2' \leq h_1'$

$\Delta h' = h_2' - h_1' - 360°$ if $|h_1' - h_2'| > 180°, h_2' > h_1'$

$\Delta H' = 2\sqrt{C_1' C_2'}\sin\frac{\Delta h'}{2}$

$\overline{H'} = (h_1' + h_2')/2$ if $|h_1' - h_2'| \leq 180°$

$\overline{H'} = (h_1' + h_2' + 360°)/2$ if $|h_1' - h_2'| > 180°, h_1' + h_2' < 360°$

$\overline{H'} = (h_1' + h_2' - 360°)/2$ if $|h_1' - h_2'| > 180°, h_1' + h_2' \geq 360°$

$$T = 1 - 0.17\,cos(\overline{H}' - 30°) + 0.24\,cos\left(2\overline{H'}\right) + 0.32\,cos\left(3\overline{H'} + 6°\right) - 0.20\,cos\left(4\overline{H'} - 63°\right)$$

$$S_L = 1 + \frac{0.015(\overline{L} - 50)^2}{\sqrt{20 + (\overline{L} - 50)^2}}$$

$$S_C = 1 + 0.045\overline{C}'$$

$$S_H = 1 + 0.015\overline{C}'T$$

$$R_T = -2\sqrt{\frac{\overline{C}'^7}{\overline{C}'^7 + 25^7}}\,sin\left[60°\,exp\left(-\left[\frac{\overline{H'} - 275°}{25°}\right]^2\right)\right]$$

D ToF-SIMS spectra of surfactants

The following figures show the ToF-SIMS spectra of surfactant residues on aluminium foil.

i) Orvus WA Paste, negative polarity (m/z ≤ 300)

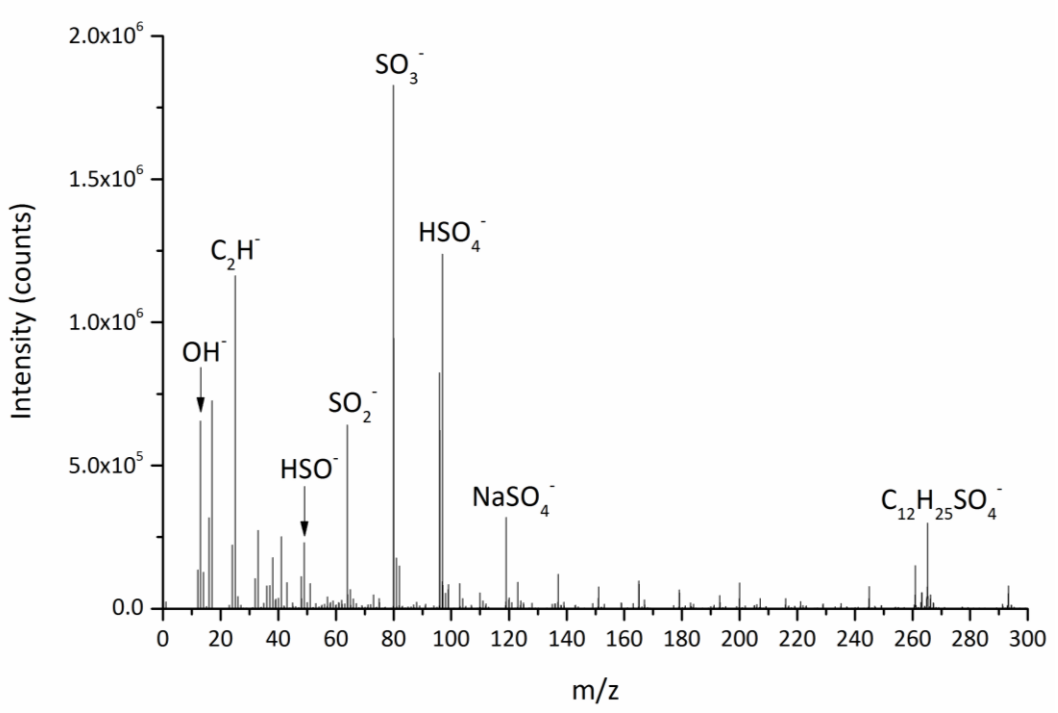

ii) Orvus WA Paste, positive polarity (m/z ≤ 200)

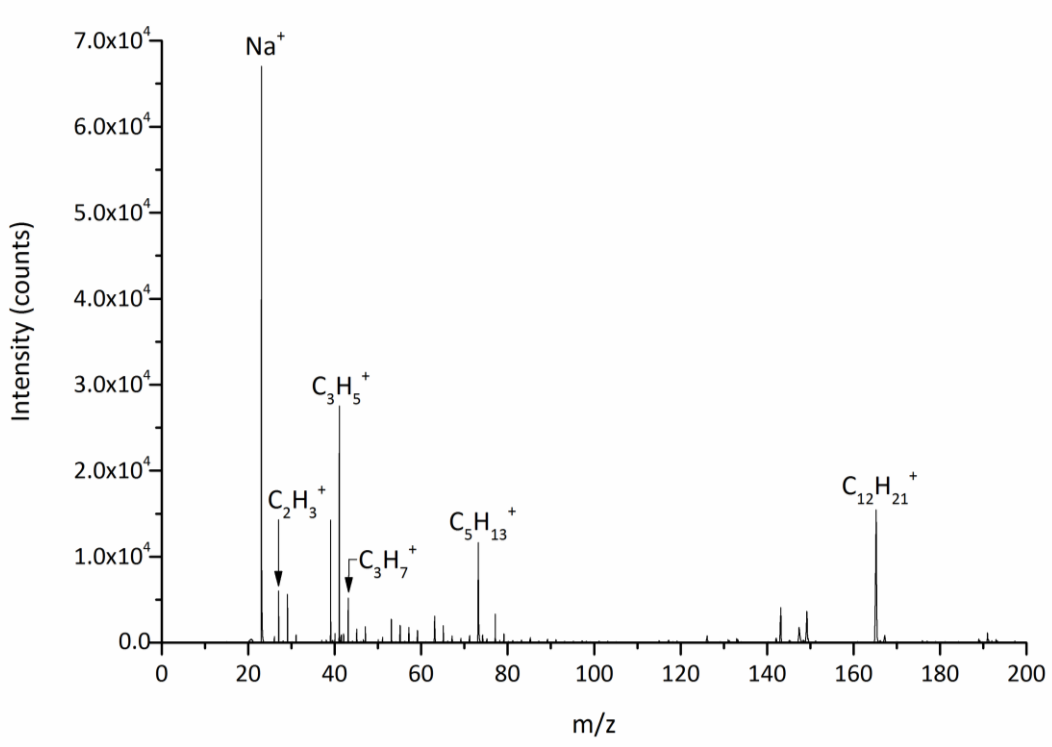

iii) Dehypon LS45, positive polarity (m/z ≤ 150)

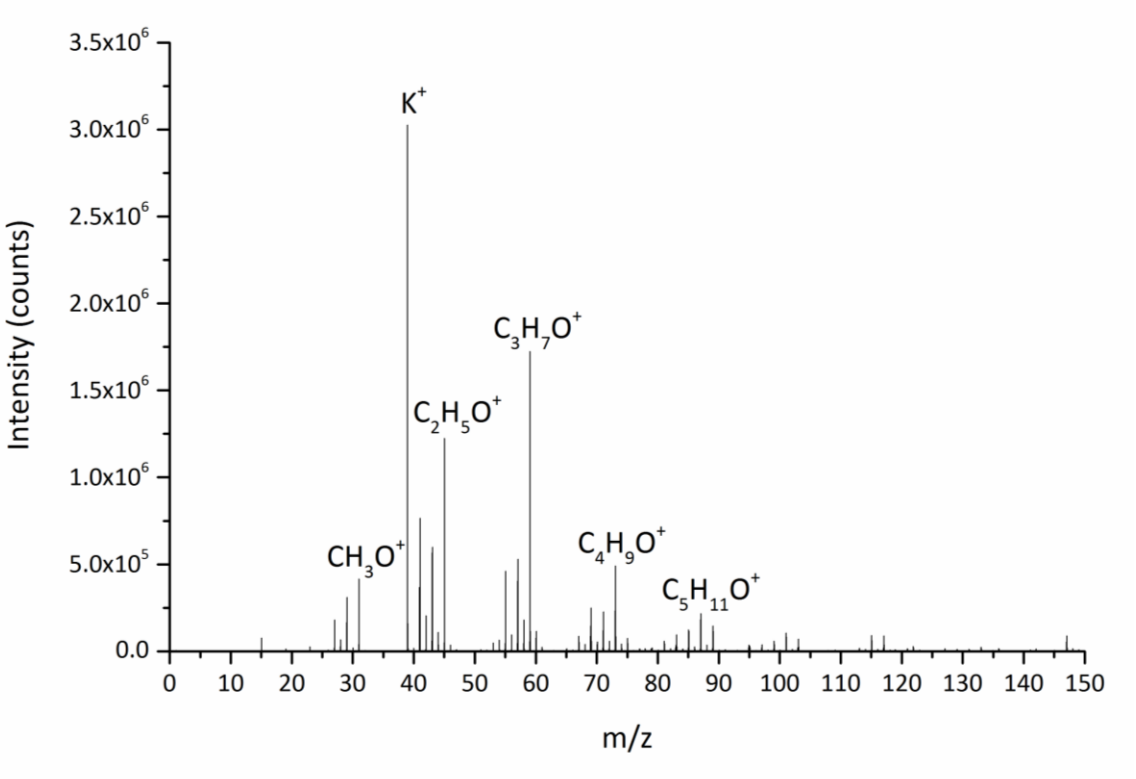

References

1. British Standards Institute. BS ISO 472:2013. *Plastics - Vocabulary*. London: BSI; 2013.
2. Plastics Europe. *Plastics - the facts 2015. An analysis of European plastics production, demand and waste data.* 2015. Available from: http://www.corepla.it/documenti/5f2fa32a-7081-416f-8bac-2efff3ff2fbd/Plastics+TheFacts+2015.pdf (accessed 20 July 2016).
3. PE International. *LCA of paper and polymer bank notes.* 2013. Available from: http://www.bankofengland.co.uk/banknotes/polymer/Documents/lcapaperandpolymerbanknotes.pdf (accessed 20 July 2016).
4. Then, E. and Oakley, V. A survey of plastic objects at The Victoria and Albert Museum. *V&A Conservation Journal*, 1993; 06:11-14.
5. Ward, C. and Shashoua, Y. *Conservation survey of objects containing plastics and rubber in the department of ethnography*. The British Museum. 1994.
6. Mossman, S. Plastics in the Science Museum, London: A curator's view. In: Grattan, D.W. ed. Canadian Conservation Institute. *Saving the Twentieth Century: The Conservation of Modern Materials*, 15-20 September 1993, Ottawa, Canada. 1993. p. 25-35.
7. Morgan, J. *A survey of plastics in historical collections*. Plastics Historical Society and The Conservation Unit of Museums and Galleries Commission. 1994.
8. Keneghan, B. *Plastics? - Not in my collection.* V&A Conservation Journal. 1996; 21:4-6.
9. Keneghan, B. et al. In what condition are my artefacts? Case studies. In: Lavédrine, B., Fournier, A. and Martin, G. eds. *Preservation of Plastic Artefacts in Museum Collections (POPART)*. Comité des travaux historiques et scientifiques (CTHS). 2012. p. 109-137.
10. Keneghan, B. A survey of synthetic plastic and rubber objects in the collections of the Victoria and Albert Museum. *V&A Conservation Journal.* 2002; 19(3):321-331.
11. Rivenc, R. *Modern materials - contemporary art.* ICOM-CC MMCA Newsletter. 2016. Available from: http://www.icom-cc.org/54/document/mmca-newsletter-june-2016/?id=1443#.V_atPvkrK70 (accessed 30 September 2016).
12. The Getty Conservation Institute. *Conservation of plastics.Conservation perspectives: The GCI Newsletter.* Spring 2014.

13. Kean, S. Does plastic art last forever? *Slate.* 2009. Available from: http://www.slate.com/articles/arts/art/2009/07/does_plastic_art_last_forever.html (accessed 20 July 2016).
14. Alberge, D. V&A conservators race to preserve art and design classics in plastic. *The Guardian*. 19 May 2015. Available from: https://www.theguardian.com/artanddesign/2015/may/19/va-conservators-race-to-preserve-art-and-design-classics-in-plastic (accessed 20 July 2016).
15. Price, B.A. et al. Naum Gabo's construction in space: Two Cones: history and materials. In: Keneghan, B. & Egan, L. eds. *Plastics: Looking at the Future & Learning from the Past.* London: Archetype Publications Ltd. 2008.
16. Bradley, S. Do objects have a finite lifetime? In: Knell, S.J. ed. *Care of Collections.* London:Taylor & Francis; 1994. p. 55-64.
17. Shashoua, Y. *Conservation of plastics: materials science,degradation and preservation*, Amsterdam: Elsevier. 2008.
18. Plastics Historical Society. *The conservation of plastics*. 2015. Available from: http://plastiquarian.com/?page_id=14326 (accessed 14 July 2016).
19. Curran, K. and Strlic, M. Polymers and volatiles: Using VOC analysis for the conservation of plastic and rubber objects. *Studies in Conservation.* 2015; 60(1): 1-14.
20. Lattuati-Derieux, A. et al. What do plastics emit? HS-SPME-GC/MS analyses of new standard plastics and plastic objects in museum collections. *Journal of Cultural Heritage.* 2013; 14(3):238-247.
21. The Institute of Conservation. *What is conservation?* 2016. Available from: http://icon.org.uk/what-is-conservation (accessed 12 July 2016).
22. The Institute of Conservation. *The Institute of Conservation's code of conduct*. 2014. Available from https://icon.org.uk/system/files/documents/icon_code_of_conduct.pdf (accessed 20 July 2016).
23. Shashoua, Y. A safe place. Storage strategies for plastics. In: The Getty Conservation Institute. *Conservation of plastics. Conservation perspectives. The GCI Newsletter*. 2014.
24. Williams, S. Care of objects made from rubber and plastic. *CCI Notes Series 15 (Modern Materials and Industrial Collections)*. Canadian Conservation Institute. 2015. Available from http://canada.pch.gc.ca/eng/1439925170961 (accessed 20 July 2016).
25. Health and Safety Executive. *The dangers of cellulose nitrate film.* 2013. Available from: http://www.hse.gov.uk/pubns/indg469.htm (accessed 30 September 2016).
26. Quye, A. Saving our polyesterdays: historical plastics conservation. *Chemistry & Industry.* 1998;(15):599-603.

27. Victoria & Albert Museum. *Collections care and conservation policy*. 2013. Available from https://www.vam.ac.uk/__data/assets/pdf_file/0020/235118/collections_care_conservation_policy_13.pdf (accessed 20 July 2016).
28. Barker, C.S. How to select gloves: An overview for collections staff. In: National Park Service. *Conserve O Gram*. September 2010. Available from https://www.nps.gov/museum/publications/conserveogram/01-12.pdf (accessed 30 September 2016).
29. Morinville, W. and Krasinski, C. Secondary ion mass spectrometry analysis of wafer contamination resulting from gloved hands. *2006 IEEE Workshop on Microelectronics and Electron Devices.*14 April 2006. Boise, Idaho. 2006. p. 35-36.
30. Strohmeier, B.R., Piasecki, J.D. and Plasencia, A. XPS surface characterization of disposable laboratory gloves and the transfer of glove components to other surfaces. *Spectroscopy.* 2012; 27(7):36.
31. Balcar, N. et al. Studies in cleaning plastics. In: Lavédrine, B., Fournier, A. and Martin, G. eds. *Preservation of Plastic Artefacts in Museum Collections (POPART)*. Comité des travaux historiques et scientifiques (CTHS). 2012. p. 225-269.
32. Morales Muñoz, C. Surface modification of plasticized PVC by dry cleaning methods: Consequences for artworks. *Applied Surface Science.* 2010;256(11): 3567-3572.
33. Shashoua, Y., et al. Wiping away the dirt - A safe option for plastics? In: *ICOM-CC Lisbon 2011: Preprints*. 19-23 September 2011. Lisbon, Portugal. 2011.
34. Morales Muñoz, C. et al. A model approach for finding cleaning solutions for plasticized poly(vinyl chloride) surfaces of collections objects. *Journal of the American Institute for Conservation.* 2014;53(4):236-251.
35. Waentig, F. Educating conservation of modern materials: case studies. In: Keneghan, B. and Egan, L. eds. *Plastics: Looking at the Future & Learning from the Past*. London: Archetype Publications. 2008.
36. Carretti, E. et al. New frontiers in materials science for art conservation: responsive gels and beyond. *Accounts of Chemical Research.* 2010;43(6):751–760.
37. Shah, B., Hunter, S. and Adams, S. Dust to dust. Access to access. *V&A Conservation Journal.* Spring 2011(59). Available from http://www.vam.ac.uk/content/journals/conservation-journal/spring-2011-issue-59/dust-to-dust.-access-to-access./ (accessed 20 July 2016).
38. Victoria & Albert Museum. *V&A annual review*. 2015. Available from: https://www.vam.ac.uk/__data/assets/pdf_file/0004/258430/Annual-Review-2015.pdf (accessed 12 July 2016).
39. Grau-Bové, J. and Strlič, M. Fine particulate matter in indoor cultural heritage: a literature review. *Heritage Science.* 2013;1(8).

40. Spafford Ricci, S. and Graham, F. The fire at the Royal Saskatchewan Museum, part 2: removal of soot from artifacts and recovery of the building. *Journal of the American Institute of Conservation.* 2000;39. Available from: http://cool.conservation-us.org/jaic/articles/jaic39-01-003.html (accessed 20 July 2016).
41. Environmental Research Group, Kings College London. *London Air Quality Network*. 2016. Available from: http://www.londonair.org.uk/ (accessed 14 July 2016).
42. Lima, C., Shah, B. and Pretzel, B. *Something old, something new: Dust monitoring at the V&A*. Unpublished work presented at the 2nd International SEAHA conference. 20-21 June 2016. Oxford, UK. 2016.
43. Smith, S., *Guidelines for the environmental control for objects on display in FuturePlan.* 2010. Available from: https://www.vam.ac.uk/__data/assets/pdf_file/0007/178612/Environmental_control_for_object_display_April_2010.pdf (accessed 20 July 2016)
44. Fenn, J., Labelling plastic artefacts. In: Grattan, D.W. ed. Canadian Conservation Institute. *Saving the Twentieth Century: The Conservation of Modern Materials*, 15-20 September 1993, Ottawa, Canada. 1993. p. 341-350.
45. Tsibouklis, J. and Nevell, T.G. Ultra-low surface energy polymers: The molecular design requirements. *Advanced Materials.* 2003;15(7-8):647-650.
46. Wu, S. *Polymer interface and adhesion*. New York: CRC Press. 1982.
47. National Physical Laboratory. Surface tensions. In: *Kaye and Laby Online Version 1.0*. 2005.
48. Carraher, C.E.J. *Carraher's polymer chemistry*. 9th ed. Boca Raton: CRC Press. 2014.
49. Young, R.J. and Lovell, P.A. *Introduction to polymers*. Florida: Taylor & Francis. 2011.
50. Vasile, C. and Pascu, M. *Practical guide to polyethylene*. iSmithers Rapra Publishing. 2005.
51. Altuglas International. *Plexiglas - Optical and transmission characteristics*. 2000. Available from http://www.plexiglas.com/export/sites/plexiglas/.content/medias/downloads/sheet-docs/plexiglas-optical-and-transmission-characteristics.pdf (accessed 9 June 2016).
52. Pilkington Glass. *Pilkington Glass Handbook.* 2010. Available from: http://www.pilkington.com/resources/glasshandbook2010english.pdf (accessed 30 September 2016)
53. Brandrup, J., Immergut, E.H. and Grulke, E.A. *Polymer handbook*. 4th ed. New York: Wiley. 1999.
54. Plazek, D.J. and Ngai, K.L. The glass temperature. In: Mark, J.E. ed. *Physical properties of polymers handbook*. New York: Springer. 2007.
55. Chapiro, A. *Radiation chemistry of polymeric systems.* High Polymers vol. 15. New York: Interscience Publishers. 1962.
56. Dawes, K., Glover, L.C. and Vroom, D.A. The effects of electron beam and g-irradiation on polymeric materials. In: Mark, J.E. ed. *Physical Properties of Polymers Handbook*. New York: Springer. 2007.

57. Brydson, J., *Plastics materials*. Oxford: Butterworth Heinemann. 7th ed. 1999.
58. British Plastics Federation. *Plastics processes*. In: *Plastipedia.* 2016. Available from: http://www.bpf.co.uk/plastipedia/processes/default.aspx (accessed 9 June 2016).
59. Shashoua, Y. Inhibiting the deterioration of plasticized poly (vinyl chloride) - a museum perspective. PhD Thesis. Technical University of Denmark. 2001.
60. Wypych, G. *Handbook of plasticizers*. Toronto: ChemTec Publishing. 2004.
61. European Parliament Council. *Directive 2005/84/EC*. 2005. Available from: http://eur-lex.europa.eu/LexUriServ/LexUriServ.do?uri=OJ:L:2005:344:0040:0043:en:PDF (accessed 9 June 2016)
62. AccuStandard. *Plastic additive standards guide*. 2013. Available from http://www.accustandard.com/assets/PLASTIC_ADD_GUIDE_2013.pdf (accessed 9 June 2016).
63. Lampman, S. ed. *Characterization and failure analysis of plastics*. ASM International. 2003.
64. Rabek, J.F. *Photodegradation of polymers: Physical characteristics and applications*. Berlin: Springer-Verlag. 1996.
65. British Standards Institute, BS EN 60904-3:2008. *Photovoltaic devices. Measurement principles for terrestrial photovoltaic (PV) solar devices with reference spectral irradiance data*. London: BSI; 2009.
66. The National Gallery. *Spectral power distribution curves.* 2016. Available from: http://research.ng-london.org.uk/scientific/spd/ (accessed 30 September 2016).
67. Baker, M.T. and McManus, E. Spacesuits: NASA's dream - Conservator's nightmare. In: Grattan, D.W. ed. Canadian Conservation Institute. *Saving the Twentieth Century: The Conservation of Modern Materials*, 15-20 September 1993, Ottawa, Canada. 1993.
68. Song, J., Fischer, C.H. and Schnabel, W. Thermal oxidative-degradation of poly(methyl methacrylate). *Polymer Degradation and Stability.* 1992;36(3):261-266.
69. Grassie, N. and Scott, G. *Polymer degradation and stabilisation*. Cambridge: Cambridge University Press. 1985.
70. Kaczmarek, H., Kaminska, A. and van Herk, A. Photooxidative degradation of poly(alkyl methacrylate)s. *European Polymer Journal.* 2000;36(4):767-777.
71. Feller, R.L. Stages in the deterioration of organic materials. In: Williams, J.C. ed. *Preservation of Paper and Textiles of Historic and Artistic Value*. American Chemical Society. 1978. p. 314-335.
72. Williams, R.S. Composition implications of plastic artifacts: A survey of additives and their effects on the longevity of plastics. In: Grattan, D.W. ed. Canadian Conservation Institute. *Saving the Twentieth Century: The Conservation of Modern Materials*, 15-20 September 1993, Ottawa, Canada. 1993.

73. Wright, D. *Failure of plastics and rubber products: Causes, effects and case studies involving degradation*. Shawbury: Rapra Technology Limited. 2001.
74. European Environment Agency. *Air quality in Europe - 2014 report*. 2014. Available at: http://www.eea.europa.eu/publications/air-quality-in-europe-2014 (accessed 9 June 2016).
75. Jellinek, H.H.G., Flajsman, F. and Rryman, F.J. Reaction of SO_2 and NO_2 with polymers. *Journal of Applied Polymer Science.* 1969;13:107-116.
76. World Health Organization. *WHO guidelines for indoor air quality: selected pollutants*. 2010. Available from: http://www.euro.who.int/__data/assets/pdf_file/0009/128169/e94535.pdf (accessed 9 June 2016).
77. Cappitelli, F. and Sorlini, C. Microorganisms attack synthetic polymers in items representing our cultural heritage. *Applied and Environmental Microbiology.* 2008;74(3):564-569.
78. Moriyama, Y. et al. Examination of fungal deterioration on plasticized polyvinyl-chloride by cryoscanning electron-microscopy. *International Biodeterioration & Biodegradation.* 1993;31(3):231-239.
79. Kerr, N. and Batcheller, J. Degradation of polyurethanes in 20th-century museum textiles. In: Grattan, D.W. ed. Canadian Conservation Institute. *Saving the Twentieth Century: The Conservation of Modern Materials*, 15-20 September 1993, Ottawa, Canada. 1993.
80. Wright, D.C. Failure of polymer products due to photo-oxidation. *Rapra Review Reports*. Rapra Technology Ltd. 2001.
81. Gray, R.L. and Lee, R.E. The influence of flame retardant structure on UV stabilization approaches in polypropylene. *Angewandte Makromolekulare Chemie.* 247:61-72. 1997.
82. Jansen, J.A. Environmental stress cracking - The plastic killer. *Advanced Materials & Processes.* 2004;162(6):50-53.
83. Van Oosten, T.B. Crystals and crazes: degradation in plastics due to microclimates. In: van Oosten, T., Shashoua, Y. and Waentig, F. ed. *Plastics in art: history, technology, preservation*. Siegl. 80-89. 2002.
84. Hansen, C.M. *Hansen solubility parameters: A user's handbook*. 2nd ed. Boca Raton: CRC Press. 2007.
85. Horie, C.V. *Materials for conservation : organic consolidants, adhesives and coatings*. Butterworths series in conservation and museology. London: Butterworths. 1987.
86. Sousa, A.R. et al. The combined effect of photodegradation and stress cracking in polystyrene. *Polymer Degradation and Stability.* 2006;91(7):1504-1512.
87. European Confederation of Conservator-Restorers' Organisations. *European Confederation of Conservator-Restorers' Organisations professional guidelines II*. 2003. Available from: http://www.ecco-eu.org/fileadmin/user_upload/ECCO_professional_guidelines_II.pdf (accessed 9 June 2016).

88. Morales Muñoz, C. Spectrocolorimetric and microscopic techniques for the evaluation of plasticized PVC cleaning: a case study applicable to three-dimensional objects at museums. *Journal of Microscopy.* 2011;243(3):257-266.

89. Pastorelli, G. et al. Environmentally induced,colour change during natural degradation of selected polymers. *Polymer Degradation and Stability.* 2014;107:198-209.

90. White, R. and Roy, A. GC-MS and SEM Studies on the effects of solvent cleaning on old master paintings from the National Gallery, London. *Studies in Conservation.* 1998;43(3):159-176.

91. Carretti, E. et al. Oil-in-water nanocontainers as low environmental impact cleaning tools for works of art: Two case studies. *Langmuir.* 2007;23(11): 6396-6403.

92. Chercoles Asensio, R. et al. Analytical characterization of polymers used in conservation and restoration by ATR-FTIR spectroscopy. *Analytical and Bioanalytical Chemistry.* 2009;395(7): 2081-2096.

93. Littlejohn, D. et al. Investigation of the degradation of cellulose acetate museum artefacts. *Polymer Degradation and Stability.* 2013;98(1):416-424.

94. Schilling, M. et al. Application of chemical and thermal analysis methods for studying cellulose ester plastics. *Accounts of Chemical Research.* 2010;43(6):888-896.

95. Van Oosten, T.B. and Aten, A. Life long guaranteed: the effect of accelerated ageing on Tupperware objects made of polyethylene. In: *ICOM Committee for Conservation. 11th triennial meeting in Edinburgh, Scotland, 1-6 September 1996: Preprints*. James & James (Science Publishers) Ltd. 1996.

96. Mitchell, G. et al. Assessment of historical polymers using attenuated total reflectance-Fourier transform infra-red spectroscopy with principal component analysis. *Heritage Science.* 2013;1:28.

97. Edwards, H.G.M. et al. Raman-spectroscopic studies of pedigree doll disease. *Polymer Degradation and Stability.*1993;41:257–264.

98. Mitchell, G. *Heritage smells: New methods of analyses for the assessment of plastics in heritage collections*. PhD Thesis. University of Strathclyde. 2014.

99. Fearn, S., McPhail, D.S. and Oakley, V. Room temperature corrosion of museum glass: an investigation using low-energy SIMS. *Applied Surface Science.* 2004;31:510-514.

100. Dowsett, M.G. et al. The use of ultra-low-energy dynamic SIMS in the study of the tarnishing of silver. *Nuclear Instruments & Methods in Physics Research Section B-Beam Interactions with Materials and Atoms.* 2005;239(1-2):51-64.

101. Abel, M.-L. and Coppitters, C. Conservation of polymers: A view to the future. *Surface and Interface Analysis.* 2008;40(3-4):445-449.

102. Keune, K. and Boon, J.J. Imaging secondary ion mass spectrometry of a paint cross section taken from an early Netherlandish painting by Rogier van der Weyden. *Analytical Chemistry.* 2004;76(5):1374-1385.
103. Benetti, F., Marchettini, N. and Atrei, A. ToF-SIMS and XPS study of ancient papers. *Applied Surface Science.* 2011;257(6):2142-2147.
104. Willneff, E.A. et al. Conservation of artists' acrylic emulsion paints: XPS, NEXAFS and ATR-FTIR studies of wet cleaning methods. *Surface and Interface Analysis.* 2014;46(10-11):776-780.
105. de Sa, M.H. et al. An AFM contribution to the understanding of surface effects caused by ageing and cleaning on acrylic glass. The Shadows by Lourdes Castro, a case study. Surface and Interface Analysis. 2011;43(8):1165-1170.
106. Necemer, M., Kump, P. and Zvanut, M. Application of energy dispersive x-ray fluorescence spectrometry for the characterization of plastic materials in synthetic polymer conservation work. *X-Ray Spectrometry.* 2012;41(2):87-92.
107. Striegel, A. et al. *Modern size-exclusion liquid chromatography: Practice of gel permeation and gel filtration chromatography*. 2nd ed. Hoboken: John Wiley & Sons. 2009.
108. Hitachi Ltd. *U-4000 spectrophotometer manual.* 1993.
109. British Standards Institute. BS EN ISO 11664-2:2011. *Colorimetry. Part 2: CIE standard illuminants*. London: BSI; 2011.
110. British Standards Institute. BS EN ISO 11664-1:2011. *Colorimetry*. *Part 1: CIE standard colorimetric observers*. London: BSI; 2011.
111. British Standards Institute. BS EN ISO 11664-3:2013. *Colorimetry. Part 3: CIE tristimulus values*. London: BSI; 2013.
112. British Standards Institute. BS EN ISO 11664-4:2011. *Colorimetry. Part 4: CIE 1976 L*a*b* colour space*. London: BSI; 2011.
113. British Standards Institute. BS EN ISO 11664-6:2014. *Colorimetry*. *Part 6: CIEDE2000 colour-difference formula*. London: BSI; 2014.
114. ASTM International. ASTM E313-15e1. *Standard practice for calculating yellowness and whiteness indices from instrumentally measured color coordinates*. 2015.
115. Zygo Corporation. *NewView 200 Manual.*1996.
116. Hesse, M., Meier, H. and Zeeh, B. Spectroscopic methods in organic chemistry. In: Enders, D., Noyori, R. and Trost, B.M. ed. *Foundations of Organic Chemistry.* New York: Thieme. 1997.
117. Pike Technologies. *Application note: ATR theory and applications*. 2011. Available from: http://www.piketech.com/files/pdfs/ATRAN611.pdf (accessed 30 September 2016).
118. National Physical Laboratory. Refractive index of optical materials. In: *Kaye and Laby Online Version 1.0*. 2005.

119. Kuo, W.C.H., Briceno, M. and Ozkaya, D. Characterisation of catalysts using secondary and backscattered electron in-lens detectors. *Platinum Metals Review.* 2014;58(2):106-110.

120. Hill, R. Analysis beams used in ToF-SIMS. In: Vickerman, J.C. and Briggs, D. ed. *ToF-SIMS: Materials Analysis by Mass Spectrometry*. Chichester: IM Publications. 2013. p. 271-290.

121. Briggs, D. *Surface analysis of polymers by XPS and static SIMS*. Cambridge: Cambridge University Press. 1998.

122. Benninghoven, A. The history of static SIMS - a personal perspective. In: Vickerman, J.C. and Briggs, D. ed. *ToF-SIMS: Materials Analysis by Mass Spectrometry*. Chichester: IM Publications. 2013. p. 39-66.

123. Schueler, B.W. Time-of-flight mass analysers. In: Vickerman, J.C. and Briggs, D. ed. *ToF-SIMS: Materials Analysis by Mass Spectrometry*. Chichester: IM Publications. 2013. p. 247-270.

124. Vickerman, J.C. Prologue: ToF-SIMS - An evolving mass spectrometry of materials. In: Vickerman, J.C. and Briggs, D. ed. *ToF-SIMS: Materials Analysis by Mass Spectrometry*. Chichester: IM Publications. 2013. p. 1-38.

125. Hagenhoff, B. Cationisation. In: Vickerman, J.C. and Briggs, D. ed. *ToF-SIMS: Materials Analysis by Mass Spectrometry*. Chichester: IM Publications. 2013. p. 193-216.

126. Briggs, D., Fletcher, I.W. and Goncalves, N.M. Positive secondary ion mass spectrum of poly(methyl methacrylate): a high mass resolution ToF-SIMS study. *Surface and Interface Analysis.* 2000;29(5):303-309.

127. Niehuis, E. and Grehl, T. Depth profiling of inorganic materials. In: Vickerman, J.C. and Briggs, D. ed. *ToF-SIMS: Materials Analysis by Mass Spectrometry*. Chichester: IM Publications. 2013. p. 613-635.

128. Mahoney, C.M. Cluster secondary ion mass spectrometry of polymers and related materials. *Mass Spectrometry Reviews.* 2010;29(2):247-293.

129. Fearn, S. *An introduction to time-of-flight secondary ion mass spectrometry (ToF-SIMS) and its application to materials science*. San Rafael: Morgan & Claypool. 2015.

130. Ninomiya, S. et al. Precise and fast secondary ion mass spectrometry depth profiling of polymer materials with large Ar cluster ion beams. *Rapid Communications in Mass Spectrometry.* 2009:23(11):1601-1606.

131. Hercules, D.M. Time-of-flight secondary ion mass spectrometry (ToF-SIMS). In: Montaudo, G. and Lattimer, R.P. eds. *Mass Spectrometry of Polymers*. Boca Raton: CRC Press. p. 311-388. 2001.

132. Gilmore, I. Role of operating conditions in ToF-SIMS. In: Vickerman, J.C. and Briggs, D. eds. *ToF-SIMS: Materials Analysis by Mass Spectrometry*. Chichester: IM Publications. 2013.

133. Pallipurath, A. et al. A chemometric study of ageing in lead-based paints. *Talanta.* 144:977-985. 2015.
134. Marengo, E. et al. Monitoring of paintings under exposure to UV light by ATR-FT-IR spectroscopy and multivariate control charts. *Vibrational Spectroscopy.* 2006;40(2):225-234.
135. Gulotta, D. et al. Anoxic treatment for the disinfestation of wood cultural heritage: assessment of the effects and harmfulness on different species. *Wood Science and Technology.* 2015;49(5):925-944.
136. Capobianco, G. et al. Pigment identification in pictorial layers by hyperspectral imaging. *Proceedings of SPIE 9106: Advanced Environmental, Chemical, and Biological Sensing Technologies XI.* 22 May 2014. Baltimore, USA. 2014.
137. Benetti, F. et al. ToF-SIMS characterization of proteinaceous binders in the wall painting "Madonna and Child enthroned with Saints" by Ambrogio Lorenzetti in the St. Augustine Church (Siena, Italy). *International Journal of Mass Spectrometry.* 2015;392:111-117.
138. Graham, D.J. and Castner, D.G. Multivariate analysis of ToF-SIMS data from multicomponent systems: The why, when, and how. *Biointerphases.* 2012;7(1-4).
139. Medard, N. et al. Characterization of additives at polymer surfaces by ToF-SIMS. *Surface and Interface Analysis.* 2002;34(1):565-569.
140. Bailey, J. et al. 3D ToF-SIMS imaging of polymer multi layer films using argon cluster sputter depth profiling. *ACS Applied Materials & Interfaces.* 2015;7(4):2654-2659.
141. Miyasaka, T., Ikemoto, T. and Kohno, T. ToF-SIMS imaging of PE/PP polymer using multivariate analysis. *Applied Surface Science.* 2008;255(4):1576-1579.
142. Keenan, M.R. and Kotula, P.G. Accounting for Poisson noise in the multivariate analysis of ToF-SIMS spectrum images. *Surface and Interface Analysis.* 2004;36(3):203-212.
143. Graham, D.J., Wagner, M.S. and Castner, D.G. Information from complexity: Challenges of ToF-SIMS data interpretation. *Applied Surface Science.* 2006;252(19):6860-6868.
144. Henderson, A. Qualitative interpretation of spectra. In: Vickerman, J.C. and Briggs, D. eds. *ToF-SIMS: Materials Analysis by Mass Spectrometry*. Chichester: IM Publications. 2013. p. 417-502.
145. Varmuza, K. and Filzmoser, P. *Introduction to multivariate statistical analysis in chemometrics*. Boca Raton: Taylor & Francis Group. 2009.
146. Procter and Gamble. *Orvus WA Paste material safety data sheet*. 2010.
147. Conservation by Design Limited. *Dehypon LS45. Technical data sheet.* 2000.
148. Casella, L. and Moore, C. Research on methods of cleaning face-mounted photographs. *Topics in Photographic Preservation.* 2009;13:200-208.
149. Kawashima, T. et al. Examination of fragment ions of polystyrene in ToF-SIMS spectra using MS/MS. *Surface and Interface Analysis.* 2014;46:92-95.

150. Miller, R.G.J. and Willis, H.A. eds. *Infrared structural correlation tables and data cards*. London: Heyden & Son Limited. 1969.

151. Nilsen, S.K. et al. Micro-fibre and ultra-micro-fibre cloths, their physical characteristics, cleaning effect, abrasion on surfaces, friction, and wear resistance. *Building and Environment.* 2002;37(12):1373-1378.

152. McLeod, J.H. and Sherwood, W.T. A proposed method of specifying appearance defects of optical parts. *Journal of the Optical Society of America.* 1945;35(2):3.

153. British Standards Institute. BS ISO 14997:2011. *Optics and photonics - Test methods for surface imperfections of optical elements*. London: BSI; 2011.

154. Pesonen-Leinonen, E. et al. Determination of soil adhesion to plastic surfaces using a radioactive tracer. *Applied Radiation and Isotopes.* 2006;64(2):163-169.

155. Koponen, H.-K., Suvanto, M. and Pakkanen, T.A. Soiling of plasticized poly(vinyl chloride). *Journal of Applied Polymer Science.* 2007;105(5):3047–3053.

156. British Standards Institute. ISO 11378-1:2000. *Textile floor coverings - Laboratory soiling tests - Part 1: Kappasoil test*. London: BSI; 2000.

157. British Standards Institute. ISO 11378-2:2001. *Textile floor coverings - Laboratory soiling tests - Part 2: Drum test*. London: BSI; 2001.

158. Galatis, P., Boyatzis, S. and Theodorakopoulos, C. An investigation of the selective removal of a synthetic soiling mixture from mastic, shellac & Laropal® K80 coatings using hydrogels. *e-Preservation Science.* 2012;9:72-83.

159. Sigma-Aldrich. *Product specification, carbon*. Available from: http://www.sigmaaldrich.com/Graphics/COfAInfo/SigmaSAPQM/SPEC/70/702102/702102-BULK_____ALDRICH__.pdf (accessed 30 September 2016).

160. Sokhi, R.S. et al. Pixe analysis of carbon-black for elemental impurities. *Nuclear Instruments & Methods in Physics Research Section B-Beam Interactions with Materials and Atoms.* 1990;49(1-4):414-417.

161. Moore, G. and Griffith, C. A laboratory evaluation of the decontamination properties of microfibre cloths. *Journal of Hospital Infection.* 2006;64(4):379-385.

162. Pociūtė , M., Lehmann, B. and Vitkauskas, A. Wetting behaviour of surgical polyester woven fabrics. *Materials Science (Medžiagotyra).* 2003;9(4):410-413.

163. Kronberg, B., Holmberg, K. and Lindman, B. *Surface chemistry of surfactants and polymers*. Chichester: John Wiley & Sons. 2014.

164. Rosen, M.J. and Kunjappu, J.T. *Surfactants and interfacial phenomena*. 4th ed. New Jersey: John Wiley & Sons. 2012.

165. Haynes, W.M. ed. *Handbook of chemistry and physics*. Boca Raton: CRC Press. 2013.

166. Feller, R.L. Accelerated ageing: Photochemical and thermal aspects. *Research in Conservation.* The Getty Conservation Institute. 1994.

167. Boye, C., Preusser, F. and Schaeffer, T. UV-blocking window films for use in museums-revisited. *Western Association for Art Conservation Newsletter.* 2010;32(1). Available from: http://cool.conservation-us.org/waac/wn/wn32/wn32-1/wn32-104.pdf (accessed 30 September 2016).

168. Piccablotto, G. et al. Study on conservation aspects using LED technology for museum lighting. *Energy Procedia*. 2015;78:1347-1352.

169. Druzik, J.R. and Michalski, S.W. *Guidelines for selecting solid-state lighting for museums*. The Canadian Conservation Institute and The Getty Conservation Institute. 2011. Available from: http://www.connectingtocollections.org/wp-content/uploads/2011/08/SSL-Guidelines-Ver.-10.0.pdf (accessed 30 September 2016).

170. Finney, L. *Basic conservation and environmental monitoring*. Zeuner, D. ed. Association of Independent Museums. 2006. Available from http://www.aim-museums.co.uk/downloads/ffe7f644-dd7d-11e1-bdfc-001999b209eb.pdf (accessed 14 September 2016).

171. South East Conservation and Restoration. *Recommended environmental conditions for museum objects*. 2011. Available from: http://www.southeastconservation.com.au/conditions.html (accessed 14 September 2016).

172. Korenberg, C. How fast do polyester fabrics age in the museum environment? *V&A Conservation Journal.* Summer 2003;(44).

173. Cucci, C., Bigazzi, L. and Picollo, M. Fibre optic reflectance spectroscopy as a non-invasive tool for investigating plastics degradation in contemporary art collections: A methodological study on an expanded polystyrene artwork. *Journal of Cultural Heritage.* 2013;14(4):290-296.

174. Maxwell, A.S. et al. *Review of accelerated ageing methods and lifetime prediction techniques for polymeric materials*. National Physical Laboratory. 2005.

175. Q-Lab Corporation. *Technical bulletin LX-5055. Spectral power distribution for Q-SUN Xe-1 and Xe-3 with daylight - Q filters*. 2011.

176. Q-Lab Corporation. *Technical bulletin LU-8054. Spectral power distribution for noon summer sunlight*. 2011.

177. National Physical Laboratory. Photometry. In: *Kaye and Laby Online Version 1.0*. 2005.

178. British Standards Institute. BS EN ISO 4892-2:2013. *Plastics - Methods of exposure to laboratory light sources. Part 2: Xenon-arc lamps*. London: BSI; 2013.

179. ASTM International. ASTM G155-13. *Standard practice for operating xenon arc light apparatus for exposure of nonmetallic materials*. 2005.

180. Quill, J. et al. *Technical Bulletin LX-5026. Quantifying the indoor light environment: testing for light stability in retail & residential environments*. Q-Lab Corporation. 2007.

181. Q-Lab Corporation. *Technical Bulletin LX-5060. A choice of filters for Q-sun xenon test chambers*. 2014.

182. Gardette, J.L., Mailhot, B. and Lemaire, J. Photooxidation mechanisms of styrenic polymers. *Polymer Degradation and Stability*, 1995;48(3): 457-470.

183. Lehocky, M. et al. Plasma surface modification of polyethylene. *Colloids and Surfaces a-Physicochemical and Engineering Aspects.* 2003;222(1-3):125-131.

184. Awaja, F. and Pigram, P.J. Surface molecular characterisation of different epoxy resin composites subjected to UV accelerated degradation using XPS and ToF-SIMS. *Polymer Degradation and Stability.* 2009;94(4):651-658.

185. Piwowar, A.M. and Winograd, N. Application of SIMS to study of biological systems. In: Vickerman, J.C. and Briggs, D. eds. *ToF-SIMS: Materials Analysis by Mass Spectrometry*. Chichester: IM Publications. 2013. p. 556-557.

186. Reich, F. *Sample handling for ToF-SIMS.* In: Vickerman, J.C. and Briggs, D. eds. *ToF-SIMS: Materials Analysis by Mass Spectrometry*. Chichester: IM Publications. 2013. p. 398.

187. ASTM International. ASTM D4265-14. *Standard guide for evaluating stain removal performance in home laundering*. 2014.

188. Cox, M.F., Smith, D.L. and Russell, G.L. Surface chemical processes for removal of solid sebum soil. *Journal of the American Oil Chemists Society.*1987;64(2):273-276.

189. *Nanorestart*. 2016. Available from: http://www.nanorestart.eu/ (accessed 28 September 2016).

List of journal publications and articles

1. **Fricker, A. L.**, McPhail, D. S., Keneghan, B. and Pretzel, B. The use of advanced surface analysis techniques to investigate the cleaning of museum-based polymers (in preparation).
2. **Fricker, A. L.**, McPhail, D. S., Keneghan, B. and Pretzel, B. Cleaning treatments for museum plastics: a closer look (in preparation).
3. **Fricker, A. L.**, McPhail, D. S., Keneghan, B. and Pretzel, B. The cleaning and conservation of plastic artefacts found in museum collections. *Proceedings of the Conference Future Talks* (in review).
4. **Fricker, A. L.**, McPhail, D. S., Keneghan, B. and Pretzel, B. The analysis of cleaning protocols for plastics in the V&A collections. *V&A Conservation Journal* (accepted for publication).

List of conference presentations

1. **Fricker, A. L.**, McPhail, D. S., Keneghan, B. and Pretzel, B. (2016). The use of surface sensitive techniques to investigate cleaning protocols for polymeric artefacts. Scientific Methods in Cultural Heritage Research, Gordon Research Conference, Sunday River, Maine, USA. 1-5 August 2016 (poster).
2. **Fricker, A. L.**, McPhail, D. S., Keneghan, B. and Pretzel, B. (2016). The use of surface sensitive techniques to investigate cleaning protocols for polymeric artefacts. Scientific Methods in Cultural Heritage Research, Gordon Research Seminar, Sunday River, Maine, USA. 30-31 July 2016 (oral).
3. **Fricker, A. L.**, McPhail, D. S., Keneghan, B. and Pretzel, B. (2016). Characterising the effect of cleaning procedures on museum polymers using secondary ion mass spectrometry. 4th International Congress Chemistry in Cultural Heritage, Brussels, Belgium. 6-8 July 2016 (poster).
4. **Fricker, A. L.**, McPhail, D. S., Keneghan, B. and Pretzel, B. (2016). Cleaning treatments for plastics: a closer look. SEAHA 2nd International Conference, University of Oxford, Oxford, UK. 20-21 June 2016 (oral).
5. **Fricker, A. L.** (2016). Scratching the surface: Examining cleaning treatments for museum plastics. Postgraduate Research Seminar, Imperial College London, London, UK. 21 March 2016 (oral).
6. **Fricker, A. L.** (2016). Deciphering the data: Using principal component analysis of ToF-SIMS spectra to examine cleaning treatments for museum plastics. Surface Analysis Seminar, Imperial College London, London, UK. 18 February 2016 (oral).
7. **Fricker, A. L.**, McPhail, D. S., Keneghan, B. and Pretzel, B. (2016). Using surface characterisation techniques to inform cleaning procedures for plastics in the museum

environment. Studying Surfaces: in vacuo, in situ, in silico, Royal Society of Chemistry, London, UK. 22 January 2016 (poster).

8. **Fricker, A. L.**, McPhail, D. S., Keneghan, B. and Pretzel, B. (2016). The use of surface analysis techniques to examine cleaning protocols for museum plastics. UK Surface Analysis Forum, Kegworth, Leicestershire, UK. 6 January 2016 (poster).
9. **Fricker, A. L.**, McPhail, D. S., Keneghan, B. and Pretzel, B. (2015). The cleaning and conservation of plastic artefacts found in museum collections. Future Talks 015, Munich, Germany. 28-30 October 2015 (oral).
10. **Fricker, A. L.**, McPhail, D. S., Keneghan, B. and Pretzel, B. (2015). A collaborative approach to evaluate cleaning protocols for museum plastics. SEAHA 1st International Conference, University College London, London, UK. 14-15 July 2015 (poster).
11. **Fricker, A. L.** (2015). The effect of cleaning treatments on plastics found in museum collections. Postgraduate Research Seminar, Imperial College London, London, UK. 23 March 2015 (poster).
12. **Fricker, A. L.**, McPhail, D. S. and Keneghan, B. (2015). Cleaning of polymeric artefacts in museum collections. Cultural Heritage Workshop, Imperial College London, London, UK, 11 February 2015 (oral).
13. **Fricker, A. L.**, McPhail, D. S. and Keneghan, B. (2014). Studies of the effects of cleaning protocols on museum-based plastics using advanced surface analysis techniques. AVS61, Baltimore, Maryland, USA, 9-14 November 2014 (oral).